Swansea University E-Theses

An investigation into embedded photodynamic therapy.

Liew, Yen Song

How to cite:

Use policy:

An Investigation into Embedded Photodynamic Therapy

Yen Song Liew

Thesis submitted to the University of Wales Swansea in fulfilment of the requirements for the degree of Doctor of Philosophy in Electrical and Electronic Engineering.

University of Wales Swansea

Supervisor:
Prof. R.M. Clement

June 2005

SUMMARY

This thesis describes investigations undertaken for a light source device embedded subcutaneously in the cancer treatment of photodynamic therapy. Photodynamic therapy involves a photosensitiser administered into tissue and using a light source to activate the photosensitiser leading to the destruction of tumour. An investigation into the current cancer treatment modality was described. The photodynamic therapy modality could be improved by the use of low cost LED device compared to laser system. The embedded LED device could be powered externally by an electromagnetic source.

A detailed study was performed to enable an understanding of photodynamic therapy process and the light-tissue interaction. A theoretical model was developed to examine the effect of embedding a light source and the effect of varying the photodynamic parameters in an effort to optimise the efficiency of photodynamic therapy.

An investigation into dielectric properties of tissues at radio and microwave frequencies was presented. A theoretical model was utilised to determine the attenuation losses in the heterogeneous tissue structures of varying frequencies. Inductive coupling and radiative coupling methods that were employed for energy coupling to power the LED device remotely were presented. Once the possible solutions were found, a complete radio frequency system and a microwave system had been constructed and evaluated. The evaluations carried out showed that the radio frequency system employing inductive coupling principle could be used to couple sufficient energy into tissue efficiently for the application in embedded photodynamic therapy.

Finally, the practical aspects of embedded photodynamic therapy were addressed. The findings and conclusions should be relevant to the wider biomedical cancer research community.

DECLARATION AND STATEMENTS

DECLARATION

This work has not previously been accepted in substance for any degree and is not being concurrently submitted in candidature for any degree.

Signed...   Candidate)

Date......22/.7./.05.....................

STATEMENT 1

This work is the result of my own investigations, except where otherwise stated. Other sources are acknowledged by footnotes giving clear references. A full reference is appended.

Signed......   (Candidate)

Date......22/7/05.....................

STATEMENT 2

I hereby give consent for my work, if accepted, to be available for photocopying and for inter-library loan, and for the title and summary to be made available to outside organisation.

Signed........   .... (Candidate)

Date...........22/.7./.05...............

ACKNOWLEDMENTS

TABLE OF CONTENTS

LIST OF FIGURES

LIST OF TABLES

CHAPTER 1   INTRODUCTION

1.1 The Medical Needs

Current studies have shown cancer is a major cause of death in the United Kingdom with more than 270,000 new cases diagnosed in year 2000.[1] It is estimated that one out of three people will be diagnosed with cancer during their lifetime. Hence, there is a critical need in the medical field for a novel method to treat cancer effectively. There are more than 200 different types of cancers. The most common types of cancer affecting men and women in the UK are breast, lung, large bowel and prostate as shown in Figure 1.1.
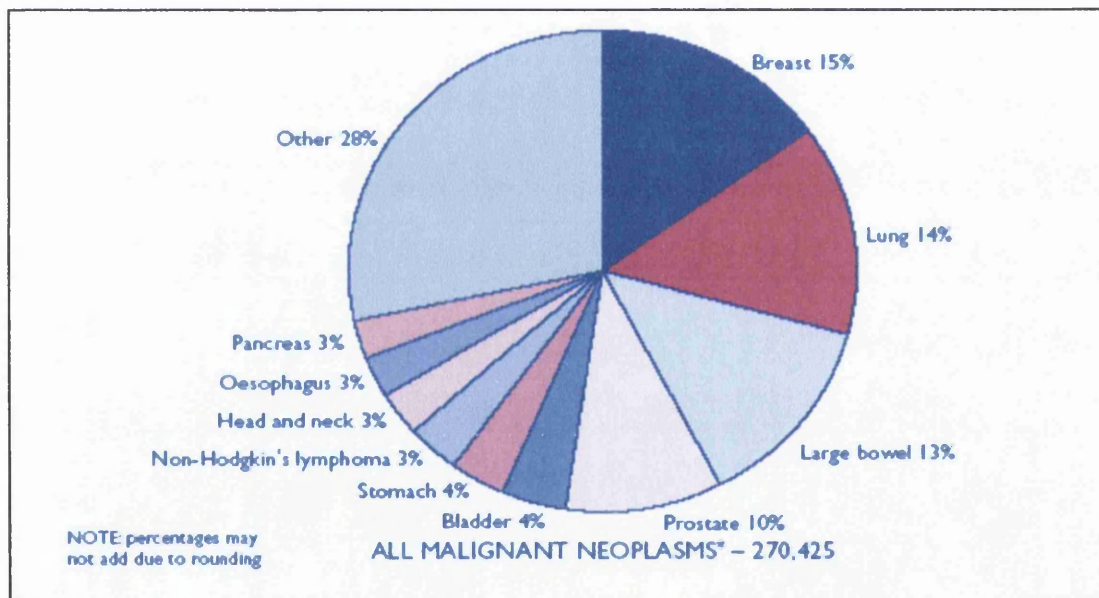
Figure 1.1: Ten most common cancers diagnosed in the UK. [1]

Cancer is an uncontrolled growth of cells that destroy normal tissues. The cancer cells are tumours which destroy the part of the body in which they are formed and then spread to other parts where they start a new growth and cause more cell destruction. The abnormal cells keep reproducing and do not mature into normal cells. With each doubling of cells, the cells become more primitive and reproduce more rapidly. The genetic information in the cancer cells are damaged or lost. It is this ability to spread fast that makes a cancer highly dangerous which has to be treated immediately.

1

1.1.1 Limitation in Current Treatment

The current cancer treatments are surgery, radiotherapy, chemotherapy, immunotherapy, gene therapy and stem cell transplant. Immunotherapy is the treatment with substances to boost the immune system of the body to fight against cancer cells. The gene therapy and stem cell transplant treatments are still in the early development stage of treating cancer safely but hold the solution to cure all types of cancer.

Surgery is one of the main methods of cancer treatment. It is mostly used to remove the tumour in only one particular part of the body and not suitable for patients whose cancer has spread to another part of the body. However, every surgery performed always carries some risks due to the trauma involved. There is always the danger that malignant tumours have already spread before surgery. There are some common problems associated with surgery. These are

- Pain.
- Local infection.
- Blood clots.
- Scarring.
- Fluid collection around the wound.

Traditional cancer therapies such as chemotherapy and radiotherapy have major drawbacks and work in the same way as carpet bombing. These methods destroy not only the cancer cells but also other healthy cells in the body. These therapies result in the loss of normal cell function because of having non-selectivity in targeting cancer cells. The radiotherapy and chemotherapy can be used to

- To shrink a cancer before surgery.
- To reduce the risk of a cancer coming back after surgery.
- To cure a cancer completely.
- To control symptoms and provide quality of life when a cancer is too advanced to cure.

Radiotherapy is the treatment using high energy rays to kill cancer cells. The high energy rays are directed at the localised part of the body being treated. To protect normal cells, doctors carefully limit the doses of radiation and spread the treatment out over time. They also shield as much normal tissue as possible while they aim the radiation at the site of the cancer. The most common side effects of radiotherapy are

- Tiredness.
- Anaemia.
- Skin problems.
- Damage to normal tissues.
- Hair loss in the treatment area.
- Infertility.

Chemotherapy is treatment with anti-cancer drugs to destroy cancer cells. Drugs can be injected intravenously or taken orally. It is a systematic method that can be used to treat cancer anywhere in the body because it circulates throughout the body in the bloodstream. Anti-cancer drugs destroy cancer cells by stopping them from growing or multiplying. The most common side effects of chemotherapy are

- Fatigue
- Damage to body organs
- Lowered resistance to infection
- Reduction in memory and concentration abilities
- Increased risk of getting another type of cancer
- Infertility

All of the cancer treatments mentioned above do not effectively target and kill cancer cells and have lots of long term side effects. With these complications and health problems assiociated with conventional cancer treatments, there is a serious need for a better treatment protocol to treat cancer effectively with fewer side effects. Another alternative method of treating cancer is the photodynamic therapy (PDT).

Recently photodynamic therapy has been utilised as the new cancer treatment for a range of cancers. The concept of photodynamic therapy is the combination of two agents, a photosensitising drug and light. This requires a systemic application of a drug containing a photosensitiser. The drug preferentially attaches itself to a diseased cell and remains at that location for a defined time. Illumination of the photosensitiser using a specific light wavelength leads to a selective tumour damage or destruction as shown in Figure 1.2. In the past, photodynamic therapy is being offered when all other cancer treatments have failed. Now, it is the preferred treatment for certain types of cancer due to its tumour selectivity and low side effects combined with high success rate. Figure 1.3 shows a patient undergoing PDT with red laser irradiated on the skin and Figure 1.4 shows the patient successful treatment results.
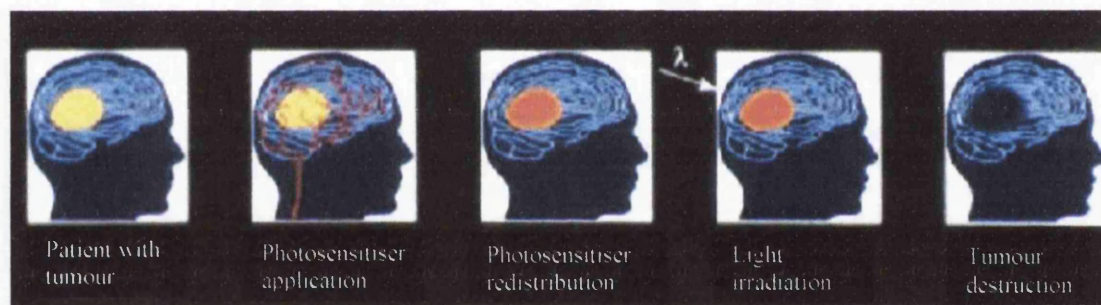
Figure 1.2: Treatment of cancer with photodynamic therapy.[33]
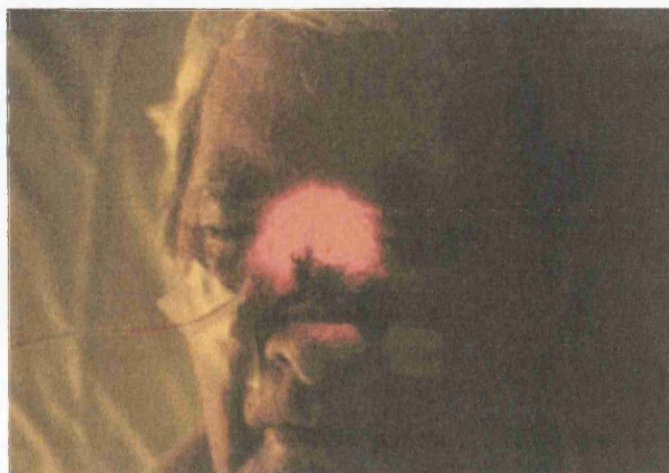
Figure 1.3: A patient undergoing photodynamic therapy treatment.[33]

Figure 1.4: Images of a patient before and after PDT treatment results. [33]

Photodynamic therapy is a technique which holds great promise; however its usage is limited by a number of factors:

I. Following an application of a photosensitiser, the tumour is illuminated by a laser. This illumination is invariably direct line of sight, thereby limiting the treatment to only surface or superficial tumours.

II. Since the laser systems utilised in the PDT are large and expensive, the treatment modality is relatively resource intensive. This includes the need for dedicated treatment rooms reflecting significant capital investment

III. In order to achieve maximum therapeutic benefit, significant drug dosages are utilised. Drugs are applied some time before exposure by laser to allow tumour uptake. The patient is then treated in a relatively short time minimising occupation of the treatment room. A major disadvantage of photodynamic therapy is that the patient develops prolonged photosensitivity to visible light for several weeks following the treatment.

1.1.2 Improvement to Current Treatment

Lasers are currently the most widely used light sources in cutaneous application to treat aged, damaged and cancer cells. In photodynamic therapy, high power laser are used to stimulate photochemical reactions between photosensitiser and oxygen. The laser's monochromatic light permits precise photosensitiser activation at the wavelength of one of its absorption peaks.

Despite these advances, laser systems are still large, expensive, and complicated to operate. Broadband non coherent light sources are typically smaller, safer to use, and less expensive to operate than laser. The development of a non coherent light source that is inexpensive could make PDT recognised as a first choice for cancer treatment. A light emitting diode (LED) device provides the alternative low cost solution for the expensive laser. LED arrays are much smaller and produce low irradiances and can be used to illuminate large tumour area.

The objective of this research is therefore to develop a new method to couple energy to a subcutaneous device that emits the required optical parameters for photodynamic therapy. The proposed device will be embedded into the skin and remotely powered by radio frequency (RF) coupling. The illumination from the subcutaneous LED will activate the photosensitiser for photodynamic therapy leading to consequent destruction of the cancer cells.

This research has two main objectives

I. To develop a computer model that simulates the light distribution of photon energy absorption in tissue and to investigate the photodynamic mechanism.

II. To investigate the RF-tissue interaction and to develop a method to couple energy required into tissue efficiently in order to power the LED device.

6

1.2 PDT Light Device

Although lasers remain good light sources for PDT of localised disease such as superficial basal cell carcinoma cancer, lasers cannot penetrate deeply into the body without causing much surface heating. Laser systems are expensive and complex to use and require a dedicated treatment room. This creates a demand for an efficient and low cost light source for PDT use. In order to meet the demand of medical needs and to improve the PDT treatment, a RF-LED based light device has been proposed.

The ideal RF-LED based light device requirements:

- Small in size, lightweight and implantable.
- Have a LED wavelength matched to the photosensitiser.
- Powered by RF energy coupling from an external source.
- Encapsulated in a biocompatible material.

The PDT light device consists of two main parts
- Light source.
- Power source.

1.2.1 Light source - LED

The benefit of using an implantable LED is that the light source is positioned closely to the tumour thus allowing deep treatment depth whereas laser can only penetrate superficially with most photons being absorbed into the skin before reaching the tumour. The layer of the skin will be intact without the undesirable heating and pigmentation frequently caused by laser. The efficacy of the PDT treatment will increase with only the tumour area being illuminated by LED and leaving the normal tissue unharmed. For this reason, it is reasonable to propose that the use of a low power LED positioned subcutaneously may be significantly more efficient than a higher power external laser that is directed at the surface of the skin. The LED device is much cheaper to manufacture and do not require complex circuitry compared to a laser system.

1.2.2 Power Source - RF Coupling

The LED light source will be powered by an external source through radio frequency coupling, this means that the embedded device does not requires a battery. It is proposed that by using radio frequency, energy can be transferred through multiple layers of tissue without much loss and heating. The benefit of using RF coupling is that the LED can be left in the patient's body indefinitely or until the tumour has been destroyed. The total fluence of light can be controlled and pulsed depending on the patient's need. Patients will have a better treatment modality compared to conventional laser treatment. They are not required to be confined to the treatment room and are able to lead a normal lifestyle. The embedded LED powered and controlled externally by using pulsed or continuous PDT effect. The photosensitiser dosage could be reduced and controlled over a longer duration of photodynamic therapy for increased treatment efficiency. This could benefit the patient by lowering the patient's skin photosensitivity.

The possible benefits of PDT light device:

- Light source can be positioned in the region of interest.
- Controlled dose of photosensitiser.
- Controlled dose of light.
- Higher photodynamic selectivity and damage.
- Enhanced treatment efficacy.
- Improved patient treatment regime.
- Lower cost of treatment.

1.3 Photodynamic Therapy

The medical definition of photodynamic therapy is the treatment of diseased cells by the use of visible or infrared light together with an administered photosensitiser and in the presence of oxygen. Light is absorbed by the photosensitiser, which in turn releases singlet oxygen. The reactive singlet oxygen then causes damage or destruction of the tumour tissue.

1.3.1 Historic Review

In 1903, Von Tappeiner had published experiments on photodynamic therapy in which tumours had been treated with Eosin, a photosensitiser dye, and exposed to visible light.[2] Von Tappeiner showed that PDT was effective for treating skin cancer. Ten years later, Meyer-Betz was the first to demonstrate long-term cutaneous photosensitivity after injecting himself with Hematoporphyrin.[3] Photodynamic therapy was shown to be a promising new modality in the treatment of cancer since the early 1960s. Lipson *et al.* created a photosensitiser drug called Hematoporphyrin Derivative (HPD) that could be localised with some degree of selectivity in tumour tissue.[4] Lipson *et al.* were also the first to use xenon arc lamp to activate HPD in a patient with recurrent breast cancer.[5] HPD was investigated as a diagnostic agent for cancer in which PDT remained an important application during the 1970s. Diamond *et al.* showed that by changing the irradiation conditions, the photodynamic effect could be achieved and the tumour could be photodegraded.[3] Diamond *et al.* also introduced the term photodynamic therapy. In 1974, Dougherty *et al.* showed that PDT was possible using HPD and light in the treatment of malignant tumours with complete effectiveness in animals and in patients.[6,7] Extensive fundamental and clinical research using porfimer sodium as a photosensitiser was carried out for a variety of malignant cancers.

There has been much development in recent years for new photosensitisers that achieve high selectivity in targeting the cancer tissues, thus increasing the efficiency of the treatment. Porfimer sodium under the trade name Photofrin® was the first photosensitiser approved by the United States Food and Drug Administration (FDA)

in 1995 and it is now licensed for use in the treatment of esophageal, lung, gastric, cervical, and bladder cancers. [8] At the same time, there has been increasing research in the development of second generation photosensitisers which are more efficient and more tumours specific.

1.3.2 Treatment Modality

The cytotoxic tumour action of PDT is a two-phase process as shown in Figure 1.5. The first phase is the intravenous injection of the photosensitiser. For systemic photosensitiser, the total patient drug dose is usually based on body weight ($2mgkg^{-1}$ for Photofrin®). After the administration of photosensitiser, the patient's skin and eyes will be very sensitive to sunlight and bright light for at least thirty days and may remain photosensitive for up to ninety days. Before the light exposure, a delay is necessary to allow photosensitiser distribution and partitioning between target cells and normal cells. Photosensitiser clearance from tissues occurs over 40-50 hours, but the tumours retain photosensitiser at a higher concentration for a longer period.[8]
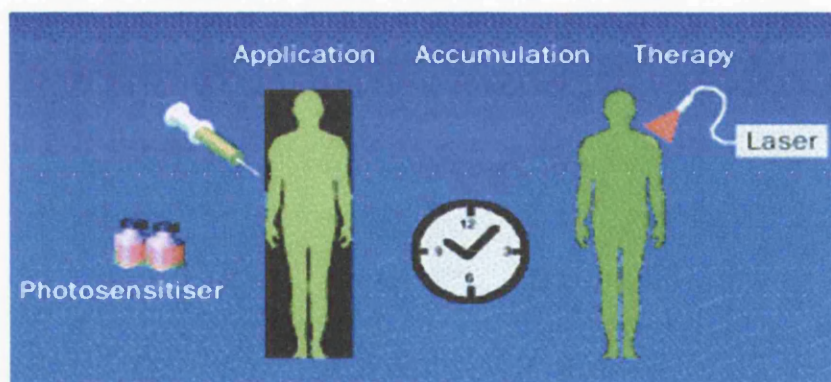
Figure 1.5: Two-phase process of PDT treatment.[9]

The illumination with laser light at 40-50 hours after injection represents the second phase of therapy. A second light application may be given 96-120 hours after injection to ensure all photosensitiser are used completely. The doctor will direct the laser light to its target through a fibre optic endoscope. The fibre optics specially designed to emit laser light are thin, flexible, transparent strands. Treatment times vary substantially and the time is related to the absorption of light by the photosensitiser and the efficiency of light energy transfer to oxygen. A burning

sensation during the irradiation also occurs and can be controlled by local anaesthetics when necessary.[9] The tumour cells death occurs through cellular damage and necrosis during the treatment. Post treatment pain is usually milder and responsive to oral analgesics.

After the treatment, the patients are advised to avoid direct exposure to sunlight and bright light. However they do not have to limit themselves to dark rooms. It is helpful to get some low power indoor light, because the low levels of light will help break down the drug in the body and reduce photosensitivity in the patients. The complete healing of treated area generally occurs within 4 to 8 weeks after treatment. For tumours to be completely destroyed, PDT has been repeated up to two or three times at intervals of 3 weeks to 3 months.[10,11]

There are two common side effects associated with PDT treatment.[8]. First, local swelling and inflammation occurring in and around the treated area may cause physical discomfort including pain in the chest, back, or abdomen and breathing difficulties. The second short term side effect is photosensitivity due to the continued presence of the drug in the skin.

1.3.3 Mechanism of Action

The PDT is a photochemical interaction that is dependent on three most important elements – oxygen, photosensitiser and light source. Photosensitiser has the ability to preferentially accumulate in cancer tissue and much less in normal tissue. Each element is harmless by itself but when the photosensitiser is activated by specific wavelength of light and reacts with oxygen, the end result is singlet oxygen. This singlet oxygen is highly cytotoxic with a short lifetime that can cause damage to the micro vasculatures of tumour.[9] The selectivity of PDT is enhanced by the increased uptake of the photosensitiser by diseased tissue and the confinement of the photosensitiser activation by restricting irradiation to only tumour area.

During PDT, the photosensitiser in the tissue is first excited by light from the ground state to a short lived, higher-energy singlet state followed by a transition to the

reactive triplet state as shown in Figure 1.6.[12] The long lifetime of triplet state enables the photosensiser to react with surrounding molecules to form either singlet oxygen or radical ions. The reactive triplet state can react in two ways as defined by Type I mechanism and Type II mechanism shown in Figure 1.7.[13,14]

The Type I mechanism involves electron transfers between the triplet state sensitiser and cellular substrate to form free radical ions. These free radicals are highly unstable and will react with molecular oxygen to produce reactive oxygen species. The reactive oxygen species produce oxidative damages that are expressed as biological lesions.

The Type II mechanism requires energy transfer between the triple state sensitiser and ground state oxygen to generate singlet oxygen molecules. These singlet oxygen molecules are extremely reactive and will interact with the surrounding cells to induce oxidative damages and cell necrosis. The Type II process predominates in PDT and generates the cytotoxic effect of PDT.[15,16] Under low oxygen concentration conditions, Type I mechanism becomes more dominant than Type II process.[12] Tissue oxygen concentration compared with photosensiser concentration can be a limiting factor for PDT in some conditions.[17]
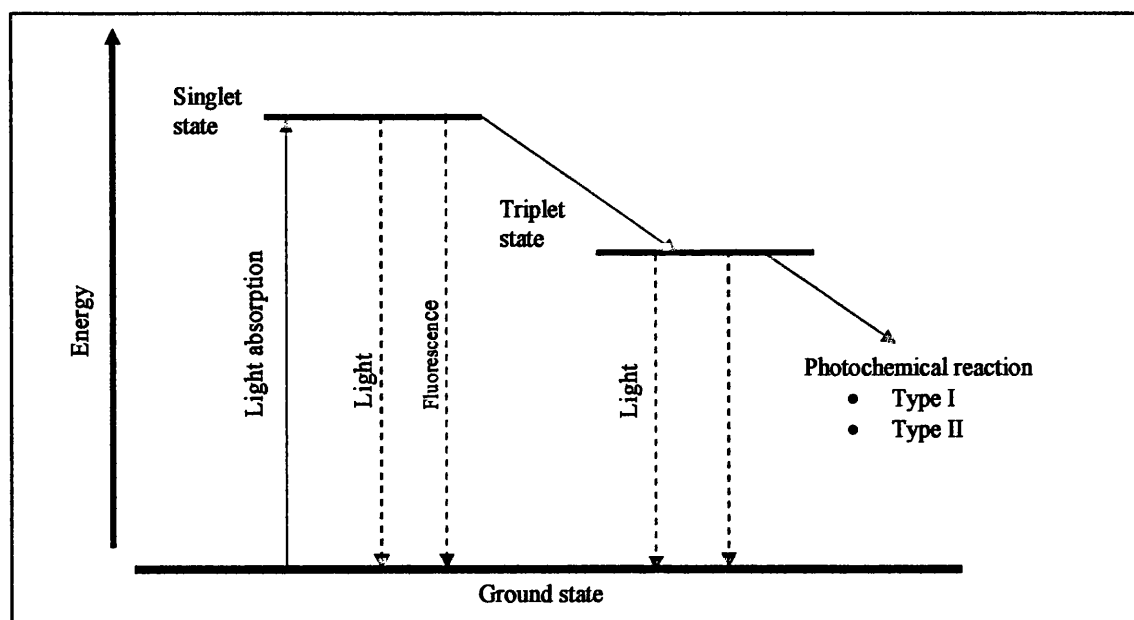
Figure 1.6: Photosensiser activation by light

$$\text{Sensitiser} \xrightarrow{\text{Light}} {}^{1}\text{Sensitiser}*$$

$${}^{1}\text{Sensitiser}* \longrightarrow {}^{3}\text{Sensitiser}*$$

Type I Mechanism

$${}^{3}\text{Sensitiser}* + {}^{3}\text{Sensitiser}* \longrightarrow \text{Sensitiser}^{+\bullet} + \text{Sensitiser}^{-\bullet}$$

$${}^{3}\text{Sensitiser}* + \text{Substrate} \longrightarrow \text{Substrate}^{+\bullet} + \text{Sensitiser}^{-\bullet}$$

$$\text{Sensitiser}^{-\bullet} + O_2(^3\Sigma_g^-) \longrightarrow \text{Sensitiser} + O_2^{-\bullet}$$

$$\text{Substrate}^{-\bullet} + O_2(^3\Sigma_g^-) \longrightarrow \text{Oxidative damage}$$

$$\text{Substrate} + O_2^{-\bullet} \longrightarrow \text{Oxidative damage}$$

Type II Mechanism

$${}^{3}\text{Sensitiser}* + O_2(^3\Sigma_g^-) \longrightarrow \text{Sensitiser} + O_2(^1\Delta_g)$$

$$O_2(^1\Delta_g) + \text{Substrate} \longrightarrow \text{Oxidative damage}$$

* is the excited state, • is the radical state

Figure 1.7: PDT mechanism of action (Type I and Type II).

1.3.4 Light Sources

Although LED arrays are currently the most widely used PDT light sources, their usage in PDT differs fundamentally from that in other cutaneous laser applications. In PDT, lasers are used for photochemical reactions between photosensitiser and oxygen, while the clinical effects of laser are the result of photothermal interactions between the photons and chromophores present in the skin. For the photothermal interactions, the principle of selective photothermolysis applies which is dependent on laser wavelength and pulse duration.[18] For PDT, photosensitiser dose and total light fluence are the important variables determining the treatment efficacy. However, lasers are absolutely required for selective photothermolysis, whereas PDT can be carried out with laser and also with non-coherent broadband light sources.

Lasers have become the standard source for PDT application because they can be efficiently coupled to flexible fibre optics to allow access to internal tissues and their monochromatic property allows precise and efficient photosensitiser activation at its absorption peak. Another relative advantageous of laser is their ability to deliver high irradiances at specific wavelength, thereby minimising overall treatment times. However, this is not necessary in PDT because low fluence rate can cause more damage than high fluence rate for the same total fluence.[19] At high fluence rate, the amount of damage may reach a threshold and fractionation of the light delivery appears to increase the amount of damage produced by a given fluence.[20] This is because for a higher fluence rate, the tissue oxygen concentration is rapidly depleted without recovery, thereby quenching the reaction.[21] Fractionation of light with short pulse duration was shown to be more effective for PDT than continuous wave light.[22] This is due to short period of oxygen recovery during the dark interval resulting in more singlet oxygen production. Sterenborg and Van Gemert suggested that at irradiances several-times higher than the photosensitiser saturation level, PDT effects depend only on the actual photosensitiser tissue concentration and not on the local irradiance.[23]

The broadband non-coherent light sources are typically smaller, easier to use and less expensive to acquire than laser system. These include xenon arc lamps, flash lamps and fluorescent tubes. The advantageous of these sources are the capability for irradiating a large treatment area and photosensitiser activation at multiple wavelengths for drugs that exhibit several absorption peaks. Light exposure can sometimes generate active photoproducts with absorption peaks that are different from the parent photosensitiser. Some of these photoproducts can be triggered to enhance the overall PDT effect.[23]

The development of alternative non-coherent light sources that are inexpensive and light weight will undoubtedly make PDT more practical for routine daily use. Current high intensity LED arrays system available are portable, produce high irradiance ($>10Wcm^{-2}$) within a narrow band ($\pm10nm$) and represent a technology that is much less expensive than laser system.

For most photosensitisers that have multiple absorption peaks, the effective treatment depth of PDT is determined by the tissue penetration of the activating wavelength of light used. To achieve deep photodynamic effect, photosensitisers with high absorption at longer wavelengths are desirable when treating tumours. Above 750nm wavelength, PDT efficiency is limited because the photon energy may be insufficient to drive photochemical reactions.[24] In contrast, shorter wavelengths are preferable for superficial photodynamic effect or when deep photodynamic effects are not needed.

1.3.5 Photosensitisers

Photosensitisers are compounds that are capable of absorbing light of specific wavelength and transforming it into functional energy for the production of reactive agents. Most photosensitisers are administered systemically and some are applied topically in the treatment of skin cancer. There are hundreds of natural and synthetic dyes that can function as photosensitisers for PDT, ranging from plant abstracts to complex synthetic macrocycles. The important attribute of any photosensitiser is the ability to selectively accumulate in cancer cells and generate enough cytotoxic agents to cause destruction of cells.

There are a number of photosensitiser agents available today for PDT with the most commonly used being the porfimer sodium and protoporphyrin. These photosensitisers are the first generation photosensitisers approved by the regulatory authorities and are marketed with the name Photofin® (Axcan Pharma Inc.) and Levulan® (Dusa Pharmaceuticals Inc.) respectively.

Photofrin® or porfimer sodium (Figure 1.8) has been accepted in the clinic in several countries for the treatment of early and late stage lung cancer, superficial and advanced oesophageal cancer, bladder cancer, superficial and early-stage gastric cancers, early stage cervical cancer and cervical dysplasia.[14] In addition, porfimer sodium is being investigated in clinical trials with promising results for conditions such as cancers of the head and neck, brain, intestine, lung, breast and skin.

With the success of porfimer sodium to treat oesophagus and lung cancer, the first generation photosensitiser still has a few disadvantages. Although porfimer sodium has a range of absorption wavelength (400-650nm), the 630nm wavelength is used clinically for tumour treatment because of its deeper tissue penetration, but the absorption band at this wavelength is the weakest, therefore the depth of effect is limited to 0.5 cm.[9] The other disadvantage is that porfimer sodium is retained by the cutaneous tissue and induces skin photosensitivity that lasts for 4 to 6 weeks.[25] Photosensitivity appears to be dose dependent according to preliminary clinical studies.[26,27] Hence, patients are required to avoid sunlight and bright artificial light for the duration of photosensitivity. These problems of prolonged photosensitivity, limited light penetration into tissue and the 48 hours delay required between drug infusion and light treatment associated with the photosensitiser have been addressed partly by the development of second generation photosensitisers.
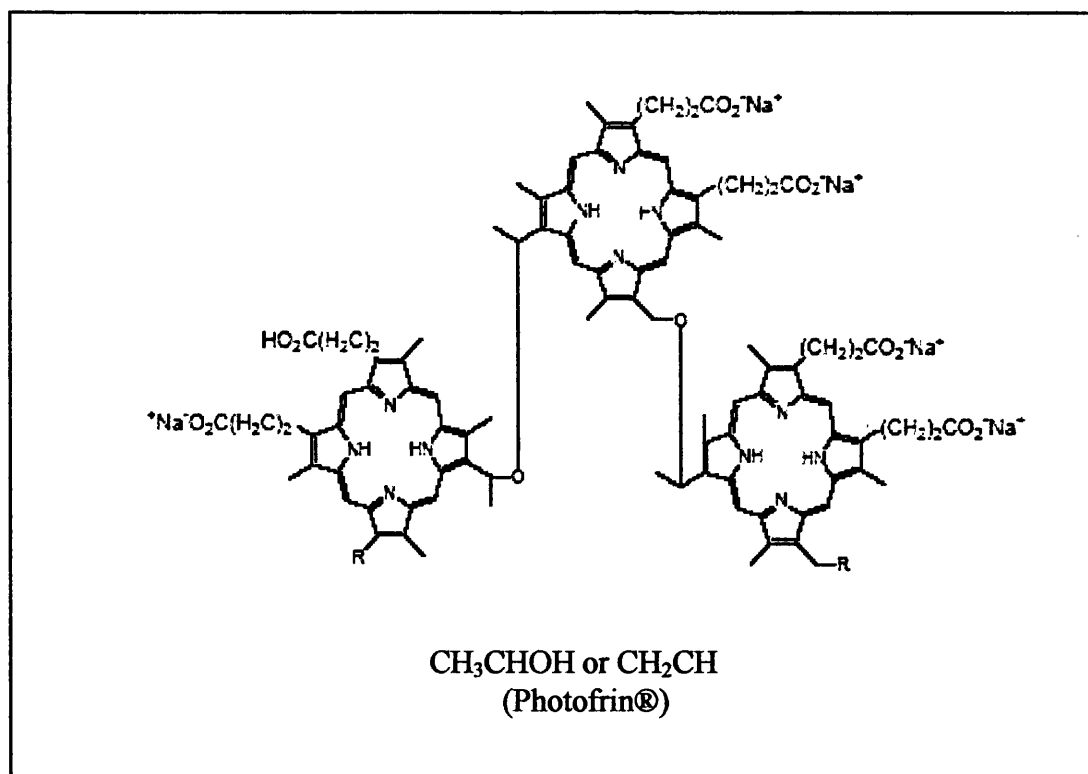
Figure 1.8: Schematic structure for Photofrin®. [14]

Levulan® or 5-aminolevulinic acid (Figure 1.9) is a naturally occurring molecule present in the human cells, and to date it has received approval only for a non-malignant disorder, actinic keratosis. The ALA is not a photosensitiser by itself, but the ALA is converted to protoporphyrin IX, a photosensitiser with photodynamic activity. The administration of ALA is by a topical route and can be activated by many light sources. The optimal wavelength for the in vivo photodynamic activation of protoporphyrin IX has been shown instances with hamsters to be 635 nm.[28] It is used mainly for cutaneous lesions such as basal-cell carcinoma due to its limited penetration depth.[10]

The ALA has been actively used in dermatology and currently exhibits the best topical efficacy of any PDT drugs. Its smaller molecular size renders it more permeable across the skin than porphyrins. The concentrations of ALA used in topical applications are 5% to 20%. Also, localised photosensitivity occurs after treatment and the patients must avoid sunlight to treatment sites. While the absence of systemic photosensitivity is a definite advantage in topical application, cutaneous ALA penetration can be highly variable from one patient to another.[29]

NH₂CH₂COCH₂CH₂CO₂H
(5-Aminolevulinic Acid)
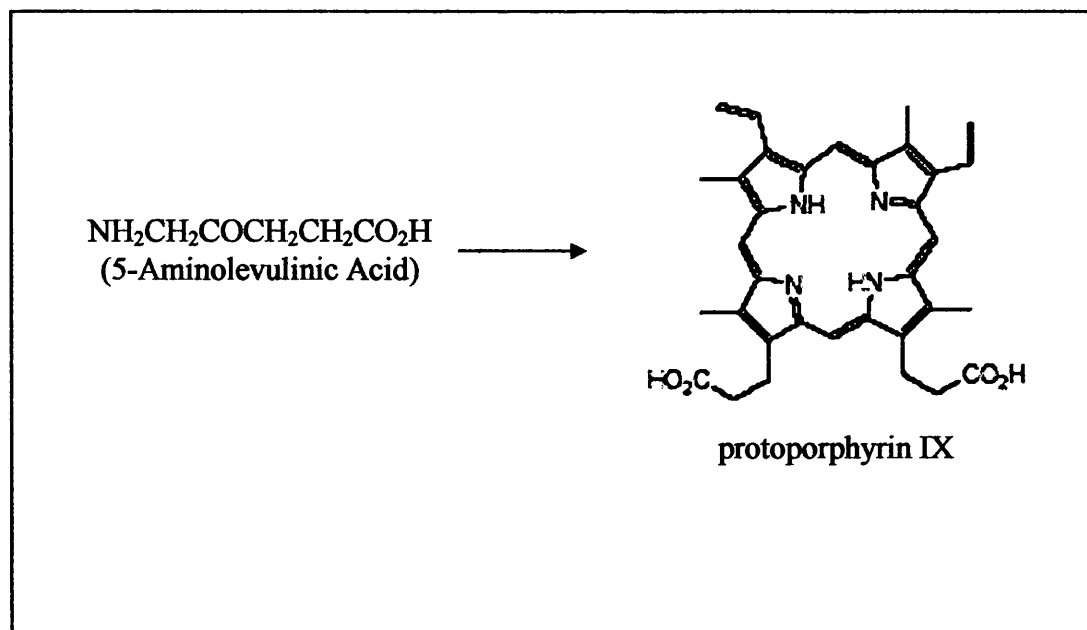
protoporphyrin IX

Figure 1.9: Schematic structure and conversion of ALA to protoporhyrin IX [14]

Although the first generation photosensitisers are widely used for PDT treatment, there are a few disadvantages associated with them. The first of the disadvantages is that the photosensitisers are not selective enough and remains in normal tissue for several weeks thus causing prolonged photosensitivity. Secondly, the absorptions of light at 630nm of the photosensitisers are the weakest. Hence, the low energy absorptions require higher photosensitiser doses and higher light doses if adequate level of excited photosensitiser is to be generated.

The development of second generation photosensitisers should have reduced the photosensitivity duration, longer activation wavelengths and therefore increased depth of penetration, higher damage by singlet oxygen, and better tumour selectivity. The photosensitiser groups that have been most actively investigated are Temoporfin, Texaphyrins, Tin-Etiopurpurins, and Phthalocyanines. These second generation photosensitisers have absorption bands between 640nm and 750 nm, being administered systemically and induced cutaneous photosensitivity for 5 to 10 days only.

Temoporfin or metatetraphyroxphenylchlorin (m-THPC) under the tradename Foscan® (Biolitec Pharma Ltd.) is a very potent photosensitiser in current development. This photosensitiser is one of the most cytotoxic of all the second-generation photosensitiser with a quantum yield of singlet oxygen of about 0.87 and with a residual photosensitivity up to two weeks.[9] It has been used for curative, palliative or adjuvant treatments of head and neck cancers.[30,31] It requires very low drug doses (0.15mgkg^{-1}) as well as very low light dose (20 Jcm^{-2}) making it 100 times more reactive than Photofrin®, which requires high drug dose (2-5 mgkg^{-1}) and high light dose (100-200 Jcm^{-2}).[14] In 2001, Foscan® has been approved in the Europe Union, as a local therapy for the palliative treatment of patients with advanced head and neck cancer who have failed prior therapies and are unsuitable for radiotherapy, surgery or chemotherapy. Foscan® is also on clinical trials for late stages oesophageal cancer and dysplasia in Barrett's oesophagus. In addition, topical formulations of temoporfin are being developed to compete with ALA against skin cancers and other dermatological conditions.[14]

The successes of Photofrin® and other second-generation photosensitiser have created a huge growth in treatment of cancer with PDT. Another photosensitiser drug currently under investigation is Hypericin. Hypericin is well documented as having photodynamic activity as it causes photo poisoning in animals that consume large quantities of plants containing this compound, often leading to skin irritation, fever and even death.[32] Hypericin which absorbs light at 590nm, is currently on phase I clinical trial studies for the treatment of psoriasis, warts and skin cancer.

At present, the pharmaceutical industry is investigating new types of chromophore that can produce a photodynamic effect upon illumination and therefore will have the possibility in the future of treating many types of cancer with greater efficacy.

CHAPTER 2   LIGHT-TISSUE INTERACTIONS

2.1 Light Transport in Tissue

As the application of lasers and LEDs in medical field becomes increasingly important, an understanding of light interaction with the biological tissue is essential. The interaction of light and tissue depends on the characteristics of the light source and the target tissue. The distribution of photons in the tissue is basis for photochemical therapy or photothermal therapy. Three interactions take place when the light enters upon biological tissue, it can be subject to reflection, scattering, and absorption through the material. Tissue is a scattering and absorbing medium which has a higher refractive index than air. A portion of light will undergo reflection at the surface of the skin while the remainder will interact in some way with the tissue. The light penetrates the tissue and goes through multiple scattering and absorption events. Scattering events occur when there is a change in the propagation distribution of incident light. Absorption events occur when the photon transfers its energy to an atom or a molecule known as a chromophore. Chromophores are substrates in the tissue that absorb the light and exhibit multiple bands of absorption at specific wavelengths.

2.1.1 Light Scattering

As light strikes the skin surface, about 5% of light reflected from skin is scattered light because of the sudden change in refractive index between air and stratum corneum.[34] When the remaining 95% of the light propagates into the tissue, it encounters multiple scattering and absorption events. The path of direction of light propagation changes because of the complex geometry of bio molecules and the inhomogeneous distribution of tissues in human body.[35] A small momentum is imparted by scattering and the photon continues along its way in different direction until it has been absorbed or back-scattered out of the tissue. In a highly scattering tissue, a large proportion of the photons are back-scattered out of the tissue, which depends on the wavelength. The size of the molecules or particles in the tissue

20

relative to the wavelength of incident light determines the spatial distribution and intensity of the scattered light.

For particles which are much smaller than the wavelength of light, Rayleigh scattering theory applies where scattering dominates at longer wavelength.[36] The scattering is weak, nearly isotropic and varies inversely with the fourth power of the wavelength

Mie scattering theory applies when the particle size is comparable to or larger than the incident wavelength. [37] The scattered particle is rather wavelength independent and is highly forward directed. Mie scattering tends to dominate over Rayleigh scattering in the band of wavelengths commonly used in the laser therapy. At longer wavelength, Rayleigh scattering becomes more dominant as the wavelength is increasingly larger than the particles size.

The distribution of scattering events is determined by an isotropic component and the phase function. The variation from isotropic scattering is given by the anisotropy factor.

2.1.1.1 Phase Function

In order to determine the angular distribution of scattered light, the phase function of scattering is used. The direction in which a photon will scatter in each event depends on an angle obtained from a phase function. The phase function represents the product of the tissue's albedo and the probability density function that a photon moving from one direction will be scattered into the different direction. The albedo is defined as the ratio of scattering coefficient to the total attenuation coefficients. It is assumed that the scattering depends only on the angle between unit vector directions s and s'. The scattering probability phase function p(s,s') can be written as

$$p(s,s') = p(\theta) \qquad \text{(Eq. 2.1)}$$

21

If the scattering is isotropic, then the phase function becomes a constant.

$$p(\theta) = \frac{1}{2\pi} \qquad \text{(Eq. 2.2)}$$

The majority of the scattering occurring in tissue is in the forward direction as light scattering in tissue is not isotropic. The Henyey-Greenstein phase function is used to represent forward scattering in tissues because it provides a reasonable approximation of scattering in the visible wavelengths.[39,40,41]

The Henyey-Greenstein phase function is defined by [39]

$$p(\theta) = \frac{1-g^2}{(1+g^2-2g\cos\theta)^{3/2}} \qquad \text{(Eq. 2.3)}$$

In a highly scattering medium, a substantial amount of light is back-scattered out to the tissue surface. The back-scattered light could either leave the tissue and be transmitted into the air or totally internally reflected. The refractive index of the medium determines the critical angle. The back-scattered light that exceeds the critical angle will undergo total internal reflection.

The critical angle is given by [40]

$$\theta_c = \sin^{-1}\left[\frac{n_1}{n_2}\right] \qquad \text{(Eq. 2.4)}$$

The type of tissue, wavelength and temperature changes affect the angle of incidence at the surface of tissue. It has been discovered that as much as 75% of incident beam may be reflected out of the tissue due to back-scattering.[34,42]

2.1.1.2 Anisotropy Factor

The anisotropy factor is used to determine the diffusion pattern of the light as it penetrates the skin. This parameter represents the mean cosine of the scattering angle.

The anisotropy factor, g, is defined by [40]

$$g = \int_{-1}^{+1} p(\mu)\, d\mu = \cos(\theta) \qquad \text{(Eq. 2.5)}$$

where θ is the scattering angle

$p(\mu)$ is the probability density function

The quantity of 'g' characterise the angular distribution of beam scattering.

when $g = -1$ light is entirely backscatter

$g = 0$ light is isotropic scatter

$g = +1$ light is purely forward scatter

Isotropic Scattering

When $g = 0$ $p(\theta) = $ constant
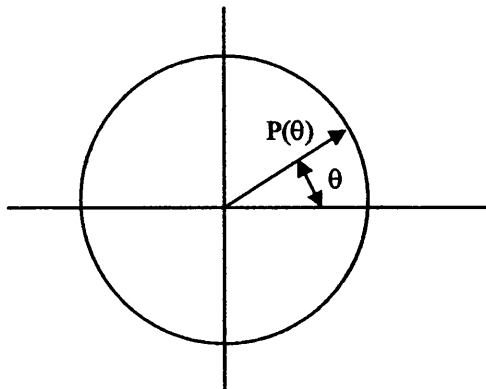
Slightly Forward Scattering

When $g = 1/6$ $p(\theta) = \text{constant} [1 + 3g \cos \theta]$
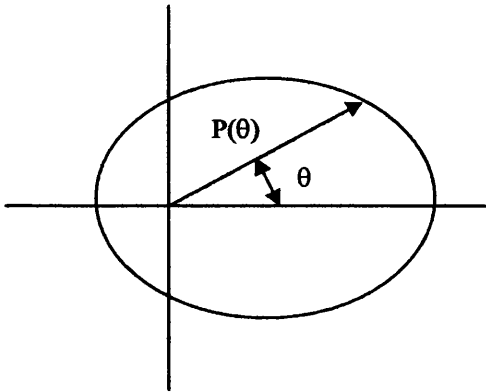
Forward Scattering

When $g = 0.78$ $p(\theta) = \dfrac{1 - g^2}{(1 + g^2 - 2g \cos \theta)^{3/2}}$
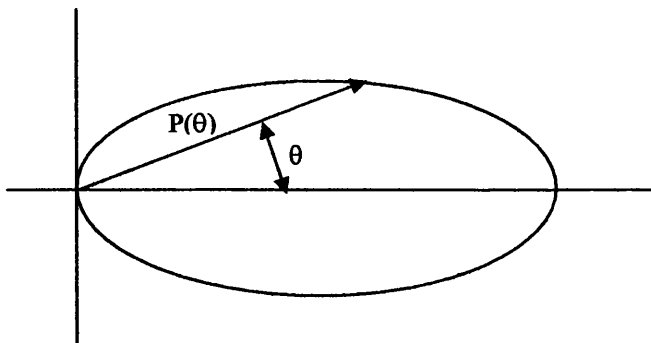
Van Gemert et al had derived a simple formula that is used to calculate 'g' value for highly scattering non-vascular layers of the skin.[38]

$$g \approx (\lambda \times 0.29 \times 10^{-3}) + 0.62 \qquad \text{(Eq. 2.6)}$$

2.1.2 Light Absorption

Another process of laser tissue interaction that occurs in the tissue is the photon absorption. Light energy is absorbed when the incident light excites a molecular resonance. Once it is absorbed, the photon energy is transferred to the chromophore and the photon ceases to exist. The chromophore becomes excited and may trigger photochemical, photothermal or photomechanical reaction. The probability that the reaction will occur depends on the total light dose and the light intensity.

The absorption spectrum of the major skin chromophores dictates most of the laser tissue interactions in the medical field. Human skin has distinctive cell structures that have different absorption spectra. The skin is a highly water based structure which comprises of 60% to 70% water and 30% to 40% organic molecules.[43] This heterogeneity allows the selectivity of target choromophores for selective photothermolysis or selective photochemical to work. The primary target chromosphores for the skin in the visible wavelengths range are the melanin and the haemoglobin. Figure 2.1 shows a three dimensional view of the human skin and its three main layers: the epidermis, the dermis and the hypodermis.
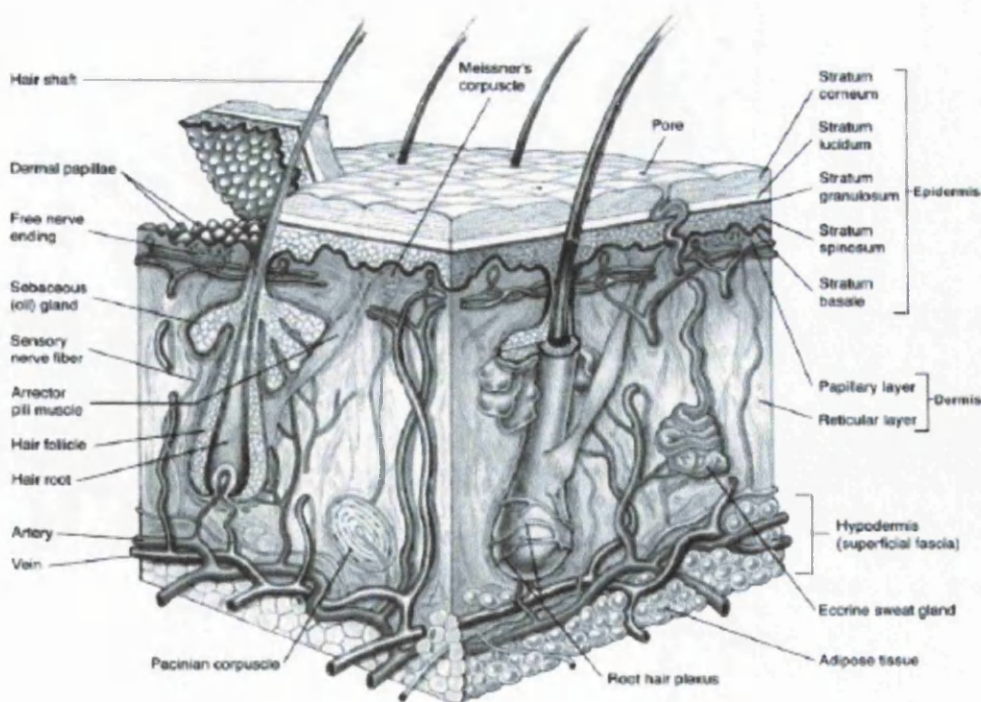
Figure 2.1: Three dimensional view of the human skin.[104]

2.1.2.1 Tissue Chromophores

Water exhibits strong absorption for far-ultraviolet region of wavelength below 200nm and in the far-infrared region of wavelength above 1200nm as shown in Figure 2.2. The advantageous of this spectra is that light energy only penetrates about 30μm into the surface of the skin if a 10.6μm wavelength CO_2 laser is used and is therefore excellent for skin resurfacing.[44] At 1200nm and above wavelengths, the optical properties of tissue are assumed to be similar to the optical properties of water.
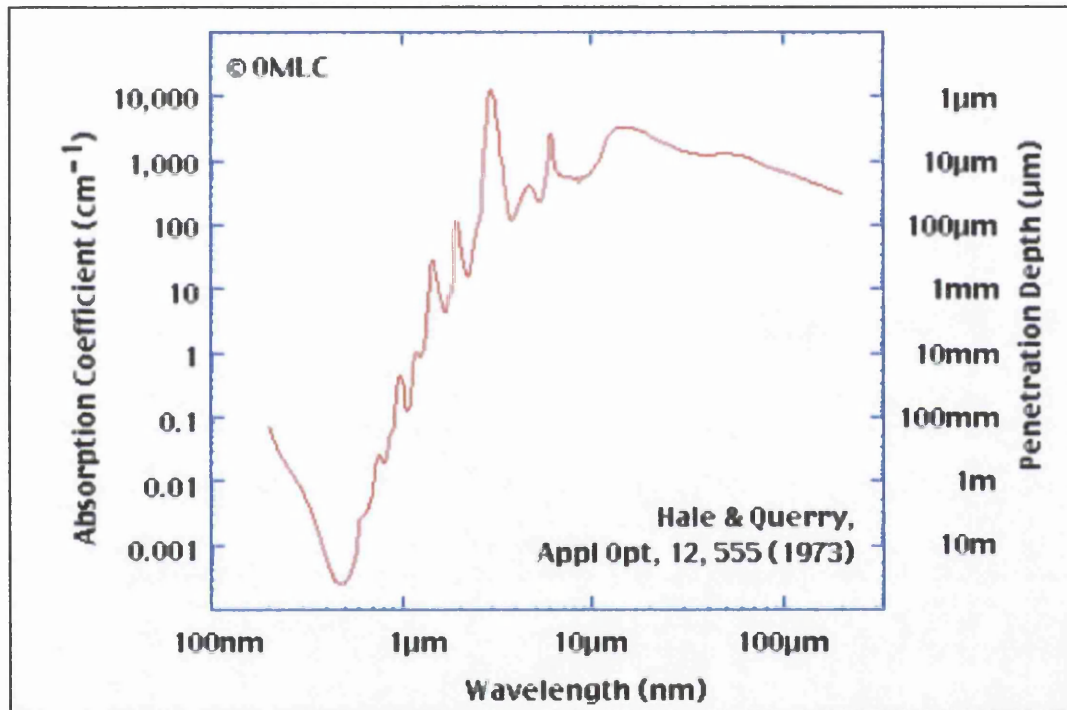
Figure 2.2: Absorption spectrum of water from 200nm to 200μm wavelengths [58,59]

Absorption by melanin dominates the epidermal optical properties for wavelength of 250nm to 1200nm (see Figure 2.3). At a far-ultraviolet region, melanin absorption is greater due to its role as a skin protector against ultraviolet sunlight damage from sunlight.[45] Melanin absorption is also dependent on the type of skin. For fairer skin, the transmission of light increases steadily from about 50% at 400nm to 90% at 1200nm while dark skin transmit light less 20% throughout the visible spectrum and rises to 90% at 1200nm.[46]

In contrast, the blood absorption is dominated by absorption of oxygenated haemoglobin and absorption of deoxygenated state haemoglobin (see Figure 2.4). Oxyhaemoglobin exhibits strong absorption at 420nm and 577nm while haemoglobin has an absorption peak at 560nm.[47]. Despite the high absorption of oxyhaemoglobin in the 420nm, limited penetration and high absorption of melanin make this region not suitable for use. The 577nm was selected for targeting superficial microvessels by selective photothermolysis because it is strongly absorbed by the blood.[48] Another wavelength chosen for selectively targeting large blood vessels is the 585nm because the depth of penetration is higher than the 577nm.[49] Beyond 600nm, absorptions by oxyhaemoglobin and haemoglobin are negligible.
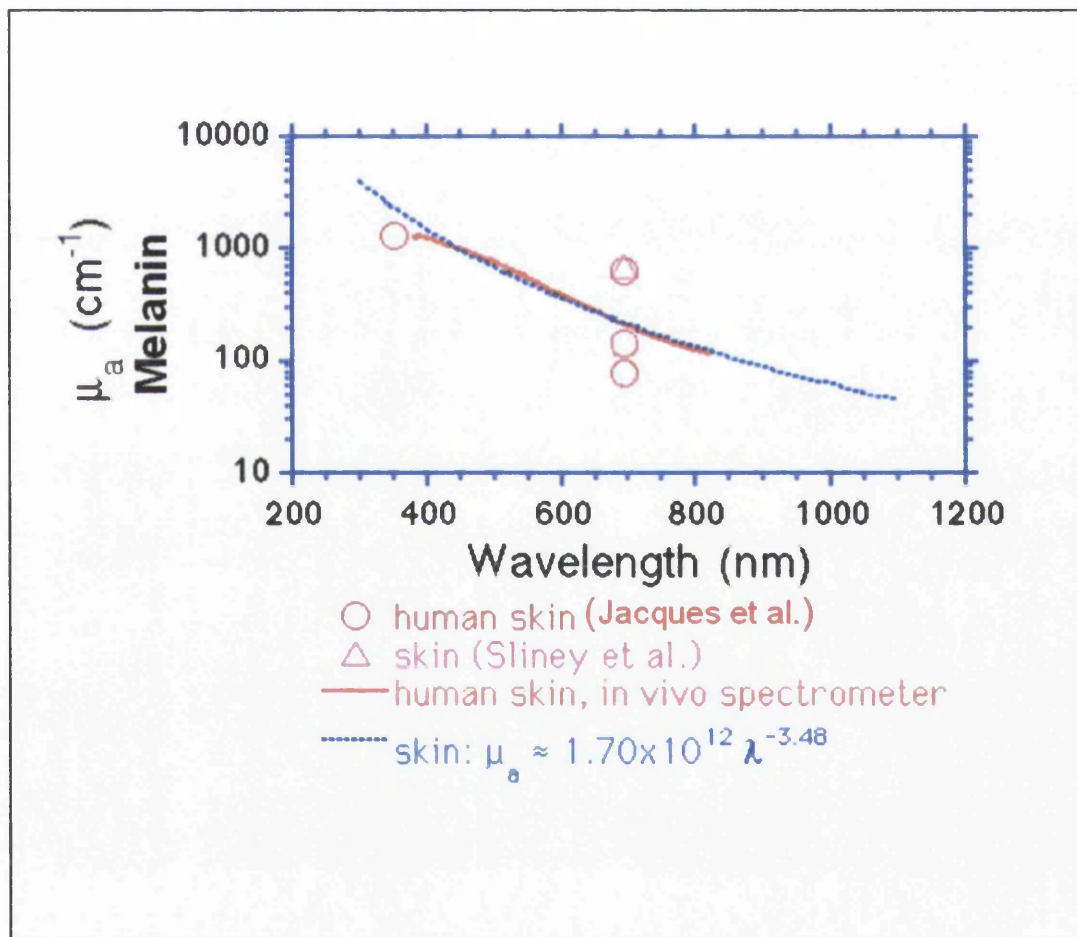
Figure 2.3: Absorption spectrum of melanin in the human skin [60,61,62]
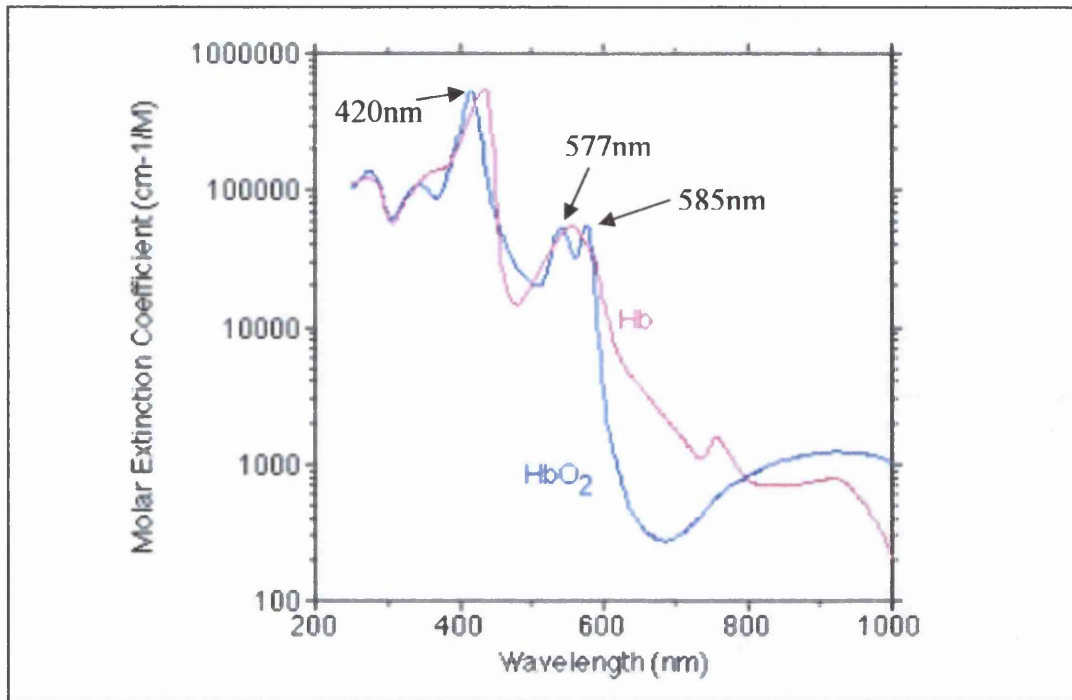
Figure 2.4: Absorption spectrums of oxyhaemoglobin (HbO$_2$) and haemoglobin (Hb) [63]

2.1.2.2 Absorption and Scattering Coefficient

A metric is defined for each of the scattering and absorption events namely absorption and scattering coefficient respectively. These coefficients represent the optical properties for various types of tissue.

The absorption coefficient, μ_a, is defined as the average number of absorptions per unit path length of photon travelled in the tissue. Similarly, the scattering coefficient μ_s is defined as the average number of scatterings per unit path length of photon travelled in the tissue

In the presence of both absorption and scattering, the total attenuation coefficient μ_t is defined by

$$\mu_t = \mu_a + \mu_s \ (cm^{-1}) \qquad\qquad (Eq.\ 2.7)$$

The mean free path between absorption events is equal to $1/\mu_a$. Similarly, the mean free path between scattering events is equal to $1/\mu_s$.

28

2.1.3 Light Distribution Models

The photon incident on the tissue experiences multiple scattering and absorbing events. In order to describe these light distribution events in the tissue, numerical models are used to provide solutions to the laser-tissue interaction. The numerical models can be divided into two types, deterministic and probabilistic. Deterministic solutions are based on a theoretical model. The most widely used theoretical models are the Lambert-Beer's Law, Radiative Transport Theory and Diffusion Approximation Theory. Probabilistic solutions involve generation of random numbers in order to simulate some random process found in the original problem. The method of using probabilistic solution to simulate the light distribution is called the Monte Carlo method.

2.1.3.1 Lambert-Beer's Law

If absorption dominates scattering $(\mu_a \gg \mu_s)$, the light exhibit exponential attenuation when it is passed through the tissue with increasing depth.[34]

This distinctive decay in intensity is called Lambert-Beer's law which states that the intensity at depth z is given by [34]

$$I(z) = I_0 \exp \left[-(\mu_a + \mu_s)z\right] \qquad \text{(Eq. 2.8)}$$

where I_0 is the intensity of the incident light at z = 0.

The above equation is valid for modelling 1-D geometries. In 2-D modelling, the spatial profile of the laser beam needs to be included. A Gaussian distribution profile is considered with e^{-2} radius of w which the intensity at a point (z,r) is given by [34]

$$I(z,r) = I_o \exp\left[\frac{-2r^2}{w^2} - \left(\mu_a + \mu_s\right)z\right] \qquad \text{(Eq. 2.9)}$$

29

The probability of the photon being either absorbed or scattered at a particular point can be calculated using the albedo method. The albedo is defined as the ratio of absorption or scattering coefficient to the total attenuation coefficients.

The probability of photon absorption is given by:

$$P\ (absorption)\ =\ \frac{\mu_a}{\mu_a + \mu_s} \qquad \text{(Eq. 2.10)}$$

The probability of photon scattering is given by:

$$P\ (scattering)\ =\ \frac{\mu_s}{\mu_a + \mu_s} \qquad \text{(Eq. 2.11)}$$

where μ_a is the absorption coefficient

μ_s is the scattering coefficient

The angle at which the photon is scattered is calculated by using the Henyey-Greenstein phase function.[50]

$$\vartheta\ =\ \frac{\mu_s}{\mu_a + \mu_s}\ \frac{\left(1 - g^2\right)}{\left(1 + g^2 - 2\cos\vartheta\right)^{3/2}} \qquad \text{(Eq. 2.12)}$$

The Lambert-Beer's law is a simple process for estimating the light distribution but gives an inaccurate solution for a highly scattered medium when the scattering coefficient is much larger than absorption coefficient. This method is not suitable for wavelengths between 450nm and 1100nm where light is mostly scattered in the tissue.[51] Hence, the Lambert-Beer's law is suitable for wavelengths below 300nm and above 1500nm where light is strongly absorbed and less scattered in the tissue.[38,52]

2.1.3.2 Radiation Transport Theory

Another numerical method of describing the light distribution in the tissue is the radiative transport theory which is also called the Boltzmann Transport Theory. Chandrasekhar first used the Boltzmann Transport Theory to describe the rate of change in radiance of light as a function of the optical properties of the medium.[53] The Boltzmann Transport Equation is described by [53]

$$(s \cdot \nabla) L(r,s) = -(\mu_a + \mu_s)L(r,s) + \frac{\mu_a + \mu_s}{4\pi} \int_{4\pi} p(s,s')L(r,s')d\omega' \quad \text{(Eq. 2.13)}$$

where $L(r,s)$ is the radiation intensity (watt per area per steradian) at position r in

direction of s

s is the direction unit vector

r is the position unit vector

ω is the solid angle

The first term of the right hand side in the above equation gives the decrease in radiation intensity per unit length $L(r,s)$ by absorption and scattering. The second term gives the increase in the radiation intensity per unit length due to scattering from all other directions. The $L(r,s')d\omega'$ term is the light radiance per unit area in direction s' at a location r confined within solid angle $d\omega'$. The solid angle integration of phase function is defined as [38]

$$\int_{4\pi} p(s,s')d\omega' = 4\pi \frac{\mu_s}{\mu_a + \mu_s} \quad \text{(Eq. 2.14)}$$

The Boltzmann Transport Theory gives a more accurate description than other models but the general solution is not available. This method of analytical solution is only suitable for simple 1-D geometries. In the 2-D and 3-D problems, the numerical solutions are too rigorous mathematically and too complex to be solved analytically which require complex numerical methods. Another type of more simplified numerical solution is the Monte-Carlo method which will be described in Chapter 3.

2.1.3.3 Diffusion Approximation

When scattering becomes dominant over absorption, the intensity of scattered light is much larger than the collimated light in the tissue. The radiance of scattered light can be estimated by using an approximation of the transport equation.[54]. This method assumes that the light is being scattered almost uniformly after encountering multiple scattering events.[34] The diffusion theory is defined mathematically by [34]

$$L(r,s) = \frac{1}{4\pi}\int_{4\pi} L(r,s)d\omega + \frac{3}{4\pi}\int_{4\pi} L(r,s)s \cdot s\, d\omega \qquad \text{(Eq. 2.15)}$$

The first term of the right hand side in the above equation represents the isotropic scattering and the second term represents the forward peak compensation.

The diffusion approximation method is appropriate for dense and highly scattering tissue. Since the method requires diffuse light within the tissue, the diffusion approximation results are not accurate at surface layers and at boundaries. Hence this method is not applicable for thin tissues or tissues with multiple layers of optical properties and complex geometries. Also the accuracy of the results decreases as the anisotropy factor g approaches value of one for highly forward scattering tissue.[55] As a simplified analytical method, it is only suitable for study of light diffusion deep within an optically uniform medium and it is easy to implement for computer simulations.[56] Analytical solutions can be obtained for 1-D geometries but 2-D geometries require a fast computer for numerical processing.[57].

2.1.4 Effects of Light -Tissue Interaction

There are three main types of light tissue interactions namely photochemical, photothermal and photomechanical effects.

Photochemical effects are caused when the photons absorbed trigger off chemical reactions within tissue cells. Low energy light sources are mostly used for photochemical effects. The interaction time is considerable long and may range from minutes to hours. Photochemical effects are applied in the area of phototherapy, photochemotherapy, and photodynamic therapy

Photothermal effects take place when the photons absorbed by the tissue chromophores are converted to heat. The effects range from photothermolysis, photohyperthermia, photocoagulation, photocarbonisation and photovaporisation. The interaction time is short and range from milliseconds to seconds.

Photomechanical effects occur when the photons absorbed induce stress gradients and pressure waves to destroy tissue molecules. Photomechanical causes mechanical destruction of the tissue. The effects range from photoablation and photodisruption. The interaction time is very short. A Q-switched Nd:Yag laser can be used to provide the necessary power in short time for the breakdown of kidney stones in lithotripsy.

This study takes into account low energy interaction only and hence photomechanical interaction is not considered. The following review will concentrate on the photochemical interaction and photothermal interaction.

2.2 Photothermal Interaction

2.2.1 Thermal transport in tissue

When a light source is used to illuminate through the tissues, photons are absorbed by the chromosphore structures in the tissues. Photon energy is transferred into the tissue and the heat is generated through the absorption of light. As soon as heat is created, it begins to dissipate by conduction, radiative transfer and convection. The basic law which apply to photothermal processes is the first law of thermodynamics. Thermodynamics is the application of the conservation energy principle to heat processes. The law states that the amount of energy gained by a closed system equals to the corresponding amount of heat lost by regions inside the closed system as defined by:

$$Q_{produced} + Q_{gained} = Q_{stored} + Q_{lost} + W \qquad \text{(Eq. 2.16)}$$

where $Q_{produced}$ is the energy produced by the body metabolism

$\quad\quad Q_{gained}$ is the energy gained from the external source

$\quad\quad Q_{stored}$ is the energy stored in the body tissue

$\quad\quad Q_{lost}$ is the energy lost through conduction, convection, radiation

$\quad\quad W \quad$ is the rate of work performed by the body

The energy conservation in biological tissue can be represented by the Pennes Bioheat Transfer Equation (BHTE).[64] The BHTE is used to calculate temperature T as a function of time t and distance r from the source in the tissue. The equation is described by [64]

$$\rho c \frac{\partial T(r,t)}{\partial t} = k\nabla^2 T(r,t) - c_b w_b (T - T_a) + Q_m + Q_{ext} \qquad \text{(Eq. 2.17)}$$

where ρ is the density of the tissue $(kg \cdot m^{-3})$

$\quad\quad c$ is the specific heat capacity of tissue $(J \cdot kg^{-1} \cdot K^{-1})$

34

k is the thermal conductivity $(W \cdot m^{-1} \cdot K^{-1})$

Q_m is the rate of metabolic heat production

Q_{ext} is the rate of external heating

c_b is the specific heat capacity of blood $(J \cdot kg^{-1} \cdot K^{-1})$

w_b is the blood perfusion $(kg \cdot m^{-3} \cdot s^{-1})$

The first term $k\nabla^2 T(r,t)$ on the RHS represents the heat conduction in the tissue while the second term $-c_b w_b (T - T_a)$ represents the heat removal by blood in microvasculature. The perfusion term w_b quantity varies with time to account for collapse of the microvasculature perfusion during heating. The value of w_b at any location and time is dependent on the Arrhenius integral.[65] The Arrhenius integral Ω is defined by [65]

$$\Omega(r,t) = \int A_{freq} \exp[\frac{-E_a}{RT(t)}] \, dt \qquad \text{(Eq. 2.18)}$$

where A_{freq} is the frequency factor

E_a is the activation energy

R is the rate constant for gas

T is the temperature

The Arrhenius integral is used to describe the time-temperature behaviour for laser-induced thermal injury in the skin.[66] The Arrhenius intregral states that the rate of denaturation is exponentially related to temperature. Therefore the accumulation of denaturated material increases exponentially with temperature and proportionally to time. As a critical temperature is reached, coagulation occurs. The thermal coagulation of tissue has a sharp, threshold character which account for cell necrosis, haemostasis and burn injuries.

Most human cells can withstand prolonged exposure to $42\,^{\circ}C$. At $45\,^{\circ}C$, cultured human fibroblasts die after about 20 minutes. However, the same cells can withstand more than $100\,^{\circ}C$ if present for only 10^{-3} seconds.[67] For exposure longer than 10^{-3}

seconds at temperature above 42°C as in hyperthermia application, the enzymes and other molecular components are affected and the structure of the membrane is loosened, causing denaturation and irreversible aggregation of macromolecules within the cell. This will lead to cell necrosis or cell death within 24 hours period. Hence, it is not temperature rise but a combination of light energy and exposure time that governs thermal damage. For most cells the critical temperature for necrosis increases by approximately 10°C to 20°C for each decade decrease in the heating time.

Photocoagulation occurs at temperature above 60°C which causes the denaturation of protein. Only a short exposure to high temperature is required and the effects are immediate and visible, such as tissue turning white. Hence it is a more obvious form of thermal injury than hyperthermia.

When the temperature in the tissue equal or exceed 100°C, the cell water starts to boil. The after shock of evaporation of water into steam causes the cell wall to rupture explosively allowing the steam to escape. Once the water has completely evaporated from the cell, complete rupture of tissue, also known as the popcorn effect, is observed.[68] The subsequent debris is rapidly raised to a higher temperature up to 300°C. When the 300°C is reached, there is a further decomposition of the molecules which causes the tissue to turn black and become carbonised. At temperatures over 500°C, the remaining tissue will burn and evaporate.

There are many variables in photothermal interaction that need to be taken into consideration. The key characteristics to obtain the desired photothermolysis or photocoagulation are optimising the laser wavelength, pulse energy and pulse duration parameters.

2.2.2 Laser parameters

2.2.2.1 Wavelength selection

The two primary factors which influence the choice of laser wavelength are the optical penetration depth of light in the skin and absorption of light by the target tissue chromophores. Light must pass through the epidermal and upper dermal regions of the skin to interact with the underlying tissue. In the visible light region of the spectrum, the skin has two main target chromophores; melanin and haemoglobin.

2.2.2.2 Pulse energy

A laser beam output with a Gaussian distribution is assumed to be incident on the skin. The laser irradiance L at point r (Wcm^{-2}) is defined by [34]

$$L(r) = \frac{P}{\pi w_o^2} \exp[-\frac{r^2}{w_o^2}]$$

(Eq. 2.19)

where P is the applied laser power (W)

w_o^2 is the beam radius (cm^2)

The relationship between w_o and the laser w_o is shown in Figure 2.5 and is defined as [34]

$$w_1 = w_o\sqrt{2}$$

(Eq. 2.20)
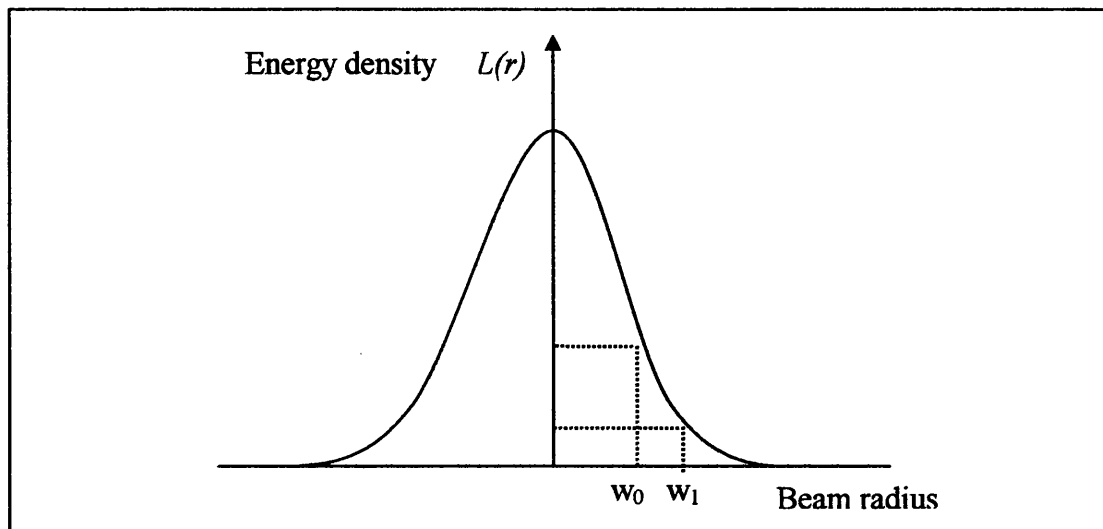
Figure 2.5: Gaussian beam intensity distribution of a laser beam.

The temporal output profile of a laser source is typically trapezoidal as shown in Figure 2.6.
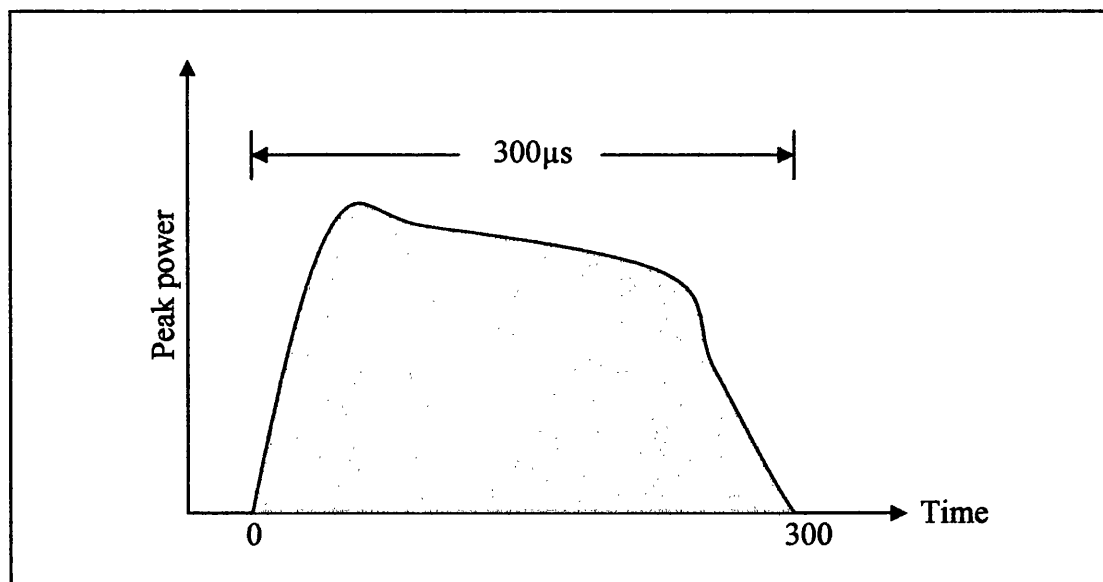
Figure 2.6: Output power against time of a flash lamp pulsed dye laser.[70]

The laser energy E (J) delivered at point *r* is defined by [34]

$$E(r,t) = \int_o^T P \, dt \qquad \text{(Eq. 2.21)}$$

where P is the laser power (W)

t is the laser exposure time (s)

The laser fluence E_t (Jcm^{-2}) is defined by [34]

$$E_t = \frac{4 \cdot E}{\pi w_1^2}$$

(Eq. 2.22)

where E is the laser fluence

πw_1^2 is the area of beam spot size

2.2.2.3 Pulse duration

For maximum effectiveness of the laser pulse, the heat must be confined to the target tissue. In order to limit the thermal damage to the intended target tissue, the pulse duration must be shorter than the thermal relaxation time of the target tissue. The thermal relaxation time is defined as the time necessary for target tissue to cool down by 50% through transfer of its heat to surrounding tissue through thermal diffusion.[69] Table 2.1 shows the thermal relaxation time for different types of target tissue.

Tissue Type	Diameter(μm)	τ
Epidermis	60	2 msec
Basal layer	20	400 μsec
Melanosome	1	0.2 μsec
Erythroctye	5	5 μsec

Table 2.1: Thermal relaxation time for different types of target tissues.

The thermal relaxation time τ for a vessel is defined by [70]

$$\tau = \frac{d^2}{16\alpha}$$ (Eq. 2.23)

where d is the vessel diameter

  α is the thermal diffusivity

For small vessel applications, laser pulses shorter than the thermal relaxation time will generate maximum temperature rise and thermal damage in the vessel. Laser pulses that are equal to the thermal relaxation time will achieve the heat confined to the vessels, which allow a significant site-specific temperature rise and maximum thermal diffusion. Laser pulses longer than the thermal relaxation time will induce non-specific damage to the surrounding tissue through thermal diffusion. Table 2.2 shows the approximate thermal relaxation time for vessels of different diameters.[48]

Diameter (μm)	τ (ms)
10	0.048
20	0.19
50	1.2
100	4.8
200	19.0
300	42.6

Table 2.2: Thermal relaxation time for vessels of different diameters.

If a target tissue can be heated sufficiently to affect it before its surrounding tissue is damaged by thermal diffusion, selective photothermolysis can be achieved.[18,48] Selective photothermolysis is based upon the principle of using laser energy to selectively injure a chromosphore target tissue while leaving the healthy surrounding tissue structures unharmed. The principle is therefore to irradiate the skin with a suitable wavelength light source which only the energy are absorbed in the target tissue and the light are passed through the epidermis and dermis. It is by far the most

precise use of heat in medical application. This selective photothermolysis theory le\d to the development of flash lamp pulsed dye lasers which have been very successful in treating port wine stain and in wrinkles reduction.

Table 2.3 below lists the current laser technology for photothermal application.[70]

Laser Type	Wavelength	Pulse duration	Output
Flash Lamp Pulsed Dye Laser	585nm	200-450 µs	20J/cm^2
Argon Laser	488nm& 511nm	0.1-1 s	3-10W Average power
Copper Vapour Laser	577nm	50ns@10- 15khz	1-5W

Table 2.3: Types of lasers and the light output specifications.

2.3 Photochemical Interaction

Photochemical interaction is applied mostly in the therapeutic medicine. The photochemical effect within the tissue can occur as phototherapy, photochemotherapy and photodynamic therapy. The relationship between three types of photochemical reaction is shown in the following Figure 2.7. Phototherapy is a general term used to describe all cases where light is used therapeutically; photochemotherapy is a subset of it, and photodynamic therapy is a subdivision of it.
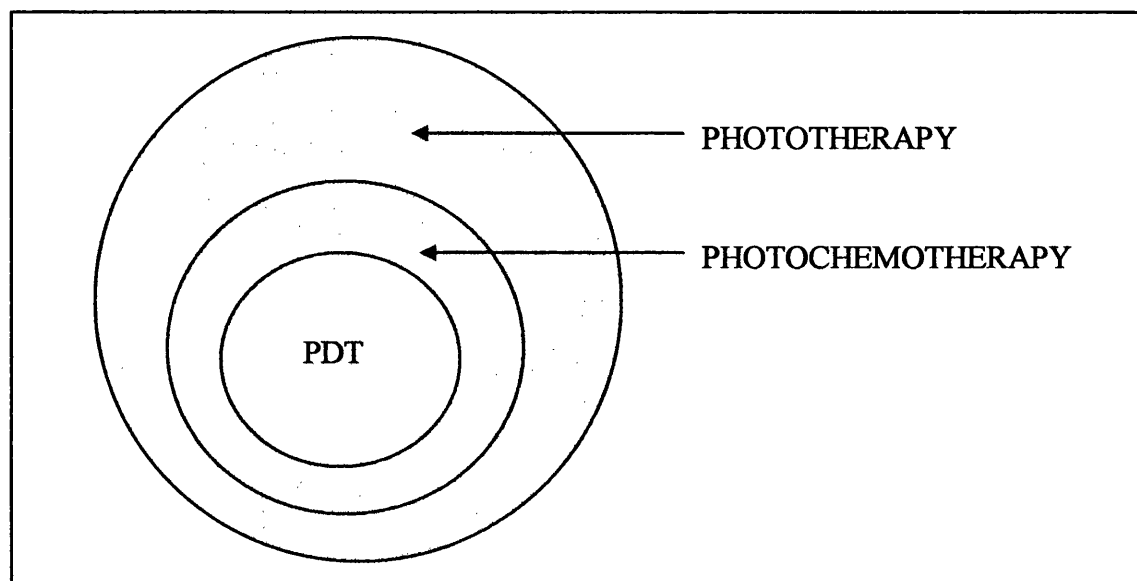
Figure 2.7: Venn diagram of photochemical reaction.

2.3.1 Photochemical Laws

The definitions of each photochemical effect are described as follows: [71]

Phototherapy

The use of ultraviolet, visible, or near infrared light in the treatment of disease. In cases where no photosensitiser is administered the light is absorbed by chromosphores present in the tissue. E.g. photogeneration of collagen.

Photochemotherapy

The use of ultraviolet, visible, or near infrared light together with an administered photosensitiser in the treatment of disease. Light is absorbed by the photosensitiser. E.g. PUVA therapy of psoriasis.

Photodynamic therapy

The treatment of disease by the use of visible or near infrared light together with an administered photosensitiser and in the presence of molecular oxygen at ambient levels. Light is absorbed by the photosensitiser, which then serves to activate oxygen. The activated oxygen then causes damage to the living system.

The three important basic laws which apply to photochemical process are [71]

Law 1 - Grotthus-Draper Law

The Grotthus-Draper Law states that only light which are absorbed by a system can cause a photochemical change. If no photons are absorbed, no photochemical reaction can occur.

Law 2 - Stark-Einstein Law

The Stark-Einstein Law states that the absorption of one photon excites one substrate molecule in the initial excitation step of a photochemical reaction. The quantum yield cannot be greater than 1.

Law 3 – Bunsen-Roscoe Law

The Bunsen-Roscoe Law states that the photochemical effect depends on the total dose (intensity x time) and not just the dose rate (intensity).

The main focus of this study is on photodynamic therapy and hence phototherapy and photochemotherapy will not be reviewed here. Photodynamic therapy is a photochemical process that is dependent on the fluence and fluence rate of the light source as well as the oxygen concentration and photosensitiser concentration in the tissue. There are many variables in photodynamic therapy that need to be taken into consideration. Figure 2.8 shows the schematic diagram for the PDT steps. Each step has its own variables and is highly dependent on other process. The two most important parameters that influence the photodynamic therapy results are

- Photosensitiser
- Light
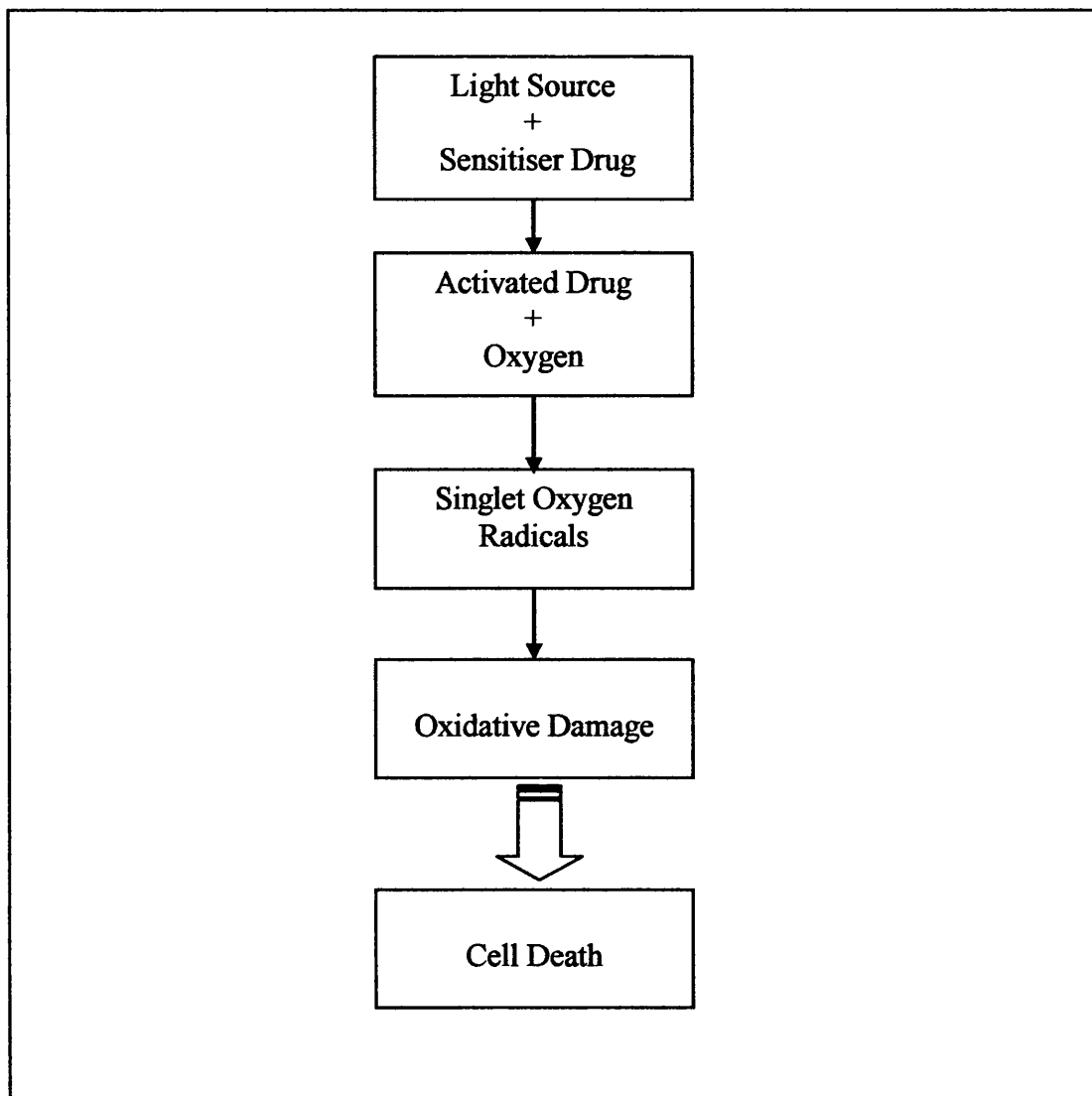
Figure 2.8: Schematic diagrams of photodynamic therapy steps

2.3.2 Photosensitiser parameters

An ideal photosensitiser suitable for PDT should have the following attributes: [71,72]

- Have a strong absorption at a longer wavelength where tissue penetration depth is at a maximum
- Preferentially drug localisation to target tissue
- Have a high quantum yield for efficient singlet-oxygen generation
- Have a minimal dark toxicity and only cytotoxic with light activation
- Rapidly excretion from the body thus inducing a low systemic toxicity

2.3.2.1 Absorption wavelength

The transmission of visible light through human tissue is dependent on the wavelength of the light. At the blue region of the visible spectrum, the absorption and scattering by melanin and oxyhaemoglobin are at their greatest. Both factors are much lessened in the red region of the visible spectrum. For maximum optical penetration depth of light into tissue and efficiently absorption, the photosensitiser needs to have a high absorption band in the region of 650-750nm.

Photofrin® has a high absorption peak in the 400nm-450nm region but it is not suitable for use due to high absorption peak of melanin in the blue region. Hence in order to achieve deep penetration of light into tissue, a wavelength of 630nm is usually used for activation. The absorption of Photofrin® at 630nm is a minimum level, thus requiring a higher dose concentration of photosensitiser. Figure 2.9 shows the absorption spectrum for various types of photosensitisers and Table 2.4 shows the characteristics of photosensitisers currently in clinical application.

Metallophythalocyanines (AlClPc) exhibit very high absorption peaks in the near UV region and the red region. The difference in absorption between AlClPc and melanin is significant in the red region and hence this region is the suitable wavelength choice for photodynamic therapy. Temoporfin (m-TMPC) has the highest absorption peak among the six photosensitisers in the blue region. If an embedded light source is used, the absorption in the melanin could be reduced or ignored, therefore greatly increasing the absorption of the photosensitiser in the blue and red regions. This method will increase the efficiency of singlet-oxygen generation and have a better PDT response. In effect, the photosensitiser dosage and the light dose can be reduced with the increased rate of singlet-oxygen production.

45
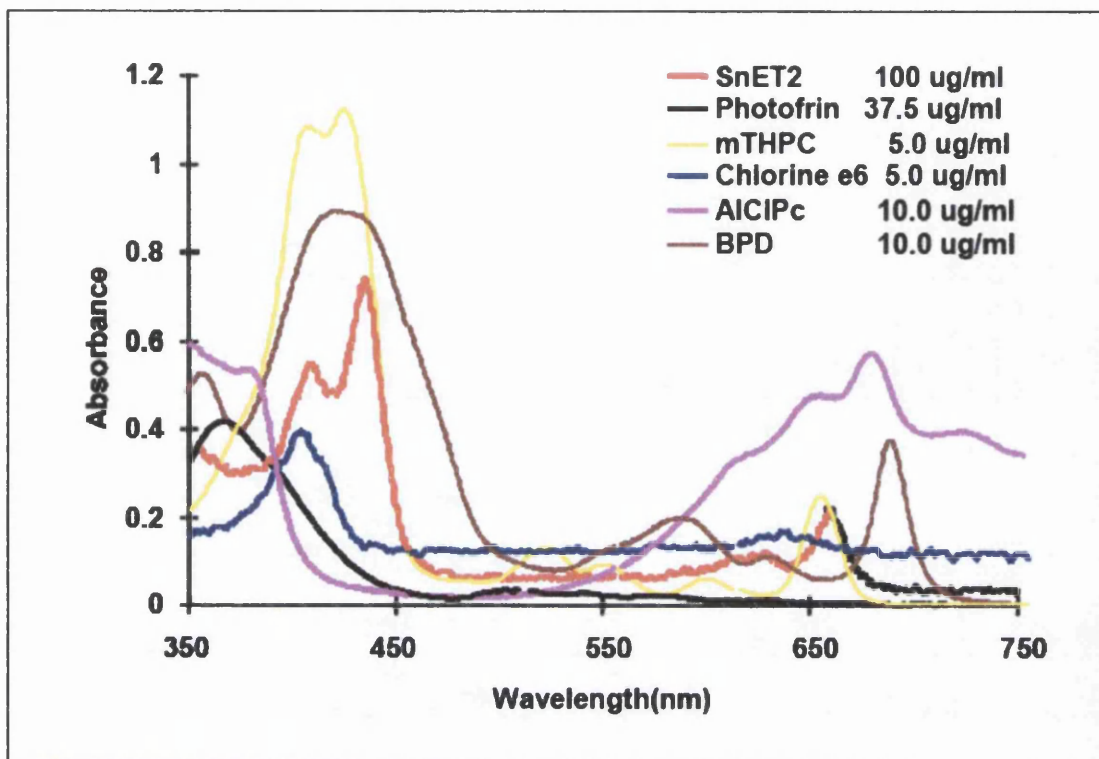
Figure 2.9: Absorption spectrum for various types of photosensitisers [33]

Photosensitiser	Activation wavelength (nm)	Dosage (mg kg^{-1})	Time post-injection
Photofrin®	630	2.0-5.0	24-48h
ALA	635	<30 (intravenous)	not available
Tin etiopurpurin	660	1.0-2.0	24h
Temoporfin (m-THPC)	652	0.1-0.3	24-48h
Texaphyrins	632	0.6-7.2	3-5h

Table 2.4: Characteristics of photosensitisers currently in clinical application [14]

2.3.2.2 Tumour selectivity

There are two main objectives in achieving tumour selectivity.

1) To reduce damage to the normal adjacent tissue, since the area surrounding the tumour will receive some irradiation during photodynamic therapy.

2) To reduce long term general photosensitivity.

The localisation of the photosensitiser is described by its concentration in various tissues with respect to time and location in the biological system. The timing of the administration of photosensitising drug relative to the time of irradiation is the key parameter in determining the localisation and the tumour uptake of the drug. The minimum post-injection time required for maximum tumour uptake of various photosensitisers is listed in Table 2.5. Most photosensitisers are found in high concentration in the metabolically vigorous tissues especially liver, spleen, kidney and lung.

One of the particular considerations is the ratio of photosensitiser in tumour cell with respect to concentrations in all the other tissues at the time of illumination. Secondly, it is desirable that the photosensitiser has zero or very low cytotoxic in the absence of light during the post-injection period. This mean the tumour photodestruction can be efficiently controlled by the light dose for a given drug dose. Table 2.5 shows the ratio of photosensitiser drug uptake into the tumour and surrounding or remote normal tissues.

Species	Drug (route, dose in mgkg⁻¹)	Tumour/normal tissue	(Time)Ratio of uptake
Hamster	Photofrin (i.v., 2.5)	pancreas ca(*in situ*)/ liver pancreas ileum	(3h) 0.3:1 2.3:1 0.8:1
Rat	HPD (i.p., 10)	colon ca (*in situ*)/ colon	(72h) 1.8:1
Rat	Photofrin (5)	bladder lesions(*in situ*)/ bladder hyperplasia non-invasive ca invasive ca	(100h) 1.3:1 2.0:1 3.5:1
Mouse	HPD (i.v., 27)	colon ca (s.c.)/ liver skin	(48h) 0.1:1 1.7:1
Mouse	HPD (i.t., 0.4 mg/ ml tumour)	bladder ca(s.c.)/ liver skin	(3h) (48h) 8.9:1 15:1 101:1 55:1
Man	HPD (i.v., 2.5)	colorectal adenoca(in situ)/ normal mucosa	(3h) 8.2:1
Man	HPD (i.v., 5)	glioblastoma(i.c.)/ BAT region normal brain	(24h) 0.9:1 35:1M
Mouse	mTHPP (i.v., 34)	astrocytoma(i.c.)/ normal brain	(24h) 100:1
Mouse	Various drugs (i.p., 25)	mammary ca(s.c.)/ liver and skin	liver (drug) skin at 24h 0.3:1 Photofrin 2.3:1 1.2:1 3THPP 3.3:1 1.1:1 TPPS4 1.7:1 1.1:1 Chl e6 4.8:1 0.1:1 AlPCTS 1.9:1 0.1:1 AlPC 1.0:1
Mouse	Chl e6 (i.v. 200)	sarcoma of kidney(s.c)/ liver and skin	(48h) 6.3:1

Table 2.5: Ratio of photosensitiser drug uptake into the tumour and surrounding normal tissues [73]

Mouse	AlPCTrS (iv, 10)	colorectal ca (s.c.)/ liver colon skin	(24h) 0.2:1 7.0:1 5.7:1
Rat	AlPCTrS	fibrosarcoma (s.c.)/ skin	(48h) 0.9:1
Rat	AlSPC	colon ca (*in situ*)/ colon	(48h) 2.2:1

Table 2.5 (Continued)

2.3.2.3 Singlet oxygen generation

The photodynamic effect is mediated largely by the generation of singlet excited oxygen. The singlet oxygen is estimated to have a short lifetime $(3-25\mu s)$ and can diffuse about $0.01\,\mu m$.[73] Hence the primary damage can only be initiated in the immediate vicinity where the photosensitiser is located. The photochemical efficiency in which various photosensitisers generate singlet oxygen is the singlet oxygen quantum yield. Since singlet oxygen generation is a key intermediate in photodynamic therapy, the importance of quantum yield of singlet oxygen formation ϕ_Δ must be considered. A value of more than 0.3 for ϕ_Δ is desirable to be used as an effective photosensitiser. Table 2.6 presents the values of quantum yields of singlet oxygen ϕ_Δ and triplet quantum yields ϕ_T for various photosensitiser compounds.

Photosensitiser type	Solvent	ϕ_Δ	ϕ_T
Protoporphyrin dme	PhH	0.57	0.80
Haematoporphyrin	MeOH/H$_2$O	0.65	0.83
Uroporphyrin	H$_2$O	0.52	0.93
m-THPC	MeOH	0.43	0.89
TPP	PhH	0.63	0.67
Photoprotoporphyrin dme	PhH	0.67	0.65
Bacteriochlorophyll a	PhH	0.32	0.32
Porphycene	PhMe	0.30	0.42

Table 2.6: Triplet quantum yields ϕ_T and singlet oxygen quantum yields ϕ_Δ production of various photosensitisers [71]

2.3.2.4 Photobleaching

The term photobleaching refers to the breakdown of photosensitiser as a result from exposure to light irradiance that leads to chemical changes in the photosensitiser. The chemical changes results in small fragments which no longer have significant absorption in the visible region. In an in vitro study, protoporphyrin IX generated from 5-ALA photosensitiser is rapidly photobleached in cells with 70-95% of protoporphyrin IX degradation at light fluences of 40-200 Jcm^{-2} at 630nm.[74] Table 2.7 shows the values of photobleaching quantum yields ϕ_{pb} of four different porphyrins at 25 °C.After a photodynamic therapy treatment, some residual part of the photosensitiser located in the normal tissue would be subject to photobleaching under ambient light conditions, thus reducing the period of photosensitivity.

Types of porphyrin	Photobleaching quantum yields (ϕ_{pb})
Haematoporphyrin	4.7×10^{-5}
Uroporphyrin	2.8×10^{-5}
TPP	9.8×10^{-6}
Photofrin	5.4×10^{-5}

Table 2.7: Photobleaching quantum yields of four different porphyrins [75]

2.3.3 Light parameters

2.3.3.1 Wavelength selection

A basic consideration in the efficacy of PDT treatment is depth of penetration of light through the tissue. In the choice of wavelength for photodynamic therapy use, two factors apply:

1) The exact wavelength selection will depend on the absorption characteristics of the photosensiter drug. The wavelength used should match the peak absorption of the photosensiter for maximum light activation of photosensitiser drug.

2) Light should be able to reach the tumour cell located deep in the tissue and generally longer wavelengths of visible light penetrate tissue more efficiently than shorter wavelengths. There is strong attenuation of light from 400nm up to 580nm largely because of high absorption of melanin and haemoglobin in this region. At 600nm to 680nm, there is a rapid rise in penetration depth due to the low absorption by haemoglobin. The penetration depth increases gradually between 700nm to 800nm.

By taking into the account the above factors, the suitable range of wavelength for photosensitiser selectivity is located in the red region. Therefore 630nm is the preferred choice of wavelength for most PDT applications.

2.3.3.2 Fluence rate

For photodynamic therapy, three important quantities that govern light exposure are total light dose, fluence rate of light source, and exposure time. The relationship between these quantities is as follows: [71]

$$\text{Exposure time(seconds)} = \frac{\text{Total light dose } (J \cdot cm^{-2}) \times 1000}{\text{Fluence rate at treatment site } (J \cdot s^{-1} cm^{-2})} \qquad \text{(Eq. 2.24)}$$

The PDT light dose to be used for treatment depends on the type and dose of photosensitiser. Low fluence rate has been shown in many studies to cause the same damage to tumour cells and highly enhanced the photodynamic efficacy compared to high fluence rate.[76,77,78,79,80,81] One of the reasons is that oxygen concentration in tissues decreases during high fluence PDT which leads to oxygen depletion.[82] Low fluence PDT lowers the rate of oxygen consumption, thus increasing the oxygenated region in the tumour. Oxygen level does not get depleted to the threshold level required for photodynamic actions and the production of singlet oxygen is not interrupted during the low fluence rate treatment. Another reason is that high fluence rate decreases the photodynamic effectiveness by limiting the photodynamic damage.[80] The photodynamic damage may reach saturation point which depends on the photosensitiser concentration. It is possible that, due to the much lower efficacy at saturation fluence levels, photobleaching would prevent administration of a photodynamic dose sufficient for complete tumour kill.[77] Therefore low fluence rate treatments can be as effective as high fluence rate treatments for the irradiation applied over the same period of time.

2.3.3.3 Fractionation of light

Studies have shown that fractionation of light was much more effective in cell killing compared to continuous light applied at the same power density. [76,77,78,83,84] This is because fractionation of light lowers the rate of oxygen consumption and the cell is reoxygenated during the short recovery time which leads to more cytotoxic effect due to greater activation of singlet oxygen. Muller et al have demonstrated that light fractions of only 0.05 s can improve PDT significantly.[85] A theoretical study by Pogue et al suggests that the optimal fractionation time is dependent with the distance between capillaries and cells and varies between 30 seconds and 60 seconds.[86] In addition, some residual tumour cell might be reoxygenated to normal level at 24 hours after first irradiation and recovery of damaged cells occurs at 48 hours later.[87] Fractionation interval of irradiation subsequently 24 hours after first irradiation greatly enhanced the photodynamic effect.

CHAPTER 3   COMPUTER MODEL

In order to understand how light interacts with the tissue, a computer model named TODDY has been developed to simulate the laser-tissue interaction in two dimensions (2-D). The computer model is based on a three-stage process.

For the first stage, a radiation transport solver is used to generate a fluence map of the tissue sample. The fluence map produced shows how light was distributed throughout the tumour site.

In the second stage, a thermal solver is used to produce a time-dependent thermal profile of the irradiated site.

The third stage of the model used a photochemical solver to generate a photodynamic damage profile of the tissue model. The photodynamic damage profile produced an estimate of the damage at every location in the tissue, especially the tumour site.

3.1 Light Transport Algorithm

An analytical solution of transport equation that describes the light distributions in the tissue is not available. Although diffusion approximation theory and Lambert Beer law have been used to calculate light flux distributions in a simplified model, these methods are not suitable to model light transport in the skin with complex geometries and heterogeneous structures. An alternative numerical solution to the transport equation is the probabilistic technique called the Monte-Carlo method.

The Monte-Carlo method involve the generation of random numbers within a predetermined range to simulate various processes that occur in the problem. In laser-tissue problems, the method may be used to randomly select individual photon scattering angles and path lengths. Cashwell and Everett were the first to establish the weighting method in the Monte-Carlo simulation for neutron transport in the field of nuclear reactor.[89] Wilson and Adam reintroduced the weighting method later in 1983 to improve the simulation's efficiency of light transport in the laser-tissue

interaction.[90] This method models the light transport in the tissue by considering the statistical average effect of a very large number of photons.

The advantages of using the Monte Carlo method is that it provides a simple solution to a problem with complex geometries and gives a reasonable accuracy comparable to the general transport theories. It also gives more accurate results near to surfaces and near to the collimated laser beam than the faster diffusion approximation. [91]

3.1.1 Two Dimensional Model

The human skin consists of multiple layers with each layer having different absorption and scattering coefficients. The skin-tumour model is represented by a simple two-dimensional, multi-planar structure which includes epidermis, basal layer, dermis and tumour as shown in Figure 3.1. The light source can be placed outside the skin for surface irradiance or embedded into the skin for subcutaneous irradiance. In this model, there are three assumptions being made. The light is assumed to irradiate perpendicularly incident into the skin thereby reducing the amount of light lost through reflection at the air-skin boundary. Secondly, the optical properties of tissue are assumed to be constant and independent of temperature changes. Thirdly, the tumour contains mostly blood vessels and the blood vessels chromophore is 100% oxyhaemoglobin which is homogeneously distributed in the vessels.
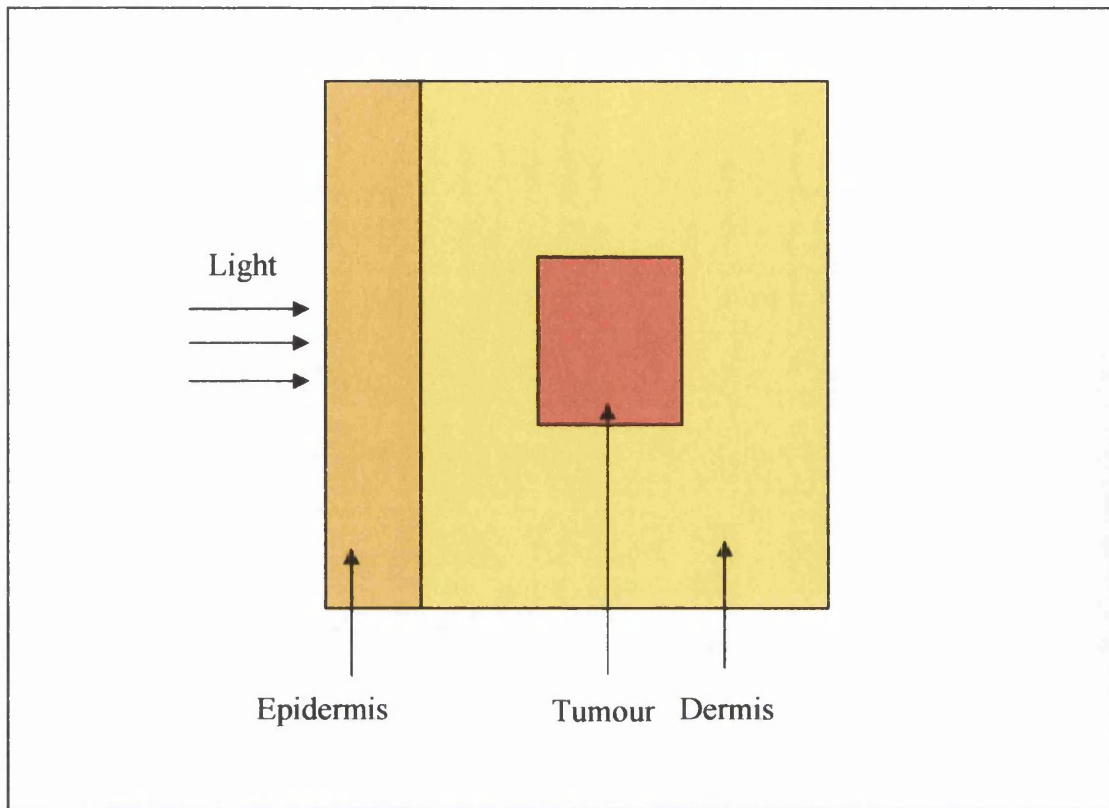
Figure 3.1: Skin-tumour model represented as parallel plane layers.

The skin-tissue model is represented as a two dimensional array of cells which uses a Cartesian grid system with spatial position (x,y) as shown in Figure 3.2. Each cell has its own absorption and scattering coefficient depending on the type of tissue. As the 2-D model is assumed to be infinite in the z direction, the volumetric photon energy is calculated and stored in an array called 'numabs[i][j]' for all values of i and j from 0 to i_{max} and j_{max} where i and j are the values that represent the depth and width of the virtual tissue sample.
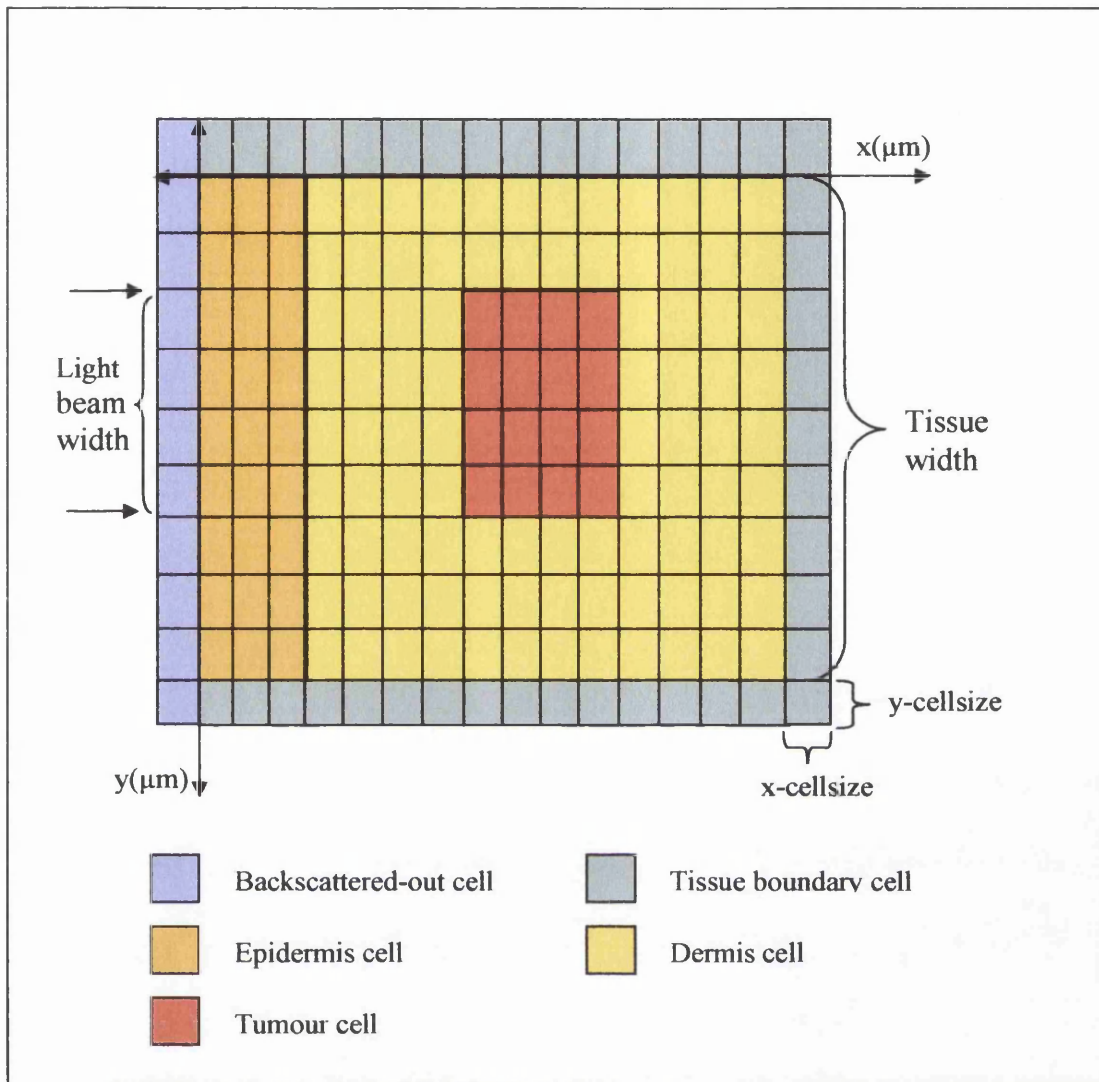
Figure 3.2: Two dimension Cartesian grid system representing the skin-tumour model.

Photons are launched at the skin boundary or at an internal point in the tissue and their paths through the tissue are tracked and recorded. The initial position of photon's launch can be varied to accommodate the starting point of embedded light source. Each photon is initially assigned a weight (W_0) equal to unity. A photon can be scattered or absorbed at each interaction. The probability of this photon being absorbed or scattered is dependent on the albedo as the weighting factor. [56]

The probability of photon absorption is given by: $\dfrac{\mu_a}{\mu_a + \mu_s}$

The probability of photon scattering is given by: $\dfrac{\mu_s}{\mu_a + \mu_s}$

The propagation of each photon is selected from an exponential distribution using a computer generated pseudo-random number. The path distance that a photon travels between successive interactions is given by [56]

$$L = \frac{-\ln(R)}{\mu_a + \mu_s}$$

(Eq. 3.1)

where R is a pseudo-random number between 0 and 1.

A photon in any given cell can be scattered into any one of eight direction cells as shown in Figure 3.3. The direction of photon scattering is calculated by generating another random number and applying it in the probability density function. Hence, the angle of scattering is determined by using the Henyey-Greenstein phase function.
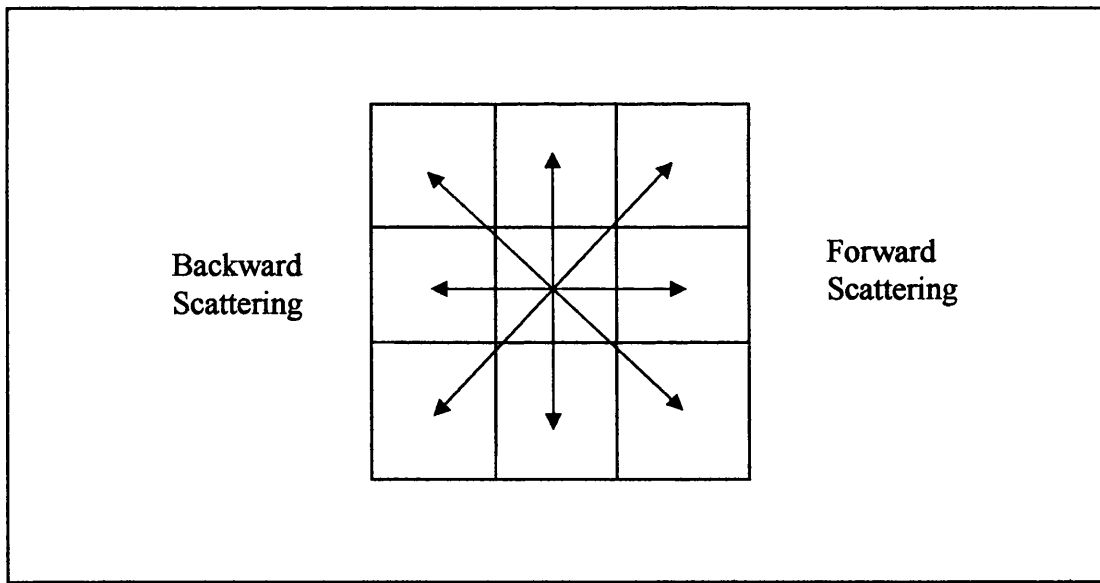
Figure 3.3: Possible photons scattering directions in one of eight direction cells.

The angle of scattering, θ, given by Henyey-Greenstein phase function is described by [56]

$$\theta = \cos^{-1}\frac{1}{2g}\left[1+g^2 -\left(\frac{1-g^2}{1-g+2gR}\right)^2\right]$$

(Eq. 3.2)

where R is a pseudo-random number between 0 and 1.

57

The new position of the photon is determined by the path length and the angle of scattering. At each interaction, a fraction of the photon's energy is being absorbed and the rest is being scattered. The photon will continue to scatter and reduce its energy until the energy falls below a given threshold value.

At each interaction point, a fraction (μ_a / μ_t) of the energy of the current weight, W_i, is deposited at the cell, The energy decreases due to multiplying it by the weight (μ_s / μ_t) at each interaction as shown in Figure 3.4. The fraction of energy absorbed and scattered at the each i interaction point are D_i and W_i respectively. The photon weight is updated following each scattering event.

Tissue surface

$$W_0 = 1$$

$$D_1 = \frac{\mu_a}{\mu_t}$$

$$W_1 = \frac{\mu_s}{\mu_t}$$

$$D_i = \frac{\mu_a}{\mu_t}\left(\frac{\mu_s}{\mu_t}\right)^{i-1}$$

$$W_i = \left(\frac{\mu_s}{\mu_t}\right)^{i}$$

Figure 3.4: Schematic diagram of photon path in the tissue.

A new propagation path for the next photon will begin when the photon is either completely absorbed, its weight fallen below a threshold level, or escaped the tissue. The whole process is repeated for every single photon used in the simulation. The photon energy deposited at each cell is accumulated in order to map out the distribution of light absorption.

A volumetric distribution of energy absorption is then obtained for each cell by dividing the deposited photon weight in that cell by its volume and by the total numbers of photons propagated. Since the 2-D model is assumed infinite in the z direction, each cell's volume is obtained by multiplying its surface by the unit length in the z direction.

The total number of photons required for propagation depends on the accuracy needed and the spatial and temporal resolution for the model. After the entire photons have been deposited, the distribution of light absorption will be known and mapped out. This volumetric distribution of photons energy is taken as a fluence source and can be used in the numerical model of the photothermal and photodynamic damage to compute the tumour damage in response to light irradiation in the tissue.

3.2 Thermal Transport Algorithm

Heat transfer in the tissue occurs mainly through conduction, convection and blood perfusion. Heat conduction in tissue is the dominant factor in this study of thermal transport. There is no cooling of skin surface used hence convection process is not considered in this study. The amount of heat transferred by blood perfusion varies during irradiation. The bioheat transfer equation includes the heat conduction and heat source.

Heat conduction at a position (x,y) is given by[105]

$$\frac{1}{\alpha} \cdot \frac{\partial T(x,y)}{\partial t} = \frac{\partial^2 T}{\partial x^2} + \frac{\partial^2 T}{\partial y^2} + \frac{Q}{k} \qquad \text{(Eq. 3.3)}$$

where T is the temperature at point r

$\quad$ Q is the heat source term (Wm^{-3})

$\quad$ k is the thermal conductivity ($Wm^{-1}\,°K^{-1}$)

$\quad$ α is the thermal diffusivity of the tissue(m^2s^{-1})

The thermal diffusivity is given by [105]

$$\alpha = k / \rho C \qquad\qquad \text{(Eq. 3.4)}$$

where k is the thermal conductivity ($Wm^{-1}\,°K^{-1}$)

$\quad$ ρC is volumetric heat capacity ($Jm^{-3}\,°K^{-1}$)

To solve the equation 3.3, a numerical solution based on the well-known Finite Difference method is used.

3.2.1 Finite Difference Method

To model the heat conduction in tissue, a two dimensional conducting region with the same thermal properties across the region is used. The conducting region of interest is

represented by a regular 2-D Cartesian grid system, where the grid spacing is Δx and Δy, as shown in Figure 3.5.
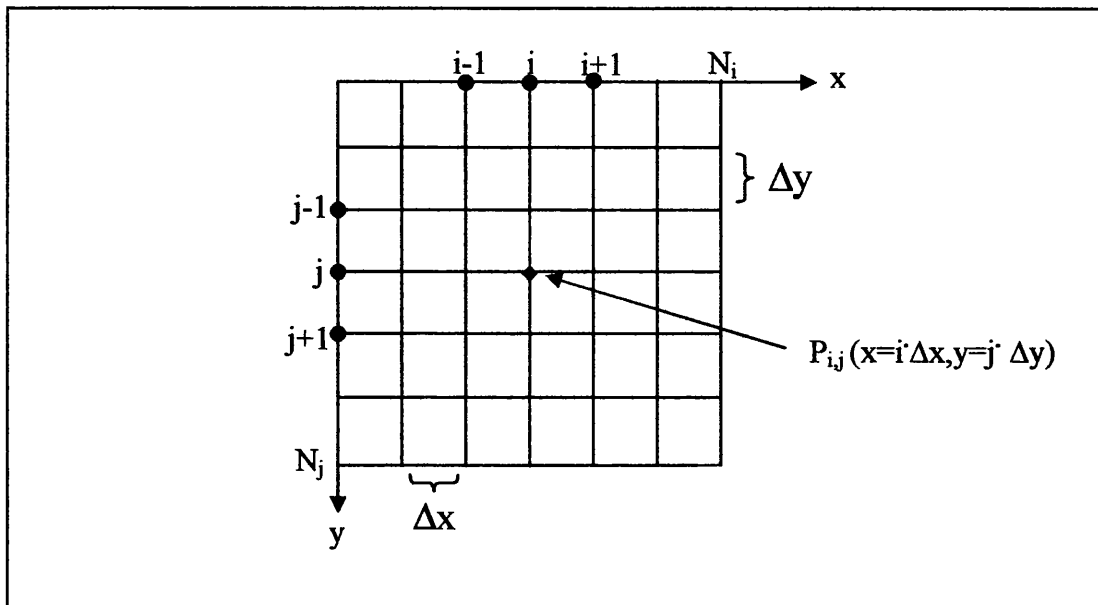
Figure 3.5: Cell point $P_{i,j}$ in the 2-D Cartesian grid with uniform grid spacing.

The basic concept of the Finite Difference method is to substitute the derivatives in the differential thermal diffusion equation by forward, backward and central differences according to Taylor series expansion. If the initial and boundary conditions are known, the differential equation can be organised into sets of algebraic equation. There are two types of finite difference are available namely the explicit method and implicit method.

3.2.2 Explicit Method

The explicit method allows the temperature at a given point at a new time level $(t + \Delta t)$ to be calculated explicitly from the temperature at nearby points at time t. This requires the first-order partial derivative (LHS of equation 3.3) to be evaluated using a forward difference representation involving $T(t + \Delta t)$ and $T(t)$ or by truncating the Taylor series expansion to obtain an estimate of error. The new LHS arrangement is written as [105]

$$\frac{\partial T}{\partial t} = \frac{T_{i,j}^{n+1} - T_{i+j}^{n}}{\Delta t} + O(\Delta t) \qquad \text{(Eq. 3.5)}$$

where i,j subscripts represent the position

n,(n+1) superscripts represent the time (t) and (t + Δt) respectively

Δt is the time step

O(Δt) indicates the truncation error term. The truncation error is of order Δt,

in order to provide a stable numerical method

In order to estimate the second-order partial derivatives in space (RHS of equation 3.3), two Taylor series expansions are added at time t. The new RHS arrangement in each direction is written as [105]

$$\frac{\partial^2 T}{\partial x^2} = \frac{T_{i+1}^{n} - 2T_{i}^{n} + T_{i-1}^{n}}{h^2} + O\left(h^2\right)$$

$$\frac{\partial^2 T}{\partial y^2} = \frac{T_{j+1}^{n} - 2T_{j}^{n} + T_{j-1}^{n}}{h^2} + O\left(h^2\right) \qquad \text{(Eq. 3.6)}$$

where h is the cell size

$O\left(h^2\right)$ indicates the truncation error term which is of order h^2

A Fourier number, F_o, is used in unsteady state heat transfer calculation. The Fourier Number describes the rate at which a body will respond to a temperature change and is essentially a function of the physical geometry and thermal characteristics of the cell. The time steps chosen for each point to determine the temperature in the cell must meet the Fourier Stability criteria.. The Fourier number is given by [105]

$$F_o = \frac{k \cdot \Delta t}{\rho C \cdot h^2} = \frac{\alpha \cdot \Delta t}{h^2} \qquad \text{(Eq. 3.7)}$$

where α is the thermal diffusivity

A restriction is placed on the Fourier number from which the matching time step can be obtained in order to keep the numerical method stable.

$F_o \leq 0.25$ in 2-D Cartesian problems

$F_o \leq 0.5$ in 1-D Cartesian problems

Substituting equation 3.5 and equation 3.6 into equation 3.3 gives [105]

$$\frac{1}{\alpha}\left(\frac{T_{i,j}^{n+1} - T_{i,j}^n}{\Delta t}\right) = \frac{T_{i+1}^n - 2T_i^n + T_{i-1}^n}{h^2} + \frac{T_{j+1}^n - 2T_j^n + T_{j-1}^n}{h^2} + \frac{Q^n}{k} \qquad \text{(Eq. 3.8)}$$

where i,j subscripts represent the position

n,(n+1) superscripts represent the time (t) and $(t + \Delta t)$ respectively

Multiplying by h^2 and inserting F_o in the equation 3.8 gives

$$\frac{1}{F_o}T_{i,j}^{n+1} = T_{i+1,j}^n + T_{i-1,j}^n + T_{i,j+1}^n + T_{i,j-1}^n - \left(4 - \frac{1}{F_o}\right)T_{i,j}^n + \frac{h^2 Q^n}{k} \qquad \text{(Eq. 3.9)}$$

The temperature at each point $P_{i,j}$ of the Cartesian grid can be obtained by solving equation 3.9 when the initial and boundary conditions are known. Although the results obtained with the explicit method are accurate, the Fourier restriction leads to very small time steps which require very long simulation times. A much quicker approach can be obtained by using an implicit method with larger time steps and coarser grid spacing.

3.2.3 Implicit Method

In an implicit method, the temperature at a given point at a new time level is obtained from temperature at nearby points at that new time levels. The first-order partial derivative in time is obtained by truncating the Taylor series expansion. The second-order partial derivatives in space are estimated by adding the two Taylor series expansions at time $(t + \Delta t)$. Rewriting the equation 3.3 at time $(t + \Delta t)$ gives [105]

$$\frac{1}{\alpha}(\frac{T_{i,j}^{n+1} - T_{i,j}^{n}}{\Delta t}) = \frac{T_{i+1}^{n+1} - 2T_{i}^{n+1} + T_{i-1}^{n+1}}{h^2} + \frac{T_{j+1}^{n+1} - 2T_{j}^{n+1} + T_{j-1}^{n+1}}{h^2} + \frac{Q^{n+1}}{k} \qquad \text{(Eq. 3.10)}$$

where i,j subscripts represent the position

        n,(n+1) superscripts represent the time (t) and (t + Δt) respectively

Multiplying by h^2 and inserting F_o in the equation 3.10 gives

$$-\frac{1}{F_o}T_{i,j}^{n} = T_{i+1,j}^{n+1} + T_{i-1,j}^{n+1} + T_{i,j+1}^{n+1} + T_{i,j-1}^{n+1} - \left(4 + \frac{1}{F_o}\right)T_{i,j}^{n+1} + \frac{h^2 Q^{n+1}}{k} \qquad \text{(Eq. 3.11)}$$

It is observed from equation 3.11 that no restriction needs to be placed on the Fourier number and larger time steps can be used. Since the temperatures at the new time level cannot be directly computed from previous known temperatures, the temperatures are obtained by solving for each time step, a set of simultaneous equations coupling the new temperature at the neighbouring points. In a 1-D problem, the linear system can be solved rapidly using matrix algorithms. However in a two dimensional problem, no rapid solution can be used and an iterative method has to be applied. This could increases the simulation time even though implicit method is faster than the explicit method. The other numerical methods used to solve this problem are the Crank-Nicholson method and the alternating direction implicit (ADI) method. The ADI method was used in the thermal model.

3.2.4 ADI Method

Another way of solving the thermal diffusion equation is the use of alternating direction implicit method. The basic of ADI method is to express the derivatives into two half steps. For the first half step, the derivative is expressed in one space direction (x) implicitly, and the other direction (y) being expressed explicitly. In the second half step, the direction for implicit representation is changed. The diffusion equation is written in tridiagonal matrix form. This matrix form requires only one set of rows or one set of columns to be solved at iteration. The tridiagonal matrix algorithm is applicable and solutions are obtained rapidly. Nevertheless, this method is much more complex to code than the fully implicit method but the simulation time could be reduced significantly, since it is half-implicit with the full implicit method stability.

The temporal profile model of a light pulse is represented as a simple functional form as shown in Figure 3.6. This consists of rise, hold and fall time which can be varied while maintaining the delivered energy constant. The beam pulse width is divided into a number of strips of width equal to the time step to create the time bands. The photons are distributed evenly between the time bands and the model steps through the temporal profile of the beam pulse with a time step less than the Fourier Number.
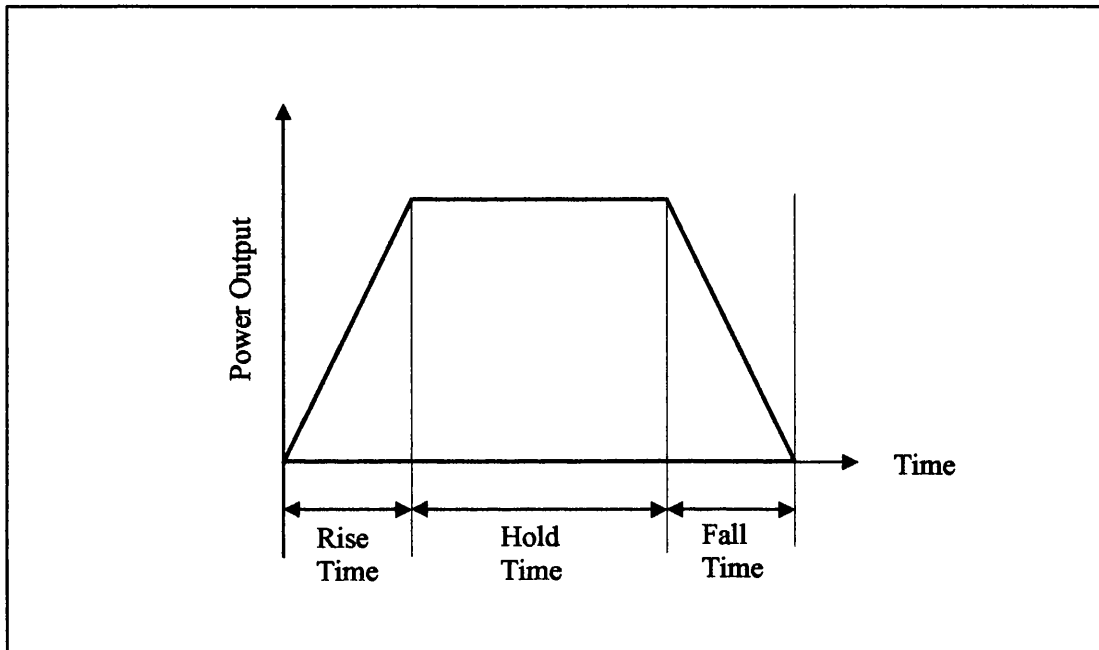
Figure 3.6: Temporal profile model with rise time, hold time and fall time.

The temperature in a given cell at given time is determined by the following process:

a) The proportion of the total energy in the pulse delivered during the time step is calculated. This takes into account the temporal profile of the light pulse.

b) The cell in matter only receives a fraction of the pulse energy, the value being determined from the result of Monte Carlo simulation. The absorption of energy produces a direct heating effect on the particular cell.

c) The temperature in the given cell has a contribution from the adjacent cell. This can either be a positive or negative heat effect.

65

The temperature calculation required steps are represented graphically in a schematic diagram as shown in Figure 3.7. These procedures are repeated for the entire duration of the light pulse to determine the temperature profile in the skin and tumour cells.
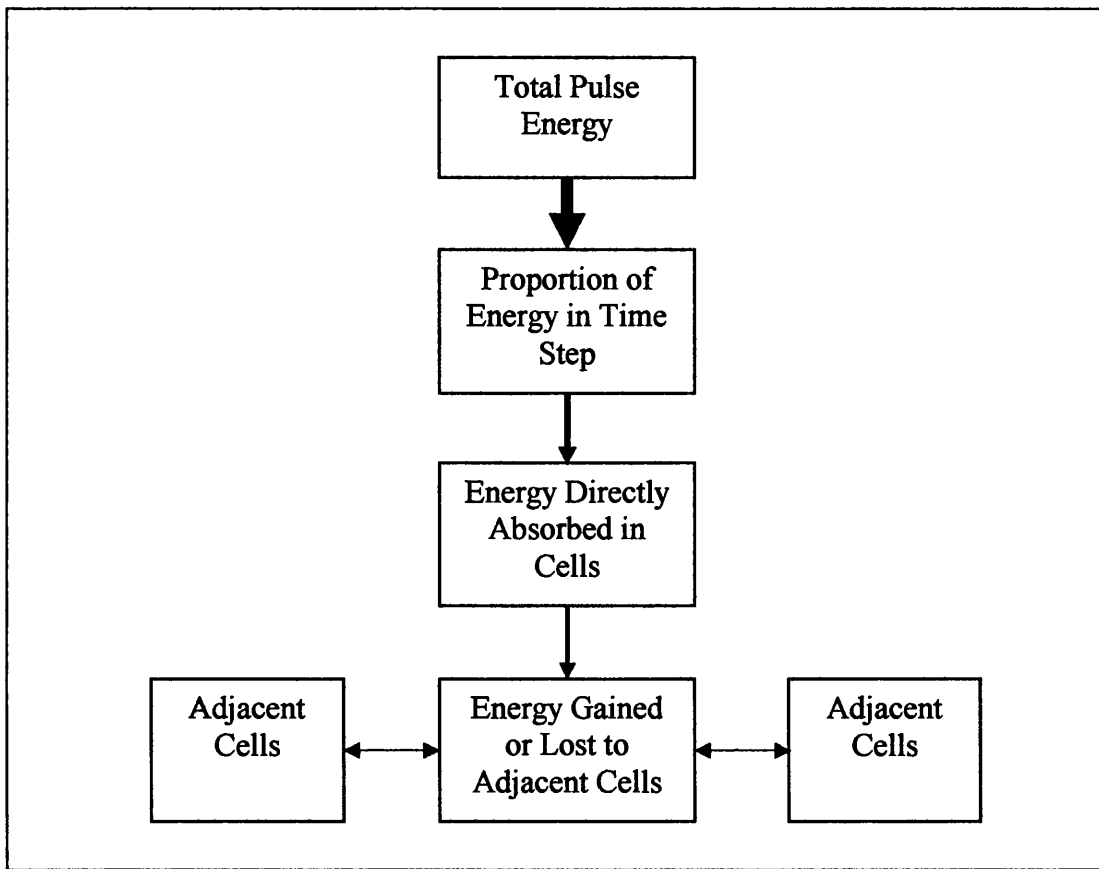
Figure 3.7: Procedures in determining the temperature rise in the cells. [70]

Taking into the account of all the factors for the calculation of the temperature in the cell, the cell temperature is given as

$$T\,(\text{cell}) = \left[\begin{array}{l}\text{Heat generated from}\\ \text{direct absorption}\end{array}\right] + \left(\begin{array}{l}\text{Heat from}\\ \text{adjacent cells}\end{array}\right) - \left(\begin{array}{l}\text{Heat lost during}\\ \text{time step}\end{array}\right)$$

The thermal model was developed to display the temperature variation of any cell at any time during the pulse period.

3.3 Chemical Transport Algorithm

3.1 Oxidative Damage Method

The photodynamic damage factor is introduced to quantify the amount of damage produced by oxidative interactions leading to photodynamic therapy. It is assumed that the rate of photodynamic damage occurring at time t is proportional to the fluence rate and the local concentration of photosensitiser and oxygen at that time. Another assumption made is that all biological damage is singlet oxygen mediated by only the Type II reaction.

The photodynamic damage occurring within a cell in tissue at time t is defined by [78]

$$PD(t) = k_{pd} \int I(t) \times P(t) \times O_2(t) \times dt \qquad \text{(Eq. 3.12)}$$

where k_{pd} is damage rate constant

$I(t)$ is the fluence rate

$P(t)$ is the photosensitiser concentration

$O_2(t)$ is the oxygen concentration

The photodynamic damage constant k_D value combines the photosensitiser absorption coefficient and the efficiency of generation of cytotoxic oxygen species.

The total fluence E delivered at a cell in tissue with time t is defined by [78]

$$E(t) = \int I(t) \times dt \qquad \text{(Eq. 3.13)}$$

where $I(t)$ is the fluence rate

The photosensitiser concentration P in a cell in tissue at time t is defined by [78]

$$P(t) = (k_{pp} - k_{pb} \int I(t) \times P(t)) \times dt \qquad \text{(Eq. 3.14)}$$

where k_{pp} is the photosensitiser production rate constant

k_{pb} is the photobleaching rate constant

$I(t)$ is the fluence rate

$P(t)$ is the initial photosensitiser concentration

$O_2(t)$ is the initial oxygen concentration

The model assumed that there is no photosensitiser formed during irradiation, hence photosensitiser production rate constant is zero. The photobleaching rate constant k_{PB} is wavelength dependent as light absorption is required.

The oxygen concentration O_2 in a cell in tissue with time t is defined by [78]

$$O_2(t) = (k_{perf} - k_{oxy} \int PD(t)) \times dt \qquad \text{(Eq. 3.15)}$$

where k_{perf} is the tissue perfusion rate constant

k_{oxy} is the oxygen removal rate constant

$PD(t)$ is the rate of photodynamic damage at time t

The k_{perf} on the RHS is for the supply of oxygen to the tissues and is assumed to be net perfusion over metabolic processes. The second term represents the rate of removal of oxygen by photodynamic processes is proportional to the amount of photodynamic damage occurring at that time.

Macroscopic damage to the tumour in photodynamic therapy could occur by two possible pathways:

1. Direct damage to tumour cells

2. Damage to endothelial cells of the vascular system and around the tumour thereby shutting off its blood flow

The death of the tumour cells occur by two distinct modes:

- Necrosis
- Apoptosis

Necrosis takes place when the membranes or other vital units are mostly damaged so that the cells can no longer sustain essential function and die. This type of destruction occurs quickly.

On the other hand, apoptosis is programmed cell death and it may take 24 hours for the program to operate and kill the cell. The apoptosis may be recognised by various biochemical markers, for example the fragmentation of DNA in the cell and mitochondrial changes. Kessel *et al* reported that two photosensitisers, which are located in the lysosomes, rapidly initiate apoptosis leading to cell death.[88]

CHAPTER 4   REMOTE COUPLING OF POWER

The embedded light source proposed for the photodynamic therapy application requires an efficient energy source to power the LED. Several possible methods to power the LED have been considered including the use of remote coupling. All of the methods have their inherent practical difficulties in the implementation.

The use of a battery is the simplest way of supplying power to the LED. The disadvantage is that the size of the device will increase considerably that it is no longer small in size to be embedded into the tissue. Furthermore, a battery has limited power and need to be removed from the tissue and disposed once the power runs out; hence the device has limited lifespan usage. A battery also contains toxic nickel or lithium materials which are harmful if accidentally leaked into the tissue.

An alternative way of supplying energy to the LED is through the use of remote coupling. This method utilises either radio frequency (RF) or microwaves as the coupling and energy transfer medium. The mechanism of energy transfer is through inductive coupling for 1-30MHz region and radiative coupling for 100MHz-10GHz frequency region. The remote coupling RF system consists of

- Transmitter - RF generator
- Receiver – RF device

The RF device is a passive device, which it does not require any internal power source. This has positive implications on the cost, life-time and environmental situation. The necessary power required to energise and activate the RF device is drawn from the localised electromagnetic field.

70

The two primary factors which influence the choice of the frequency for remote coupling are:

a) *How much of the energy is lost or attenuated in the tissue?*

b) *How does the frequency affect the penetration depth of the waves in the tissue?*

Once an ideal frequency has been selected, a third and highly significant issue that must be solved is

How could the energy be coupled into a small antenna receiver efficiently?

An understanding of the electromagnetic waves and the tissue dielectric properties are required in order to achieve maximum efficiency of energy transfer into tissues.

4.1   E.M. Waves Propagation in Tissue

For this study, it is assumed that all electromagnetic waves are transmitted as plane waves to describe the propagation of waves into a tissue. The use of plane waves is a good approximation to the actual system and a useful mathematical description because it simplifies the analysis of electromagnetic waves.

The propagation of electric and magnetic fields is described by the differential form of the complex time-harmonic steady-state Maxwell's equations. The Ampere's law of static magnetic field is one of the Maxwell's equations and is defined by [94]

$$\nabla \times H = J + j\omega\varepsilon_o\varepsilon_r E \qquad\qquad \text{(Eq. 4.1)}$$

where H is the complex vector of magnetic field intensity

E is the complex vector of electric field intensity

ω is the angular frequency

ε_o is the permittivity of free space

ε_r is the relative permittivity of medium

The electric field of the incident plane wave, E generates a current density J [94]

$$J = \sigma E \qquad \text{(Eq. 4.2)}$$

where σ is the conductivity (S/m)

Substituting equation 4.2 into equation 4.1 gives

$$\nabla \times H = j\omega\varepsilon_o\varepsilon_r \left(1 - j\frac{\sigma}{\omega\varepsilon_o\varepsilon_r} \right) E \qquad \text{(Eq. 4.3)}$$

The complex permittivity ε_d is defined as [94]

$$\varepsilon_d = \varepsilon' + j\varepsilon'' = \varepsilon_r - j\frac{\sigma}{\omega\varepsilon_o} \qquad \text{(Eq. 4.4)}$$

where ε_r' is the real part of ε_d and is equal to relative permittivity ε_r

ε_r'' is the imaginary part of ε_d and is equal to $-\sigma/\omega\varepsilon_o$

The equation 4.3 can be rewritten as

$$\nabla \times H = j\omega\varepsilon_o\varepsilon_d E \qquad \text{(Eq. 4.5)}$$

For propagation in a homogeneous dielectric medium, the plane wave expressions for E and H will include a propagation constant.

The propagation constant γ is defined as [94]

$$\gamma = \alpha + j\beta \qquad \text{(Eq. 4.6)}$$

where β is the phase constant of medium

α is the attenuation constant of medium

The solution for plane waves in a dielectric medium is given by [94]

$$E = E_o \exp[j(wt - \beta z)]\exp[-\alpha z] \qquad \text{(Eq. 4.7)}$$

The above solution shows that the plane waves have a sinusoidal part and an exponential part whose magnitude decays as either α or z increases.

4.1.1 Characteristics of Plane Waves

The plane waves transmitted in the air are normally incident on a tissue to the boundary of the tissue. A plane wave is a wave where there are spatial variations only in the direction of travel. The path of travel is in the z direction into the tissue as shown in Figure 4.1. There are three plane waves to consider at the boundary : the incident wave , the reflected wave and the transmitted wave. The origin of z coordinates start on the air-tissue boundary. The boundary condition to apply to the electric field at a boundary is that the total tangential electric field on one side of the boundary must equal the total tangential electric field on the other side of the boundary. The total electric field on transmitted side of the boundary is just E_t, hence the first boundary condition gives [95]

$$E_i + E_r = E_t \qquad \text{(Eq. 4.8)}$$

where E_i is the incident wave

E_r is the reflected wave

E_t is the transmitted wave
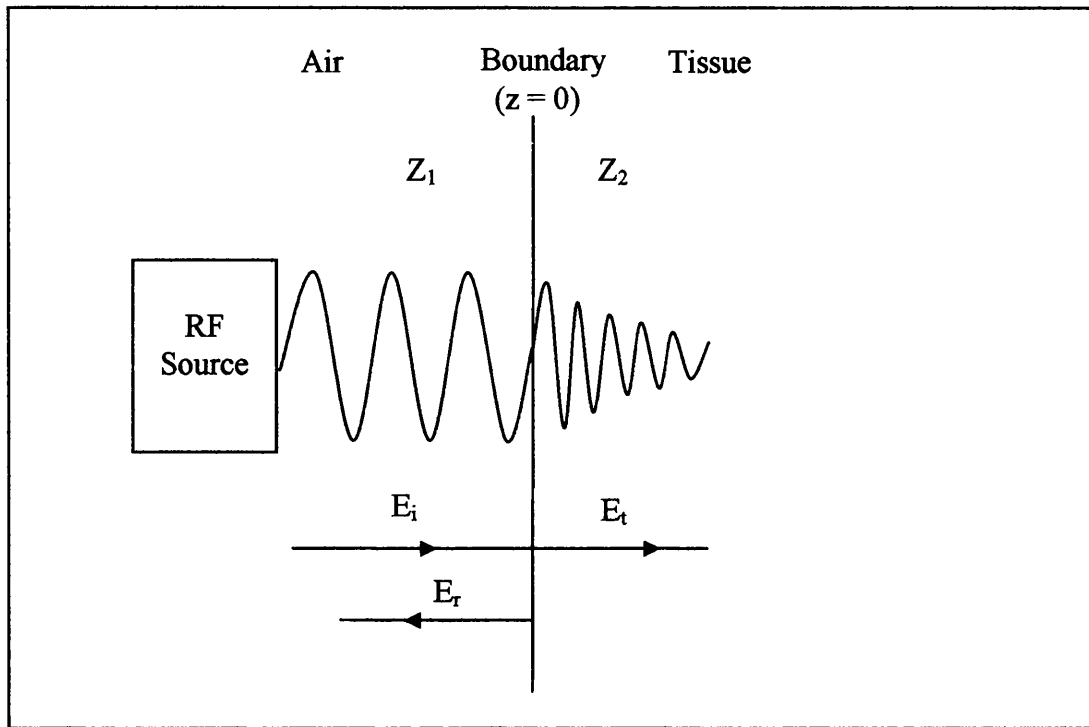
Figure 4.1: Plane waves propagation into tissue

Power conservation states that the total power is constant as the wave is incident on the boundary. The average power in the incident, reflected and transmitted plane wave are given by $\dfrac{E_i^2}{Z_1}$, $\dfrac{E_r^2}{Z_1}$ and $\dfrac{E_t^2}{Z_2}$ respectively. Hence, the second boundary condition gives [95]

$$\frac{E_i^2}{Z_1} = \frac{E_r^2}{Z_1} + \frac{E_t^2}{Z_2}$$

(Eq. 4.9)

The wave impedance Z_1 in air and the wave impedance Z_2 in tissue are given by [95]

$$Z_1 = Z_0 \sqrt{\frac{\mu_1}{\varepsilon_1}} \qquad Z_2 = Z_0 \sqrt{\frac{\mu_2}{\varepsilon_2}}$$

where Z_0 is the impedance of free space.

ε_1 is the permittivity of free space.

ε_2 is the relative permittivity of tissue.

μ_1 is the permeability of free space.

μ_2 is the relative permeability of tissue.

Inserting equation 4.8 into equation 4.9 and solving both gives the reflected waves and transmitted wave relative to the incident wave.

Hence, the reflected wave relative to the incident wave is given by

$$\frac{E_r}{E_i} = \frac{Z_2 - Z_1}{Z_2 + Z_1} = \frac{\sqrt{\varepsilon_1} - \sqrt{\varepsilon_2}}{\sqrt{\varepsilon_1} + \sqrt{\varepsilon_2}} \qquad \text{(Eq. 4.10)}$$

The transmitted wave relative to the incident wave is given by

$$\frac{E_t}{E_i} = \frac{2Z_2}{Z_2 + Z_1} = \frac{2\sqrt{\varepsilon_1}}{\sqrt{\varepsilon_1} + \sqrt{\varepsilon_2}} \qquad \text{(Eq. 4.11)}$$

The solution relates the amplitudes of the reflected wave to the impedance of the waves or the permittivity of the tissue. The ratio E_r/E_i is the reflection coefficient ρ and it is not dependent on the actual power in the plane wave.

The amplitude of decaying electric field of plane wave with the depth z is defined by [94]

$$E(z) = E_o \exp^{-\alpha z} \qquad \text{(Eq. 4.12)}$$

where α is the attenuation constant

The power absorbed from a plane wave in a tissue dielectric is defined by [94]

$$P(z) = \sigma E_o^2 \exp^{-2\alpha z} \qquad \text{(Eq. 4.13)}$$

where σ is the tissue conductivity

Tissue is a dielectric that has a very small conductivity and therefore a very small loss. The amount of attenuation of a plane wave is determined by the conductivity σ of the tissue. Higher tissue conductivity corresponds to a larger attenuation of the plane wave. The tissue conductivity σ is defined by [94]

$$\sigma = \omega \varepsilon_0 \varepsilon_r^{''} \qquad \text{(Eq. 4.14)}$$

where ω is the angular frequency

ε_o is the permittivity of free space

$\varepsilon_r^{''}$ is the imaginary part of the complex permittivity ε_d

The loss tangent, $\tan(\delta)$ is used to describe the amount of loss in the tissue. The same tissue that can influence plane waves differently at different frequencies. The loss tangent increases as the conductivity increases or the frequency decreases or the permittivity decreases. The loss tangent is defined by [94]

$$\tan(\delta) = \left| \frac{\varepsilon_r^{''}}{\varepsilon_r^{'}} \right| = \frac{\sigma}{\omega \varepsilon_o \varepsilon_r} \qquad \text{(Eq. 4.15)}$$

where $\tan \delta \ll 1$ for waves in low conductivity tissue

$\tan \delta \gg 1$ for waves in high conductivity tissue

ε_o is the permittivity of free space

ε_r is the relative permittivity of tissue

The attenuation constant α is defined by [96]

$$\alpha = \left(\frac{\omega}{c} \right) \sqrt{ \frac{\mu_r \varepsilon_r^{'}}{2} \left(\sqrt{1 + \left(\varepsilon_r^{''} / \varepsilon_r^{'} \right)^2} - 1 \right) } \qquad \text{(Eq. 4.16)}$$

where c is the speed of light

μ_r is the relative permeability

ω is the angular frequency

ε_r' is the real part of the complex permittivity ε_d

ε_r'' is the imaginary part of the complex permittivity ε_d

The attenuation constant value is dependent on the frequency, the relative permittivity, the conductivity and the relative permeability of the tissue.

The penetration depth δ is the distance where the field amplitude is 1/e of the value at the surface and is defined by [98]

$$\delta = \frac{1}{\alpha} \qquad \text{(Eq. 4.17)}$$

where α is the attenuation constant of tissue

The phase constants β is defined by [98]

$$\beta = \omega\sqrt{\mu_r \varepsilon_r} \qquad \text{(Eq. 4.18)}$$

where ω is the angular frequency

μ_r is the relative permeability

ε_r' is the relative permittivity

The wavelength λ in the tissue is defined by [98]

$$\lambda = \frac{2\pi}{\beta} \qquad \text{(Eq. 4.19)}$$

where β is the phase constant of tissue

The wave velocity v in the tissue is defined by [98]

$$v = \frac{\omega}{\beta} \qquad \text{(Eq. 4.20)}$$

where β is the phase constant of tissue

4.1.2　Tissue Dielectric Properties with Frequency

Tissue is a dielectric material characterised by permittivity and conductivity of the tissue. The key factors that determine a wave interaction in tissue are the dielectric properties of the tissue. The relative permittivity and conductivity values of tissue are highly dependent on the frequency. The characteristic of tissue whose permittivity changes with frequency is called a dispersive tissue. [94] It means that if a group of frequencies are sent through a tissue, the separate frequencies will be delayed by different amounts so that the energy will be dispersed at the other end.

An analysis of dielectric properties of tissues over the range of radio frequencies through to microwave frequencies is required for better understanding of the wave's behaviour in tissues. The tissues chosen for the analysis are the skin, fat, muscle and blood. The data used in this study for the dielectric properties of tissues are taken from C.Gabriel.[92]

The main dielectric properties constants are:

- Wave frequency (f)

- Tissue real complex permittivity $\left(\varepsilon_r^{'}\right)$

- Tissue imaginary complex permittivity $\left(\varepsilon_r^{"}\right)$

- Tissue conductivity (σ)

- Loss tangent $(\tan(\delta))$

- Attenuation constant (α)

78

4.1.2.1 Skin

The tissue dielectric properties of skin for the frequency range of 1 MHz to 10 GHz are shown in Table 4.1. [92] The real and the imaginary parts of complex permittivity of skin gradually decrease with increase in frequency. The conductivity values increase with increasing frequency. The attenuation constant increases exponentially with frequency. Hence it is recognised that at microwave frequencies, skin conducts easily so that it is highly attenuating. Figure 4.2 shows the percentage of power transmitted as a function of tissue depth for skin tissue at International Standard Medical (ISM) frequencies.

f	ε_r'	ε_r''	σ (S/m)	$\tan(\delta)$	α (m^{-1})
1 MHz	990.7595	237.9348	0.013237	0.240154	0.078657
10 MHz	361.6703	354.6898	0.197323	0.980699	1.783913
100 MHz	72.93031	88.30124	0.491242	1.210762	9.557896
1 GHz	40.93626	16.1742	0.899811	0.395107	26.0064
10 GHz	31.29022	14.40529	8.014023	0.460377	263.306

Table 4.1: Tissue dielectric properties of skin.
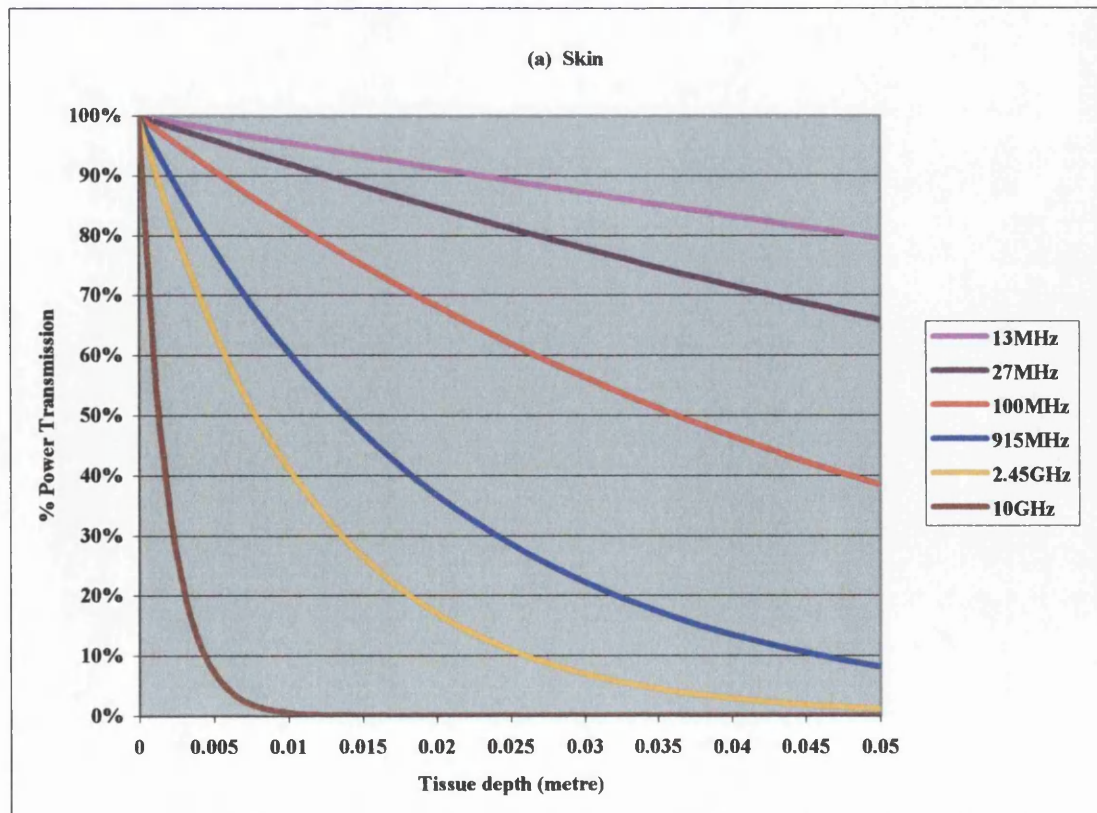
Figure 4.2: Power transmitted vs. tissue depth in skin tissue.

4.1.2.2 Fat

The tissue dielectric properties of fat for the frequency range of 1 MHz to 10 GHz are shown in Table 4.2. [92] The real and the imaginary parts of complex permittivity of fat gradually decrease with increasing frequency. The conductivity values remain very low at the lower MHz frequencies and increase gradually in the GHz region. The attenuation constant increases exponentially with frequency. This shows that at microwaves frequencies, fat conducts easily so that it is highly attenuating. Figure 4.3 shows the percentage of power transmitted as a function of tissue depth for fat tissue at ISM frequencies.

f	ε_r'	ε_r''	σ (S/m)	$\tan(\delta)$	α (m^{-1})
1 MHz	50.80411	791.8606	0.044053	15.58654	0.403874
10 MHz	29.58111	94.56821	0.052611	3.196912	1.235533
100 MHz	12.70134	12.29615	0.068407	0.968099	3.306151
1 GHz	11.29422	2.091768	0.11637	0.185207	6.494951
10 GHz	8.801566	3.069381	1.707573	0.348731	106.8514

Table 4.2: Tissue dielectric properties of fat.
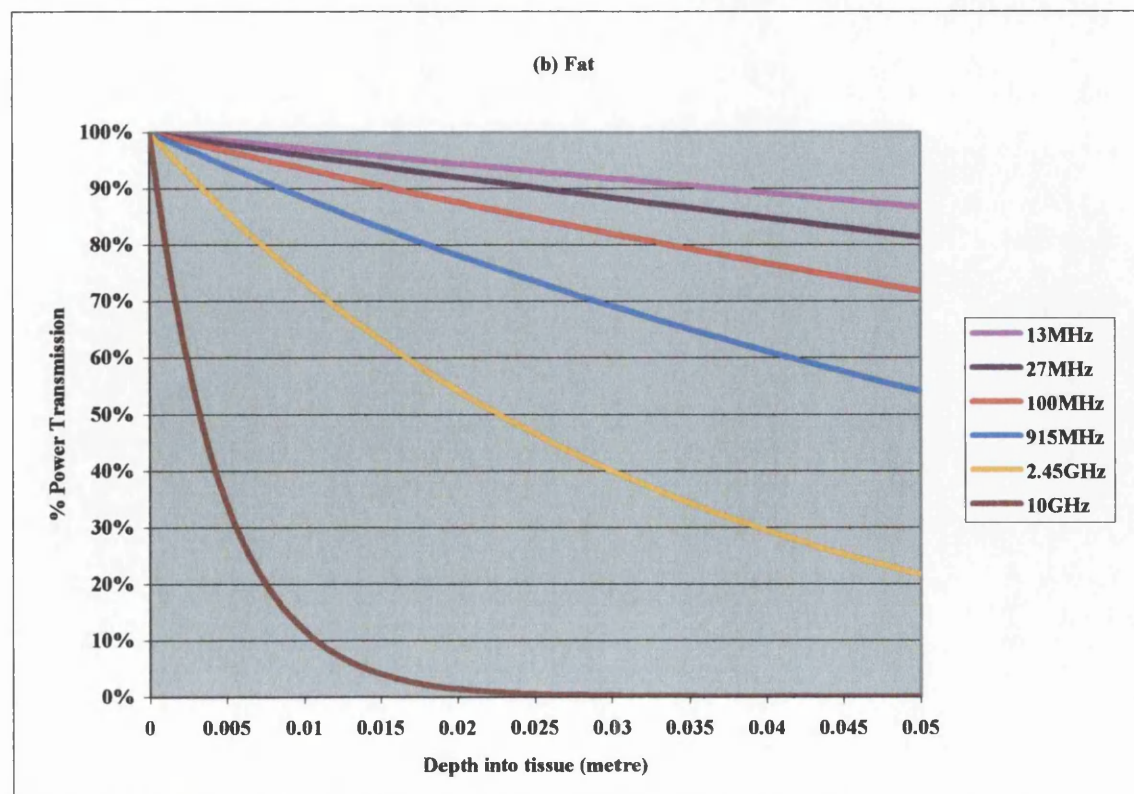
Figure 4.3: Power transmitted vs. tissue depth in fat tissue.

4.1.2.3 Muscle

The tissue dielectric properties of muscle for the frequency range of 1 MHz to 10 GHz are shown in Table 4.3. [92] The value of the real and the imaginary parts of complex permittivity of blood reduce with increasing frequency. The conductivity values remain approximately constant at the MHz region and rise in the GHz region of the spectrum. The attenuation constant increases exponentially with frequency. Thus, it is identified that at microwaves frequencies, muscle conducts easily so that it is highly attenuating. Figure 4.4 shows the percentage of power transmitted as a function of tissue depth for muscle tissue at ISM frequencies.

f	$\varepsilon_r^{'}$	$\varepsilon_r^{''}$	σ (S/m)	$\tan(\delta)$	α (m^{-1})
1 MHz	1836.314	9035.812	0.502685	4.920625	1.273491
10 MHz	170.726	1108.754	0.616828	6.494346	4.57042
100 MHz	65.97206	127.1904	0.707592	1.927943	13.03052
1 GHz	54.81103	17.583	0.978186	0.320793	24.58134
10 GHz	42.76354	19.10054	10.62611	0.446655	299.0463

Table 4.3: Tissue dielectric properties of muscle
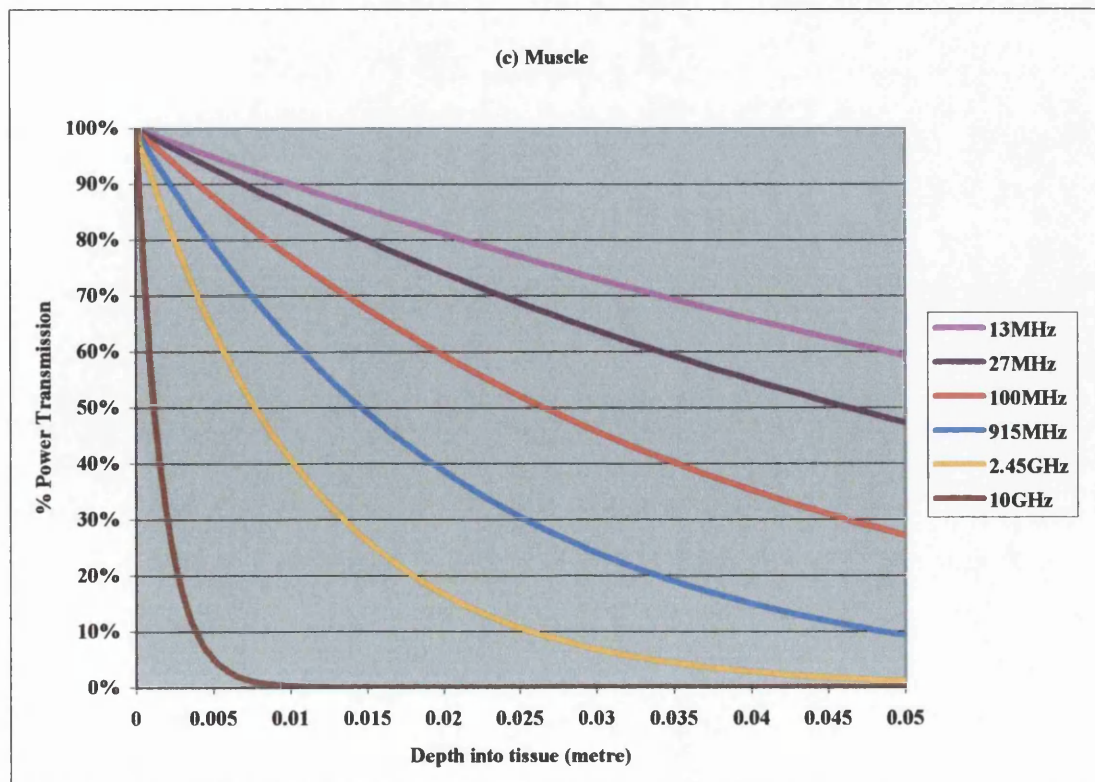
Figure 4.4: Power transmitted vs. tissue depth in muscle tissue

4.1.2.4 Blood

The tissue dielectric properties of blood for the frequency range of 1 MHz to 10 GHz are shown in Table 4.4. [92] The real and the imaginary parts of complex permittivity of blood gradually decrease with increasing in frequency. The conductivity values remain approximately constant at the lower frequencies and increases in the higher frequencies region. The conductivity constants are apparently proportional to frequency but the frequency dependence of the complex permittivity often dominates. The attenuation constant increases exponentially with frequency. Consequently, at the microwave region, blood conducts easily so that it is highly attenuating. Figure 4.4 shows the percentage of power transmitted vs. tissue depth for muscle tissue at ISM frequencies.

f	ε_r'	ε_r''	σ (S/m)	$\tan(\delta)$	α (m^{-1})
1 MHz	3026.738	14777.52	0.82211	4.882325	1.627324
10 MHz	280.0937	1971.54	1.096817	7.038861	6.130559
100 MHz	76.82191	221.6598	1.233149	2.885372	18.61488
1 GHz	61.06537	28.45584	1.58307	0.46599	37.21117
10 GHz	45.10917	23.60412	13.13156	0.523267	356.9846

Table 4.4: Tissue dielectric properties of blood
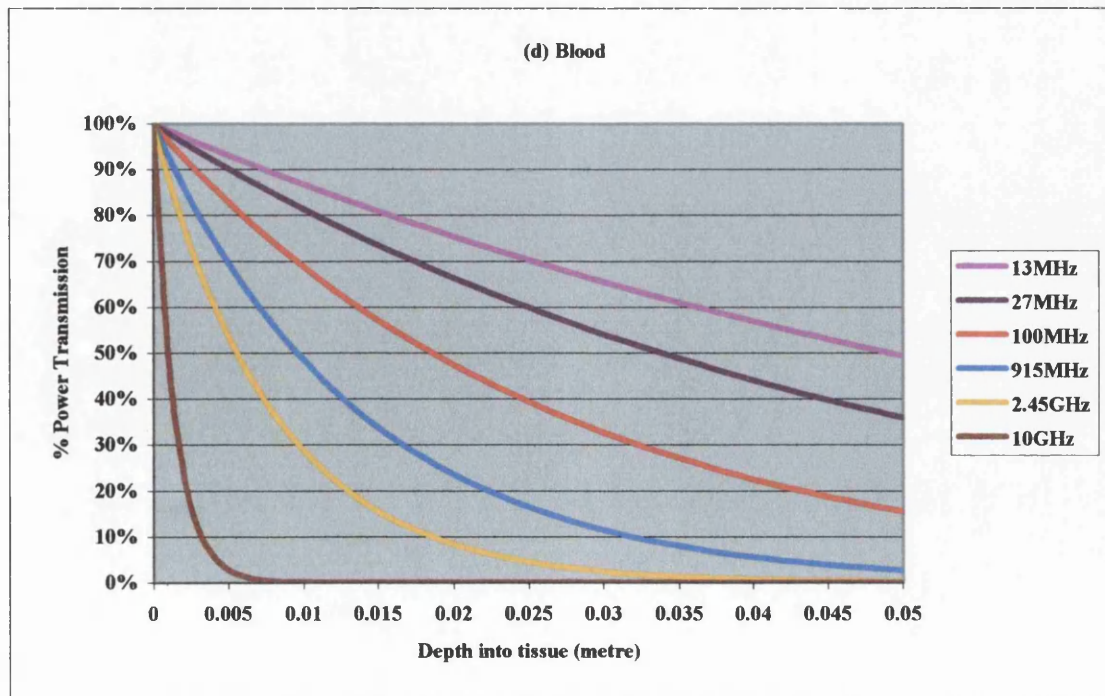
Figure 4.5: Power transmitted vs. tissue depth in blood tissue

82

4.1.3 Summary of the Frequency Analysis

The analysis of various tissue dielectric properties shows that blood is the most attenuating tissue in comparison with the other tissues. This is followed by muscle, skin and lastly fat as the least attenuating tissue. The tissue penetration depth achieved at low frequencies is much higher than at microwaves frequencies. This is because at lower frequency, there is less attenuation in these tissues and therefore more power could be transmitted through the tissues. At microwave frequencies, the waves could only be penetrating up to 1-2 cm depth in which most of the power is being absorbed in the first centimetre of the tissues.

4.2   Wave Propagation Model

A wave propagation model named WAVEP was developed to predict the penetration depth of a plane wave propagating through a human body. The human body is represented by a simple one dimensional, multi-layer structure incorporating the skin, fat, muscle and tumour. Each layer has its own tissue dielectric properties, namely relative permittivity ε_x and attenuation constant α_x. The physical dimensions of skin, fat, muscle and tumour were taken as representative of a tumour located in the body. The tumour was assumed to contain blood vasculatures. It was assumed that the plane wave was perpendicular incident to the skin surface to simplify the complex reflection of waves in the tissues.

Figure 4.6 shows five boundaries with a single wave incident on the first boundary. At the first boundary, the wave is partially reflected and partially transmitted and the same thing happens at the second boundary. A part of the wave is reflected back to the first boundary which is then partially reflected and partially transmitted. The result is that the total field at the first boundary consists of multiple individual waves. The wave is partially reflected and partially transmitted at each boundary until it reaches the final end of the tissues.
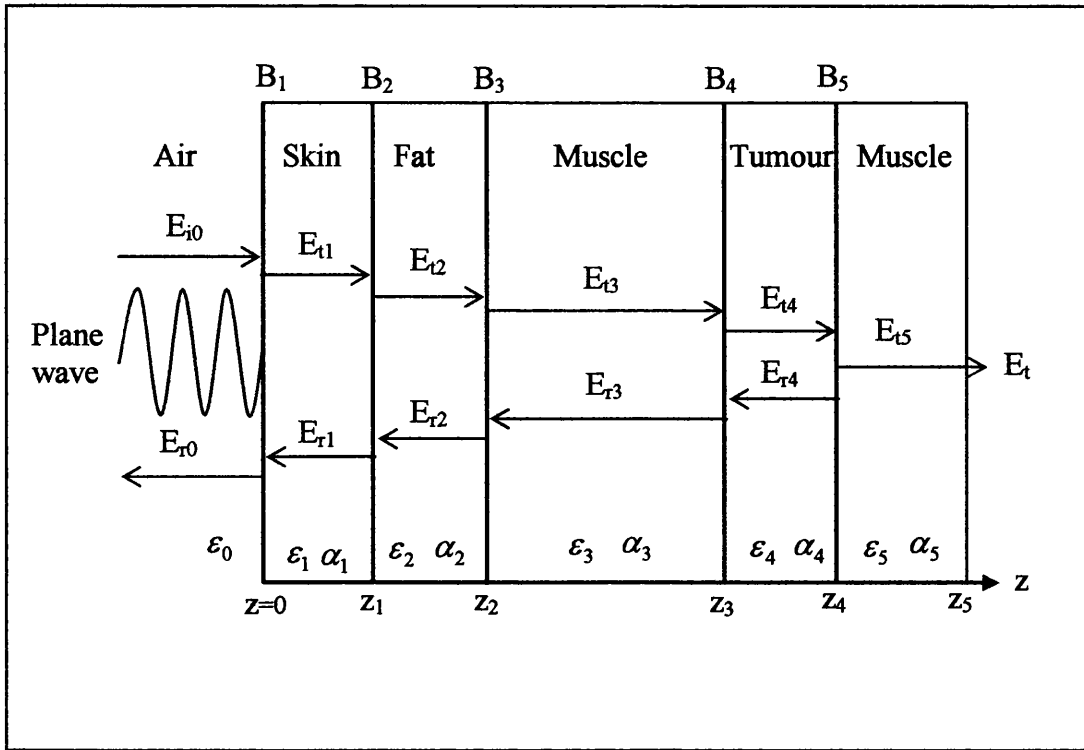
Figure 4.6: Simplified model of RF waves propagation into human body

The total electric field amplitude in each boundary consists of the sum of the individual components. The following total electric field equations were derived from equation 4.8 and equation 4.12.

In the first boundary B_1, the total field at $z = 0$ is given by

$$E_{t1} = E_{i0} + E_{r0}$$ (Eq. 4.21)

In the second boundary B_2, the total field at z_1 is given by

$$E_{t2} = E_{t1} \exp^{-\alpha_1 z_1} + E_{r1} \exp^{-\alpha_1 z_1}$$ (Eq. 4.22)

In the third boundary B_3, the total field at z_2 is given by

$$E_{t3} = E_{t2} \exp^{-\alpha_2 z_2} + E_{r2} \exp^{-\alpha_2 z_2}$$ (Eq. 4.23)

In the fourth boundary B$_4$, the total field at z$_3$ is given by

$$E_{t4} = E_{t3} \exp^{-\alpha_3 z_3} + E_{r3} \exp^{-\alpha_3 z_3} \qquad \text{(Eq. 4.24)}$$

In the fifth boundary B$_5$, the total field at z$_4$ is given by

$$E_{t5} = E_{t4} \exp^{-\alpha_4 z_4} + E_{r4} \exp^{-\alpha_4 z_4} \qquad \text{(Eq. 4.25)}$$

The total transmitted field at the end of the tissues or z$_5$ is given by

$$E_t = E_{t5} \exp^{-\alpha_5 z_5} \qquad \text{(Eq. 4.26)}$$

The solution to the problem requires that the values of E$_{t1}$, E$_{t2}$, E$_{t3}$, E$_{t4}$, E$_{t5}$ and E$_{r0}$, E$_{r1}$, E$_{r2}$, E$_{r3}$, E$_{r4}$ relative to E$_{i0}$ to be found. This requires a total of ten boundary equations to be solved. The following boundary equations were derived from equation 4.10 and equation 4.11.

For boundary condition 1,
$$\frac{E_{r0}}{E_{i0}} = \frac{\sqrt{\varepsilon_0} - \sqrt{\varepsilon_1}}{\sqrt{\varepsilon_0} + \sqrt{\varepsilon_1}}$$

For boundary condition 2,
$$\frac{E_{t1}}{E_{io}} = \frac{2\sqrt{\varepsilon_0}}{\sqrt{\varepsilon_0} + \sqrt{\varepsilon_1}}$$

For boundary condition 3,
$$\frac{E_{r1}}{E_{i0}} = \left(\frac{\sqrt{\varepsilon_1} - \sqrt{\varepsilon_2}}{\sqrt{\varepsilon_1} + \sqrt{\varepsilon_2}} \right) \times \left(\frac{2\sqrt{\varepsilon_0}}{\sqrt{\varepsilon_0} + \sqrt{\varepsilon_1}} \right)$$

For boundary condition 4,
$$\frac{E_{t2}}{E_{i0}} = \left(\frac{2\sqrt{\varepsilon_1}}{\sqrt{\varepsilon_1} + \sqrt{\varepsilon_2}} \right) \times \left(\frac{2\sqrt{\varepsilon_0}}{\sqrt{\varepsilon_0} + \sqrt{\varepsilon_1}} \right)$$

For boundary condition 5,

$$\frac{E_{r2}}{E_{i0}} = \left(\frac{\sqrt{\varepsilon_2} - \sqrt{\varepsilon_3}}{\sqrt{\varepsilon_2} + \sqrt{\varepsilon_3}}\right) \times \left(\frac{2\sqrt{\varepsilon_1}}{\sqrt{\varepsilon_1} + \sqrt{\varepsilon_2}}\right) \times \left(\frac{2\sqrt{\varepsilon_0}}{\sqrt{\varepsilon_0} + \sqrt{\varepsilon_1}}\right)$$

For boundary condition 6,

$$\frac{E_{t3}}{E_{i0}} = \left(\frac{2\sqrt{\varepsilon_2}}{\sqrt{\varepsilon_2} + \sqrt{\varepsilon_3}}\right) \times \left(\frac{2\sqrt{\varepsilon_1}}{\sqrt{\varepsilon_1} + \sqrt{\varepsilon_2}}\right) \times \left(\frac{2\sqrt{\varepsilon_0}}{\sqrt{\varepsilon_0} + \sqrt{\varepsilon_1}}\right)$$

For boundary condition 7,

$$\frac{E_{r3}}{E_{i0}} = \left(\frac{\sqrt{\varepsilon_3} - \sqrt{\varepsilon_4}}{\sqrt{\varepsilon_3} + \sqrt{\varepsilon_4}}\right) \times \left(\frac{2\sqrt{\varepsilon_2}}{\sqrt{\varepsilon_2} + \sqrt{\varepsilon_3}}\right) \times \left(\frac{2\sqrt{\varepsilon_1}}{\sqrt{\varepsilon_1} + \sqrt{\varepsilon_2}}\right) \times \left(\frac{2\sqrt{\varepsilon_0}}{\sqrt{\varepsilon_0} + \sqrt{\varepsilon_1}}\right)$$

For boundary condition 8,

$$\frac{E_{t4}}{E_{i0}} = \left(\frac{2\sqrt{\varepsilon_3}}{\sqrt{\varepsilon_3} + \sqrt{\varepsilon_4}}\right) \times \left(\frac{2\sqrt{\varepsilon_2}}{\sqrt{\varepsilon_2} + \sqrt{\varepsilon_3}}\right) \times \left(\frac{2\sqrt{\varepsilon_1}}{\sqrt{\varepsilon_1} + \sqrt{\varepsilon_2}}\right) \times \left(\frac{2\sqrt{\varepsilon_0}}{\sqrt{\varepsilon_0} + \sqrt{\varepsilon_1}}\right)$$

For boundary condition 9,

$$\frac{E_{r4}}{E_{i0}} = \left(\frac{\sqrt{\varepsilon_4} - \sqrt{\varepsilon_5}}{\sqrt{\varepsilon_4} + \sqrt{\varepsilon_5}}\right) \times \left(\frac{2\sqrt{\varepsilon_3}}{\sqrt{\varepsilon_3} + \sqrt{\varepsilon_4}}\right) \times \left(\frac{2\sqrt{\varepsilon_2}}{\sqrt{\varepsilon_2} + \sqrt{\varepsilon_3}}\right) \times \left(\frac{2\sqrt{\varepsilon_1}}{\sqrt{\varepsilon_1} + \sqrt{\varepsilon_2}}\right) \times \left(\frac{2\sqrt{\varepsilon_0}}{\sqrt{\varepsilon_0} + \sqrt{\varepsilon_1}}\right)$$

For boundary condition 10,

$$\frac{E_{t5}}{E_{i0}} = \left(\frac{2\sqrt{\varepsilon_4}}{\sqrt{\varepsilon_4} + \sqrt{\varepsilon_5}}\right) \times \left(\frac{2\sqrt{\varepsilon_3}}{\sqrt{\varepsilon_3} + \sqrt{\varepsilon_4}}\right) \times \left(\frac{2\sqrt{\varepsilon_2}}{\sqrt{\varepsilon_2} + \sqrt{\varepsilon_3}}\right) \times \left(\frac{2\sqrt{\varepsilon_1}}{\sqrt{\varepsilon_1} + \sqrt{\varepsilon_2}}\right) \times \left(\frac{2\sqrt{\varepsilon_0}}{\sqrt{\varepsilon_0} + \sqrt{\varepsilon_1}}\right)$$

The boundary conditions and the total electric field equations at the boundaries require the relative permittivity and attenuation constant of the tissues to be known. The relative permittivity and the attenuation constant of skin, fat, blood and muscle for the model are obtained from C.Gabriel.[92] By using 100% incident power as the source, the wave propagation through the tissues was modelled. The result of this model indicated what percentage of incident wave power reached the target tumour after passing through the upper layers of the skin, fat and muscle tissues. The physical parameters in Table 4.5 are taken as being representative of tissues in the body.

Tissue Structure	Thickness
Skin	2.5mm
Fat	2.5mm
Muscle (Top)	1cm
Blood (Tumour)	4mm
Muscle (Bottom)	3cm

Table 4.5: Physical dimension of the tissues in the body

4.2.1   Wave Propagation Model Results

Figure 4.7 below shows the results of the wave propagation in tissues for a range of ISM frequencies using the physical properties of the human body in Table 4.5.
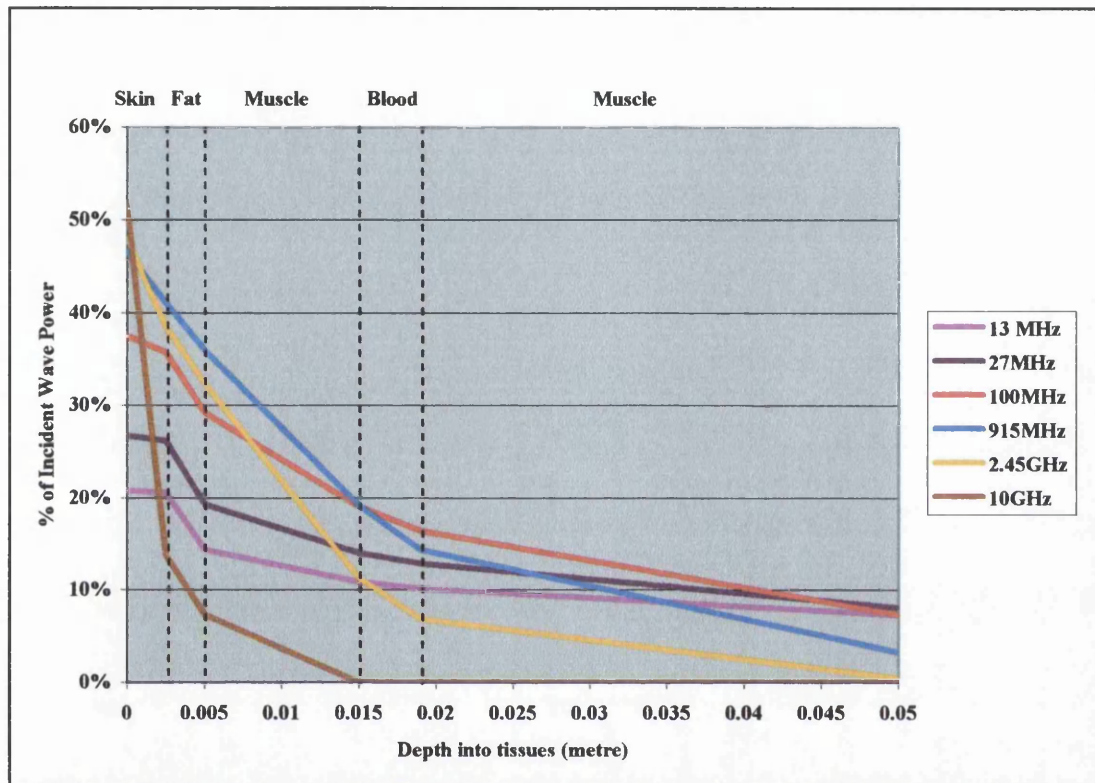
Figure 4.7: Power transmitted as a function of tissue depth from air into tissues

The wave propagation model shows that at least half of the incident waves power at all frequencies is being reflected out of the surface skin. This is due to the impedance mismatch between the air and the layer of the skin. Although the waves have less attenuation in the tissues at 13 MHz and 27 MHz, most of the incident waves at these frequencies are reflected out of the body. This means less energy absorbed in the tissues from a very low initial coupling into tissues. At the microwave frequencies 2.45GHz and 10GHz, the amount of power reflected at the skin boundary are lower. Hence, there are more power coupled into the tissues but the waves are highly attenuated inside the tissues. The power level decreases rapidly with increasing tissue depth as most of the power is absorbed by the tissues. This gives a very low penetration depth of 1-2 cm into tissues. If the embedded device is assumed to be located close to the blood vessel, the best frequency for energy transfer would be the

100 MHz. The 100 MHz frequency provides 20% incident wave power at 1.5 cm depth with lower absorption in the skin and fat layers compared to 915MHz.

In order to reduce the incident wave reflected out of the body, the incident waveguide may be filled with low loss dielectrics. An example is a water-filled waveguide used in direct contact with skin. Water has a relative permittivity value of approximately 80. The impedance of water (42 Ohms) is closely matched to the skin impedance range (10-70 Ohms) in comparison to the impedance of free space (377 Ohms). Figure 4.8 below shows the results of the wave propagation in tissues for various ISM frequencies using a water-filled waveguide.
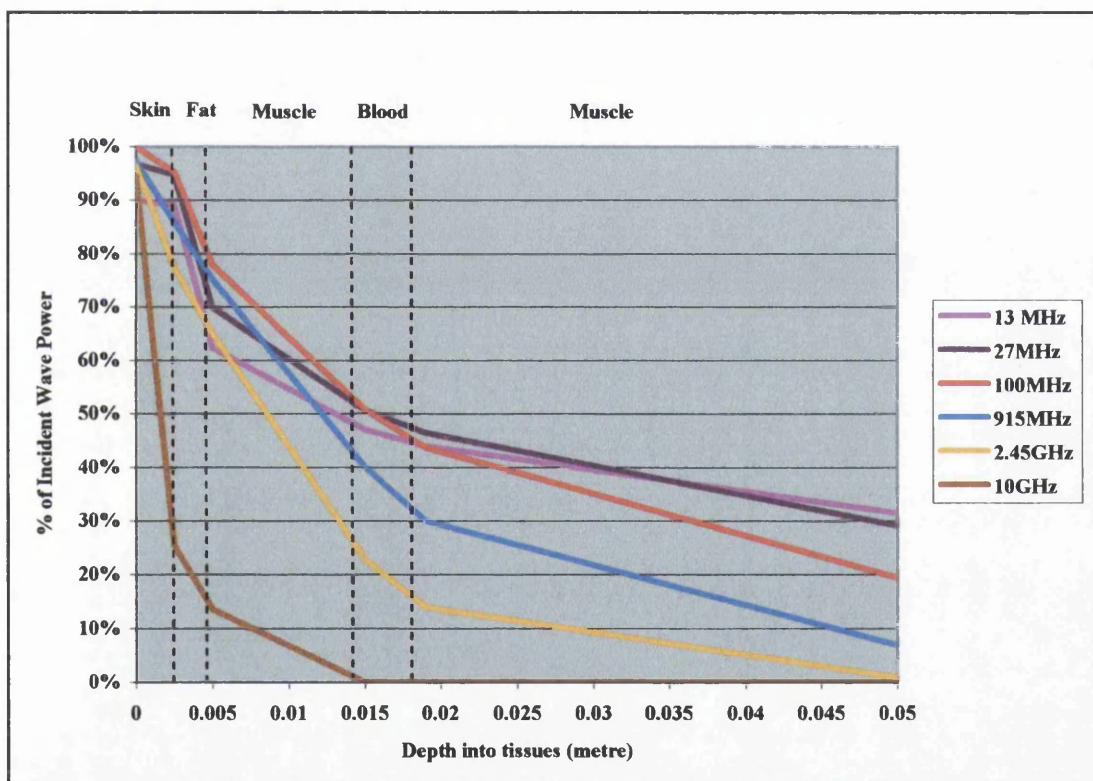
Figure 4.8: Power transmitted as a function of tissue depth from water into tissues

The wave propagation model shows a significant increase in the initial coupling power and very little power is being reflected out of the body. This is due to the impedance matching between the water and the layer of the skin. At lower frequencies of 13MHz and 27MHz, the waves can penetrate deeper into the tissues with less energy absorbed in the tissues. This gives higher coupling power at greater tissue depth compared to other frequencies. At microwaves frequencies, the range of penetration depths that can be achieved is still only 1cm to 3cm.

4.3 Remote Coupling Methods

Two methods to distinguish and categorise remote coupling are inductive coupling and radiative coupling. Both methods are based on two different operating principles. Inductive coupling is based upon close proximity magnetic field and radiative coupling is based upon electromagnetic waves propagation.

4.3.1 Radiative Coupling

RF systems operating in the ultra high frequency (UHF) and microwaves range make use of conventional electromagnetic wave propagation for energy transfer. Devices placed within the field are immersed in this propagating wave and receive the energy as it passes. The amount of energy available at any particular point is related to the distance from the transmitter and may be expressed as $1/d^2$ where d is the distance from the transmitter. On the contrary of a induction system, the field strength of the transmitted energy drops at $1/d^3$ depending on the orientation of the device to the transmitter.[98] In practice, the operating range is dependent on the radiated power of the transmitter, the operating frequency and the size of the receiver antenna.

The power density is not influenced by frequency but by the effective radiated power, however, the received coupled power is dependent on antenna size. The amount of energy collected is a function of the length of the receiving antenna, which in terms is related to the wavelength.

For resonant effect in the receiver, the minimum length required for a dipole antenna is half a wavelength[99] Table 4.6 shows the minimum length required for dipole antennas at UHF and microwave frequencies.

Frequency	Wavelength	½ Wavelength
433MHz	70cm	35cm
915MHz	32cm	16cm
1GHz	30cm	15cm
2.45GHz	12cm	6cm
5GHz	6cm	3cm
10GHz	3cm	1.5cm

Table 4.6: Minimum dipole length at UHF and microwaves frequency

In the UHF, the minimum length for dipole antennas range from 16cm to 35 cm which makes it impossible for practical use. Design of dipoles to operate at lower frequencies (<5 GHz) usually leads to impractical dimensions for the antenna. In the microwave region, the reasonable wavelength needed for practical application falls in between 5GHz and 10GHz. At these wavelengths, the waves are highly attenuating in tissues and have very low penetration depth into tissues. Over ninety percent of the power could be lost or absorbed in the first 2cm of the tissue, as predicted in the wave propagation model. The receiving antenna may be made physically smaller, but there are tradeoffs to reducing the antenna size, such as the reduction in the critical tuning and coupling power. Hence, this suggests that radiative coupling method is not suitable for energy transfer into tissues for the embedded device application.

4.3.2 Inductive Coupling

The basic operating principle of inductive coupling is energy transfer by the use of the magnetic field component. A small antenna of the transmitter consists of induction coils that generate a magnetic field which induces a voltage in the coils in the receiver and supplies the device with energy. The magnetic flux linkage and energy exchange occurs between the two resonant loop coils having the small but finite coefficient of coupling between them as shown in Figure 4.9. The inductive coupling method is commonly operated in the range 10-30MHz. At frequencies less than 10MHz, much higher coil currents are required, while operating at frequencies greater than 30MHz may results in increased heating of superficial tissues.[100]
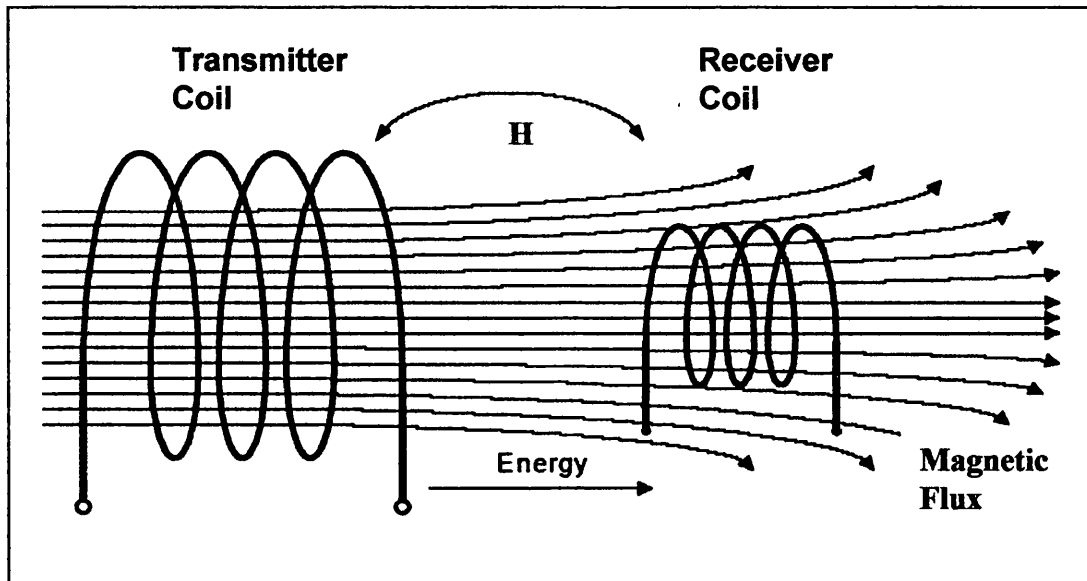
Figure 4.9: Energy transfer between two induction coils

The benefit of using a low frequency is that the energy transfer is primarily magnetic. Unlike UHF and microwave systems, the magnetic field at 10-30MHz is not absorbed by water or human tissues, which allows operation through human body. The magnetic field will penetrate human tissues with little or no loss in field strength. This is due to the fact that the relative permeability of human tissues in the body is equal to unity. Hence, it is suggested that a RF receiver device could be remotely powered while embedded inside human body.

4.3.2.1 Magnetic Field in Transmitter Coil

Ampere's law states that current flowing in a conductor produces a magnetic field around the conductor. The magnetic field produced by a transmitter circular loop coil is given by [101]

$$H = \frac{\mu_o N I A^2}{2r^3}$$
(Eq. 4.27)

where H is the magnetic field strength

μ_o is the permeability of free space

N is the number of turns of coils in loop

I is the current flowing through loop

A is the radius of loop

r is the distance from the centre of the loop

The optimum transmitter coil diameter is given by [101]

$$A = \sqrt{2}r$$
(Eq. 4.28)

where A is the radius of loop

r is the required coupling distance

The equation 4.6 shows that the magnetic field strength decays with the $1/r^3$, which means that the required transmission power decreases with $1/r^6$. The $1/r^3$ relationship has its advantageous, as the system will have a high magnetic field level in its immediate proximity but a very low level in the far field. Hence the magnetic field generated will not cause interference with other electronic devices in a distant space. The field has maximum amplitude in the plane of the loop and directly proportional to both the current and the number of turns, N. The operating region of inductive coupling systems is in the near field of the transmitter coil, which results in achievable operating distances of approximately the radius of the transmitter coil.

The inductance of a single turn circular coil is given by [101]

$$L = 0.01257(A)\left[2.303\log_{10}\left(\frac{16A}{d} - 2\right)\right]$$ (Eq. 4.29)

where A is the radius of loop

  d is the diameter of wire

The inductance of N-turn single layer circular loop coil is given by [101]

$$L = \frac{(AN)^2}{22.9A + 25.4l}$$ (Eq. 4.30)

where A is the radius of loop

  N is the number of turns of coil

  l is the length of the loop

The inductance of an N-turn multilayer circular loop coil is given by [101]

$$L = \frac{0.31\,(AN)^2}{6a + 9h + 10b}$$ (Eq. 4.31)

where A is the radius of loop

  N is the number of turns of coil

  b is the winding thickness

  h is the winding height

4.3.2.2 Induced Voltage in Receiver Coil

Faraday's law states that a time-varying magnetic field through a surface bounded by a closed path induces a voltage around the loop. The induced voltage in the loop causes a flow of current on the loop.

The induced voltage in a receiver tuned loop coil is given by [101]

$$V_o = 2\pi f NSQH \cos\theta$$ (Eq. 4.32)

where f is the frequency of the transmitter

N is the number of turns of coils in the loop

S is the area of the loop

Q is the quality factor of circuit

B is the magnetic field strength available at the loop

θ is the angle of rotation

The inductive coupling system is relatively immune to the orientation of the device with respect to the transmitter. When a transmitter coil and a receiver coil are placed in the same plane, the coupling between them will be a maximum. A rotation away from optimum alignment will therefore result in a reduction in the coupling by the cosine of angle of rotation. Table 4.7 shows the reduction in coupled energy with rotation of coil.

Angle	Coupling
0°	100 %
15°	96%
30°	86%
45°	70%
60°	50%
75°	25%
80°	17%
88°	3%
90°	0%

Table 4.7: Angle of rotation of coil with coupled energy.

As the angle turns towards 90°, there will still be coupling, even though at reduced range. In practical systems, the effect of device orientation with respect to the transmitter coil is not very critical as the transmitter coil can be placed in the same plane as the device. [102] The inherent curvature of the magnetic flux lines also assists coupling to the device under suboptimum device orientations.

4.3.2.3 Tuned Resonant Circuit

The receiver's ability to draw energy efficiently from the transmitter is based on the electrical resonance effect. To enable maximum transfer of power, the receiver should have a tuned resonant circuit. An example of a parallel resonant circuit is shown in Figure 4.10.
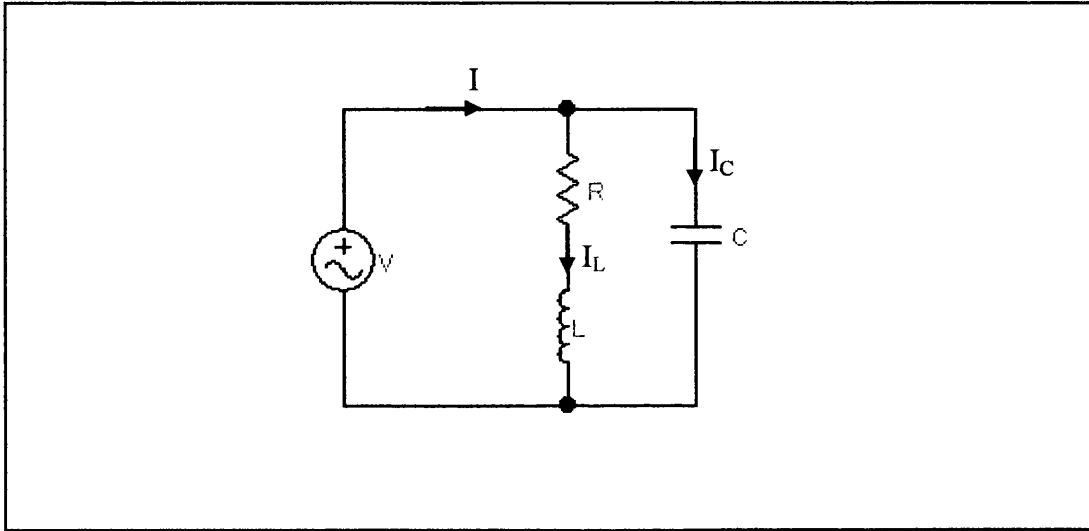
Figure 4.10: Parallel resonant circuit.

The inductor L and capacitor C are connected in parallel with the series resistance R of the coil. An alternating voltage V is applied across both L and C, and the current through the inductor is given by [103]

$$I_L = \frac{V}{\sqrt{R^2 + (2\pi fL)^2}}$$

(Eq 4.33)

The current through the capacitor is given by [103]

$$I_C = 2\pi fCV$$

(Eq. 4.34)

When the currents I_L and I_C are such that the resultant current I is in phase with the voltage, the circuit is said to be in parallel resonance. An example of a phase diagram of the resonance circuit is shown in Figure 4.11.
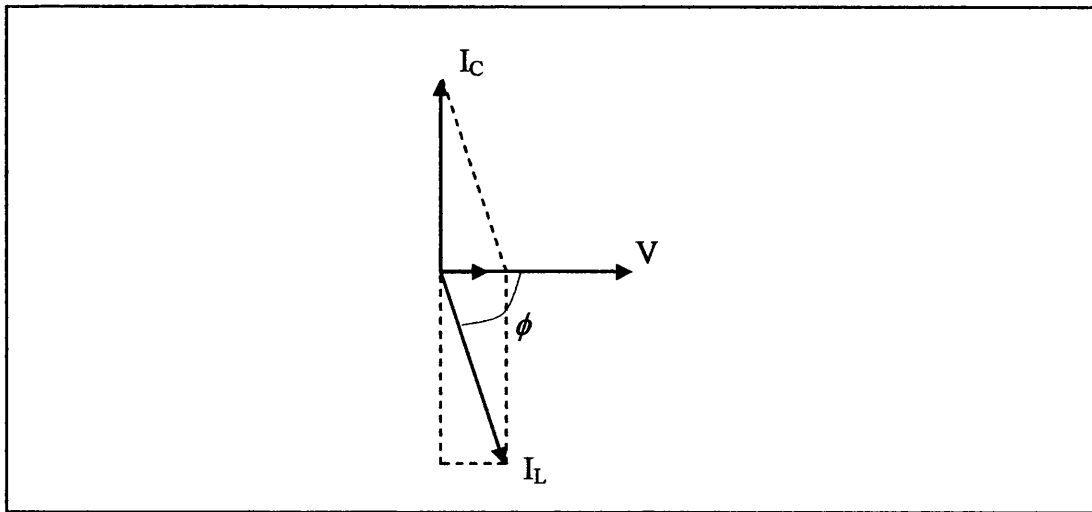
Figure 4.11: Phase diagram

When in resonance,

$$I_C = OA = I_L \sin\theta \qquad \text{(Eq 4.35)}$$

$$\text{where} \quad \sin\theta = \frac{\text{reactance of coil}}{\text{impedance of coil}} = \frac{2\pi fL}{\sqrt{R^2 + (2\pi fL)^2}}$$

Substituting equation 4.33 and equation 4.34 to equation 4.35 gives

$$f = \frac{1}{2\pi L \sqrt{\left(\dfrac{L}{C} - R^2\right)}} \qquad \text{(Eq. 4.36)}$$

If the R is small compared with $2\pi fL$, then equation 4.36 becomes [103]

$$f = \frac{1}{2\pi\sqrt{LC}} \qquad \text{(Eq. 4.37)}$$

This shows that the receiver circuit must be tuned to the operating frequency to maximize power efficiency.

The quality factor of the coupling inductor defines how well the resonating circuit absorbs power over its relatively narrow resonance band. The phase diagram in Figure 4.11 shows that when resonance occurs in parallel circuits, the current circulating in L and C will be many times greater than the resulting current. The quality factor of the circuit is given by

$$Q = R\sqrt{\frac{C}{L}}$$ (Eq. 4.38)

Figure 4.12 illustrates the effect of resistance on the quality factor of a parallel resonant circuit. At resonance, the induced RF voltage produced across the tuned circuit and delivered to the device will be few times greater than for frequencies outside of the resonant bandwidth. The resultant current in a resonant parallel circuit is in phase with the supply voltage, with the impedance given by

$$\frac{V}{I} = \frac{V}{I_c}\tan\theta = \frac{L}{CR}$$ (Eq. 4.39)
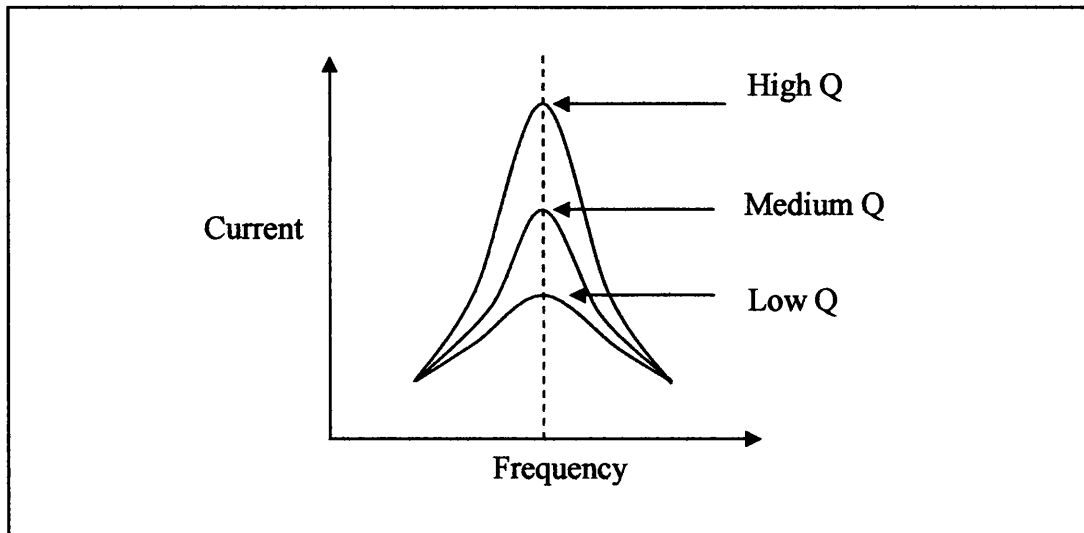
Figure 4.12: Effect of quality factor on a parallel tuned circuit

Therefore, a parallel resonant circuit is equivalent to a resistor of L/CR and is termed the dynamic impedance of the circuit.

The energy in a resonant circuit which is partly electromagnetic and partly electrostatic, is given by

$$E = \frac{1}{2}LI^2 + \frac{1}{2}CV^2$$

(Eq. 4.40)

At the moment when the capacitor is completely discharged, the energy is stored entirely in the inductor; while a quarter of a cycle later, when the current is zero, the energy is stored entirely in the capacitor. The cycle continues to change from one form to the other during the continuance of the oscillation.

4.4 Design and Evaluation of RF System

4.4.1 Transmitter and Receiver Design

The RF system consists of a RF transmitter operating at 13.56MHz and a RF receiver as shown in Figure 4.13. The advantageous of using a 13.56MHz RF system are listed as follows:

- The frequency band 13.56MHz is an ISM frequency.
- Technology widely available in the RFID security system.
- No user licenses or RF-shielded rooms required (ISM band).
- Defined and localised coupling area.
- Immunity to electrical interference.
- Attenuation effects are relatively small as magnetic field penetrates dense tissues.
- Minimal reflection effects from the human body.
- Cost effective antenna coil manufacturing.
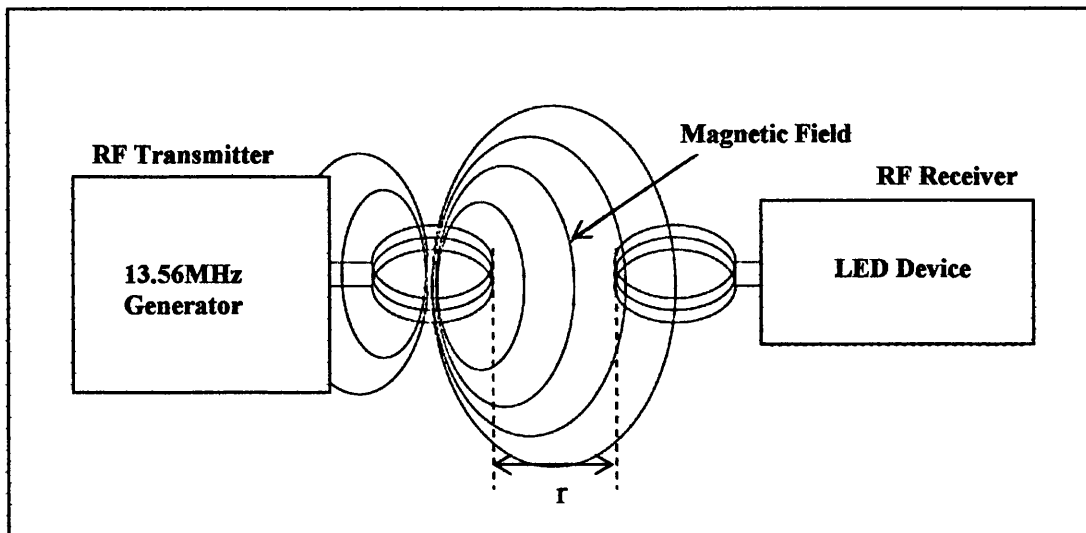
Figure 4.13: Schematic diagram of a RF system

The design of a RF system based on the 13.56MHz generator and the LED device uses equivalent electrical circuits as shown in Figure 4.14.
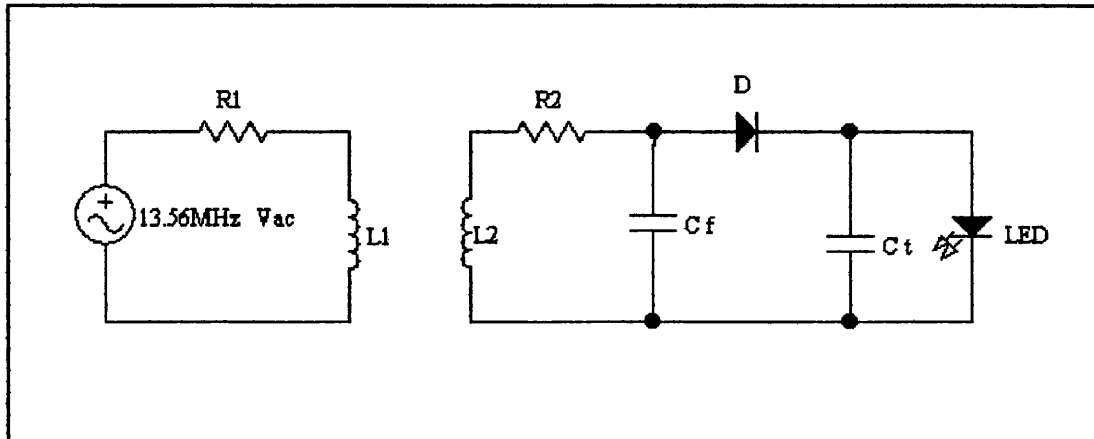
Figure 4.14: Equivalent circuits of the RF transmitter and the RF receiver

where R1, R2 is the series resistance of the coil

L1 is the transmitter circular loop coil inductance

L2 is the receiver coil inductance

C_f is the device parallel capacitance

C_t is the device tuning capacitance

D is the device diode

LED is the light source

From the equation 4.27 and equation 4.32, the parameters to optimise the maximum induced voltage in the device are:

a) Current flowing through L1 coil

b) Angle of L1 magnetic flux to L2 magnetic flux

c) Distance between L1 and L2 coils

d) Radius and number of turns of L1 coil

e) Surface area and number of turns of L2 coil

f) Quality factor of parallel resonant circuit

The 13.56MHz RF generator used in the tests was an Advanced Energy RFX-600 as shown in Figure 4.14(a). The RFX-600 is a two-stage power generator using a modular power amplifier and a switch mode dc power supply for main power and control. It is capable of 600Watts maximum output power into a 50 Ohms load.

Figure 4.14(a): Advanced Energy RFX-600 RF generator

The transmitter coils used for L1 was a 15AWG copper enamelled wire as shown in Figure 4.15. Three different loop sizes and N-turn of coils were used in the tests.

Wire diameter	1.5mm
Resistance	3.18 Ohms / 1000 feet
Insulation Coating	Polyurethane

Figure 4.15: 15AWG copper enamelled wire

The two inductors of different sizes for L2 used in the tests were 10µH ferrite core rod inductor and 10µH surface mount inductor.

a)   10µH ferrite core rod inductor ($L2_{rod}$) as shown in Figure 4.16.

Diameter	9.5mm
Length	30.5mm
Resistance	10.0mΩ

b)   10µH surface mount inductor ($L2_{sm}$) as shown in Figure 4.17.

Diameter	9.7mm
Length	5mm
Resistance	47mΩ
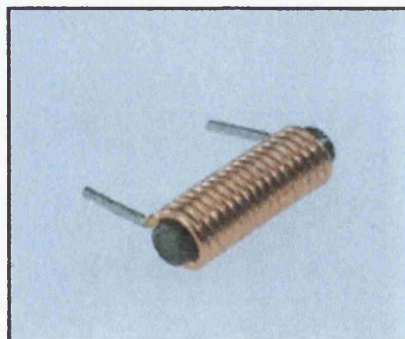
Figure 4.16: Ferrite core rod inductor.
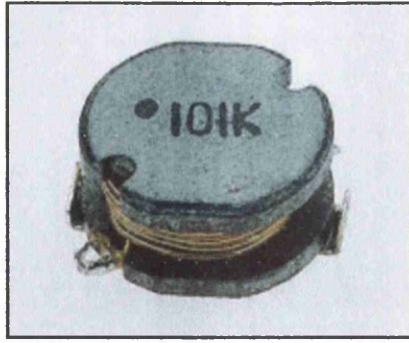
Figure 4.17: Surface mount inductor.

A sub-miniature HLMP-Q150 645nm LED was used in the receiver circuit as shown in Figure 4.18.

Length x Width x Height	2.15mm x 2.2mm x 2.15mm
Peak wavelength	645nm
Forward voltage	1.6 V
Typical forward current	1 mA
Maximum forward current	20mA
Luminous intensity	1.8mcd @ 1mA
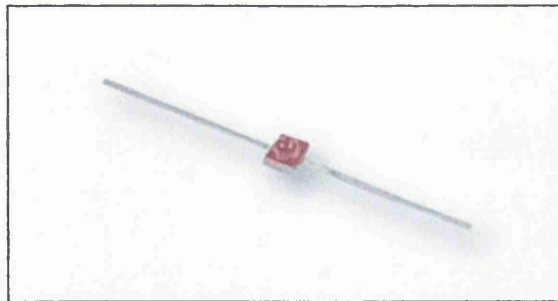
Figure 4.18: HLMP-Q150 LED.

4.4.2 Induced Voltage against Distance

Figure 4.19 below shows the equivalent electrical circuit of Test 1 setup.

where   L1 = 0.48µH   R1 = 3.84 mΩ   L2$_{rod}$ = 10µH   R2$_{rod}$ = 10mΩ

L2$_{sm}$ = 10µH   R2$_{sm}$ = 47mΩ
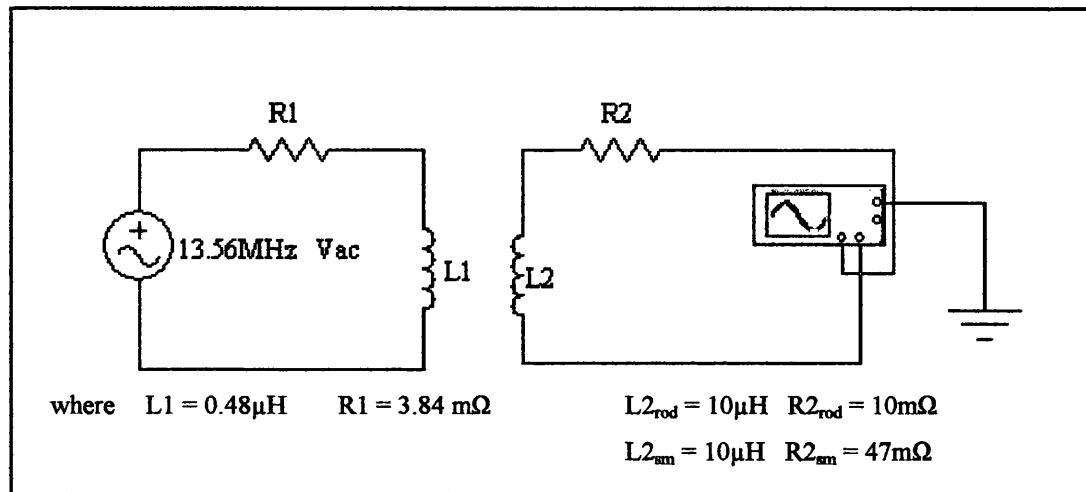
Figure 4.19: Equivalent electrical circuit of Test 1

To examine the effect of current flowing through the L1 coils, two values of transmitter powers 5W and 10 W were used. A 12cm diameter single turn circular coil was used for L1. Two different size of 10µH inductors were used for L2 namely rod inductor (L2$_{rod}$) and surface mount inductor (L2$_{sm}$). The inductor L2 positions were varied from the centre of the loop of L1 up to 10cm distance in the z-axis as shown in Figure 4.20.
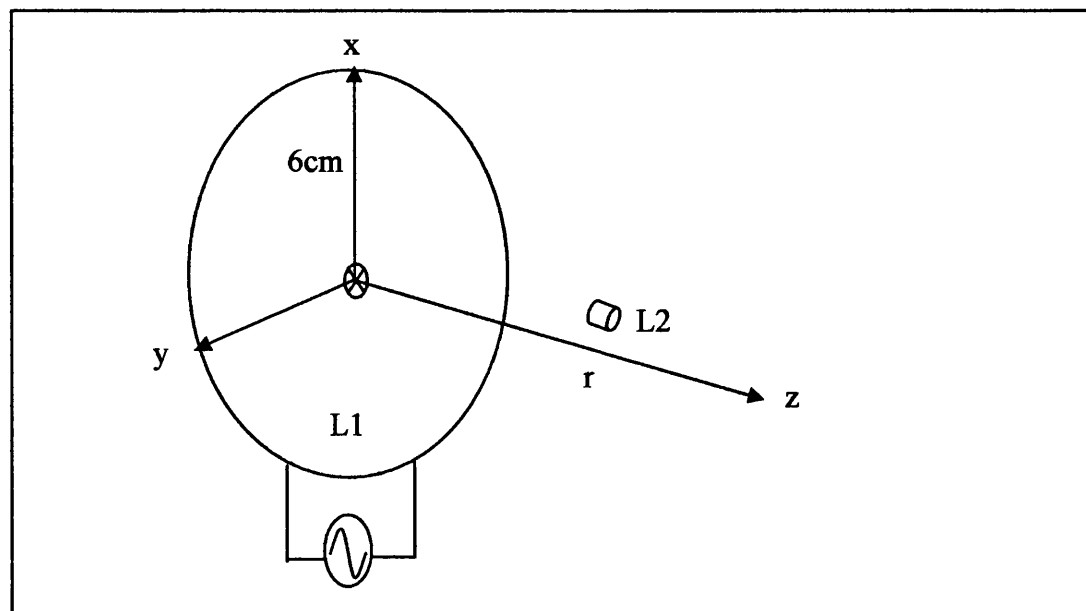
Figure 4.20: Inductor L2 positions (r) in the z-axis

The magnetic field strength produced with the 5W power was

$$H = 0.263 \text{mA/m} @ \ I_{rms} = 0.146A$$

The magnetic field strength produced with the 10W power was

$$H = 0.389 \text{mA/m} @ \ I_{rms} = 0.216A$$

The induced voltage of $L2_{rod}$ and $L2_{sm}$ were measured using an Agilent Signal Oscilloscope S4622D. Figure 4.21 and Figure 4.22 show the maximum induced voltage V_{L2} across $L2_{rod}$ and $L2_{sm}$ as a function of distance.

The first test results showed that when the transmitted power were doubled, more current flows through L1 and therefore induced voltages in $L2_{rod}$ and $L2_{sm}$ are higher. The induced voltage decays exponentially due to decrease in the magnetic field strength with distance. $L2_{rod}$ has a higher induced voltage compared to $L2_{sm}$ for the same amount of transmitted power. This is because of the greater $L2_{rod}$ surface area and length.
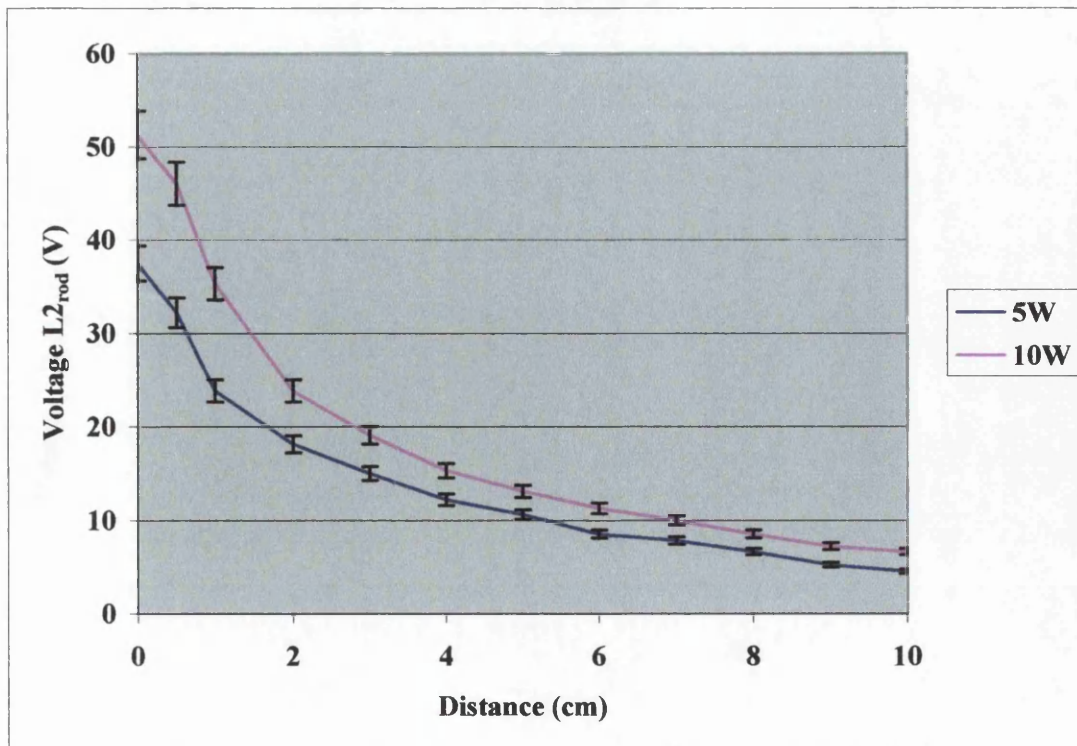
Figure 4.21: Maximum induced voltage in the rod inductor
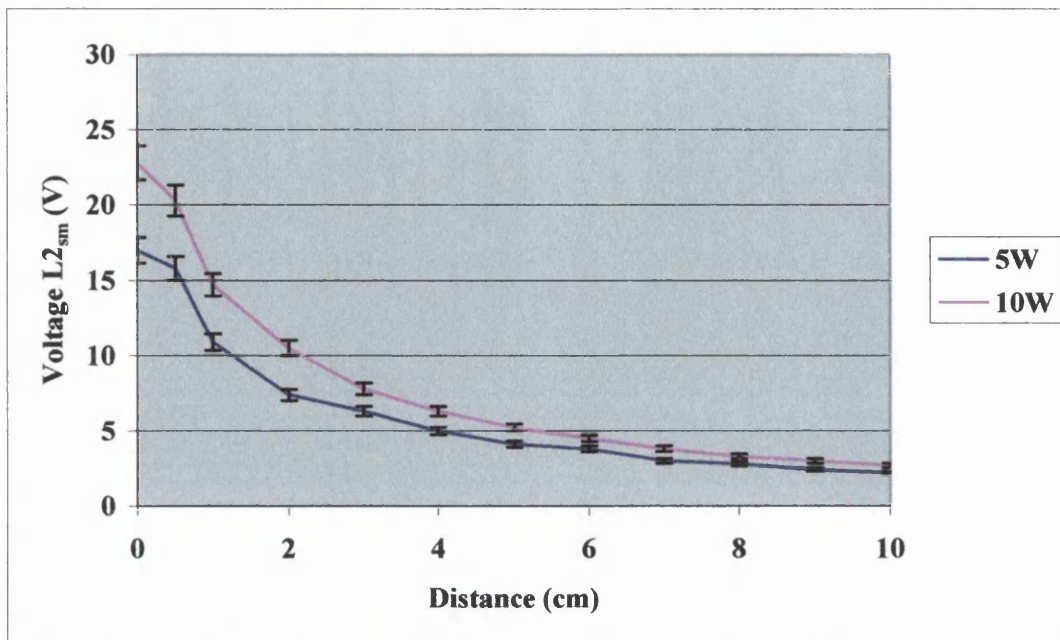
Figure 4.22: Maximum induced voltage in the surface mount inductor

To determine the effect of the angle of L1 magnetic flux to L2 magnetic flux, the orientation of L2 to L1 was adjusted and placed so that the induced voltage of L2 was at the minimum and maximum. Figure 4.23 and Figure 4.24 show the maximum and minimum induced voltage V_{L2} across $L2_{rod}$ and $L2_{sm}$ as a function of distance at 10W transmitted power.
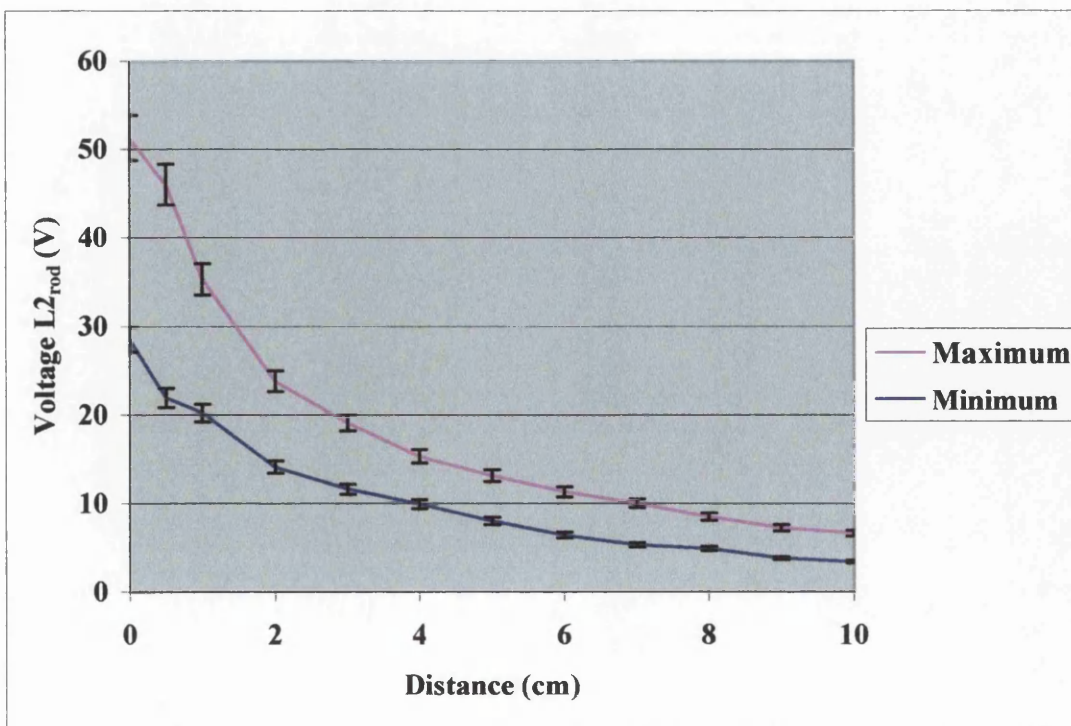
Figure 4.23: Induced voltage in the rod inductor at 10W power.
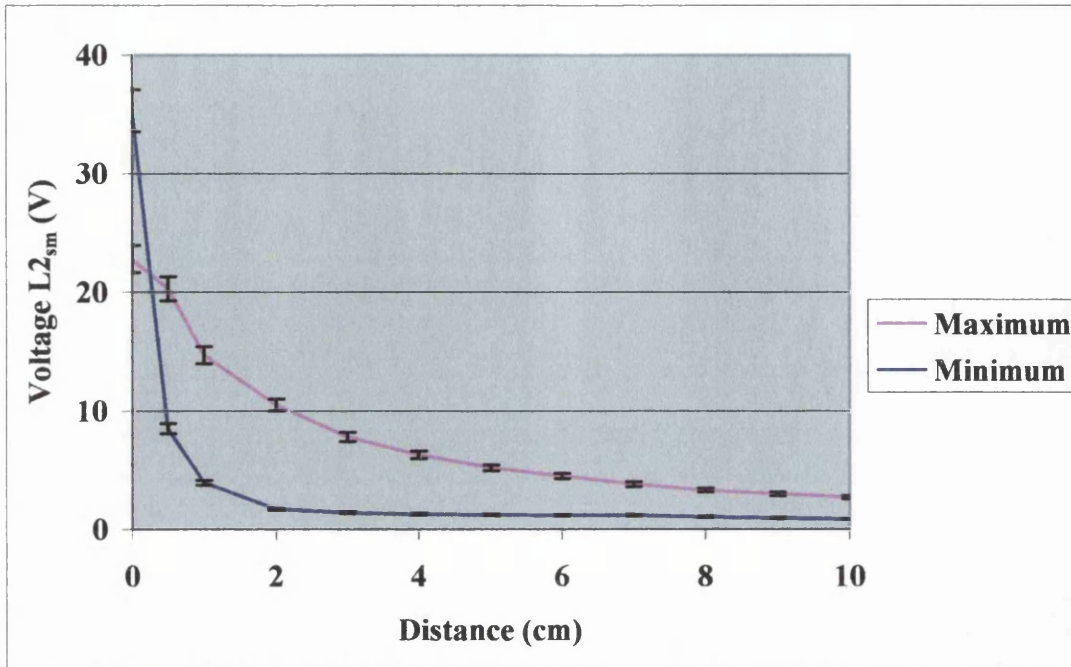
Figure 4.24: Induced voltage in the surface mount inductor at 10W power

The inductor displacement test results showed a large reduction in the induced voltage for L2 when the position of L2 was tangential to the position of L1. The maximum induced voltage is only achieved when L2 was placed parallel to the L1 magnetic flux plane.

4.4.3 Generated Current against Distance

Figure 4.25 below shows the equivalent electrical circuit of Test 2 setup.

where $L1 = 0.48\mu H$ $R1 = 3.84\ m\Omega$ $L2_{rod} = 10\mu H$ $R2_{rod} = 10m\Omega$

                                                 $L2_{sm} = 10\mu H$ $R2_{sm} = 47m\Omega$
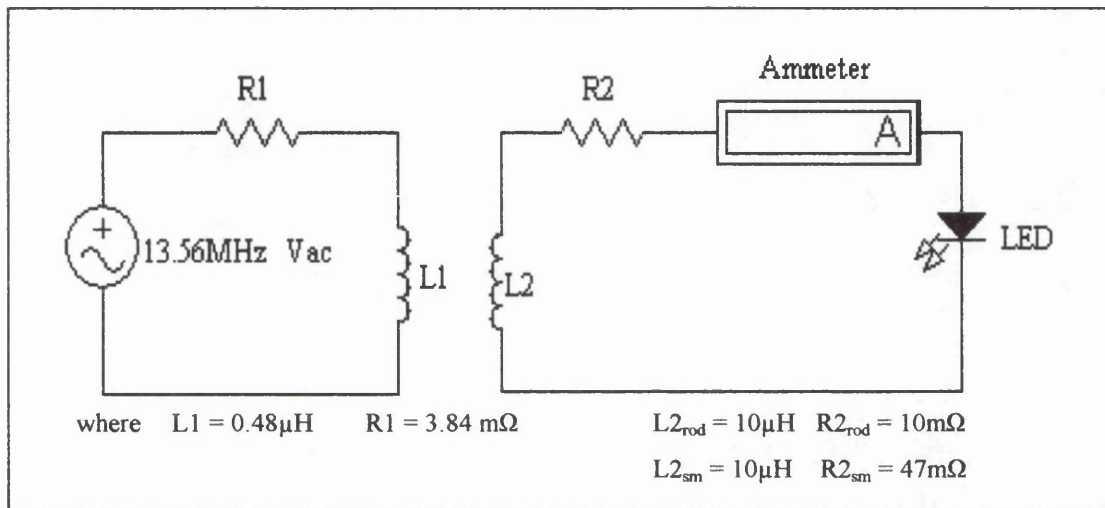
Figure 4.25: Equivalent electrical circuit of Test 2

To determine the minimum power requirement of the transmitter to generate 1mA of current into the LED, the range of 1-50W transmitter powers were used. The current flowing through the LED was measured using an ammeter. Figure 4.26 and Figure 4.27 show the LED current for $L2_{rod}$ and $L2_{sm}$ as a function of transmitter power at the distance of 1-3cm.
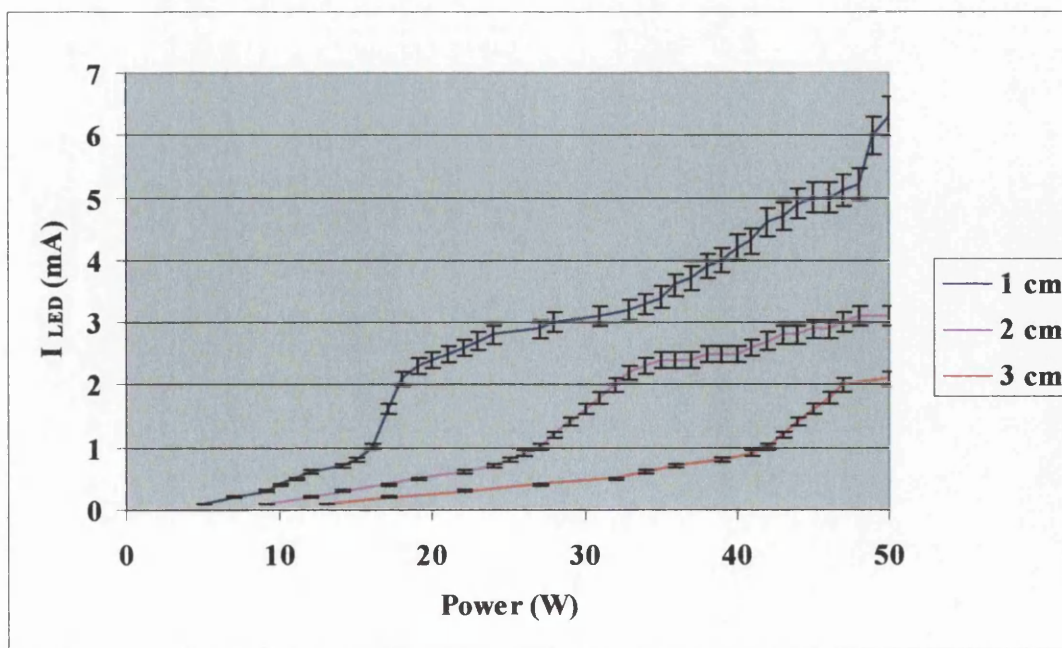
Figure 4.26: LED current vs. transmitter power for $L2_{rod}$
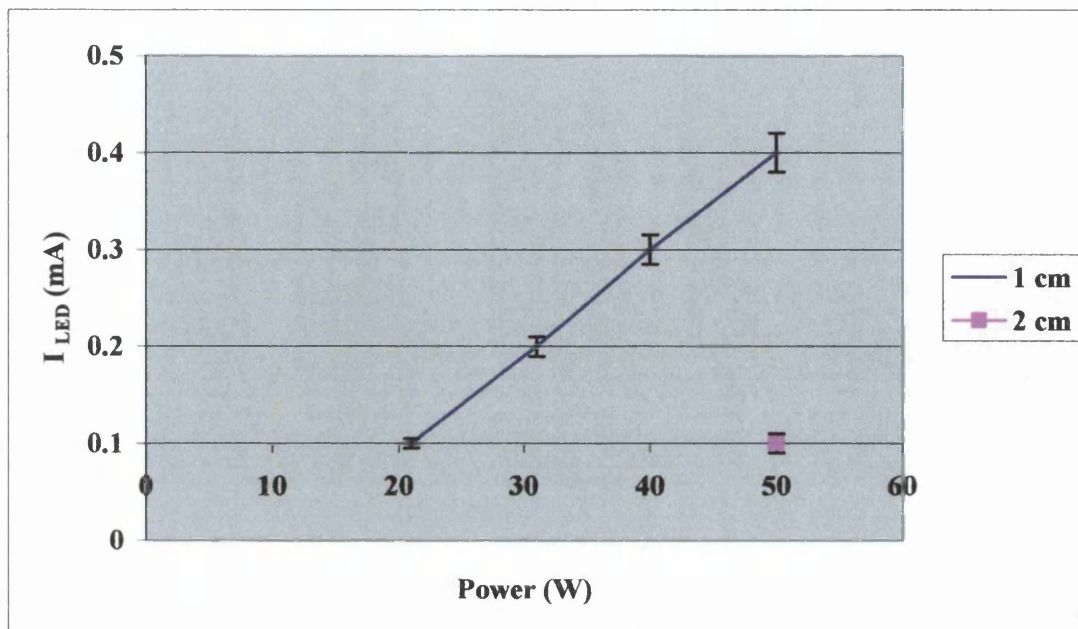
Figure 4.27: LED current vs. transmitter power for L2$_{sm}$

The second test results showed that the power required for L2$_{rod}$ to provide 1mA current into LED at 1cm distance is 16W. At 2cm distance, the power needed increases to 27W. The maximum distance allowable for LED operation is 4cm at 50W transmitted power. For the L2$_{sm}$, the highest LED current attainable from 1cm distance is 0.4mA at 50W transmitter power. This is because of the higher resistance and less induced voltage across L2$_{sm}$.

4.4.4 Induced Voltage in RLC against Distance

A parallel resonant circuit (RLC) with a resonant capacitor C_f , a tuning capacitor C_t and a diode were added to the receiver circuit. Figure 4.28 shows the equivalent electrical circuit of Test 3 setup.

The resonant circuit was connected to an oscilloscope and the tuning capacitor was tuned while observing the signal amplitude on the oscilloscope. The tuning was stopped at the maximum voltage. Figure 4.29 show the maximum induced voltage across C_t as a function of distance at 10W transmitted power.
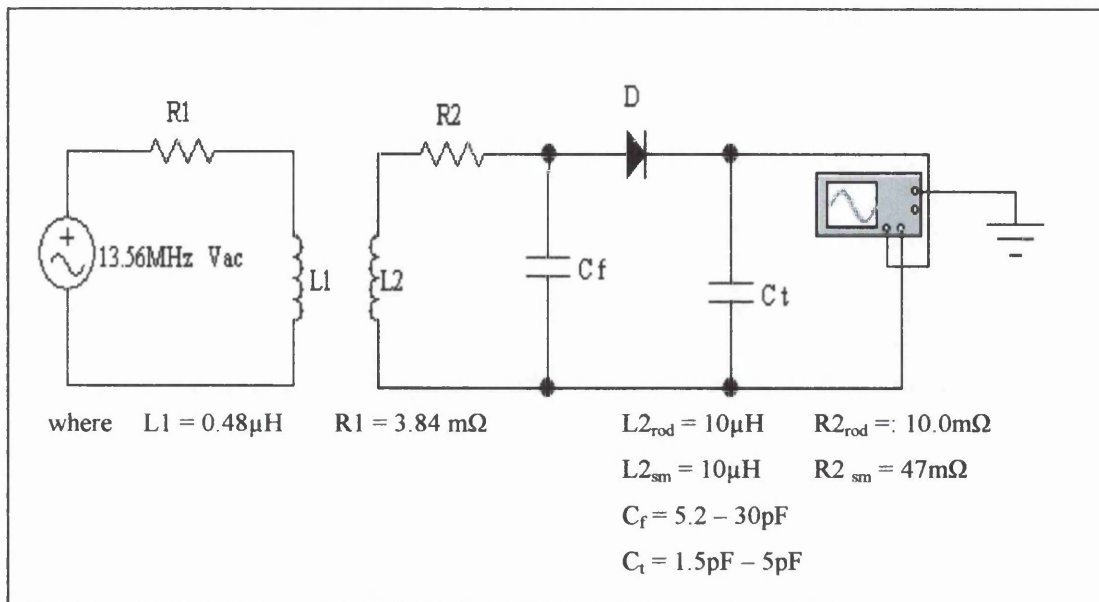
Figure 4.28: Equivalent electrical circuit of Test 3

where L1 = 0.48µH   R1 = 3.84 mΩ   L2$_{rod}$ = 10µH   R2$_{rod}$ =: 10.0mΩ

L2$_{sm}$ = 10µH   R2$_{sm}$ = 47mΩ

C$_f$ = 5.2 – 30pF

C$_t$ = 1.5pF – 5pF
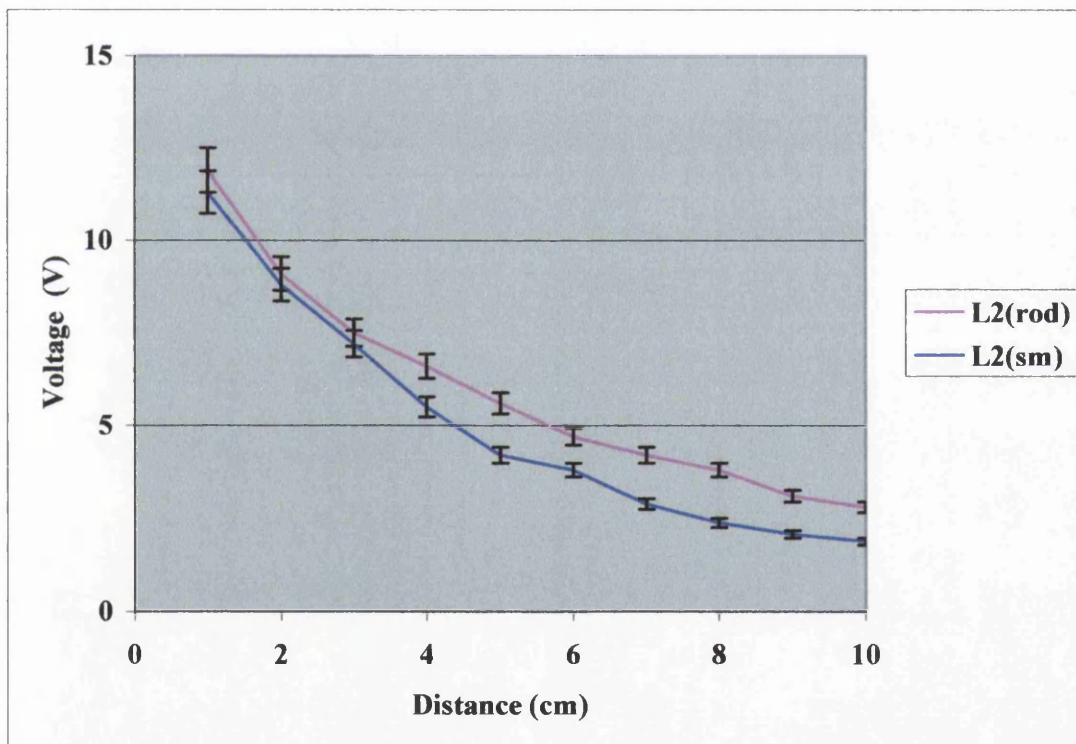
Figure 4.29: Induced voltages for L2$_{rod}$ and L2$_{sm}$ at 10W power

The third test results showed that the induced voltages for L2$_{rod}$ and L2$_{sm}$ decay with distance. Again, the voltage induced in the L2$_{rod}$ is higher than the L2$_{sm}$ because the L2$_{rod}$ has a larger surface area and length.

4.4.5 Generated Current in RLC against Distance

Figure 4.30 below shows the equivalent electrical circuit of Test 4 setup.

where   L1 = 0.48μH   R1 = 3.84 mΩ $L2_{rod} = 10μH$ $R2_{rod} =: 10.0mΩ$

$L2_{sm} = 10μH$ $R2_{sm} = 47mΩ$

$C_f = 5.2 – 30pF$

$C_t = 1.5pF – 5pF$
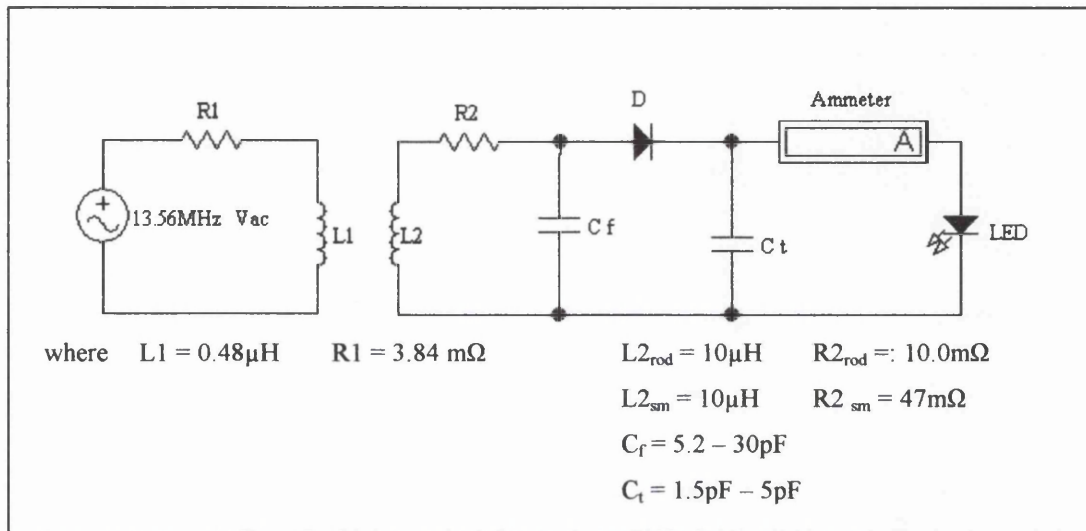
Figure 4.30:   Equivalent electrical circuit of Test 4

To compare the power requirement of the transmitter to generate 1mA current in the LED of a resonant circuit (RLC) and a non-resonant circuit (non-RLC), the range of 1-50W transmitter powers were used. The current flowing through the LED was measured using an ammeter. Figure 4.31 and Figure 4.32 show the LED current at resonance and non-resonance for $L2_{rod}$ and $L2_{sm}$ as a function of power.
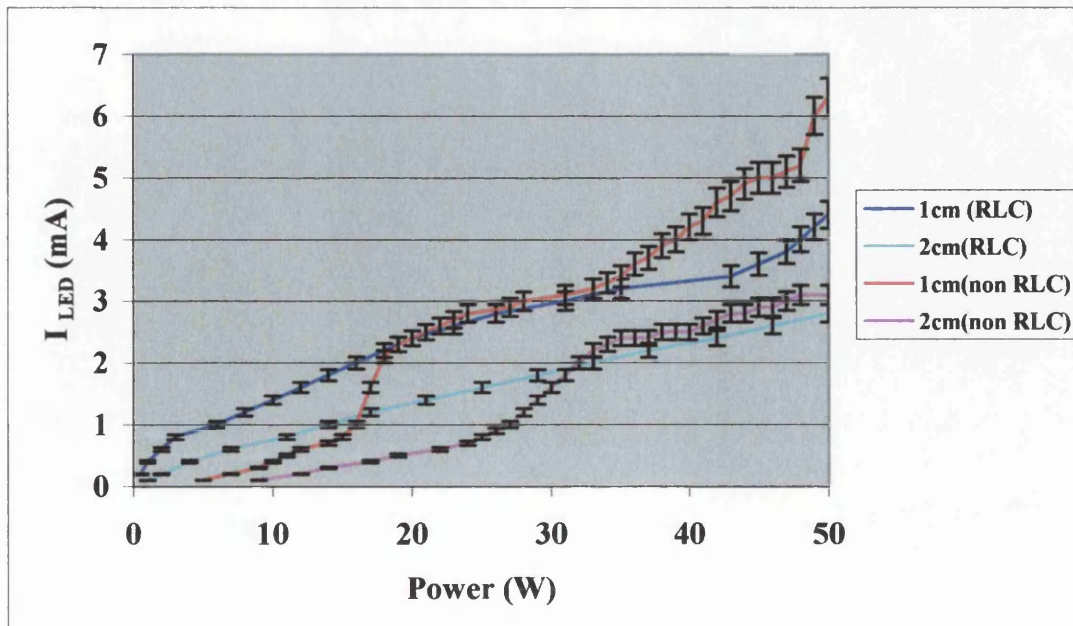
Figure 4.31: LED current for $L2_{rod}$ in the resonant and non-resonant circuits.
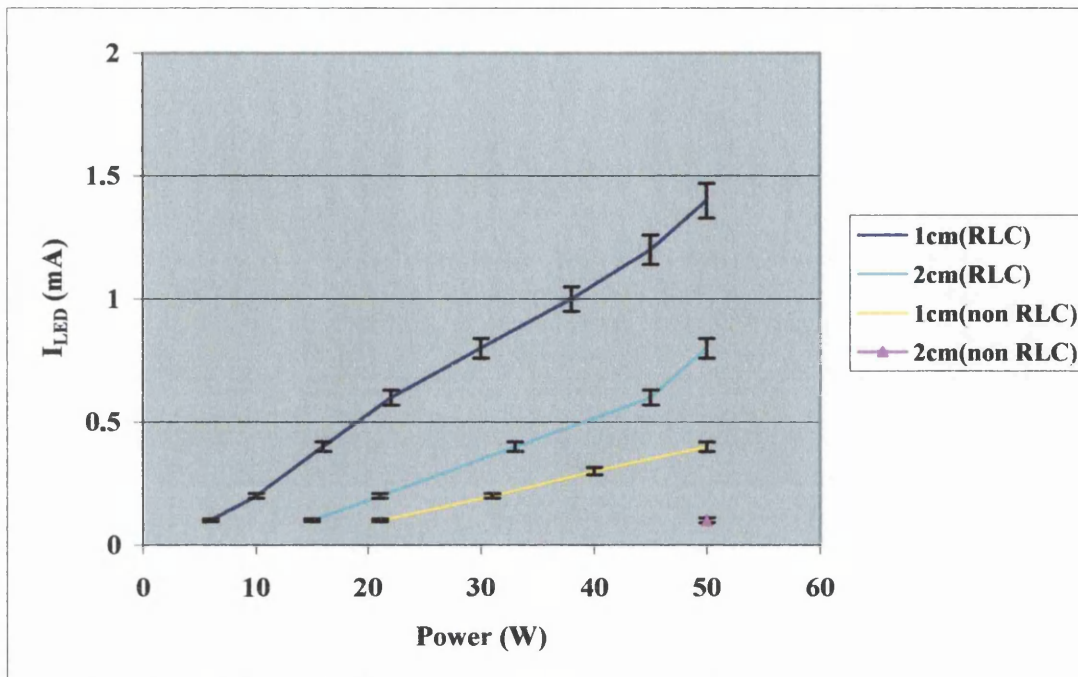
Figure 4.32: LED current for $L2_{sm}$ in the resonant and non-resonant circuits.

The fourth test results showed that less power is required to provide 1mA current into LED with resonant circuit compared to non-resonant circuit at a fixed distance. This is because the quality factor of the parallel resonant circuit increases the current available in the capacitor.

4.4.6 Effects of Transmitter on Induced Voltage

The same setup of Test 3 was used in this Test 5 with the use of three different L1 configurations. The three L1 configurations that were used to investigate the effects of the transmitter on the L2 induced voltage were

a) 12cm diameter single turn circular coil ($L1_{12} = 0.48\mu H$)

b) 6cm diameter single turn circular coil ($L1_6 = 0.22\mu H$)

c) 12 cm diameter 3-turn circular coil ($L1_{12a} = 2.18\mu H$)

Figure 4.33 and Figure 4.34 show the maximum induced voltage in $L2_{rod}$ and $L2_{sm}$ for three L1 configurations.
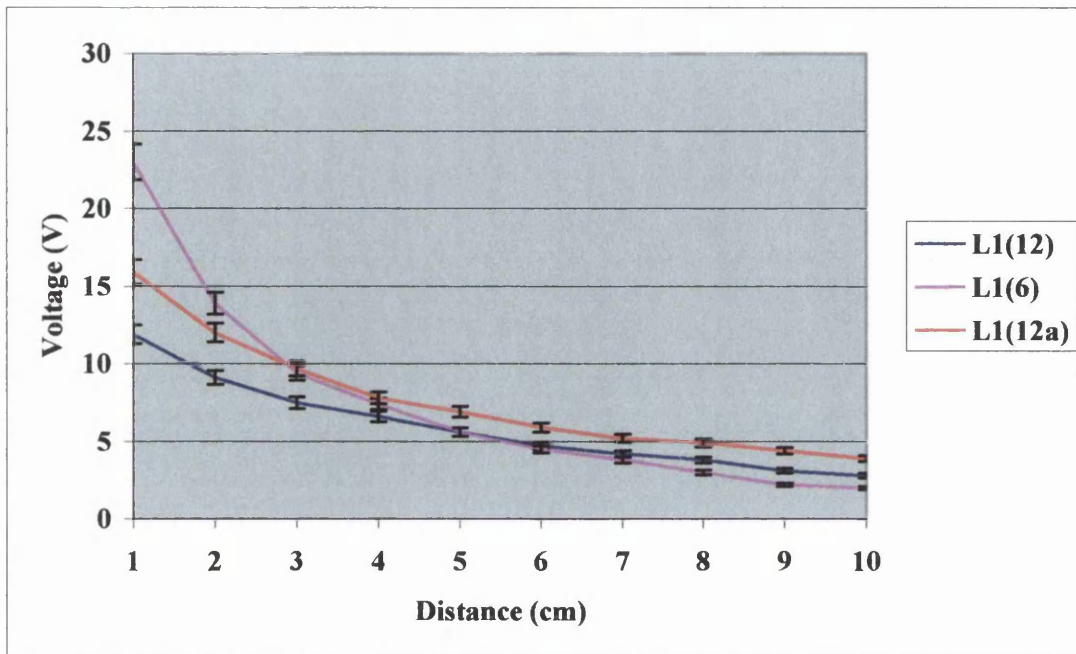
Figure 4.33: Induced voltage in L2$_{rod}$ at 10W power.
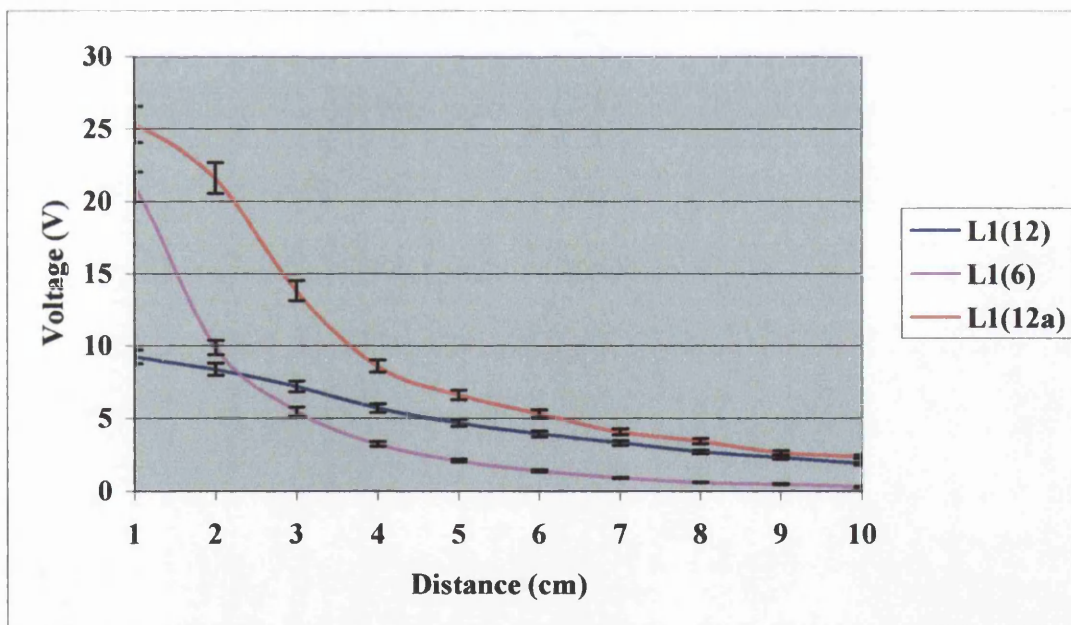
Figure 4.34: Induced voltage in L2$_{sm}$ at 10W power.

The fifth test results showed that L1$_{12}$ was best coupled with L2$_{rod}$ and L2$_{sm}$ at distance up to 3cm. Beyond 3cm distance, the use of L1$_{12a}$ generates a higher induced voltage than L1$_{12}$ and L1$_6$. The L1$_{12a}$ induced the highest voltage over the entire 10cm distance in the L2$_{sm}$ .This showed that the radius of L1 determined the optimum operating distance of L2. The increase in number of turns of L1 coil also helped to increase the induced voltage in L2.

114

Next, the identical setup of the Test 5 was used in the transmitter y-axis test. In this test, the inductor L2 positions were varied inside the L1 loop from the centre of the loop (0cm) to the outer circle of the loop in the y-axis as shown in Figure 4.35.
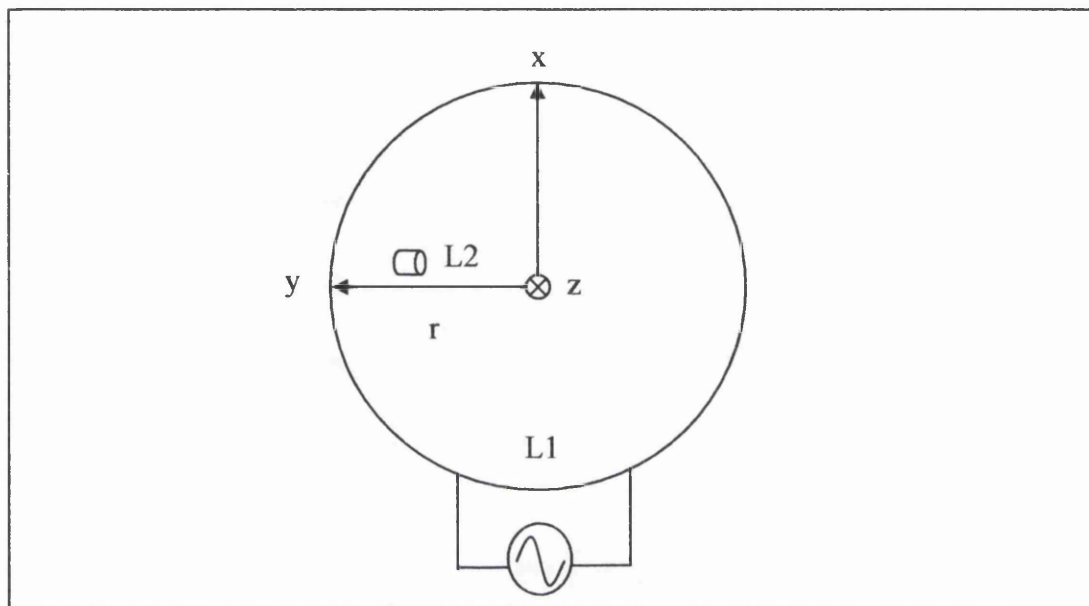
Figure 4.35: Inductor L2 positions (r) in the y-axis.

Figure 4.36 and Figure 4.37 show the maximum induced voltage in $L2_{rod}$ and $L2_{sm}$ for three L1 configurations.
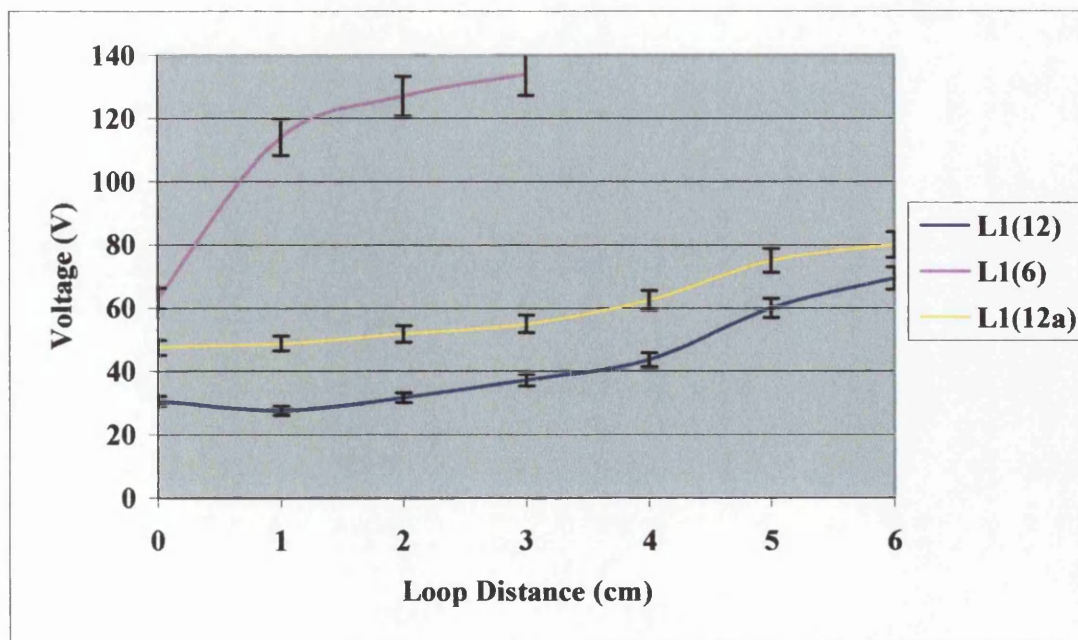
Figure 4.36: Induced voltage in $L2_{rod}$ at 10W power.
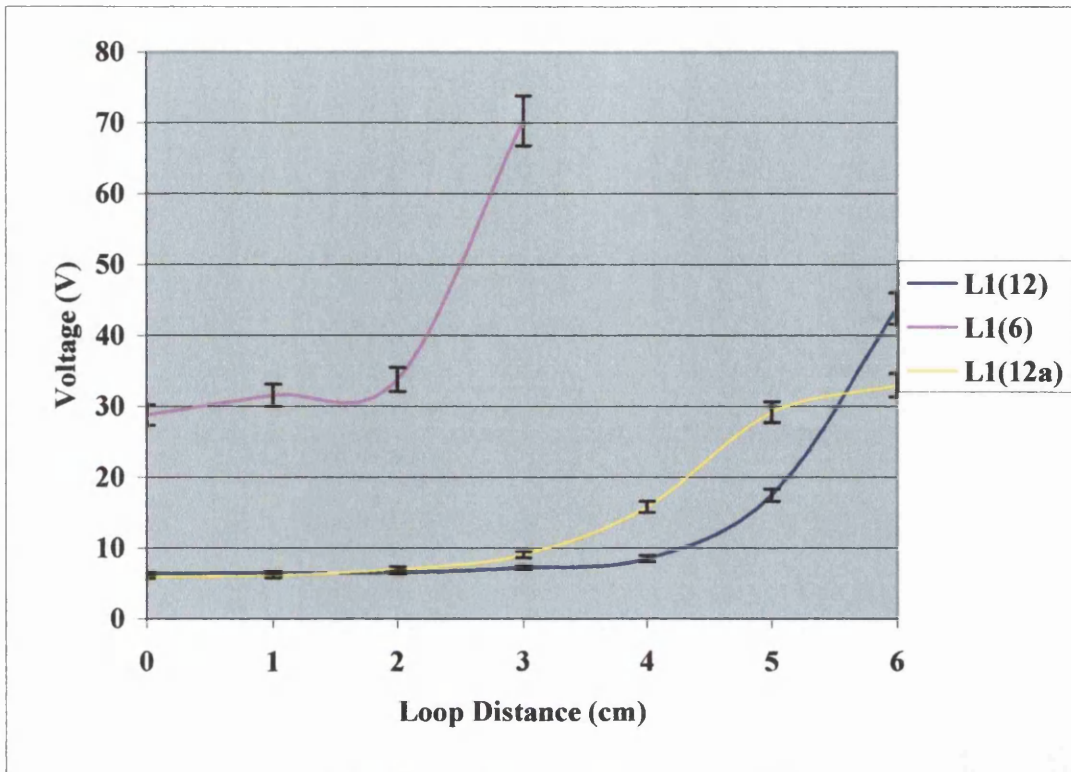
Figure 4.37: Induced voltage in $L2_{sm}$ at 10W power.

The curves of Figure 4.30 and Figure 4.31 showed that L2 induced voltage increases when the L2 was positioned nearest to the outer loop of L1. This means that at the centre of the loop, the magnetic field is the weakest. The $L1_6$ induced the highest voltage throughout the loop distance as the magnetic flux was more concentrated due to area of $L1_6$ being smaller. $L1_{12}$ and $L1_6$ had a lower induced voltage in the centre of the loop and the outer loop which suggest that increasing the loop size could cause the magnetic field in the centre of the loop to drop to zero. Hence, this test showed that the inductor position in the transmitter y-axis produce a higher voltage than the inductor position in the transmitter z-axis. This suggests that transmitter loop coil could be wrapped around the human hand or the human leg to couple the magnetic field energy into tissue for embedded photodynamic therapy.

4.4.7 Effects of Bacon Tissue on Induced Voltage

The next test was to examine the effect of tissue on the coupled magnetic field and the induced voltage. The transmitting coil L1 and the receiver coil L2a were positioned 3cm apart. The induced voltage across the air was recorded as the air reference level. Next, a bacon tissue of 2cm thickness was placed in between L1 and

L2a. The induced voltage across the bacon was recorded. It was observed that the induced voltages across the air and across the bacon have the same voltages. This showed that the bacon tissue has no effect on the induced voltage and therefore, does not absorb the magnetic field energy. These finding suggest that the magnetic field energy is able penetrate deeply into tissues without the attenuation losses.

4.4.8 Summary of the RF System

The techniques to generate maximum magnetic field strength at the transmitter coil are:

- The optimum coil diameter of the transmitter coil should be two times the coupling distance between transmitter and receiver for maximum magnetic flux density.

- The wire used in transmitter coil should be low resistance wire to allow maximum current flowing through the coil.

- The increase in number of turns of transmitter coil increases the magnetic field coupled into the receiver.

- The centre of the transmitter coil should be placed at the receiver and parallel to the receiver for efficient coupling.

The methods to induce maximum voltage in the receiver and to reduce the dimension of the receiver are:

- When higher operating frequency is used for the transmission, the size of the receiver coil could be reduced considerably.

- The length and the diameter of the receiver coil should be chosen to the smallest dimension required as possible.

- The transmitter power can be controlled to compensate for the low induced voltage in a smallest receiver coil size.

- The capacitor and inductor values must be tuned to the operating frequency for resonance in the circuit.

- The quality factor of resonant circuit increases the current available to the LED very much.

- The LED and the capacitor could be added into an integrated chip that has a very small silicon area.

The RF investigational tests carried out clearly suggests that, the use of inductive coupling principle is an efficient method to couple energy into the human body to power the embedded LED device without the attenuation losses in tissues..

4.5 Design and Evaluation of Microwave System

The microwave system consists of a microwave generator, a network analyser and an input-output test set. The microwave generator is a Wiltron 68137A Sweep Generator with frequency range of 2 GHz to 20 GHz and maximum output power of +13dBm. The network analyser is a Wiltron 360B Vector Network Analyser. The Wiltron equipments used are shown in Figure 4.38 and the equivalent circuit diagram is shown in Figure 4.39.
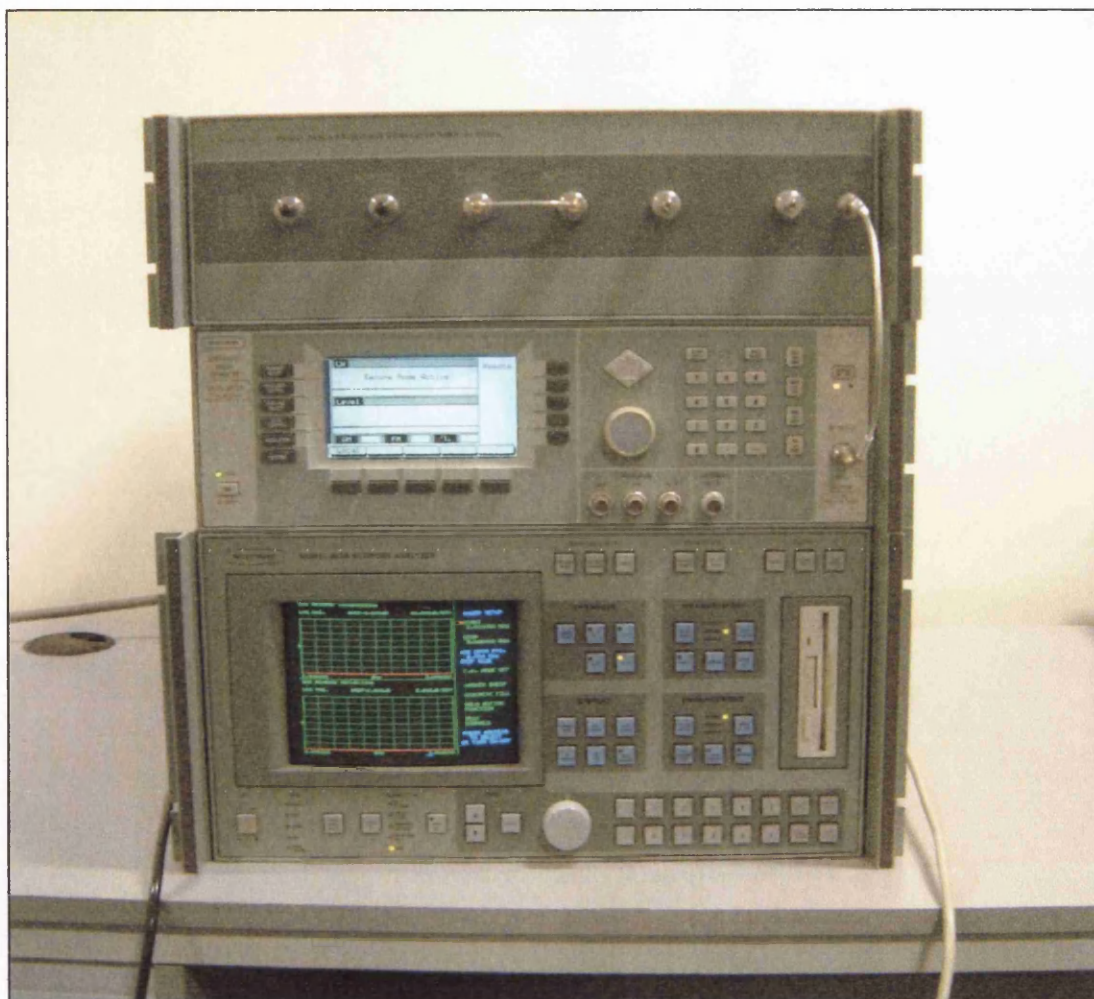
Figure 4.38 Wiltron microwave equipments.
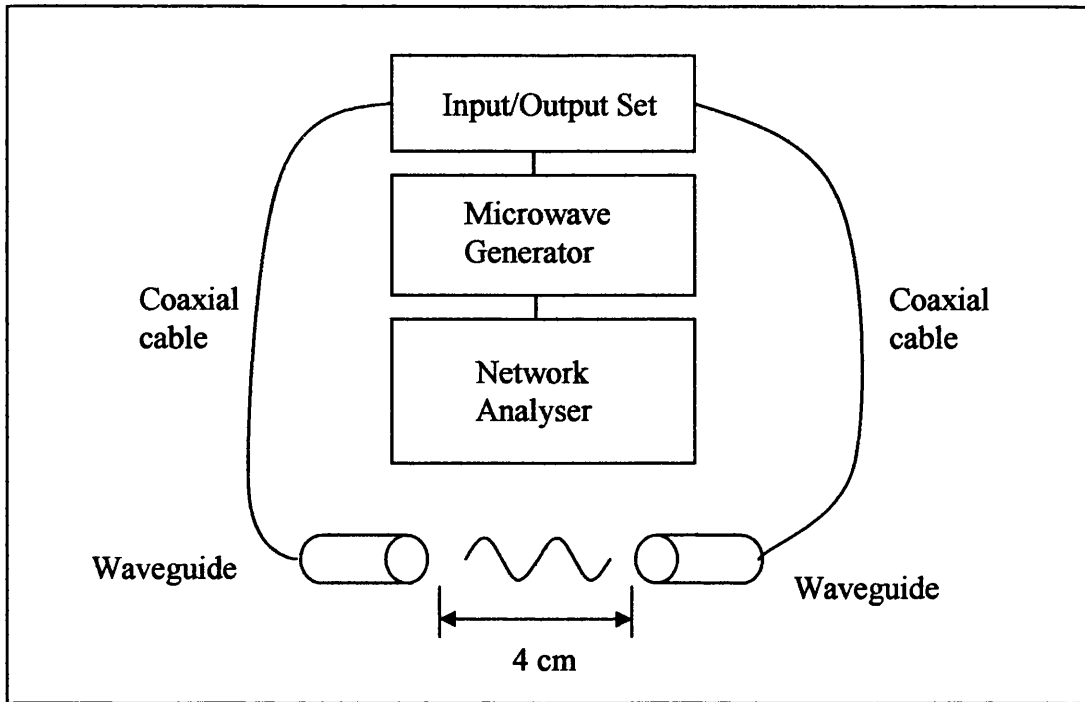
Figure 4.39 Equivalent circuit diagram of a microwave system.

Three different types of animal tissues that were used in the analyses are

a)   Chicken Skin

b)   Bacon

c)   Ham

The wavelengths that were used for the analyses range from 2.55GHz to 3GHz. The source power of the microwave generator was set at 5dBm or 3.16mW. Both of the waveguides were cylindrical tubes with 3cm monopoles to match a cut-off frequency of 2.5GHz. The waveguides were separated at 4cm distance apart. Then, the animal tissues were placed in between the waveguides. The attenuation losses in the tissues were measured using the Wiltron network analyser.

4.5.1 Attenuation against Frequency for Chicken Skin Tissue

In this analysis, a 1mm thickness fresh chicken skin was used. Firstly, the measurements of the power across the air were taken as the reference level. Next, a slice of chicken skin was placed in between the waveguides and the microwave power across the skin was measured. Figure 4.40 shows the attenuation in the chicken skin as a function of frequency.
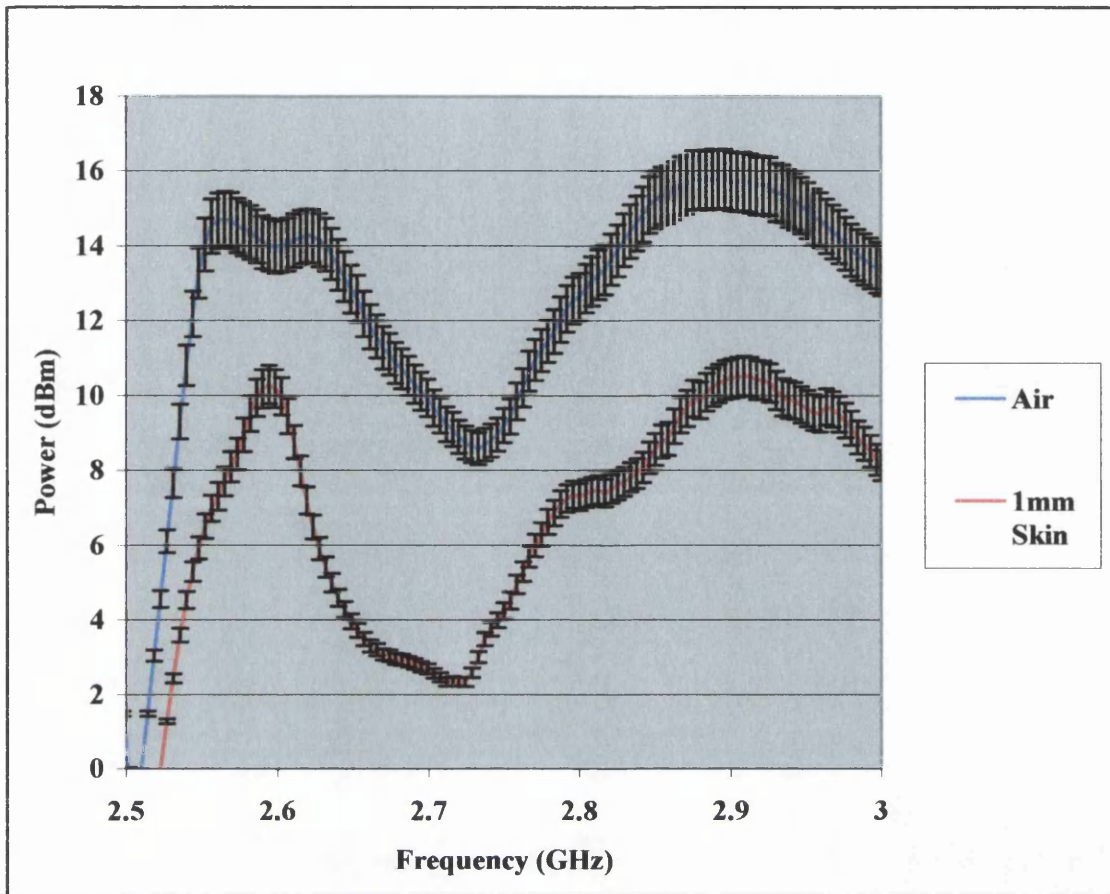
Figure 4.40: Attenuation in the chicken skin as a function of frequency.

The results showed that the microwave power diminish through the skin and vary with frequencies. At 2.6GHz, there was a loss of -3.727dBm or -57.6% reduction of power. The impedance mismatch between the air and skin causes most of the incident microwave power being reflected at the skin surface. The results were comparable with the RF propagation model which predicted -57% loss of power in a 1mm human skin. The reflection loss at the skin-air surface was assumed to be 45% of the incident microwave power.

The microwave power available at a thickness x in the tissue is given by [95]

$$P(x) = (P_o - P_r)\exp(-2\alpha x) \qquad \text{(Eq. 4.41)}$$

where $P(x)$ is the power at thickness x

P_0 is the power of the incident microwave at thickness $x = 0$

P_r is the power reflected

α is the attenuation coefficient

121

An estimate for the attenuation coefficient of a chicken skin at 2.6GHz frequency was calculated by using equation 4.41, to be

$$P(0.1) = 0.424 = (1 - 0.45)\exp(-2 * 0.1 * \alpha) \qquad \text{(Eq. 4.42)}$$

$$\alpha = 1.30\text{cm}^{-1} \pm 0.21$$

4.5.2 Attenuation against Frequency for Bacon Tissue

In this investigation, four slices of fresh bacon were used with each slice has an average thickness of 4mm. The measurements of power across the air were taken as reference level. Next, a slice of bacon was placed in between the waveguides and power measurements were taken. Subsequently, another slice of bacon was added and the power measurements were repeated. This process continued until four slices of bacon were used up. Figure 4.41 shows the attenuation in the bacon as a function of frequency.
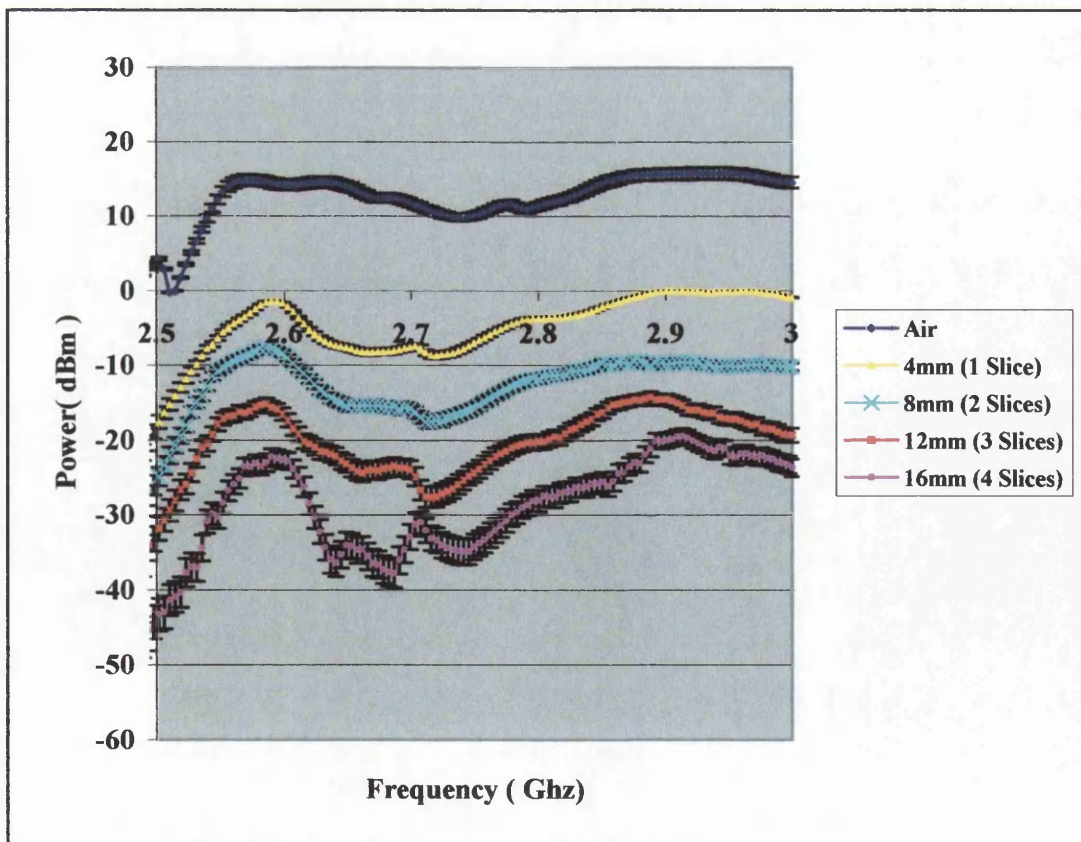
Figure 4.41 Attenuation in the bacon as a function of frequency.

The results of Figure 4.42 showed that the power loss increases exponentially with the increasing bacon thickness. At 2.6GHz, the power loss in the 4mm bacon was -16.335dBm. The power loss increased to -23.918dBm in the 8mm bacon. The power reflected at the bacon-air surface was calculated to be 87.3% of the incident microwave power using linear regression line analysis. The attenuation coefficient of a bacon at 2.6GHz was calculated by using equation 4.41, to be

$$P(0.4) = 0.0233 = (1 - 0.873)\exp(-2 * 0.4 * \alpha) \qquad \text{(Eq. 4.43)}$$

$$\alpha = 2.12 \text{cm}^{-1} \pm 0.24$$

The results of the power loss in the bacon as a function of bacon depth are shown in Figure 4.42. The curves showed that almost 90% of the incident microwave power was absorbed at the 4mm depth. Hence, at these microwave frequencies, the penetration depth is only limited to 4mm thickness.
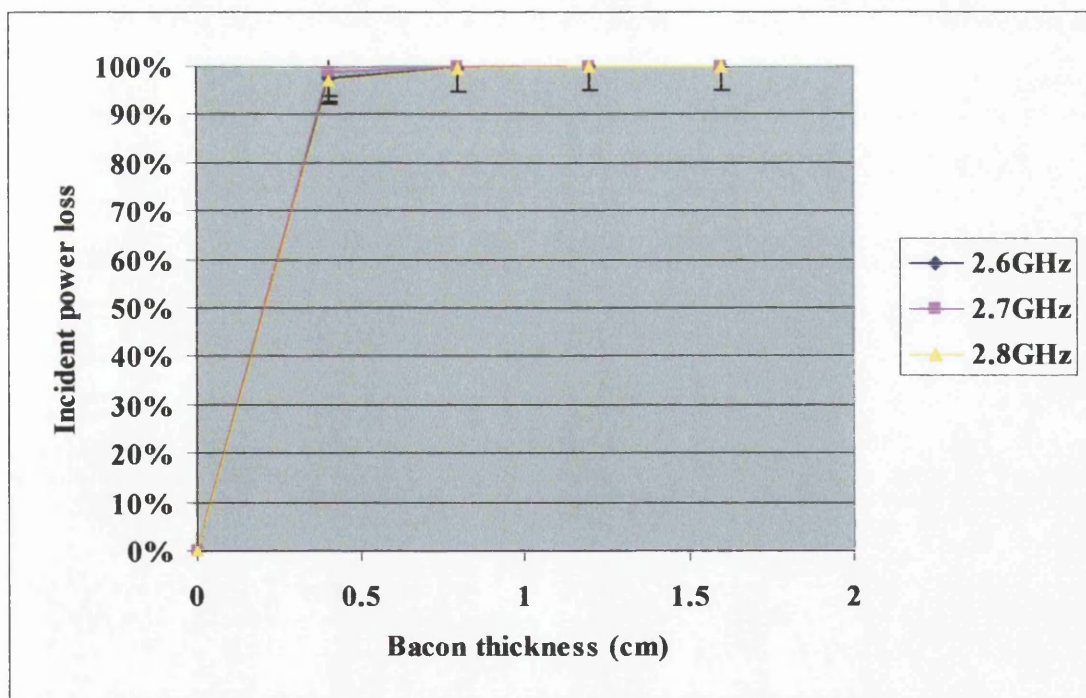
Figure 4.42 Power loss in the bacon as a function of bacon thickness.

4.5.3 Attenuation against Frequency for Ham Tissue

Next, the analysis of attenuation in the ham was carried out and each slice of ham has an average thickness of 1mm. Figure 4.43 shows the attenuation in the ham as a function of frequency.
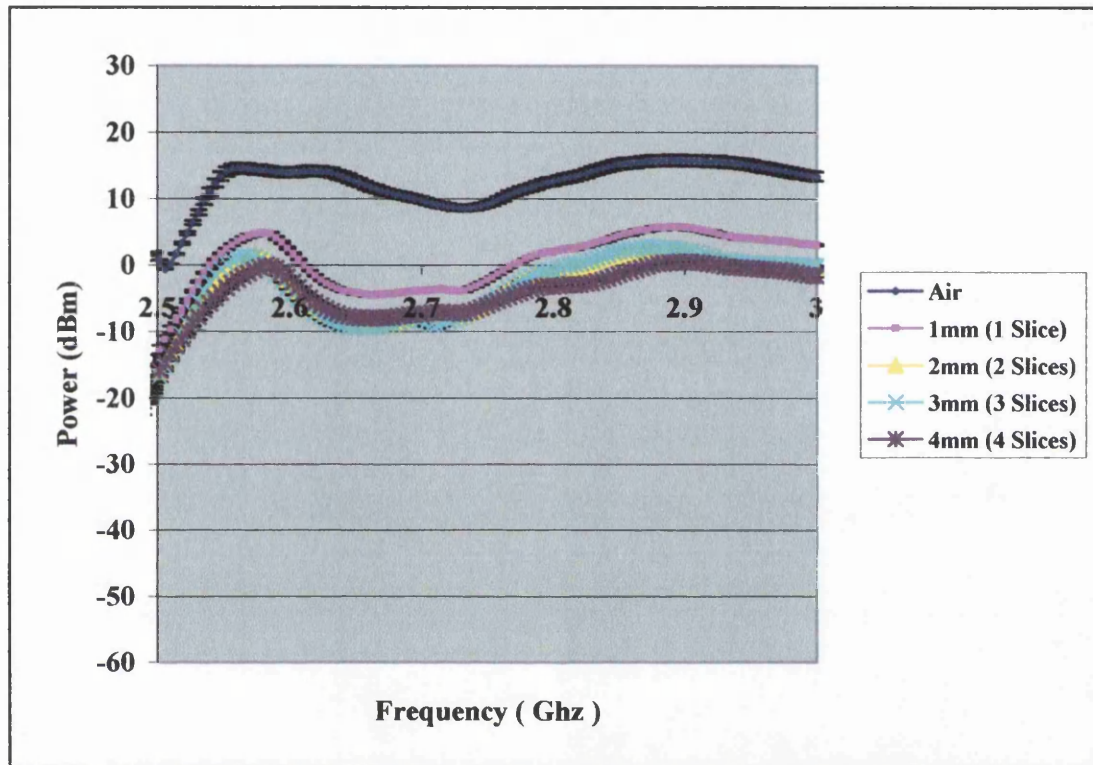
Figure 4.43 Attenuation in the ham as a function of frequency.

The results of Figure 4.43 showed that the 1mm ham had a high power loss due to most microwave power being reflected. For increasing ham thickness, the reduction in power loss becomes less significant. The power reflected at the ham-air surface was calculated to be 91.8% of the incident microwave power.

The attenuation coefficient of a ham at 2.6GHz was calculated by using equation 4.41, to be

$$P(0.1) = 0.0594 = (1 - 0.918)\exp(-2*0.1*\alpha)$$

$$\alpha = 1.612\text{cm}^{-1}(\pm 0.713)$$

The power loss in the ham as a function of ham depth was plotted in Figure 4.44. The curves showed that at least 90% incident microwave power was absorbed at 1mm.

This analysis again showed that the penetration depth at these microwave frequencies is limited to 1mm thickness.
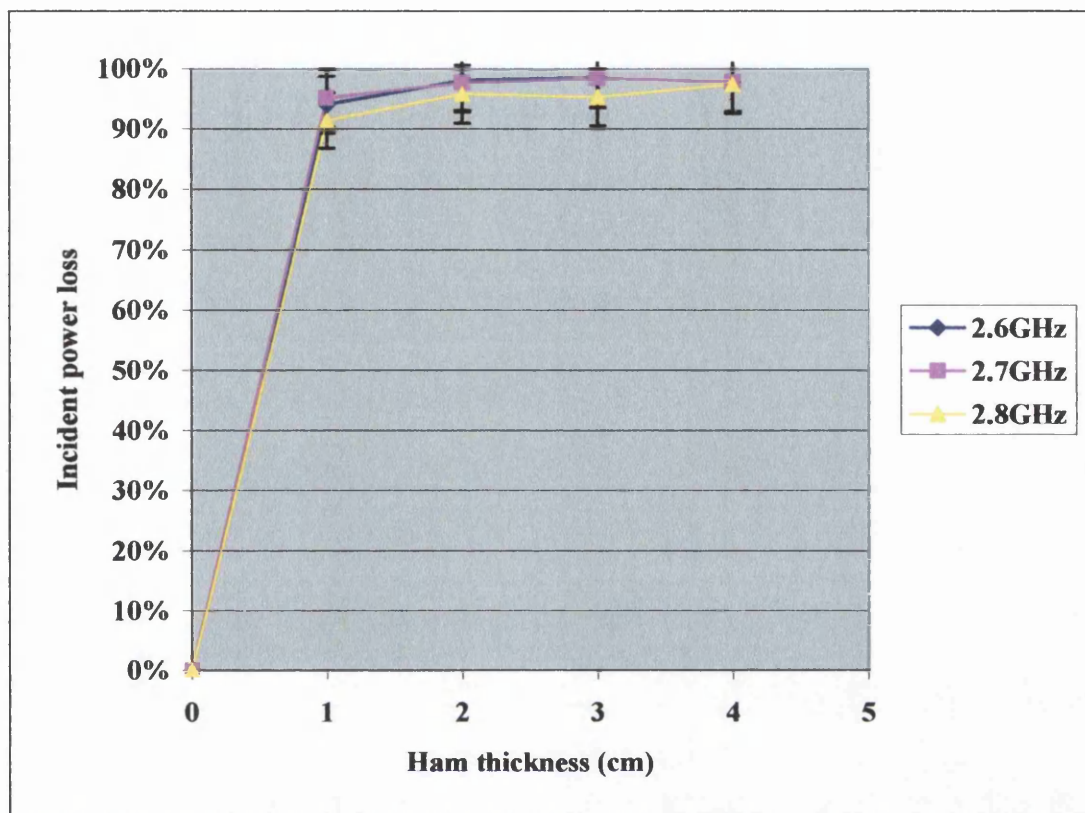
Figure 4.44 Power absorbed in the ham as a function of ham thickness.

4.5.4 Summary of the Microwave System

The microwave system requires that the minimum dipole length to be half wavelengths for the resonance effect. The minimum dipole length for a 2.5GHz system is 6cm which is still an impractical size for embedded use. The analyses showed that the chicken skin, bacon and ham tissues have high attenuation losses at microwave frequencies. These findings suggest that increasing the coupling frequency could reduce the incident microwave's penetration depth into tissue. The high energy absorption in tissue and the high reflection losses at the surface are the main reasons that the microwave radiative coupling principle is not an efficient method for energy transfer. The microwave system evaluation concludes that the use of microwave system to couple energy into tissue is not suitable for embedded photodynamic therapy because there is insufficient microwave energy penetrates deep enough into tissue for any significant energy coupling.

125

CHAPTER 5   COMPUTATIONAL STUDY

This chapter describes the procedures for running and optimising the TODDY computer model to investigate the absorption of light in two-dimensional model of tissue. The parameters needed to control the simulation were described in detail. A tumour was modelled as a single layer between the upper dermis and lower dermis. The second part describes the predicted temperature rise in tumour as a result of the absorption of photons in tissue and the subsequent photothermal damage arises from temperature increase. The final part describes the amount of photodynamic damage that occurs in the tissue. A number of radiation and photodynamic parameters were analysed and evaluated in order to optimise the ideal conditions to cause maximum damage to the tumour and minimise damage to the surrounding normal tissue.

5.1 TODDY Model G.U.I.

The TODDY model graphic user interface (G.U.I.) is the link between the user and the program. It enables the user to input the tissue geometry and to set parameters for the Monte Carlo, thermal and damage calculations and finally show the results as colour-coded intensity profiles after the calculations were completed.

5.1.1   Reference Model Properties

The grid dimension of 400 x 400 cells was used in the model. The fine grid dimension was chosen to have a more accurate representation of the results. This gives a total number of 160,000 cells in the Monte-Carlo computational space. The total number of photon count used for the study was 250,000. It is best to use the highest photon count as possible so that the result of photon absorption in tissue becomes consistent at each simulation run in order to ensure statistical convergence.

The reference tissue model (Figure 5.1) consists of

- 100μm thick epidermis layer
- 3000μm thick upper dermis
- 4000μm thick lower dermis
- 1000μm thick x 1000μm width tumour located in the lower dermis
- 10,000μm tissue width
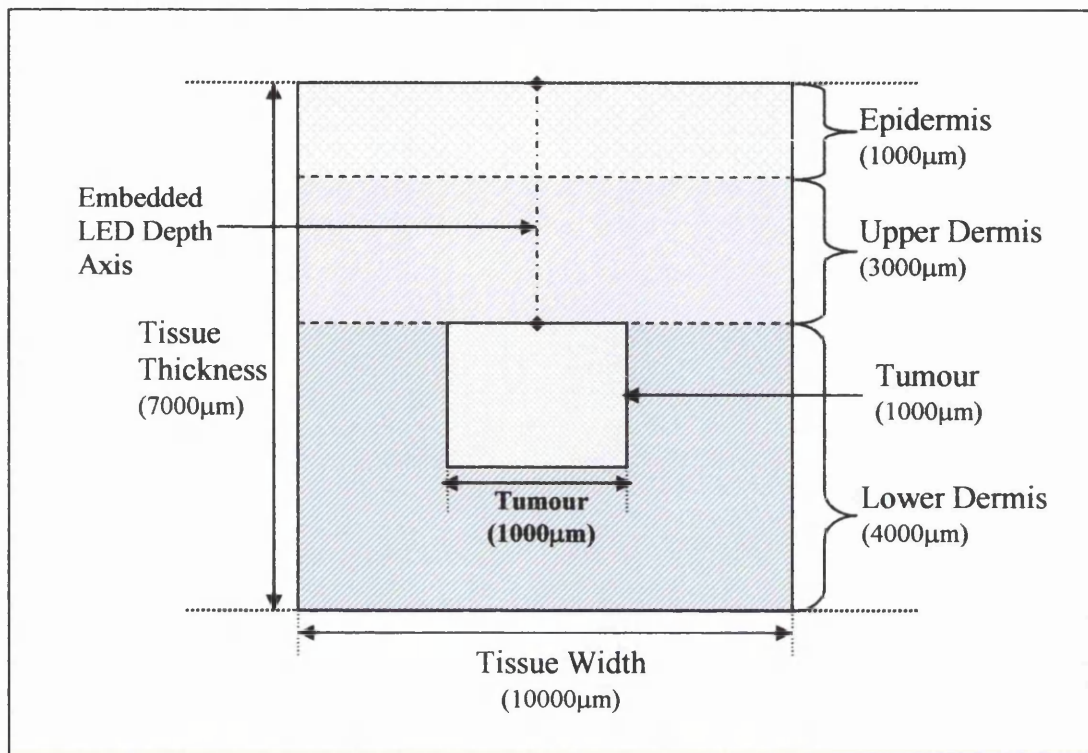
Figure 5.1: Reference tissue model

5.1.2 Optical, Thermal and Photodynamic Properties

The **standard** optical, thermal and photodynamic properties for the reference tissue model were summarised and listed in Table 5.1 - 5.6. These standard properties were used in the following computational analyses unless otherwise stated.

Wavelength	630nm	LED Depth	2600μm
Pulse time	300μs	Fluence	2.5 Jcm^{-2}
Beam diameter	5 mm	Time step	1.0 e^{-6}

Table 5.1: Light parameters

Tissue	μ_a(cm^{-1})	μ_s(cm^{-1})	g
Epidermis	0.18	580.00	0.789
Melanin	345.83	34.58	0.789
Dermis	2.29	225.00	0.789
Tumour (Blood)	159.06	468.00	0.980

Table 5.2: Tissue optical properties at 585nm wavelength

127

Tissue	$\mu_a(cm^{-1})$	$\mu_s\,(cm^{-1})$	g
Epidermis	0.18	580.00	0.789
Melanin	308.33	30.83	0.789
Dermis	2.18	220.00	0.789
Tumour (Blood)	3.17	468.00	0.980

Table 5.3: Tissue optical properties at 630nm wavelength

Tissue	$\mu_a(cm^{-1})$	$\mu_s\,(cm^{-1})$	g
Epidermis	0.18	580.00	0.789
Melanin	270.00	27.00	0.789
Dermis	2.12	217.00	0.789
Tumour (Blood)	1.85	468.00	0.980

Table 5.4: Tissue optical properties at 652nm wavelength

Tissue	$K\,(Wm^{-1}{}^{o}C^{-1})$	$\rho\,(kgm^{-3})$	$C\,(Jkg^{-1})$
Epidermis	1.06	1050	3350
Dermis	1.06	1050	3350
Tumour (Blood)	0.62	1000	3500

Table 5.5: Tissue thermal properties

Damage rate constant (k_{pd})	0.001
Photobleaching rate constant (k_{pb})	0.00025
Tissue perfusion rate constant (k_{perf})	0.01
Oxygen removal rate constant (k_{oxy})	1.0
Oxygen concentration in tissue	1.0
Photosensitiser concentration in tumour to normal tissue (Contrast ratio)	0.67/0.33 (2:1)

Table 5.6: Photodynamic properties

5.1.3 Melanin Distribution

The absorption in the epidermis is usually dominated by melanin absorption in most individuals. The actual net epidermis absorption combines the baseline epidermis absorption and the melanin absorption. The melanin distribution used in the reference epidermis layer was based on the G. Daniel and K. Donne single epidermal layer model with the melanin concentration distributed according to the normal skin type as shown in Figure 5.2. [93]
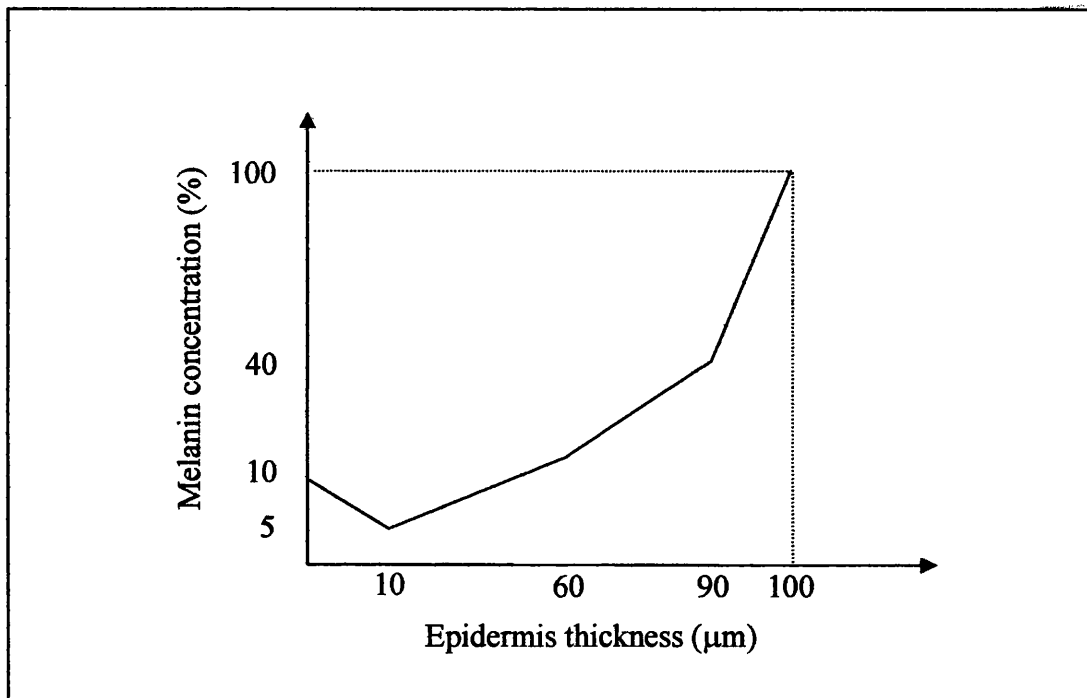
Figure 5.2: Melanin distribution in the epidermis layer

5.2 Effects of LED Depth in the Tissue at 585nm

The light source can be positioned in the centre of the tissue at various depths to model an LED embedded subcutaneously into tissue. To investigate the benefits of using an embedded light source in PDT, the position of the LED in relation to tissue depth was varied in the model. The photons were then launched at the centre of tissue from the depth of the LED. The reference tissue model and standard optical, thermal and photodynamic properties at 585nm were used in the following analyses.

5.2.1 Light Absorption against LED Depth

The LED depths were varied in the steps of 600μm from 0μm up to 3000μm. Figure 5.3 shows the light absorption profiles in tissue at each step as the LED was positioned between 0μm to 3000μm tissue depth. The results of Figure 5.3 show that the light distribution penetrates deeper into tissue as the LED position was moved closer to the tumour. The maximum photon absorption in the tumour was achieved when the LED was positioned near to the tumour. It is interesting to note the low photon absorption in the centre of the tumour. Figure 5.4 shows the percentage of energy being absorbed in tumour and upper dermis for an LED depth ranging from 0μm to 3000μm. The curve shows that the energy being absorbed in a tumour increases gradually with the LED depth. It can be seen that at 3000μm LED depth, the percentage of total photons being absorbed in the tumour was highest at 42.72%. The energy absorbed in the upper dermis starts to decrease at 1200μm LED depth in tissue as the LED was located far from the epidermis. When the LED was placed far from the tumour, the percentage of total photons being absorbed in the tumour reduces to 13.2% at 1200μm LED depth. In fact, an LED placed at the surface of epidermis generates the lowest deposited photon in tumour of 1.48%. A high percentage of the photons were being backscattered out of tissue. In addition, the presence of melanin in the lower part of the epidermis causes a higher photon absorption in the epidermis layer of 19.83%. These findings show that an LED positioned near to the tumour has the maximum energy absorption in the tumour and lowest energy absorption in the upper dermis. For PDT treatment, it is desirable to achieve maximum photon absorption in the tumour with minimum energy absorption in the normal tissues, to enhance the efficiency of PDT and to minimise damage to the surrounding tissues. For this reason, the suggested depth for the LED placement is 80% of the tumour depth in tissue. The photon energy absorption versus the tumour thickness in the cross section of the tumour for an LED depth at 0μm, 1000μm, and 2600μm was shown in Figure 5.5. The result shows that almost all of the photons energy was being absorbed in the tumour by a 600μm tumour thickness. The energy deposited in the tumour drops rapidly with tumour thickness. This is because the tumour has a high optical absorption coefficient and a high anisotropy factor value. Hence, the light was highly attenuated as it penetrates the deepest

tumour layer. Beyond 600μm thickness, the energy absorbed was mainly from photons scattering in the lower dermis. These findings show that the deposited energy in the tumour was a lot higher at 2600μm tissue depth compared to 0μm and 1000μm tissue depth.

(0 μm L.D.)

(600 μm L.D).

(1200 μm L.D).
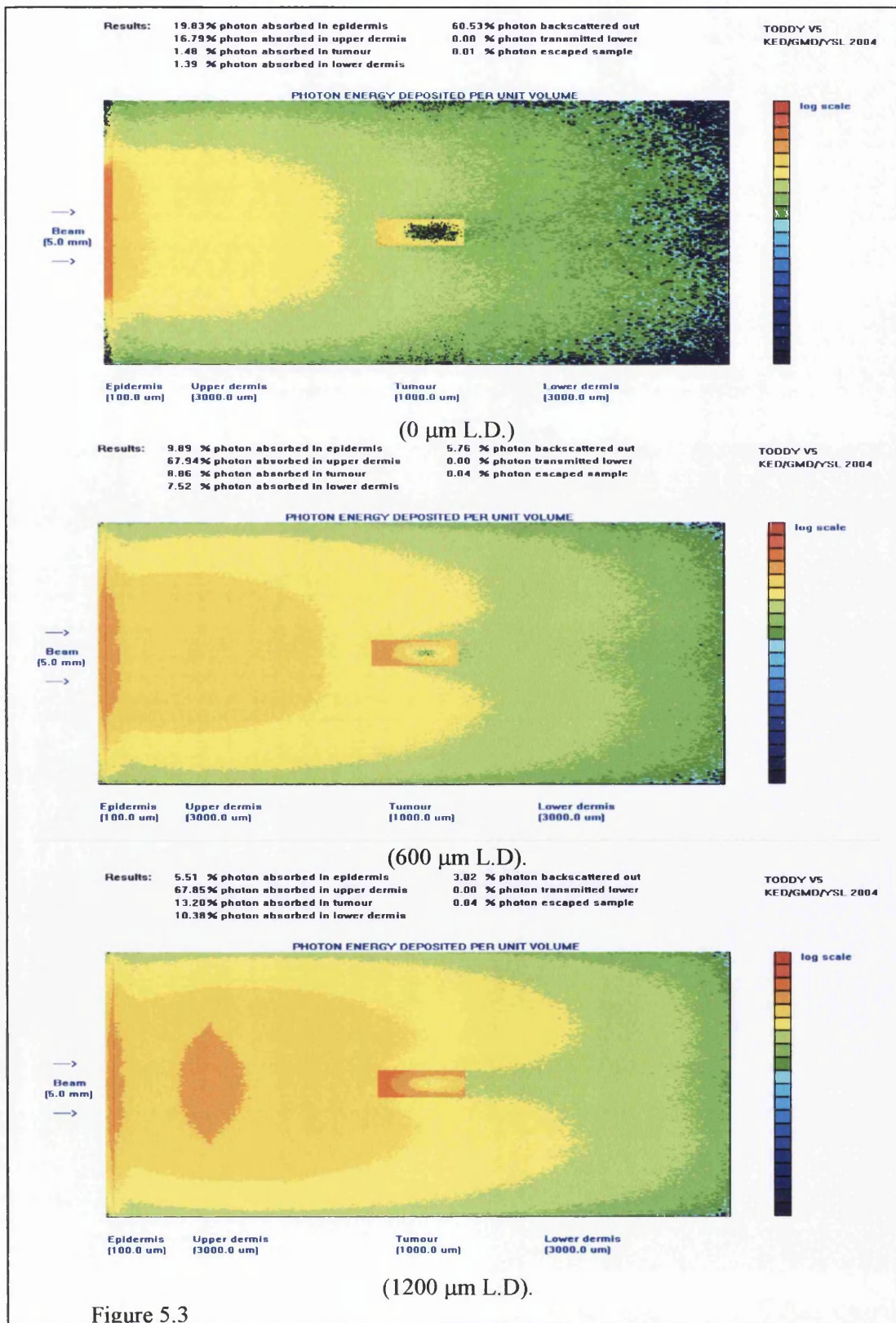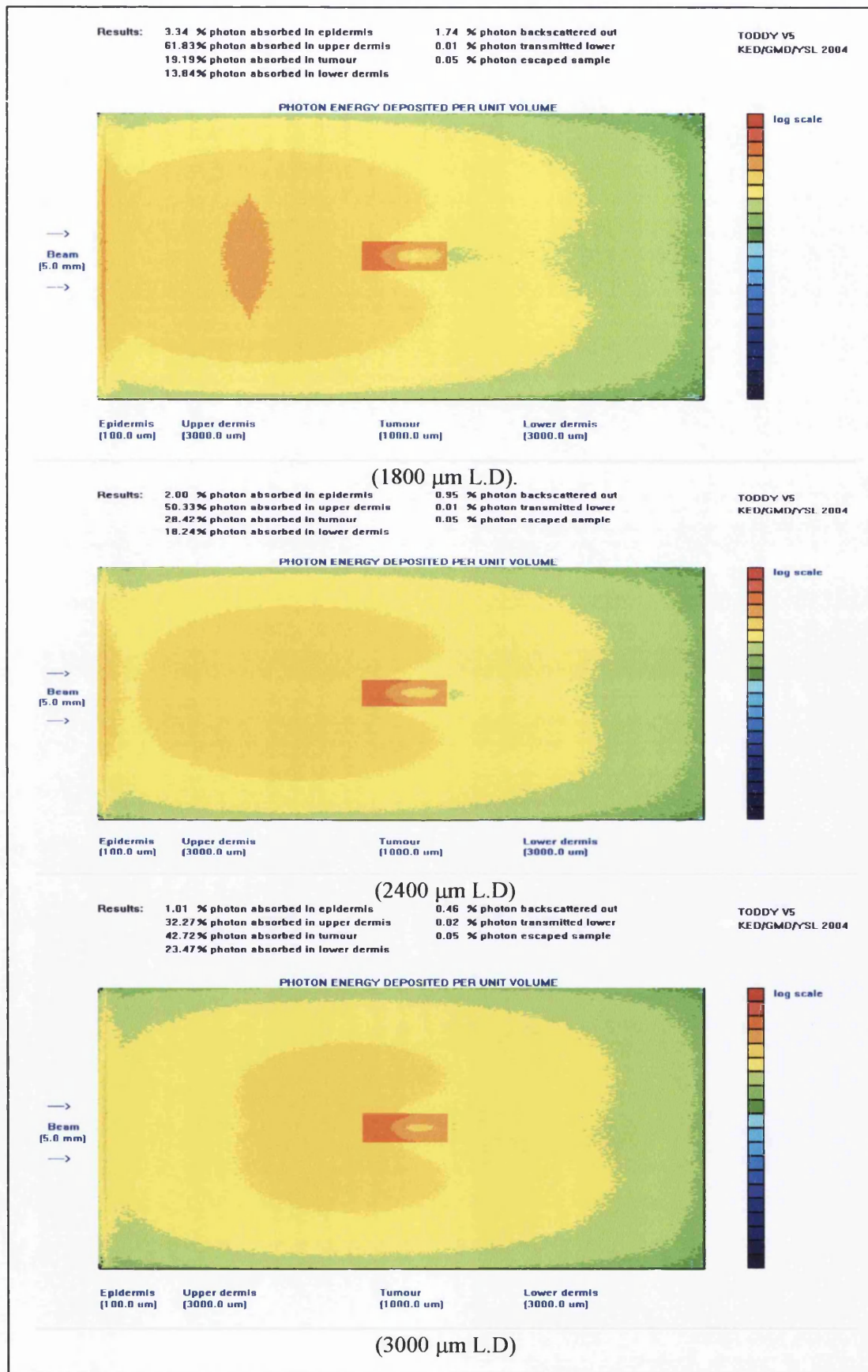
Figure 5.3

Figure 5.3: Light absorption profiles for various LED depths (L.D) from 0µm to 3000µm in tissue at 585nm wavelength.
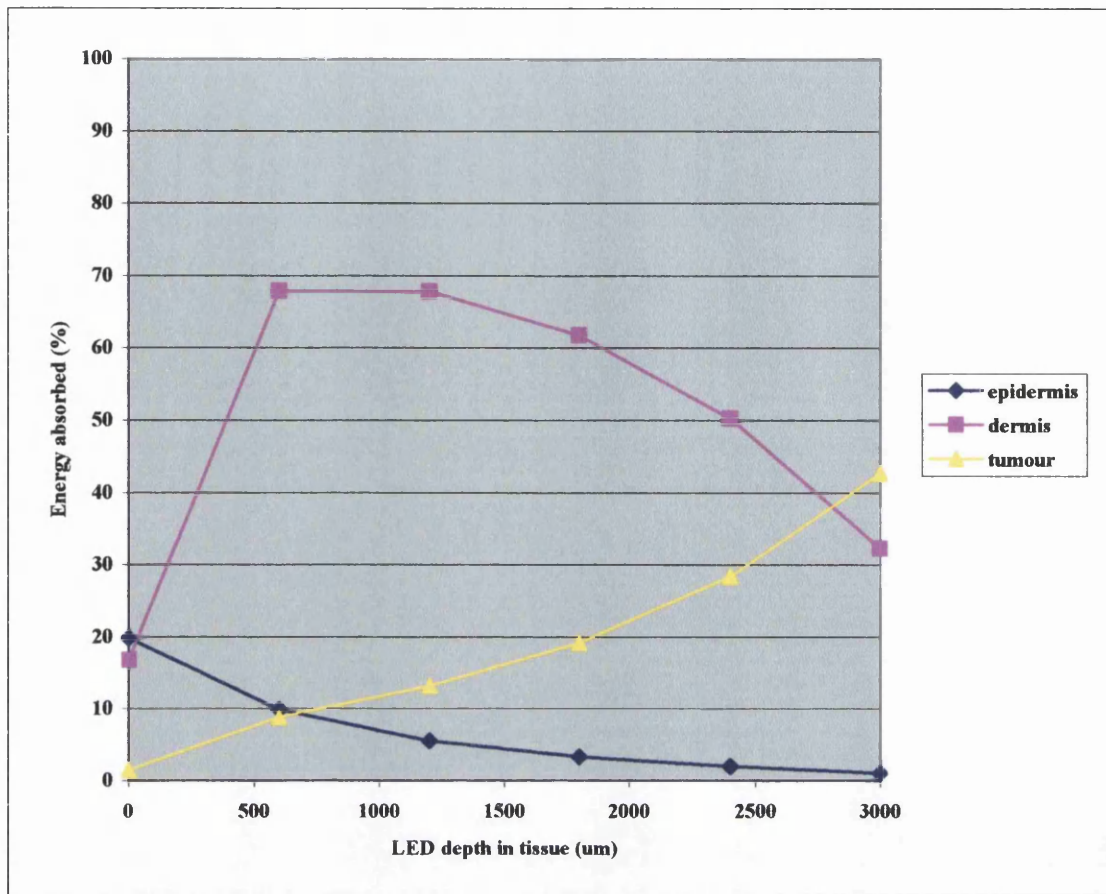
Figure 5.4: Energy absorbed in epidermis, upper dermis layer and tumour layer as a function of the LED depth in tissue.
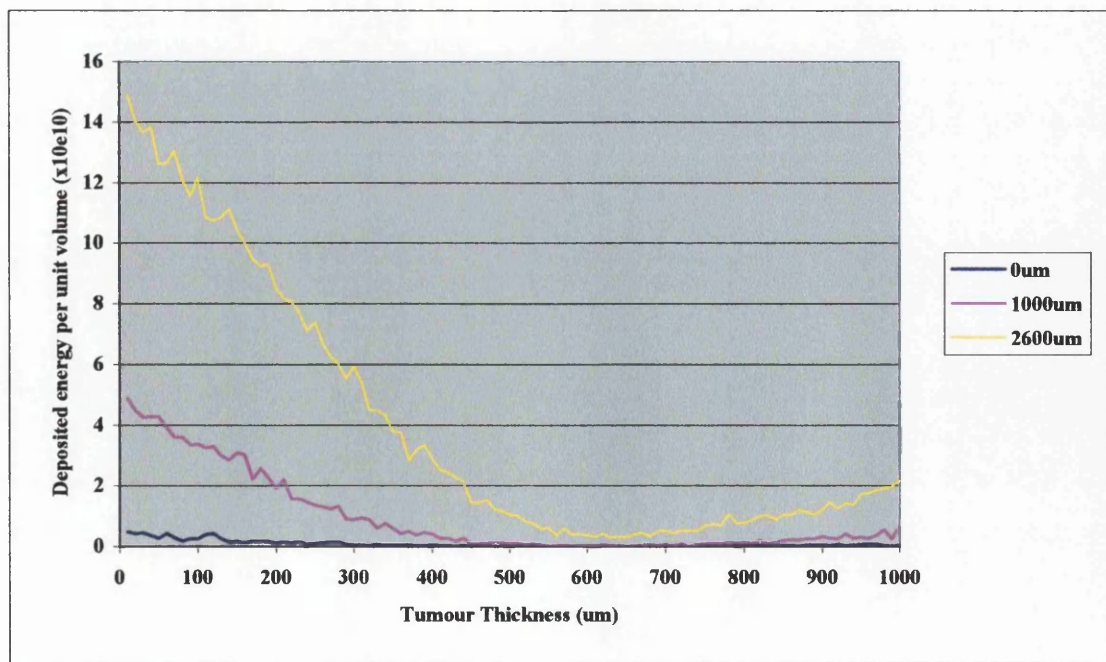
Figure 5.5: Deposited energy per unit volume vs. tumour thickness of the cross section of the tumour for the LED depth at 0μm, 1000μm and 2600μm.

5.2.2 Temperature against LED Depth

To determine the effects of LED position on the temperature rise in a tumour, a high fluence of $2.5 Jcm^{-2}$ was used in this analysis. The maximum temperature in the tumour and middle point of the tumour was plotted in Figure 5.6. The curve in Figure 5.6 show that the maximum temperature in the tumour increases rapidly with the LED depth. There is only a small increase of the temperature in middle point of the tumour due to low energy absorption in the centre of the tumour. The highest temperature in the tumour was achieved as the LED was placed near to the tumour.
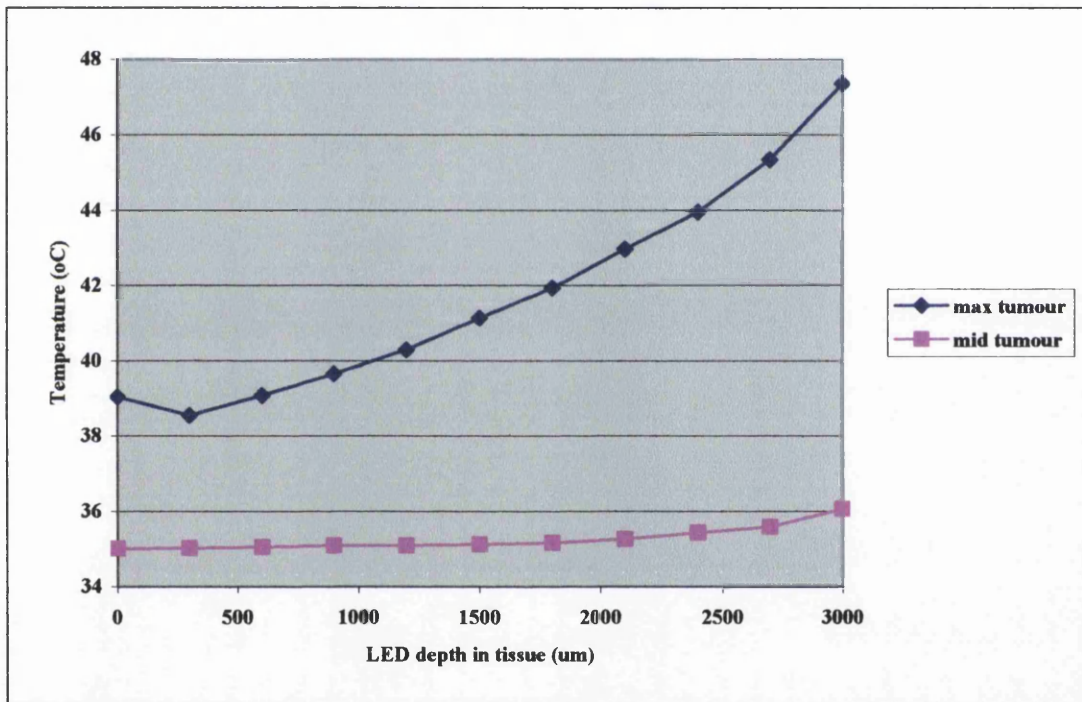
Figure 5.6: Temperature rise in the tumour and middle point of the tumour as a function of the LED depth in tissue.

5.2.3 Photothermal Damage against LED Depth

It was assumed here that at temperatures of 45°C and above, the tumour was damaged by hyperthermia corresponding to the photothermal damage scale of 1.0 and above. This assumption is valid only for the standard short pulse duration. The total photothermal damage in tumour as a function of LED depth in tissue was plotted in Figure 5.7. The results show that photothermal damage increases with the

LED depth. The amount of photothermal damage was approximately proportional to the temperature rise in the tumour.
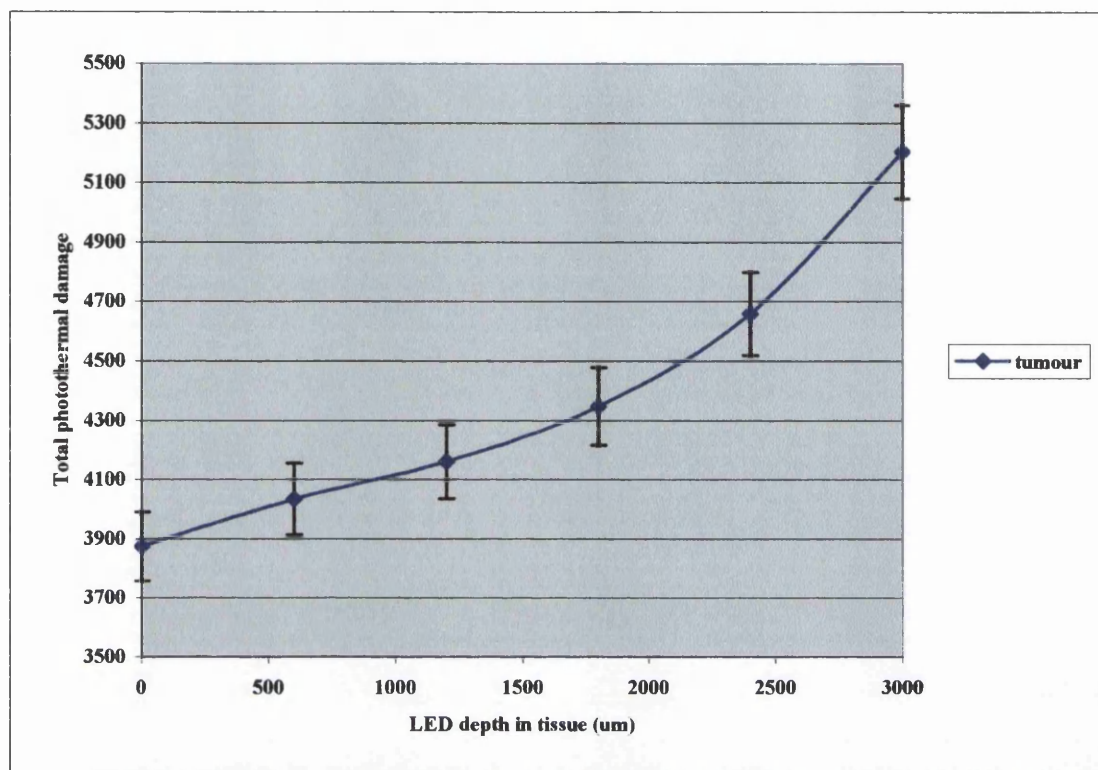
Figure 5.7: Total photothermal damage in the tumour as a function of the LED depth in tissue.

The photothermal damage profiles in the tumour for an LED positioned between 0μm to 3000μm tissue depth were shown in Figure 5.8. At 0μm tissue depth, there was not enough energy absorption to cause any substantial photothermal damage in the tumour. The highest profile of photothermal damage arises when the LED was placed in 3000μm tissue depth. However, the maximum damage occurs mostly in the top wall of the tumour as seen at 3000μm LED depth in tissue. These results once more show that the LED positioned near to the tumour generates the maximum photothermal damage in the tumour.
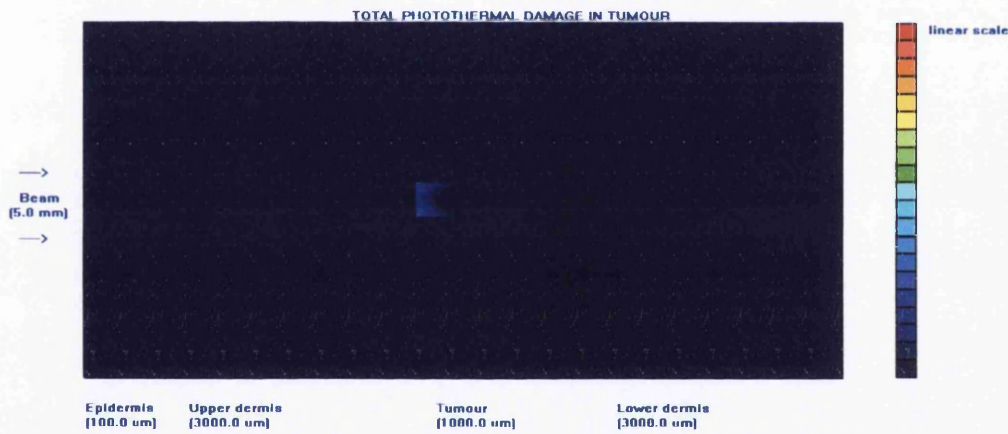
(0 um L.D.)

(600 um L.D.)

Figure 5.8 (1200 um L.D.)
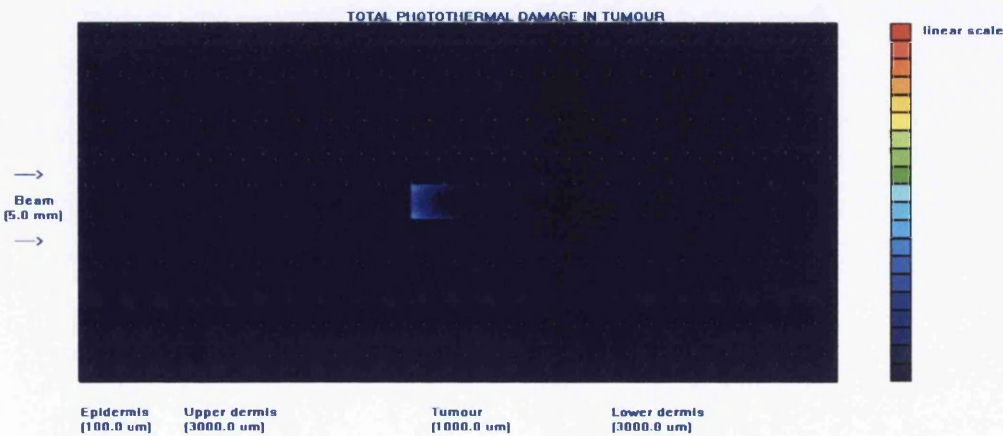
(1800 um L.D.)

(2400 um L.D.)

(3000 um L.D.)
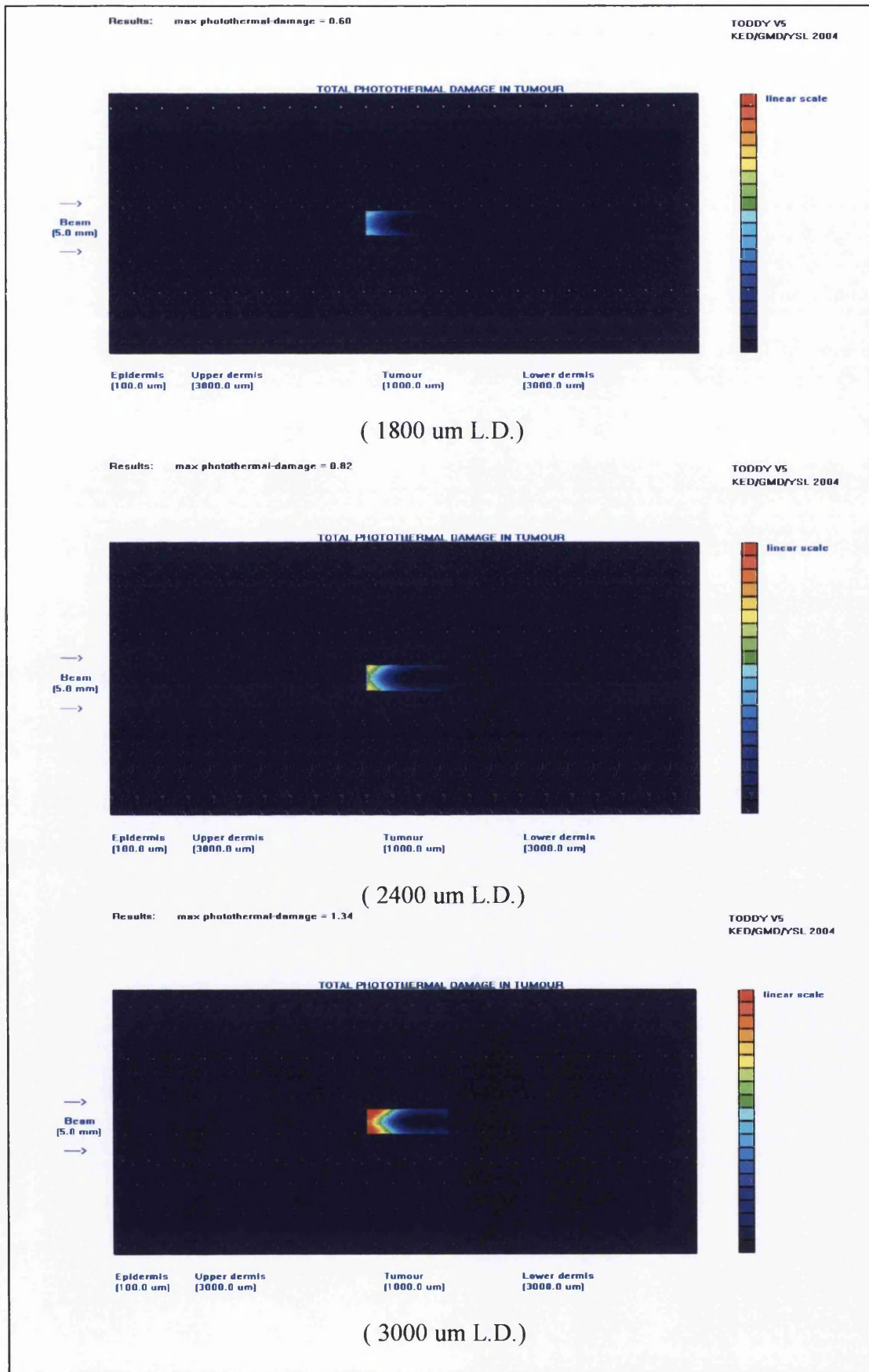
Figure 5.8: Photothermal damage profiles for various LED depths (L.D.)

from 0μm to 3000μm in tissue at 585nm wavelength.

5.2.4 Photodynamic Damage against LED Depth

Figure 5.9 below shows the total photodynamic damage in a tumour as a function of the LED depth in tissue. The amount of photodynamic damage rise greatly with LED depth in tissue from 0μm to 1200μm. When the LED was placed beyond the 1200μm tissue depth, the damage starts to saturate and slowly increases. The photodynamic damage profile in the tumour varies along the LED depth in tissue as shown in Figure 5.10. The photodynamic damage in tissue has a wider and more uniform distribution as the LED was positioned closer to the tumour.
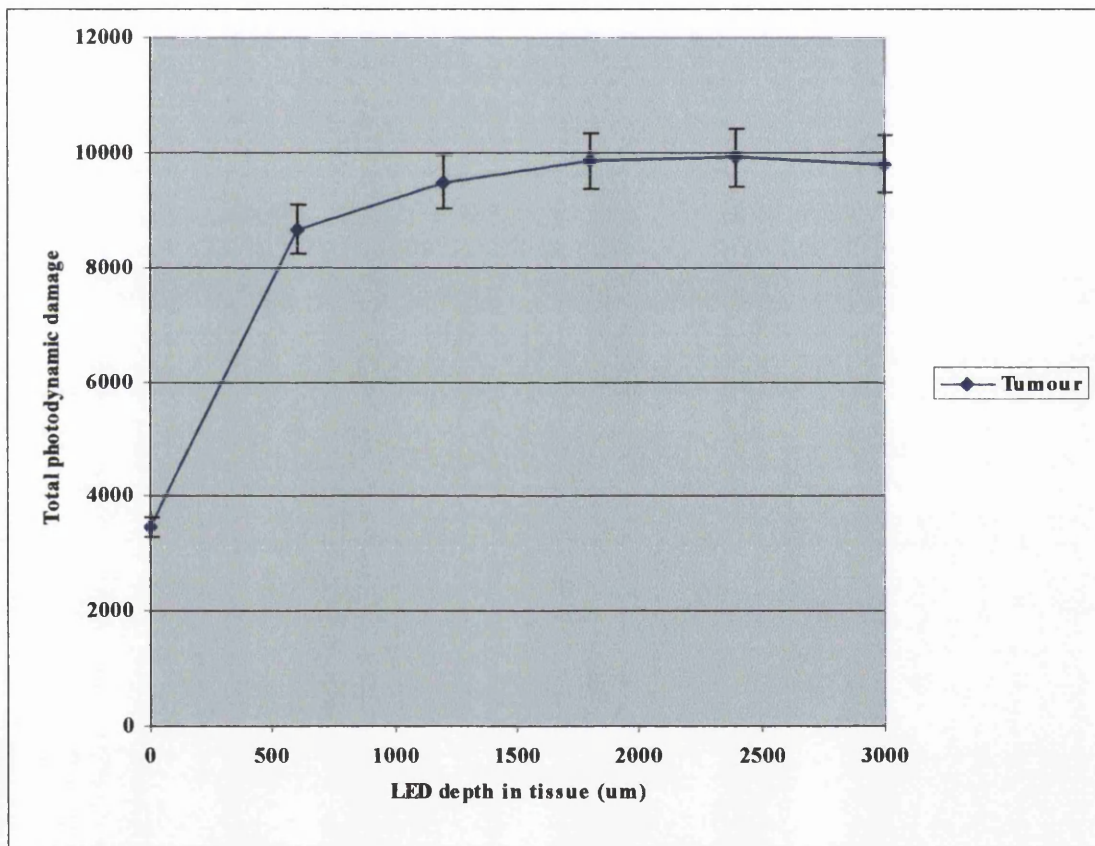
Figure 5.9: Total photodynamic damage in the tumour as a function of the LED depth in tissue.

Results: max pd-damage in epidermis = 1.320   max pd-damage = 2.613   TODDY V5
            max pd-damage in upper dermis = 1.295   KED/GMD/YSL 2004
            max pd-damage in tumour= 2.613
            max pd-damage in lower dermis = 0.158

ACCUMULATED PHOTODYNAMIC DAMAGE IN CELLS   linear scale

Beam
[5.0 mm]
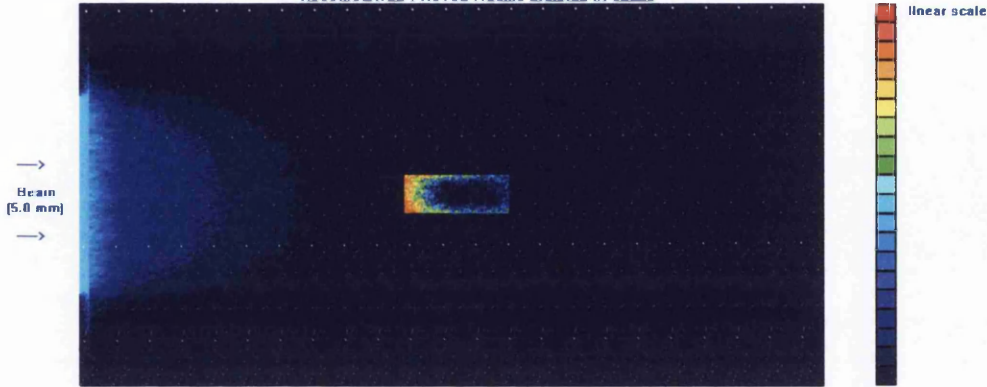
Epidermis   Upper dermis   Tumour   Lower dermis
[100.0 um]   [3000.0 um]   [1000.0 um]   [3000.0 um]

(0 um L.D.)

Results: max pd-damage in epidermis = 1.320   max pd-damage = 2.655   TODDY V5
            max pd-damage in upper dermis = 1.320   KED/GMD/YSL 200
            max pd-damage in tumour= 2.655
            max pd-damage in lower dermis= 0.397

ACCUMULATED PHOTODYNAMIC DAMAGE IN CELLS   linear scale

Beam
[5.0 mm]
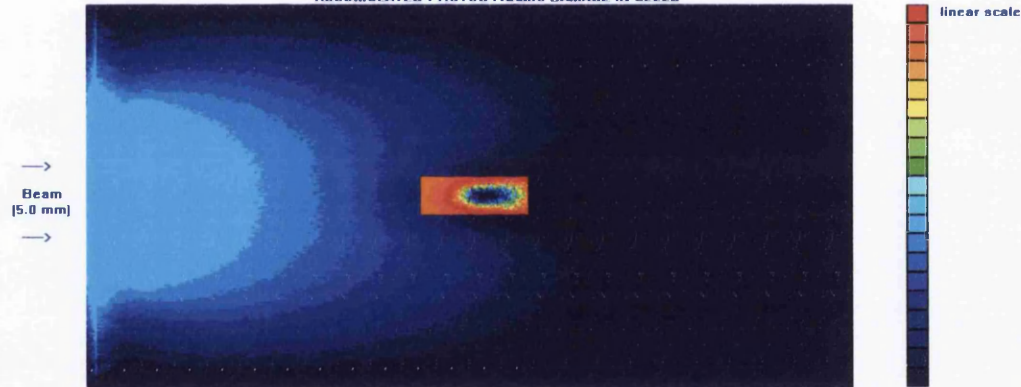
Epidermis   Upper dermis   Tumour   Lower dermis
[100.0 um]   [3000.0 um]   [1000.0 um]   [3000.0 um]

(600 um L.D.)

Results: max pd-damage in epidermis = 1.320   max pd-damage = 2.655   TODDY V5
            max pd-damage in upper dermis = 1.320   KED/GMD/YSL 2004
            max pd-damage in tumour= 2.655
            max pd-damage in lower dermis= 0.609
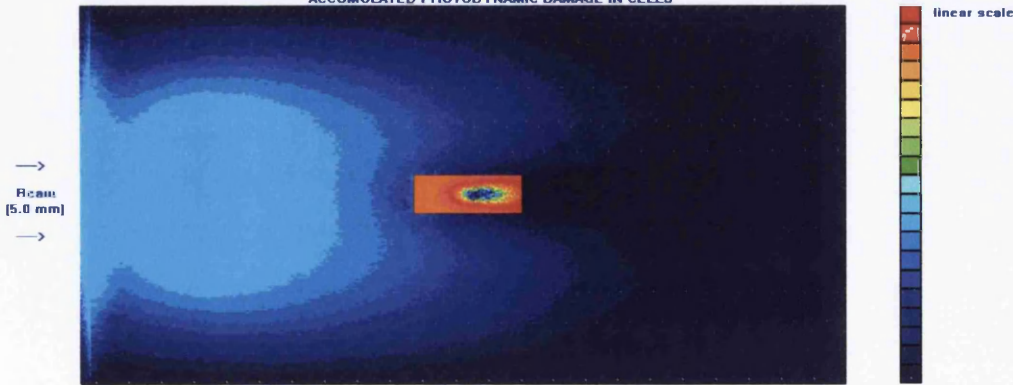
ACCUMULATED PHOTODYNAMIC DAMAGE IN CELLS   linear scale

Beam
[5.0 mm]

Epidermis   Upper dermis   Tumour   Lower dermis
[100.0 um]   [3000.0 um]   [1000.0 um]   [3000.0 um]

Figure 5.10   (1200 um L.D.)
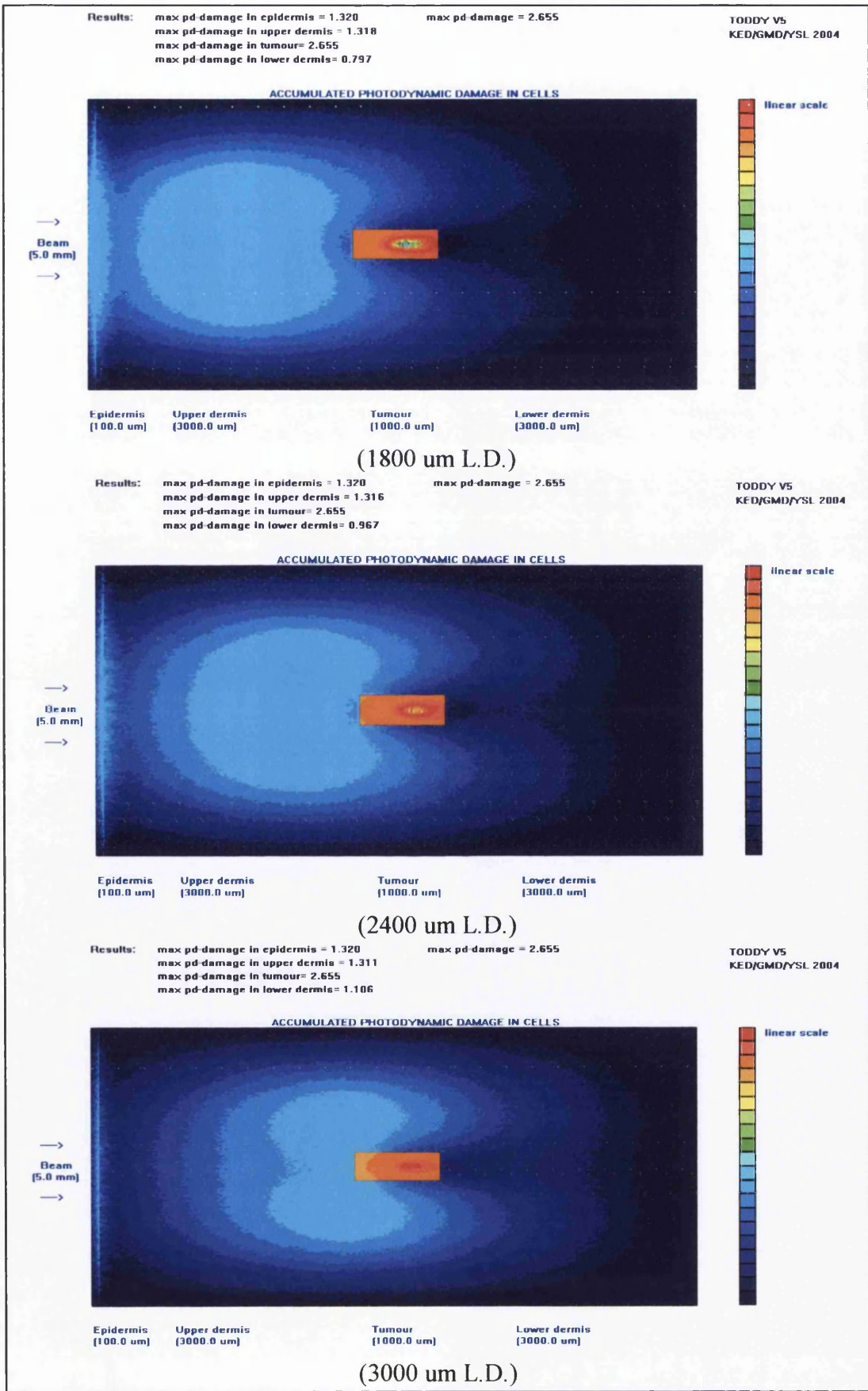
Figure 5.10: Photodynamic damage profiles for various LED depths (L.D.)

from 0um to 3000um in tissue at 585nm wavelength.

5.2.5 Conclusions

All of these analyses above suggest that when an embedded light source was placed near to the tumour, maximum photon energy will be absorbed in the tumour region. This gives a higher light penetration depth into tissue at the same wavelength. Also, the epidermis layer absorbs less photons and almost all the emitted energy was contained inside the tissue. The temperature in the tumour increases and has an effect on the maximum photothermal damage in the tumour. The tumour achieves maximum photodynamic damage in the entire tumour region. In contrast, the maximum photodynamic damage only occurs in the epidermis layer and in the top wall of the tumour for surface light source. This proves that an embedded light source offers a better PDT response compared to conventional surface light source.

5.3 Effects of Wavelength Selection

In this section, the effect of the light source wavelength on the light absorption distribution and photodynamic damage profile in the tumour was considered. Three wavelengths - 585nm, 630nm, and 652nm - were chosen to show the benefits of using shorter or longer wavelengths. The reference tissue model and standard optical, thermal and photodynamic properties were used in the following analyses.

5.3.1 Light Absorption Profile against Wavelength

At a 585nm wavelength, the percentage of photons being absorbed in the tumour was 32.45% (Figure 5.11). For a longer wavelength of 630nm, the percentage of total photons being absorbed in the tumour reduces to 5.34%, as shown in Figure 5.12. Figure 5.13 shows the percentage of total photons being absorbed in the tumour drop further to 3.37% at 652nm wavelength. The light distribution for both 630nm and 652nm wavelengths were much more uniform inside and around the tumour layer.
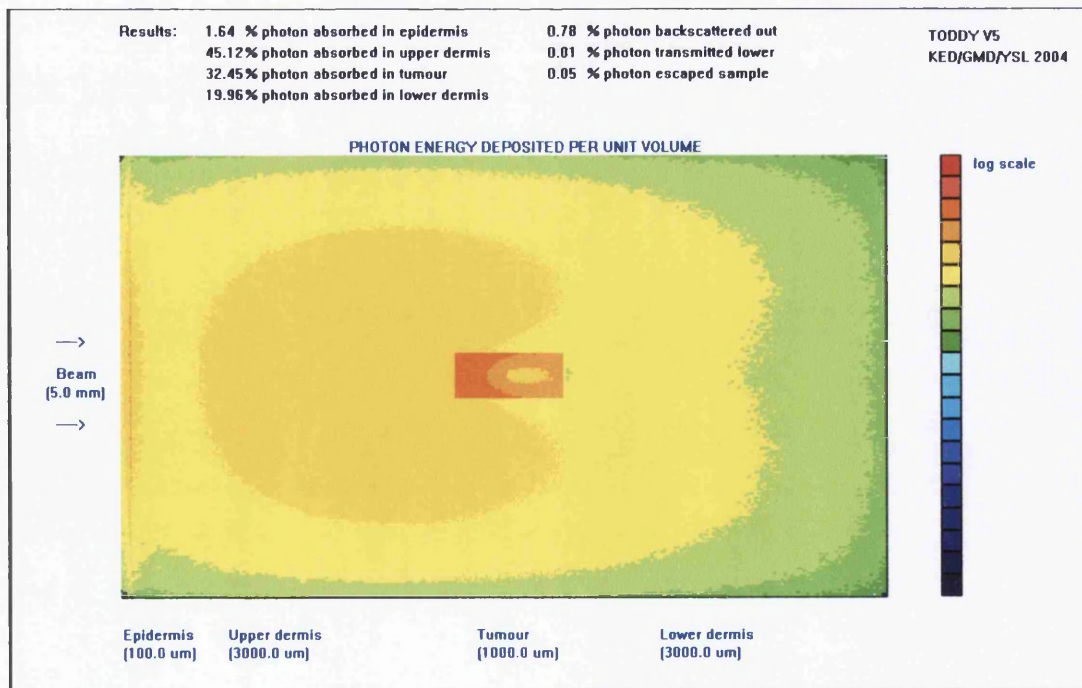
Figure 5.11: Light absorption profile at 585nm wavelength

Results: 1.38 % photon absorbed in epidermis   0.50 % photon backscattered out   TODDY V5
          55.15% photon absorbed in upper dermis   0.03 % photon transmitted lower   KED/GMD/YSL 2004
          5.34 % photon absorbed in tumour   0.07 % photon escaped sample
          37.53% photon absorbed in lower dermis

PHOTON ENERGY DEPOSITED PER UNIT VOLUME

log scale

—→
Beam
(5.0 mm)
—→

Epidermis   Upper dermis   Tumour   Lower dermis
(100.0 um)   (3000.0 um)   (1000.0 um)   (3000.0 um)

Figure 5.12: Light absorption profile at 630nm wavelength

Results: 1.89 % photon absorbed in epidermis   0.96 % photon backscattered out   TODDY V5
          55.35% photon absorbed in upper dermis   0.03 % photon transmitted lower   KED/GMD/YSL 2004
          5.16 % photon absorbed in tumour   0.07 % photon escaped sample
          36.54% photon absorbed in lower dermis

PHOTON ENERGY DEPOSITED PER UNIT VOLUME

log scale

—→
Beam
(5.0 mm)
—→

Epidermis   Upper dermis   Tumour   Lower dermis
(100.0 um)   (3000.0 um)   (1000.0 um)   (3000.0 um)

Figure 5.13: Light absorption profile at 652nm wavelength

Figure 5.14 and Figure 5.15 show the energy deposition in the cross section of a tumour for 585nm, 630nm and 652nm wavelengths. There was a significant difference in the total amount of energy absorbed between 585nm with 630nm and 652nm. This was because at 585nm, the absorption coefficient for the tumour was much higher compared to 630nm and 652nm. Light was highly attenuated and the photon energy drops off rapidly with increasing in tumour depth. Whereas, at 630nm 652nm, the deposited energy pattern was more consistent on all tumour thickness. At a longer wavelength, the penetration depth of light was much higher, which leads to a more uniform absorption profile compared to 585nm wavelength. This explains why the majority of photosensitisers in the market have absorption wavelength in the red region. When comparing the difference between 630nm and 652nm wavelengths, the energy deposition at 630nm was slightly higher by 20% than the energy deposition at 652nm. This was because the variation in the absorption coefficient for both wavelengths was small. Shorter wavelengths generate a higher energy deposition of the photons. Conversely, longer wavelengths carry lower energy with less of the thermal effect and deeper photodynamic effect. To achieve deeper penetration of light into the tumour and uniform distribution in the tumour, it is suggested that both wavelengths 630nm and 652nm are more suitable for PDT application. The wavelength selection between 630nm and 652nm is dependent upon the photosensitiser used for PDT. The peak wavelengths for Photofrin and m-TPHC photosensitiser are 630nm and 652nm respectively. When the photon wavelength matches the peak wavelength in which the photosensitiser absorption coefficient is at its peak point, the efficiency of generation and damage by singlet oxygen could be greater. Thus, for m-TPHC photosensitiser, the 652nm wavelength is a much better choice for PDT, although the 630nm wavelength offers a higher energy deposition in the tumour layer compared to 650nm.
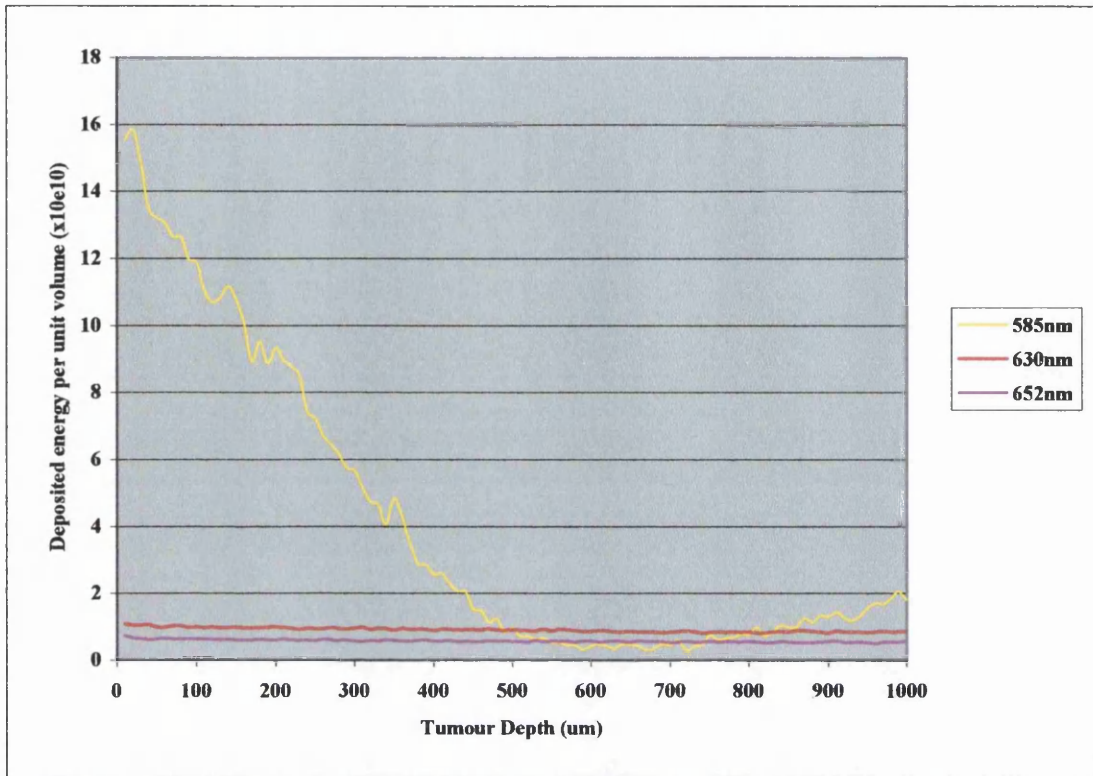
Figure 5.14: Deposited energy per unit volume vs. tumour depth of the cross section of the tumour for 585nm, 630nm and 652nm wavelengths.
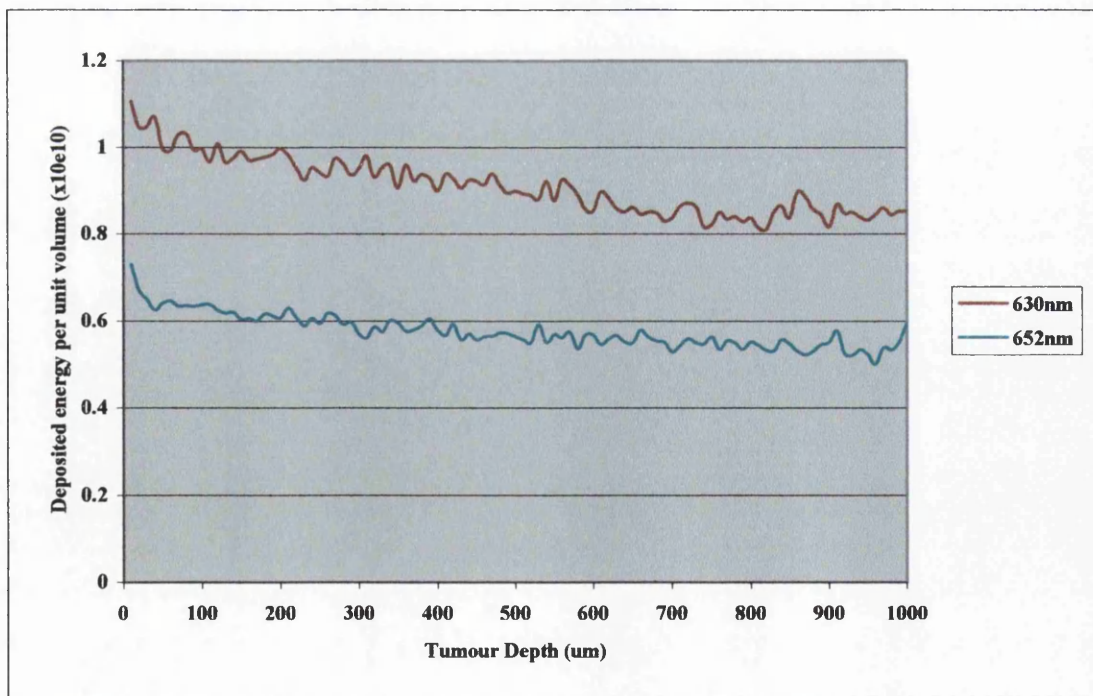
Figure 5.15: Detailed comparison of deposited energy per unit volume for 630nm and 652nm wavelengths.

5.3.2 Temperature against Wavelength

Next, the peak temperatures in tissue for 585nm, 630nm and 652nm wavelengths were simulated. High fluence of 2.5 Jcm^{-2} was used in this study. The end results of the temperatures in different layers of tissue were listed in Table 5.7.

Wavelength	Skin surface temp (°C)	Upper dermis temp (°C)	Tumour core temp (°C)	Tumour wall temp (°C)
585nm	35.11	35.23	35.53	45.01
630nm	35.15	35.30	35.49	35.44
652nm	35.14	35.30	35.32	35.59

Table 5.7: Peak temperatures in the different layers of tissue at 585nm, 630nm and 652 wavelengths.

The tumour wall temperature was much higher at 585nm than at 630nm and 652nm wavelengths. The temperature difference between the tumour core and the tumour wall noted at 585nm wavelength was due to higher energy absorption at the tumour wall. At red region wavelengths, the temperature rise was much the same in the tumour core and the tumour wall.

5.3.3 Photothermal Damage against Wavelength

In the previous section, it was observed that the 585nm wavelength produces the highest temperature rise in the tumour wall. Table 5.8 shows the total photothermal damage attainable in the tumour.

Wavelength	Total photothermal damage in the tumour
585nm	4805.470
630nm	3915.805
652nm	3867.091

Table 5.8: Total photothermal damage in the tumour at 585nm, 630nm and 652 wavelengths

At 585nm wavelength, almost all of the total damage occurs mostly in the tumour wall with no significant damage in the tumour core, as shown in Figure 5.16. At 630nm and 652nm wavelengths, the photothermal damage in the tumour does not exist, as it was below the lower limit damage of 4000 for the tumour cells, hence, no figures were shown.
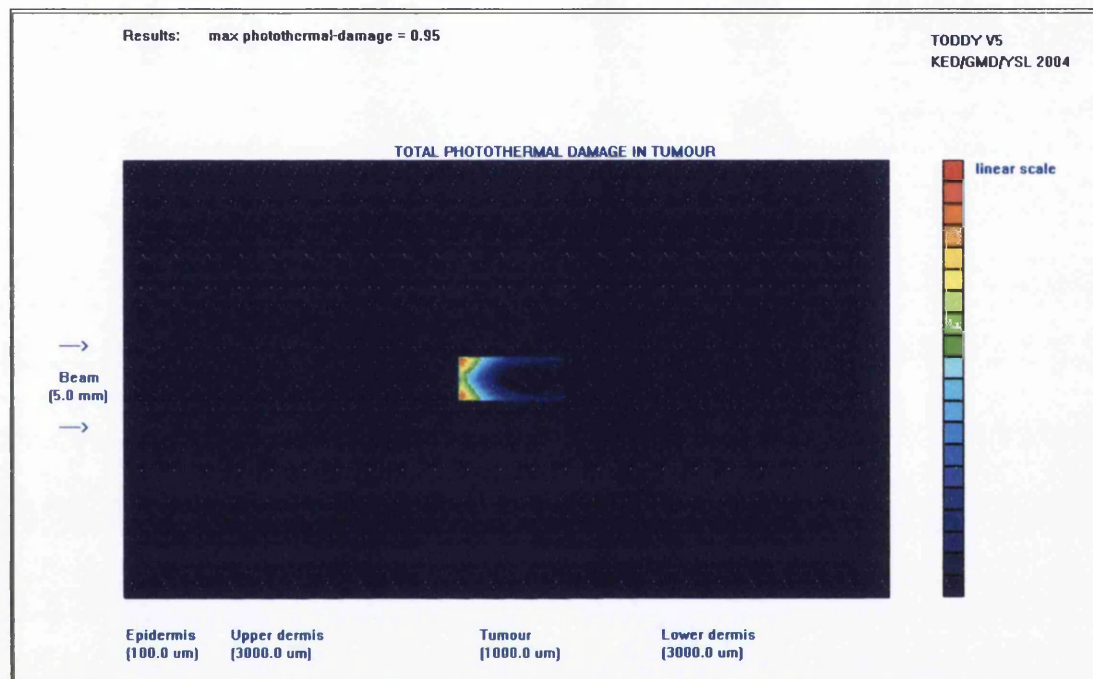
Figure 5.16: Photothermal damage profile at 585nm wavelength.

5.3.4 Photodynamic Damage against Wavelength

Next, the effect of each different wavelength on the photodynamic damage was examined. The total photodynamic damage occurred in the tumour was highest at 630nm wavelength among the three wavelengths as listed in Table 5.9.

Wavelength	Total photodynamic damage in the tumour
585nm	9890.630
630nm	10607.291
652nm	10417.248

Table 5.9: Total photodynamic damage in the tumour at 585nm, 630nm and 652nm wavelengths

However, the photodynamic damage profile in tissue varies with wavelength. It is shown in Figure 5.17, that not every section of the tumour receives maximum photodynamic damage at 585nm wavelength. The maximum damage was limited to the tumour core only when compared to 630nm and 652nm wavelengths. For 630nm and 652nm, the profile of photodynamic damage was more uniform in the tumour region as shown in Figure 5.18 and Figure 5.19. Also at these wavelengths, the light penetrates deeper into tissue and this generates a higher damage in the lower dermis.
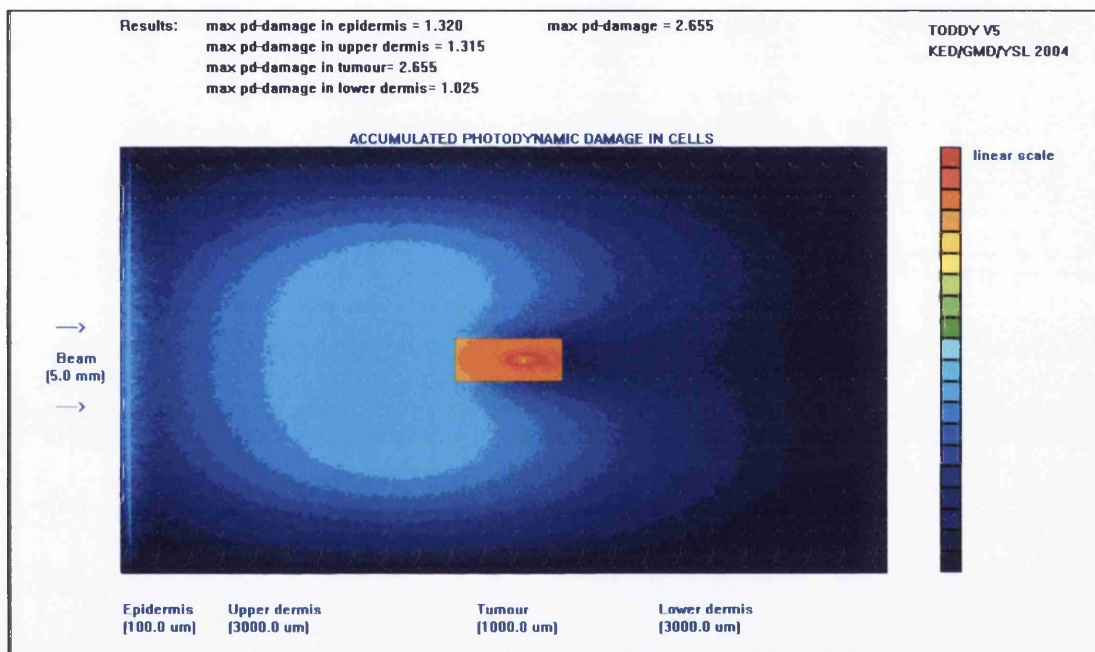
Figure 5.17: Photodynamic damage profile at 585nm wavelength
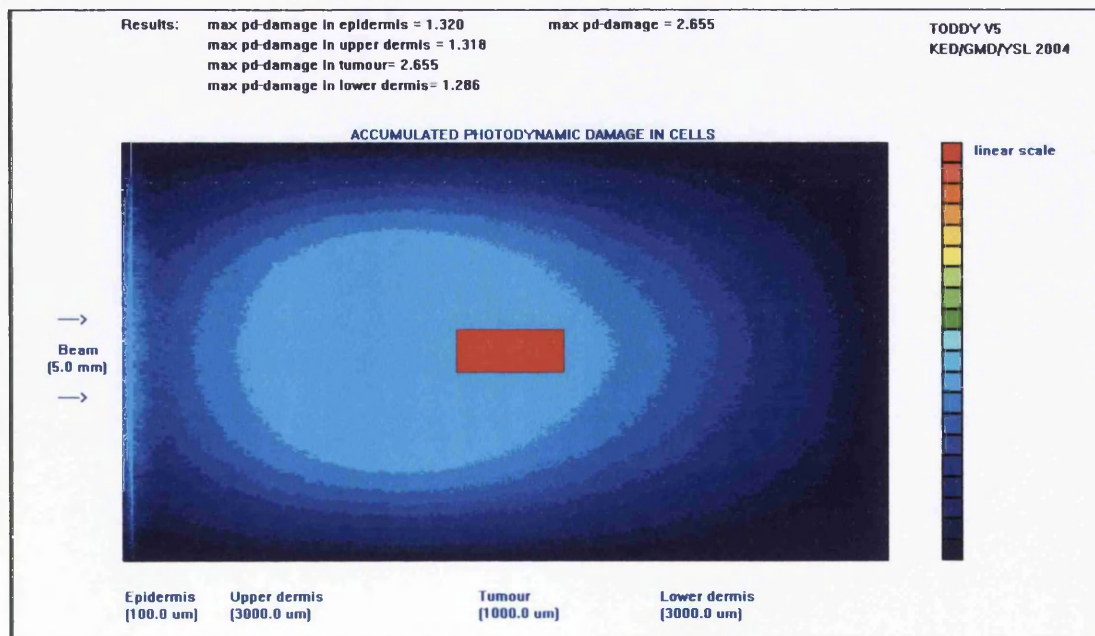
Figure 5.18: Photodynamic damage profile at 630nm wavelength
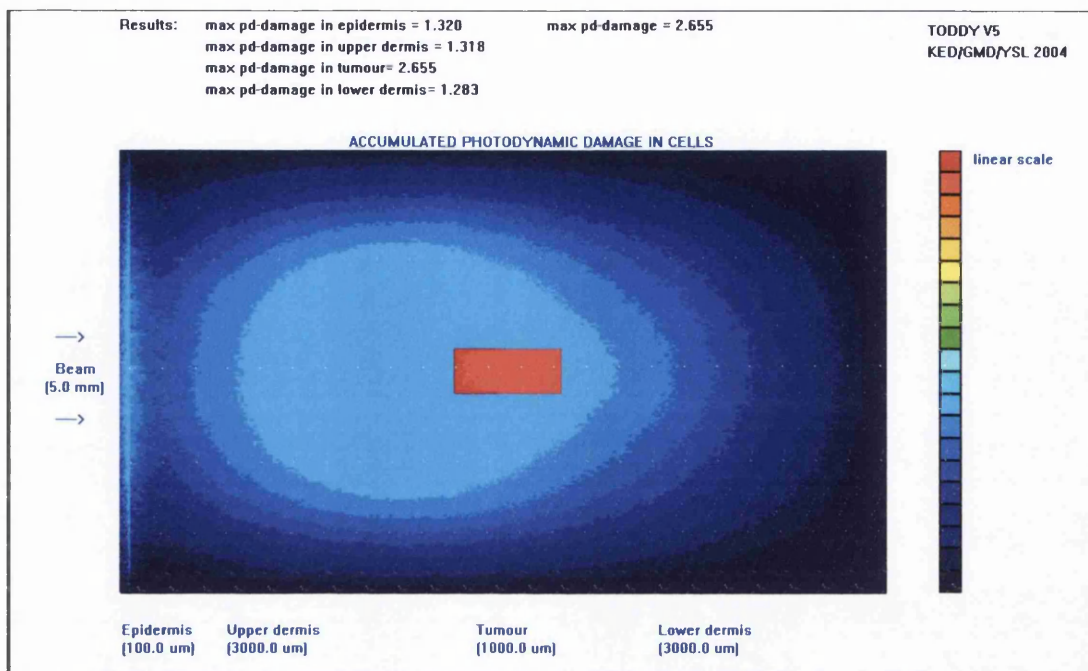
Figure 5.19: Photodynamic damage profile at 652nm wavelength

5.3.5   Conclusions

The analyses of wavelength selection demonstrate that at a longer wavelength or the red region, the penetration of light into tissue was higher than the yellow region. This gives a lower and more uniform energy absorption in the tumour area. The photon absorption was sufficient to produce a uniform photodynamic damage profile in the tumour with minimum temperature rise and maximum photothermal damage in the tumour. An important consideration in the wavelength selection is that the light source wavelength matches the photosensitiser peak wavelength for maximum absorption and generation of cytotoxic singlet oxygen. The red region wavelengths are well suited for the peak wavelength of the majority of photosensitisers used in PDT. Hence, it is suggested that the wavelengths in the red region have a much better PDT efficiency compared to shorter wavelengths.

5.4 Effects of Fluence Selection

The source power for the embedded light source comes from inductive coupling method. Consequently, the light source's energy output can be controlled by the amount of RF energy transmitted into tissue.

To investigate the effects of fluence against the photothermal damage and photodynamic damage in the tumour, the light source's fluence was varied from 0.005 Jcm^{-2} to 6.0 Jcm^{-2} as shown in Table 5.10. These fluence ranges were selected to reproduce the energy of low, medium and high intensity light through a 5mm beam spot. The irradiation duration was kept constant for the equivalent fluence range tested. The reference tissue model and standard optical, thermal and photodynamic properties at 630nm were used in the following analyses.

Fluence (Jcm^{-2})	Light energy (mJs^{-1})	Intensity
0.005	1.0	Low
0.05	9.8	Low
0.5	98.4	Low
1.0	196.4	Medium
2.0	392.3	Medium
3.0	589.1	High
6.0	1178.0	High

Table 5.10: Fluence with the equivalent light energy and intensity

5.4.1 Temperature against Fluence

The maximum temperatures in the tumour for fluence range between 0.005 Jcm^{-2} to 6.0 Jcm^{-2}, were plotted in Figure 5.20. The linear line plot in Figure 5.20 shows that the temperature rise in the tumour was proportional to the fluence of the light source. Even at the highest fluence, the maximum temperature increase in the tumour was only limited to 1.4 $^{\circ}C$.
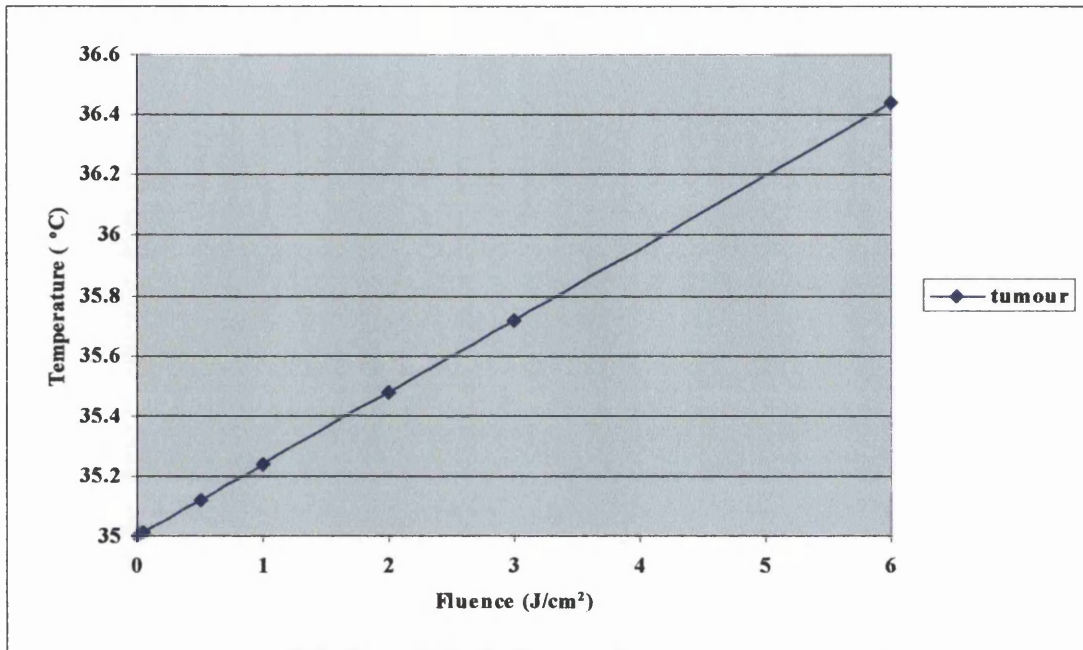
Figure 5.20: Maximum temperature in the tumour as a function of fluence.

5.4.2 Photothermal Damage against Fluence

Next, the effect of temperature rise in previous section on the photothermal damage was examined. The maximum photothermal damage in the tumour for the fluence range was plotted in Figure 5.21.
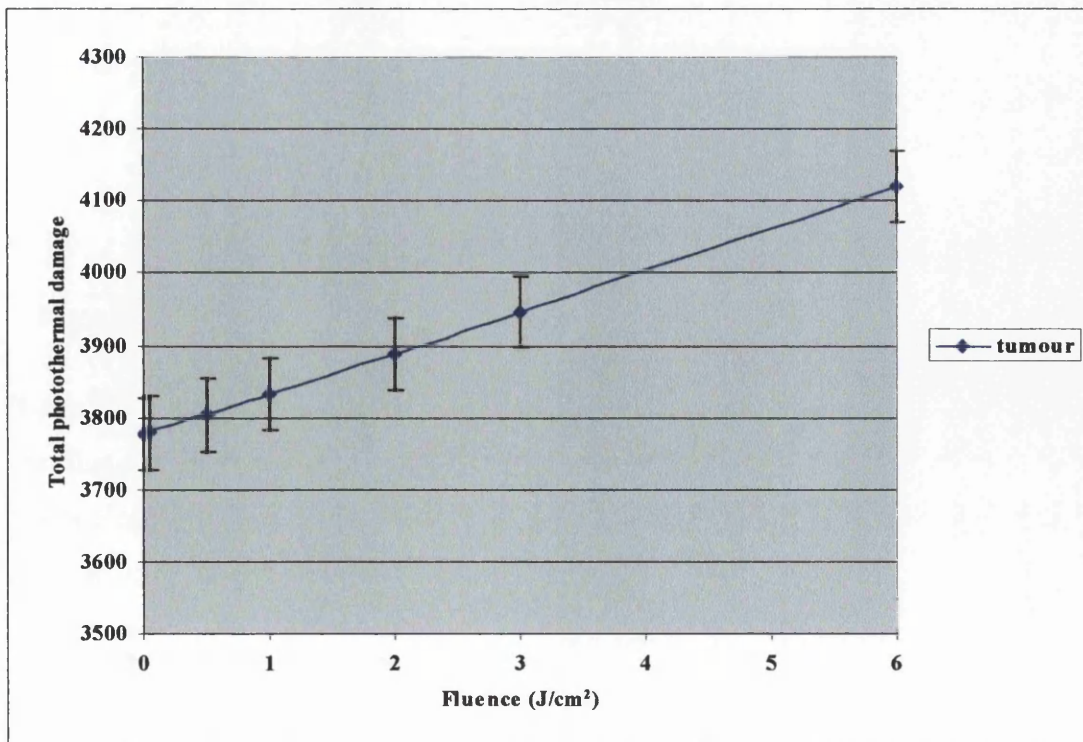
Figure 5.21: Total photothermal damage in the tumour as a function of fluence.

The amount of photothermal damage increases by a small amount throughout the fluence range. This is because the temperature rise in the tumour was too low to cause any substantial photothermal damage.

5.4.3 Photodynamic Damage against Fluence

The effects of fluence on the photodynamic damage were investigated in this subsection. The maximum photodynamic damage in the tumour as a function of fluence was plotted in Figure 5.22.
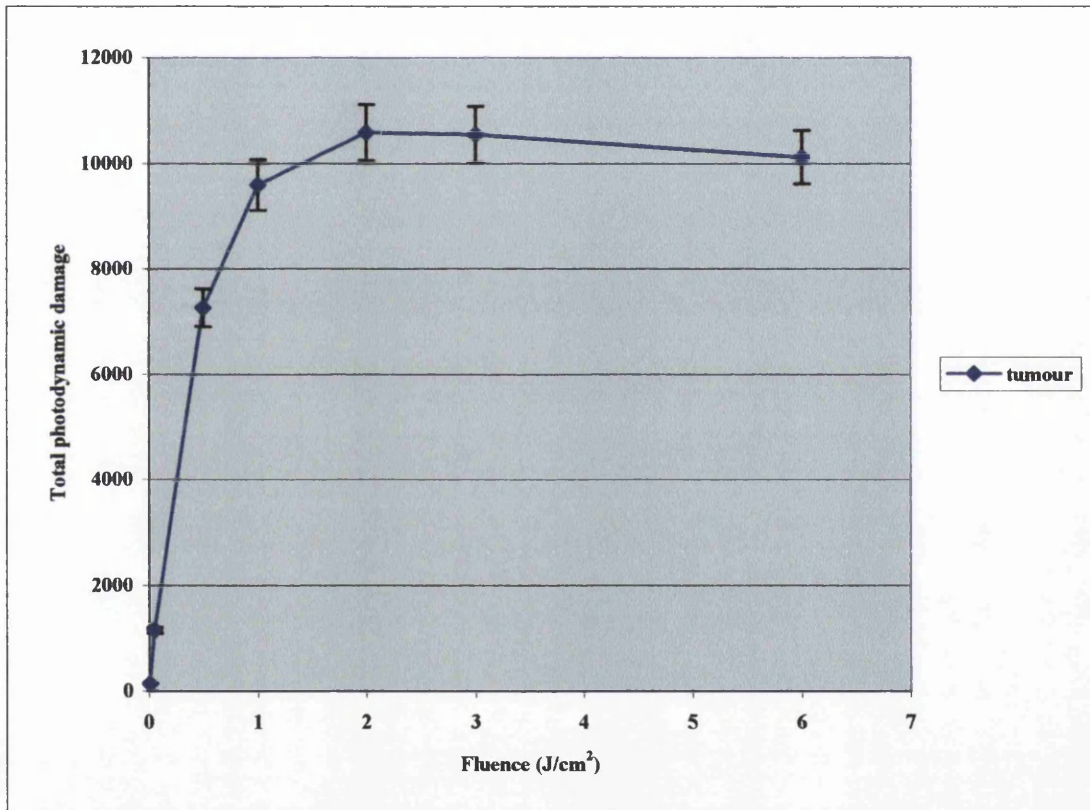
Figure 5.22: Total photodynamic damage in the tumour as a function of fluence.

It can be seen from Figure 5.22 that the highest photodynamic damage occurs when the fluence was 2.0 Jcm^{-2}. The photodynamic damage increases rapidly at low fluence range (0-1 Jcm^{-2}) and starts to saturate at medium fluence range (1-3 Jcm^{-2}). At low fluence of 0.5 Jcm^{-2}, the photodynamic damage achieves at least 80% efficiency of the peak photodynamic damage. The saturation effect of photodynamic damage observed in the medium fluence range is as a result of limited photosensitiser concentration in the tumour being exhausted. Saturation decreases the photodynamic

effectiveness by limiting the rate of photodynamic damage to a maximum value. Although it can be seen as a disadvantage, the benefit of saturation is that the photodynamic effect is only dependent on the concentration of the photosensitiser and not on the fluence. This suggests that pulsing may be advantageous in repopulating the photosensitiser in the tumour. It is interesting to note that at high fluence range (3-6 Jcm^{-2}), there was a slight reduction in the photodynamic damage. A reasonable explanation for this is that high fluence increases the rate of photobleaching in the tumour. At high fluence, photobleaching would prevent administration of light dose sufficient for complete tumour damage. Thus, low fluence may be necessary to achieve an equivalent photodynamic effect when lower photosensitiser doses were used. Figure 5.23 shows that photodynamic damage profile varies with fluence range between 0.005 Jcm^{-2} to 6.0 Jcm^{-2}. From the results of Figure 5.23, 0.5 Jcm^{-2} fluence was enough to generate 80% PDT effectiveness with the advantage of minimum damage in the upper dermis and lower dermis as compared to 2.0 Jcm^{-2} fluence.
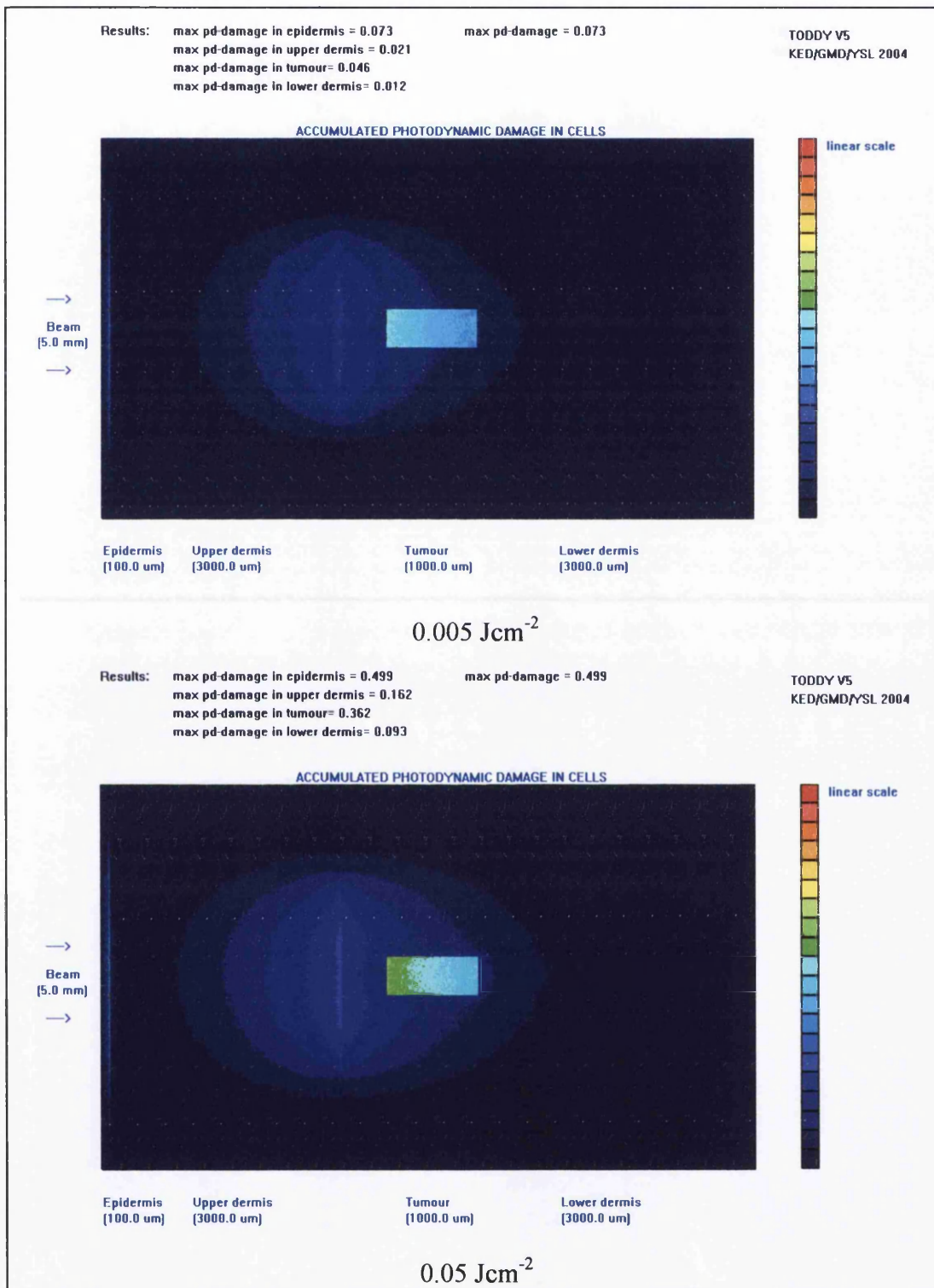
0.005 Jcm^{-2}

0.05 Jcm^{-2}

Figure 5.23: Photodynamic damage profile for fluence range between 0.005 Jcm^{-2} to 6.0 Jcm^{-2}.

Results: max pd-damage in epidermis = 1.309   max pd-damage = 2.052
             max pd-damage in upper dermis = 0.962
             max pd-damage in tumour= 2.052
             max pd-damage in lower dermis= 0.684

TODDY V5
KED/GMD/YSL 2004

ACCUMULATED PHOTODYNAMIC DAMAGE IN CELLS

linear scale

Beam
[5.0 mm]

Epidermis   Upper dermis   Tumour   Lower dermis
[100.0 um]   [3000.0 um]   [1000.0 um]   [3000.0 um]

$0.5 \ Jcm^{-2}$

Results: max pd-damage in epidermis = 1.320   max pd-damage = 2.533
             max pd-damage in upper dermis = 1.223
             max pd-damage in tumour= 2.533
             max pd-damage in lower dermis= 1.014

TODDY V5
KED/GMD/YSL 2004

ACCUMULATED PHOTODYNAMIC DAMAGE IN CELLS

linear scale

Beam
[5.0 mm]

Epidermis   Upper dermis   Tumour   Lower dermis
[100.0 um]   [3000.0 um]   [1000.0 um]   [3000.0 um]

$1.0 \ Jcm^{-2}$

Results: max pd-damage in epidermis = 1.320   max pd-damage = 2.655
             max pd-damage in upper dermis = 1.313
             max pd-damage in tumour= 2.655
             max pd-damage in lower dermis= 1.249

TODDY V5
KED/GMD/YSL 2004

ACCUMULATED PHOTODYNAMIC DAMAGE IN CELLS

linear scale

Beam
[5.0 mm]

Epidermis   Upper dermis   Tumour   Lower dermis
[100.0 um]   [3000.0 um]   [1000.0 um]   [3000.0 um]

Figure 5.23 $2.0 \ Jcm^{-2}$

Results: max pd-damage in epidermis = 1.320   max pd-damage = 2.653   TODDY V5
          max pd-damage in upper dermis = 1.319   KED/GMD/YSL 2004
          max pd-damage in tumour= 2.653
          max pd-damage in lower dermis= 1.304

ACCUMULATED PHOTODYNAMIC DAMAGE IN CELLS

linear scale

Beam
[5.0 mm]

Epidermis   Upper dermis   Tumour   Lower dermis
[100.0 um]   [3000.0 um]   [1000.0 um]   [3000.0 um]

$3.0 \ Jcm^{-2}$

Results: max pd-damage in epidermis = 1.320   max pd-damage = 2.557   TODDY V5
          max pd-damage in upper dermis = 1.320   KED/GMD/YSL 2004
          max pd-damage in tumour= 2.557
          max pd-damage in lower dermis= 1.320

ACCUMULATED PHOTODYNAMIC DAMAGE IN CELLS

linear scale

Beam
[5.0 mm]

Epidermis   Upper dermis   Tumour   Lower dermis
[100.0 um]   [3000.0 um]   [1000.0 um]   [3000.0 um]

$6.0 \ Jcm^{-2}$

Figure 5.23 (continued)

5.4.4 Photosensitiser Concentration against Fluence

Next, the effects of fluence on the rate of photosensitiser concentration consumption and the rate of photodynamic damage in the tumour were analysed. Figure 5.24 shows the photodynamic damage and photosensitiser concentration in the tumour as a function of time for 0.5 Jcm^{-2}, 1.0 Jcm^{-2} and 3.0 Jcm^{-2} fluence. It can be seen at high fluence that the photodynamic damage in the tumour reaches saturation point in the shortest duration as the photosensitiser concentration in the tumour was expended. At medium fluence, the rate of photodynamic damage was slower than high fluence but faster than low fluence. Although the rate of photodynamic damage at low fluence was the slowest among all, it still reaches the peak photodynamic damage level of high fluence at the expense of longer irradiation duration. This has an added benefit of maintaining a high level of oxygen concentration in the tumour throughout the irradiation duration.
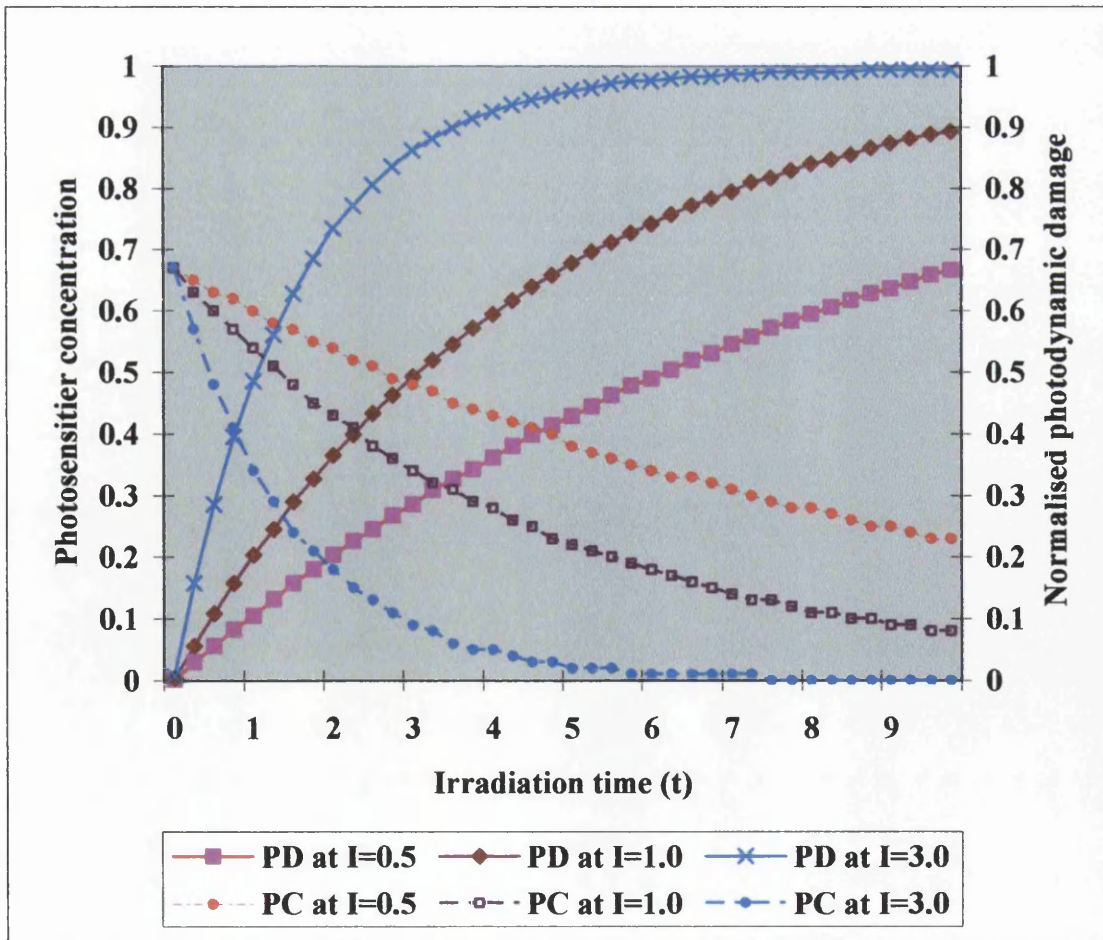
Figure 5.24: Photosensitiser concentration with normalised photodynamic damage in the tumour as a function of irradiation time.

5.4.5 Conclusions

These findings suggest that low fluence outcome was just as effective as medium fluence and high fluence. To avoid thermal effects, the fluence should be kept below the photothermal damage lower threshold. This opens up the possibility of using a low intensity LED embedded into tissue for PDT. However, the total light dose required for PDT is high hence time of treatment will be longer if low fluence is used. Thus, an example of using m-THPC as a photosensitiser in cancer treatment, the total light dose may typically be 100.0 Jcm^{-2} and the fluence is 0.5 Jcm^{-2}. The time of treatment required is therefore 200 seconds (100/0.5) or just over three minutes. If the fluence of 0.05J/cm^2 is used, the time of treatment required is 2000 seconds or 34 minutes. The embedded LED can be programmed to pulse continuously to deliver the minimum total light dose required and then switched off. The inactivated LED is left inside tissue for subsequent treatment. This method allows PDT to be repeated as many times as needed at intervals of two weeks to completely destroy the tumour while maintaining the PDT efficiency at each treatment.

5.5 Effects of Photosensitiser and Oxygen Concentration

In this section, the importance of photosensitiser concentration and oxygen concentration in the normal and tumour tissue were demonstrated. The ratio of photosensitiser intake in the tumour tissue compared to the normal tissue determines the selectivity of photodynamic damage in tissue. The oxygen concentration in tissue governs the amount of photodynamic effect occurring at that time. These two key parameter values were varied and analysed in the following subsections.

5.5.1 Photodynamic Damage against Photosensitiser Contrast Ratio

The ratio of photosensitiser intake in tumour and normal tissue for different types of photosensitiser were listed in Table 5.11. The photosensitiser initial total dose in tissue were normalised to a value of 1.0.

Photosensitiser	Ratio of photosensitiser intake in tumour/normal tissue [73]	Concentration of photosensitiser in tumour/normal tissue (Total dose of 1.0)
Photofrin	0.3:1	0.23/0.76
AlPCTrS	1:1	0.5/0.5
HPD (1)	1.7:1	0.63/0.37
Chl e6	6.3:1	0.86/0.14
HPD (2)	8.9:1	0.9/0.1

Table 5.11: Ratio of photosensitiser intake in the tumour and normal

tissue for various photosensitisers

The amount of photodynamic damage in the tumour and in the dermis as a function of photosensitiser concentration in the tumour was plotted in Figure 5.25. The photodynamic damage profiles for each photosensitiser ratio of intake were shown in Figure 5.26 to Figure 5.30. It can be said that the minimum concentration required for photosensitiser localisation in the tumour was 60% of the total dose or the ratio of 1.5:1 to improve the selectivity of photodynamic effect in the tumour. The ratio of 8.9:1 of HPD (2) intake achieves the best tumour selectivity along with the highest photodynamic damage in the tumour.
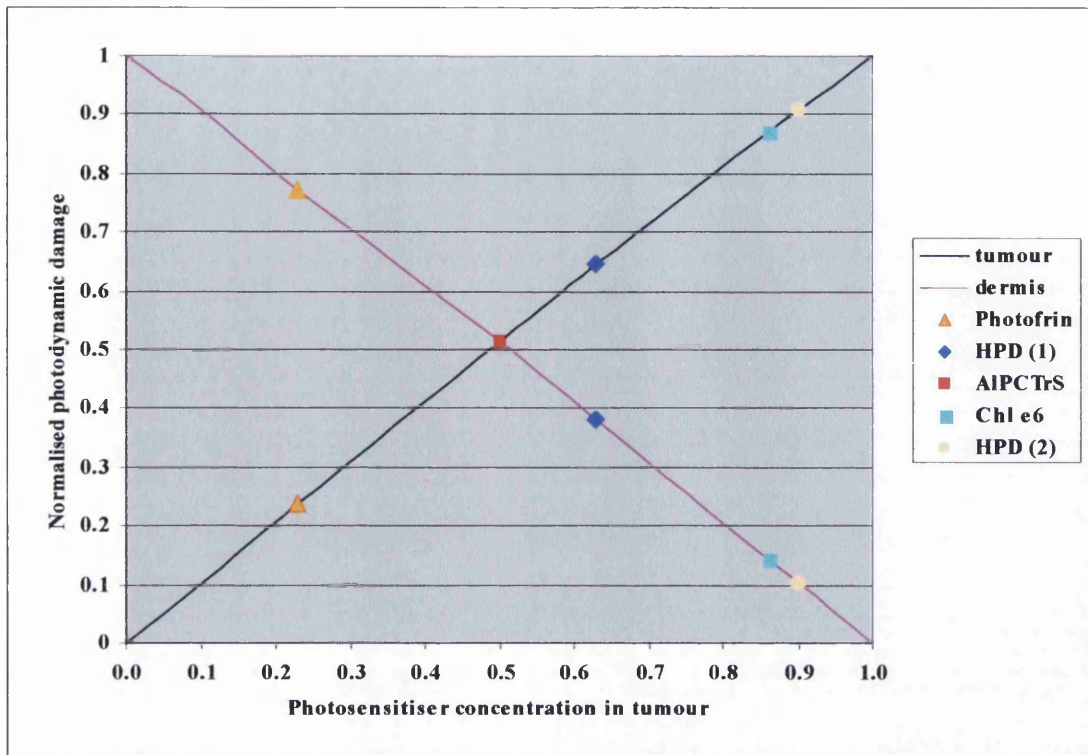
Figure 5.25: Photodynamic damage in the tumour and in the dermis as a function of photosensitiser concentration in the tumour
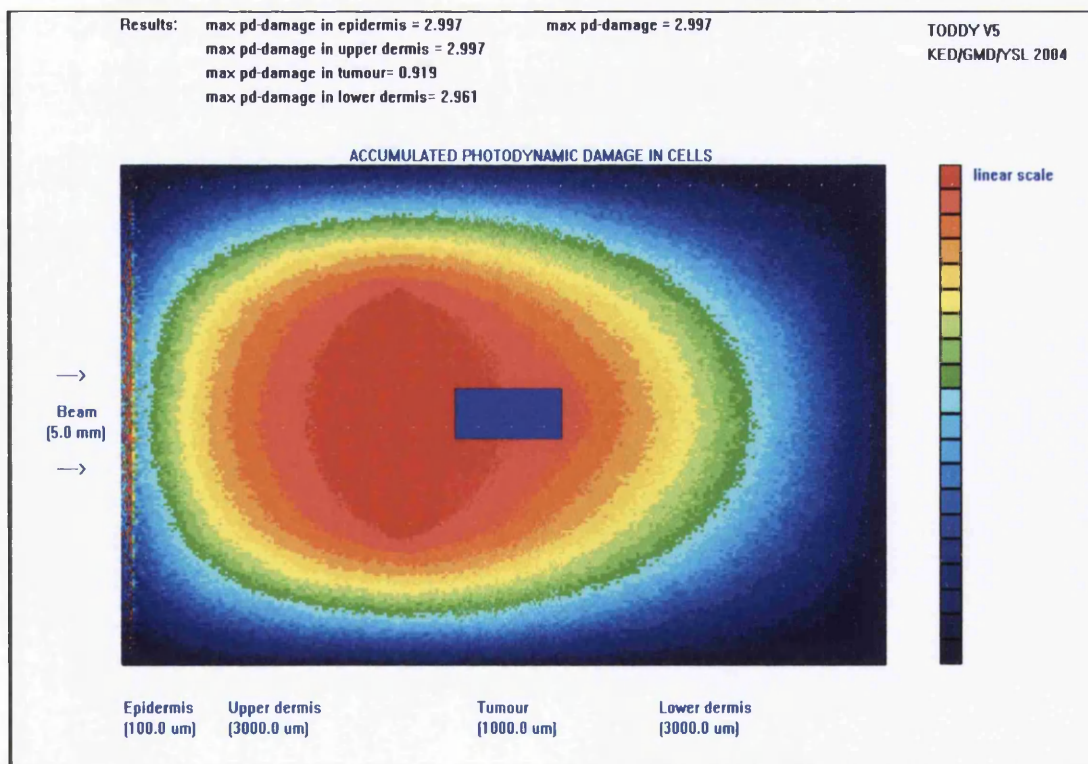
Figure 5.26: Photodynamic damage profile for 0.3:1 ratio of photosensitiser intake in tumour tissue and normal tissue.
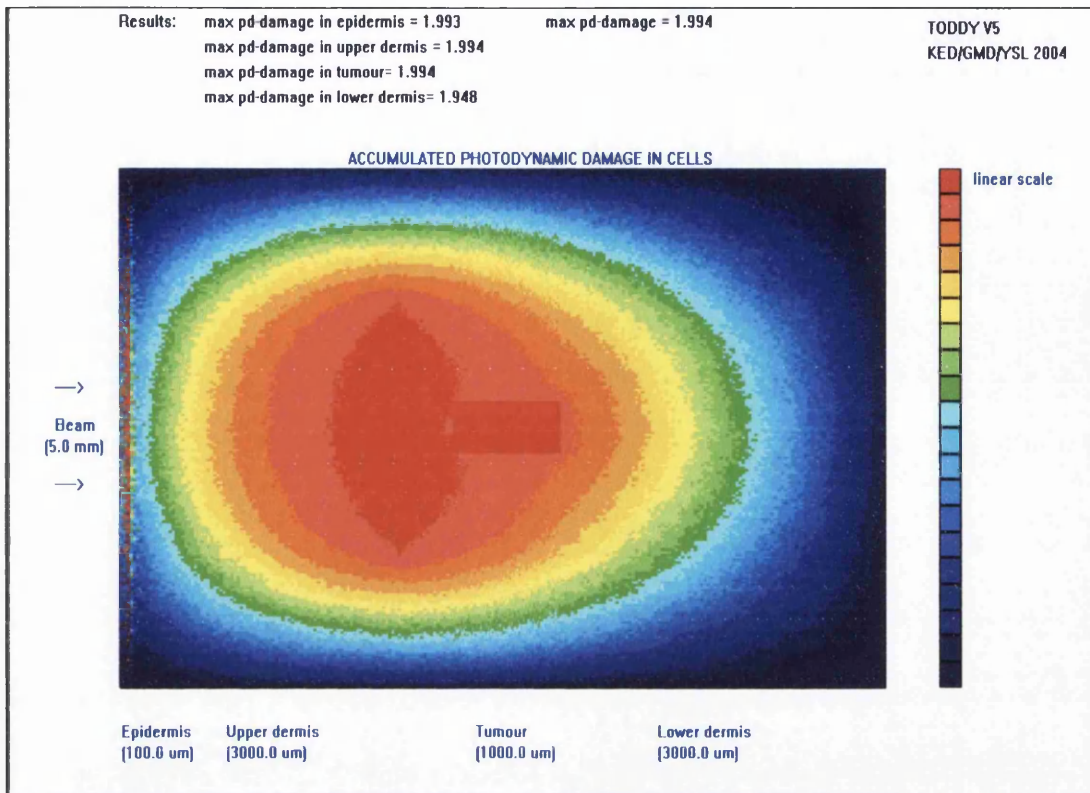
Figure 5.27: Photodynamic damage profile for 1:1 ratio of photosensitiser intake in tumour tissue and normal tissue.
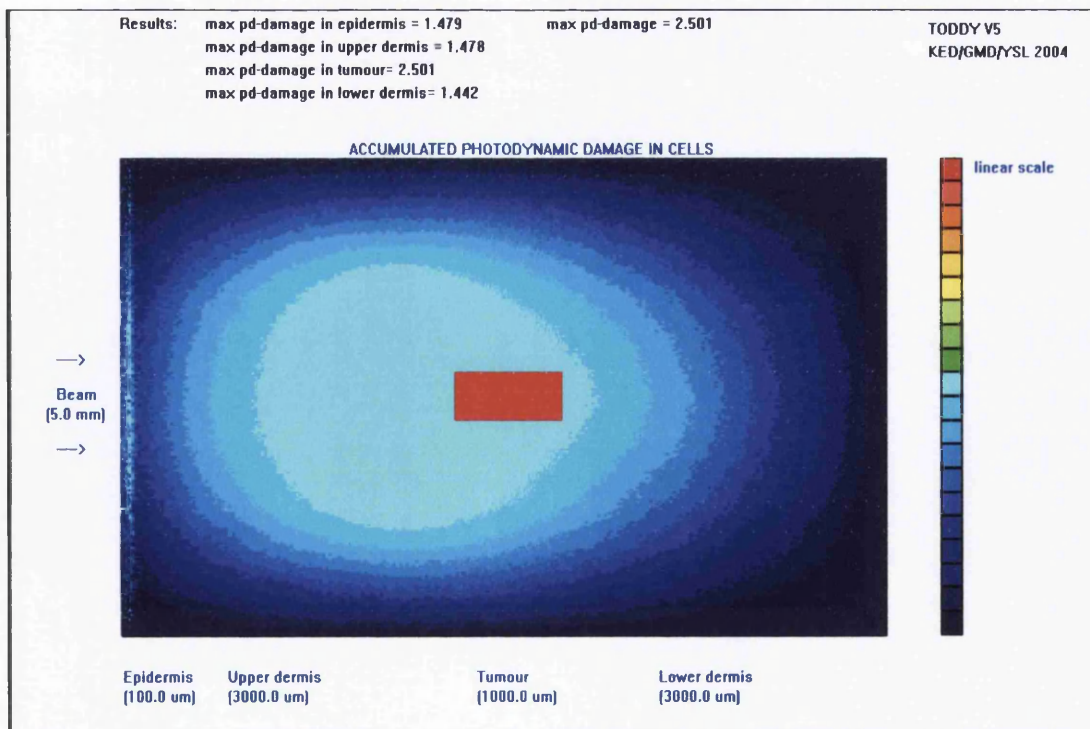
Figure 5.28: Photodynamic damage profile for 1.7:1 ratio of photosensitiser intake in tumour tissue and normal tissue.
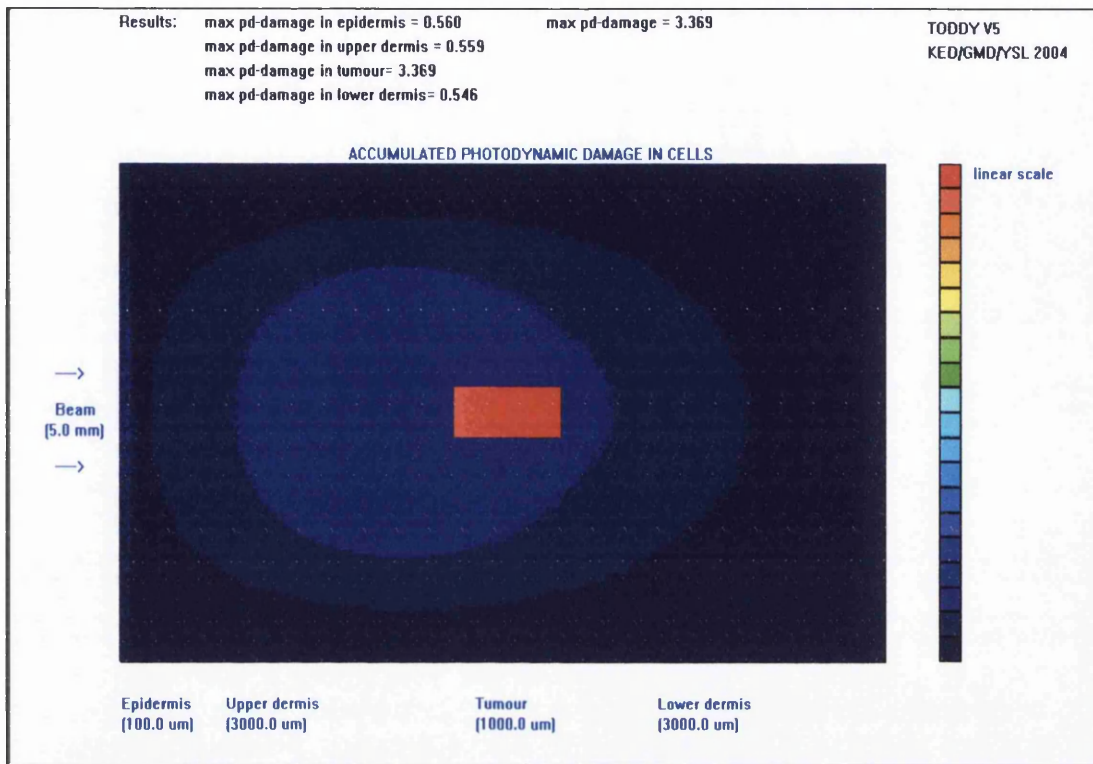
Figure 5.29: Photodynamic damage profile for 6.3:1 ratio of photosensitiser intake in tumour tissue and normal tissue.
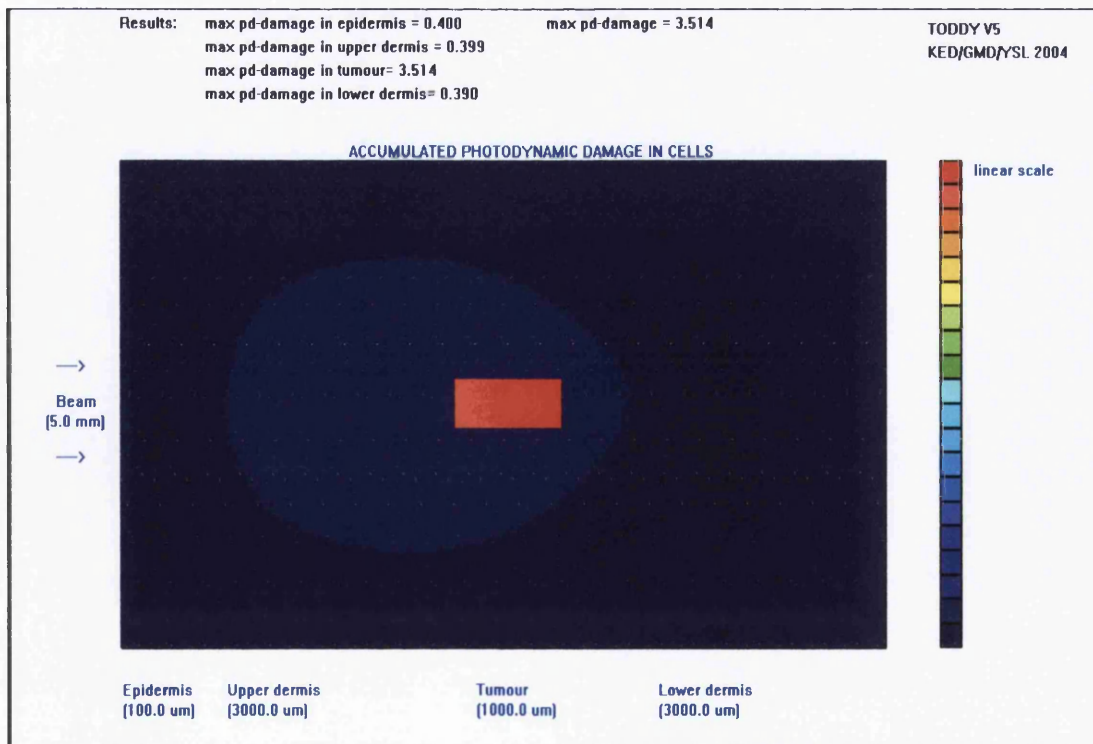
Figure 5.30: Photodynamic damage profile for 8.9:1 ratio of photosensitiser intake in tumour tissue and normal tissue.

5.5.2 Photodynamic Damage against Photosensitiser Dose

Next, the effects of photosensitiser dose on the photodynamic damage in the tumour were examined. The photosensitiser initial total dose was varied to reflect the high photosensitiser dose and low photosensitiser dose applied in the PDT. The ratio of 2:1 of photosensitiser intake in the tumour and normal tissue was used in the analysis. Table 5.12 shows the percentage of photosensitiser dose with the photosensitiser concentration in the tumour and normal tissue.

Percentage of control dose	Normalised photosensitiser dose	Concentration of photosensitiser in tumour/normal tissue
200%	2.0	1.33/0.67
150%	1.5	1.0/0.5
100%	1.0 (control dose)	0.67/0.33
50%	0.5	0.33/0.17
25%	0.25	0.17/0.08
0%	0	0/0

Table 5.12: Photosensitiser dose with photosensitiser concentration in the tumour/normal tissue

The results of Figure 5.31 show that the increase in photodynamic damage in the tumour was proportional to the photosensitiser concentration in the tumour. When the photosensitiser dose was doubled, the damage in the tumour increases correspondingly. Moreover the photodynamic damage in the surrounding tissue also increases relatively. When there was no photosensitiser dose absorbed, the damage occurring in the tumour and normal tissue was zero. These findings confirm that the photosensitiser dose used for PDT should be just adequate for tumour annihilation. An increase in photosensitiser dose does not help the selective photodynamic effect in the tumour.
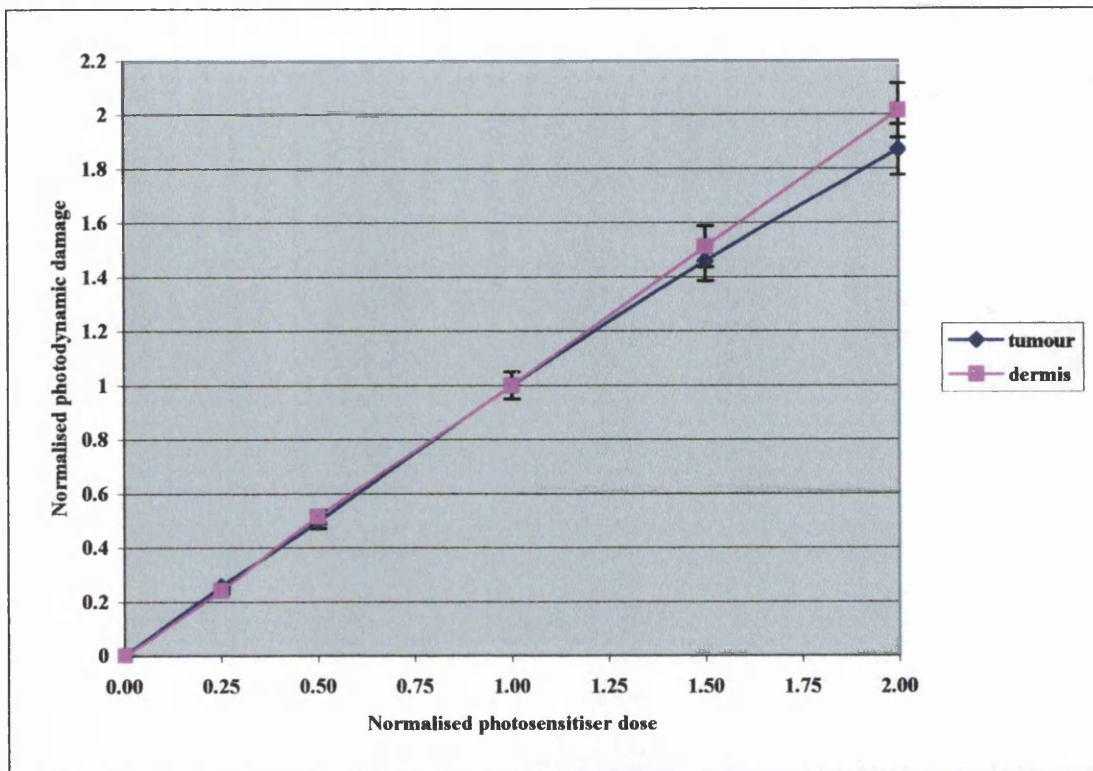
Figure 5.31: Photodynamic damage in the tumour and dermis as a function of photosensitiser dose

5.5.3 Photodynamic Damage against Oxygen Concentration

To help show the importance of oxygen in effect to the photodynamic effect, the initial oxygen concentration in the tumour was varied according to the percentage of oxygenation in the tumour. Table 5.13 shows the percentage of oxygenation in the tumour with the oxygen concentration in the tumour.

Figure 5.32 shows the amount of photodynamic damage in the tumour as a function of oxygen concentration in the tumour. It can be seen in Figure 5.32 that the photodynamic damage in the tumour increases with increasing oxygen concentration in the tumour. When there was no oxygen available, the damage occurring in the tumour was zero. It is best to increase the amount of oxygen available to the tumour for maximum photodynamic effect. The amount of oxygen available to the tumour is dependent on the percentage of oxygenation in the blood and tissue perfusion rate. Oxyhemoglobin blood carries a higher percentage of oxygen level than deoxyhemoglobin blood. Increasing the tissue perfusion rate also helps replacing the oxygen lost during irradiation and maintaining the initial oxygen level in the tumour.

Percentage of oxygenation in the tumour	Equivalent initial oxygen concentration in the tumour
100%	1.0
90%	0.9
80%	0.8
70%	0.7
60%	0.6
50%	0.5
40%	0.4
30%	0.3
20%	0.2
10%	0.1
0%	0

Table 5.13: Percentage of oxygenation in the tumour with oxygen concentration in the tumour
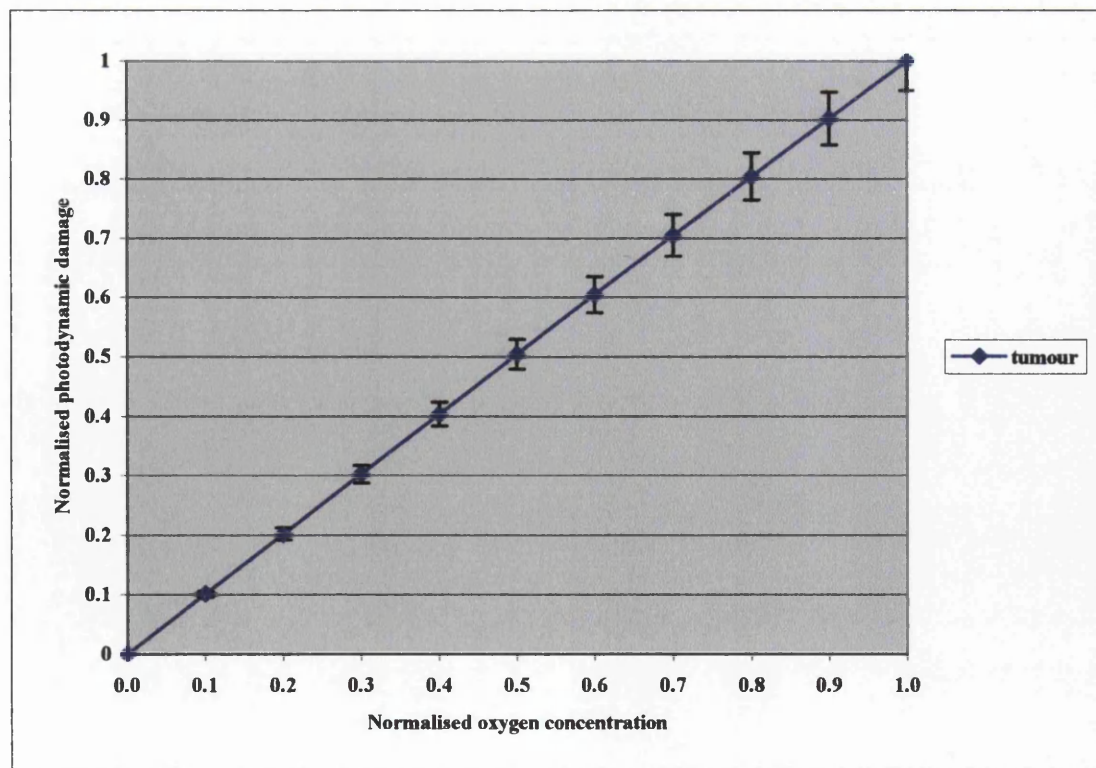
Figure 5.32: Photodynamic damage in the tumour as a function of oxygen concentration for constant perfusion rate

5.6 Sensitivity Analysis of Photodynamic Reaction Rate Constants

5.6.1 Damage Rate Constant (k_{pd}) Variation

The role of damage rate constant combines the photosensitiser absorption coefficient and the efficiency of generation of cytotoxic oxygen species. This is dependent on the light's wavelength and photosensitiser used for PDT treatment. The quantity of damage rate was varied to demonstrate the efficiency of the photosensitiser with effect to the photodynamic damage as shown in Table 5.14.

Percentage of damage rate	k_{pd}
200%	0.002
150%	0.0015
100%	0.001 (control constant)
50%	0.0005
25%	0.00025
1%	0.00002

Table 5.14: Percentage of damage rate with k_{pd} quantity

The results of photodynamic damage in the tumour as a function of damage rate variation were plotted in Figure 5.33. The graph in the Figure 5.33 shows that the increase in photodynamic damage in the tumour is proportional to the efficiency of the photosensitiser. The efficiency of various photosensitisers in generating singlet oxygen is dependent on the singlet oxygen quantum yield. This means that a high singlet oxygen quantum field photosensitiser should be used to produce singlet oxygen for maximum photodynamic effect. Furthermore, high photodynamic damage rate is achieved if the wavelength of the light source matches the photosensitiser peak wavelength. When the absorption coefficient is at the peak level, the efficiency of generation of oxygen radical is higher than any other wavelengths used. Overall, the photosensitiser dose used in the PDT can then be reduced to generate the same amount of photodynamic damage with the added benefit of less photosensitivity endured by the patients.
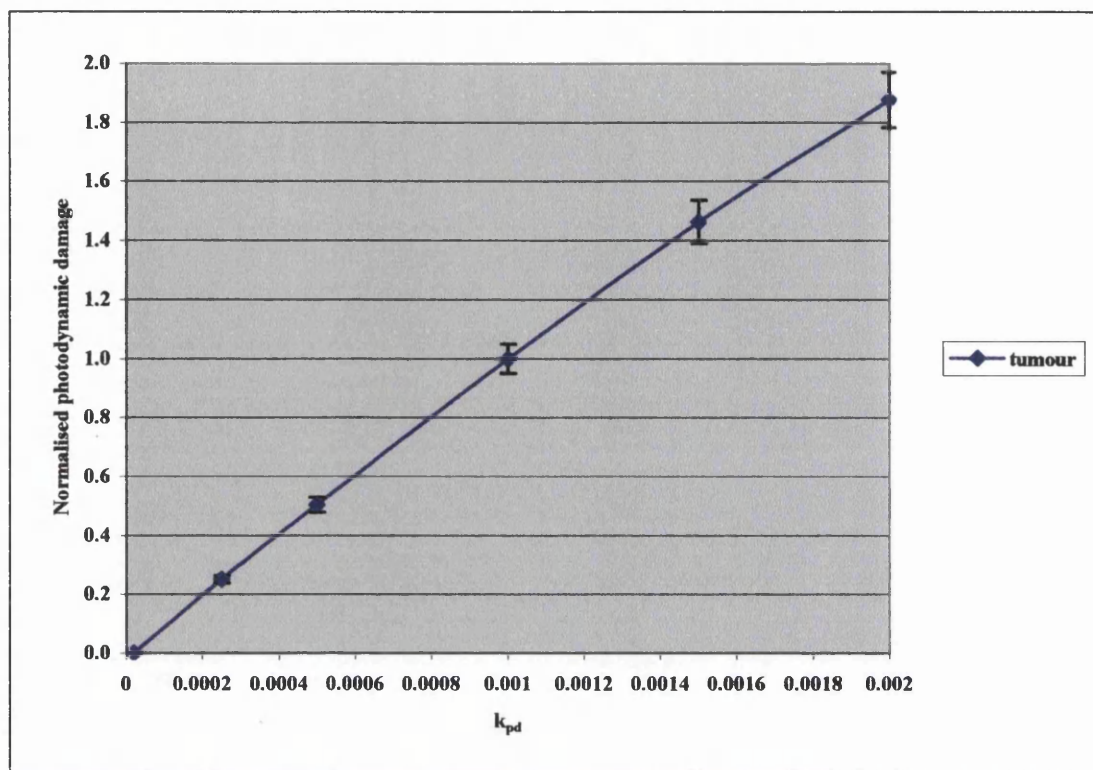
Figure 5.33: Photodynamic damage in the tumour as a function of damage rate

5.6.2 Photobleaching Rate Constant (k_{pb}) Variation

Next, the effect of photobleaching rate on the photodynamic damage in the tumour was examined. The rate of photobleaching of various photosensitisers is dependent on the photobleaching quantum yield. The initial photobleaching rate was varied as listed in Table 5.15.

Percentage of photobleaching rate	k_{pb}
200%	0.00050
150%	0.000375
100%	0.00025 (control constant)
50%	0.000125
25%	0.0000625
1%	0.0000025

Table 5.15: Percentage of photobleaching rate with k_{pb} quantity

Figure 5.34 show the photodynamic damage in the tumour as a function of photobleaching rate variation. The curve shows that, by decreasing the

167

photobleaching rate, the photodynamic damage increases greatly in the tumour. It was observed that by reducing the photobleaching rate by half, the amount of photodynamic damage was doubled in the tumour. Hence, this finding shows that the use of a photosensitiser with low photobleaching quantum yields generates a better PDT response than a high photobleaching quantum yield photosensitiser.
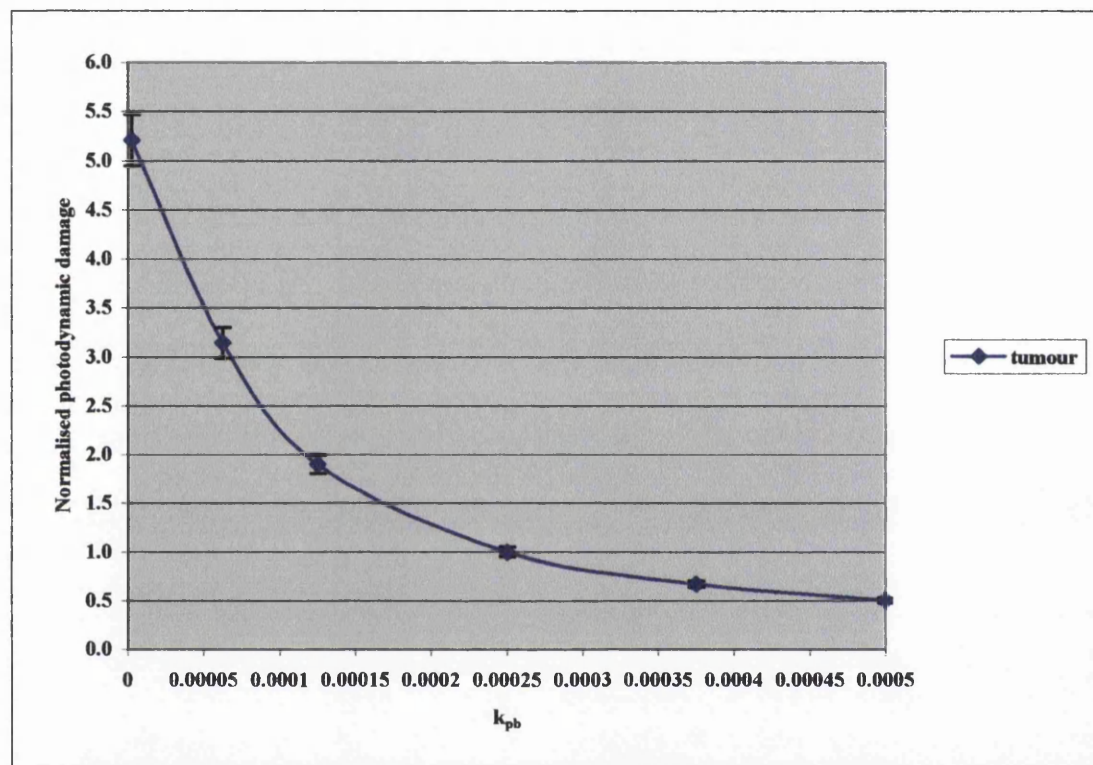
Figure 5.34: Photodynamic damage in the tumour as a function of photobleaching rate

5.6.3 Tissue Perfusion Rate Constant (k_{perf}) Variation

In this subsection, the effect of tissue perfusion rate on the photodynamic damage in the tumour was analysed. The initial tissue perfusion rate was varied as shown in Table 5.16. The results of photodynamic damage in the tumour as a function of tissue perfusion rate variation were shown in Figure 5.35. Increasing the tissue perfusion rate to 200% only increases the photodynamic effect by 1%. Also, when the tissue perfusion rate dropped to 50% of the initial value, the photodynamic damage decreased by 3%. This was mainly because the oxygen levels in the tumour and normal tissue were already at their peak level. The rate of photodynamic damage at medium fluence does not deplete the oxygen level to a great extent that the oxygen

level remained high throughout the total irradiation duration. Hence, the increase or decrease in the tissue perfusion rate provides a small effect on the overall efficiency of the PDT treatment. In conclusion, all of the rate constant analyses were for the standard short pulse duration at medium fluence. For low fluence, the pulse time is much longer; therefore the variation of damage with the perfusion rate will be sensitive to the pulse length over which the damage was achieved.

Percentage of tissue perfusion rate	k_{perf}
200%	0.02
150%	0.015
100%	0.01 (control constant)
50%	0.005
25%	0.0025
1%	0.0002

Table 5.16: Percentage of tissue perfusion rate with k_{perf} quantity
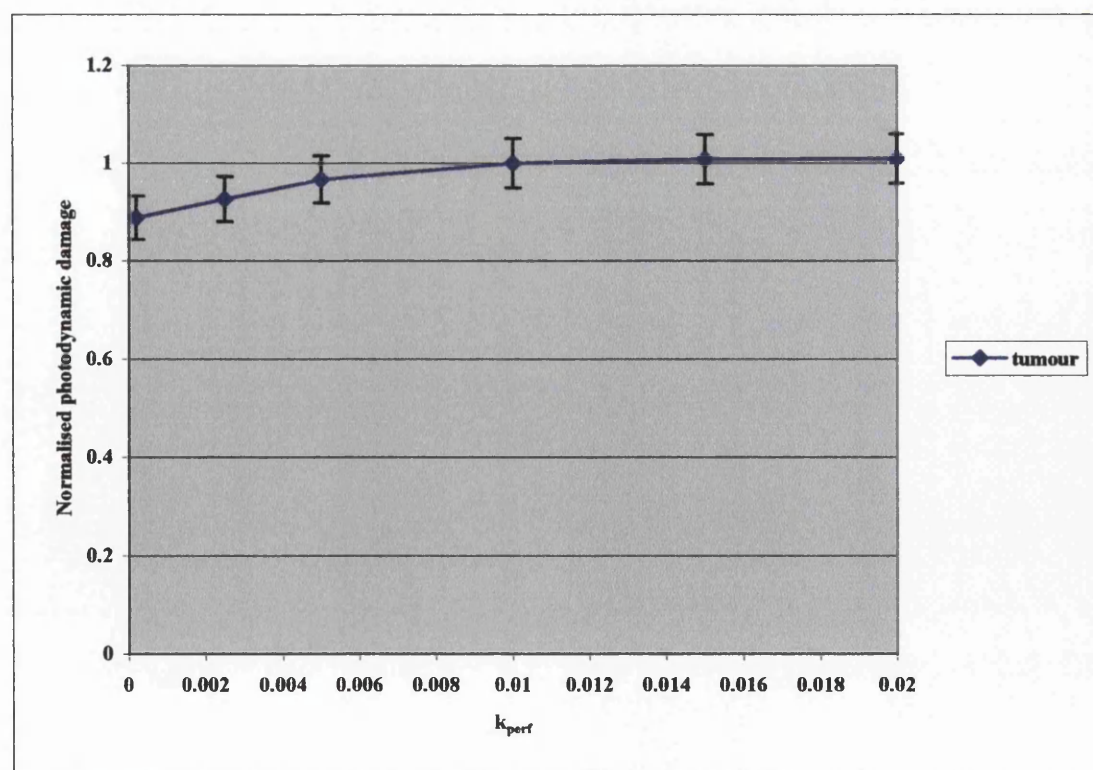

Figure 5.35: Photodynamic damage in the tumour as a function of tissue perfusion rate

5.7 Summary of Computational Study

A simple model of a light source embedded in tissue based on the Monte Carlo light transport was developed and used to study the light absorption distributions in tissue. In this chapter, it is shown that an embedded light source increases the total photon absorption being absorbed in the tumour. The LED position in tissue determines the amount of photon energy deposition in the tumour. The energy gained between surface light irradiation and light source placed next to the tumour was at least 40%. Another added benefit was that light absorption in the epidermis-melanin layer can be bypassed and reduced to almost zero when the LED was placed deep inside tissue. Also by using an embedded LED, the light penetration depth into tissue can be increased without the use of longer wavelengths. This generates higher temperature increase and photothermal damage in the tumour. The photodynamic induced damage in the tumour penetrates more deeply when the LED was placed near to the tumour.

The wavelength analyses showed that the use of longer wavelengths at 630nm and 652nm were preferable than 585nm since these wavelengths offer deeper light penetration depth and match the peak wavelength of most photosensitisers. Also, the temperature rise in tissue was much lower and the photodynamic damage was more uniform in the entire tumour region.

In the fluence analyses, the use of low fluence photodynamic therapy has been shown to be as effective as high fluence. Low fluence does not generate any temperature rise and photothermal damage in tissue. The only disadvantage was that low fluence requires a longer treatment time than high fluence to offer maximum photodynamic damage for the same total light dose. However, low fluence does not consume photosensitiser or deplete oxygen as fast as high fluence. This maintains a high level of oxygen in tissue and provides a steady rate of photodynamic damage in the tumour.

The use of a photosensitiser with high ratio of photosensitiser intake in the tumour and normal tissue together with high singlet oxygen quantum yields and low

photobleaching quantum yields achieves the maximum photodynamic damage and selectiveness in the tumour. Second generation photosensitisers offer better tumour selectivity and higher efficiency of singlet oxygen generation compared to first generation photosensitisers. Higher photosensitiser dose generates a higher photodynamic effect in the tumour but also in the normal tissue. Thus, the photosensitiser dose should be just sufficient for the total light dose to avoid photosensitivity experienced by patients after PDT treatment.

The role of oxygen in tissue plays an important factor in the photodynamic process. Low oxygenation in tissue generates a lower photodynamic damage compared to high oxygen concentration. High tissue perfusion rate was favoured to replenish the oxygen depleted by photodynamic process during irradiation.

All of these findings showed that the use of an embedded LED with low fluence offers the possibility of continuous light pulsing (e.g. 2 seconds on and 1 second off) at low photosensitiser dose in favour for hours of uninterrupted photodynamic effect with the convenience of patients staying at home.

As for the accuracy of the model was concerned, the two dimensional model was only capable of predicting the amount of damage in the tumour and normal tissue based on the photodynamic parameters. The photosensitiser efficiency as well as the exact photosensitiser and oxygen concentration available at treatment site at the start of irradiation were arbitrary values used in the model. The real values of these quantities used in PDT would need to be inserted into the model for absolute values of damage to be estimated. However, the model clearly shows the benefits of using optimised values for the fluence and photodynamic properties. The computed photodynamic damage model needs to be calibrated to the clinical observation of tumour cell death in photodynamic therapy.

CHAPTER 6   CONCLUSIONS

The review of the current literature indicated that photodynamic therapy is the emerging treatment of choice for a wide range of cancers. PDT is a complex photochemical process of light activation of photosensitiser in the presence of oxygen which generates the singlet oxygen excited state to cause damage in the cells. The Type II mechanism of action dominates the PDT process under normal oxygen concentration to generate the singlet oxygen to induce oxidative damage and cell necrosis. The selectivity of PDT is enhanced by the high contrast absorption of photosensitisers in the tumour and the confinement of the photosensitiser activation by controlling irradiation to only the tumour area.

The main setback for PDT extensive use is the costly and complex operation of laser systems. The disadvantages of photodynamic therapy are essentially the need for dedicated treatment rooms and the numerous treatment sessions to effectively kill the tumour. With high photosensitiser dose, a patient develops prolonged photosensitivity to visible light for several weeks following the PDT treatment. A significant point of the study is that photodynamic therapy is a photochemical reaction that is dependent on the total light dose and not the intensity of the light. Therefore, a low power LED system can be utilised as a cheaper method to treat cancer effectively. However, the low intensity irradiation of a LED system means that the light cannot penetrate the skin deeply to reach a deep centred tumour. The author's hypothesis was to use a novel method, in which the light source is embedded subcutaneously into the tissue which is powered remotely by RF energy. The embedded device, when positioned correctly in the tissue, has the ability to focus light to the treated tumour area to increase the absorption of light in the tumour and to minimise damage to the surrounding tissue. This method increases the efficiency and selectivity of the photodynamic damage and, in effect, lower photosensitiser drug dose can be used. It is reviewed that for tumours to be completely destroyed, PDT needs to be repeated up to two or three times at intervals of three weeks to three months. With the embedded device, each treatment sessions can be done periodically with the convenience of patients treated at home. Patients are able avoid the photosensitivity to sunlight and artificial light by staying at home for several days

after the treatment. This is a cost-effective technology that could enable the treatment of cancer to be available to a wider patient base.

A numerical model, written in Visual C++, has been developed to simulate photon transport and subsequent energy transfer in tissue. This model extends the previous TODDY computer model developed by G. Daniel and K. Donne by adding the chemistry kinetics of the photodynamic process as well as photothermal damage integration. [104] The theoretical computer model has shown that by positioning the LED next to the tumour, the absorption of light energy increased by 400% when comparing to surface irradiation. The embedded light source eliminated the light backscattered out of the tissues and reduced the absorption in the melanin layer. The low fluence delivered by a low energy light source is shown to be as effective as high fluence for photodynamic damage effect. The drawback with low fluence is essentially that the time of treatment required will be longer. However, at low fluence, the oxygen and photosensitiser can be replenished during the irradiation period to achieve optimum photodynamic effect. Second generation photosensitisers that have higher contrast ratio of absorption in the tumour relative to normal tissue combined with the LED wavelength selection achieves the best selectivity photodynamic damage in the tumour. It is also been shown that increasing the oxygen level and the tissue perfusion rate in the tissue increases the photodynamic damage effect.

The technique of using and embedded light source requires an energy source to power the LED. Obviously, a battery can be used but the main drawbacks with batteries are the size, limited power and toxicity. The author's hypothesis was to use electromagnetic waves as a method for energy transfer into tissues. There are two possible methods, namely the inductive coupling method and the radiative coupling method. Inductive coupling system operates at 10 MHz - 30 MHz radio frequency with magnetic field as the medium of transfer, while radiative coupling system operates at 2 GHz -10 GHz microwave frequency with electric field as the medium of transfer. Inductive coupling is based on the loop coils and radiative coupling is based on the antennas such as dipoles.

The absorption of electromagnetic wave energy in the tissue is dependent on the dielectric properties of tissue. On examination of the dielectric properties, the conductivity of the tissues increases with the wave frequency. At microwave frequency, the conductivity of the tissues is very high and exhibits high attenuation of energy in the tissues. The theoretical wave model showed that for 10 GHz frequency, half of the microwave energy is reflected out of the skin and only 5% of the incident power is available at 1cm tissue depth. The energy loss from reflection is due to the difference in the permittivity of free space and relative permittivity of the tissue. Hence, the microwave energy cannot penetrate deeply into tissue because of high attenuation loss. This has been confirmed experimentally with the microwave system operating at 2.5 GHz – 3.0 GHz using chicken skin, bacon and ham tissues. High energy absorption in tissues together with high reflection losses, are the main reasons that the radiative coupling method is not efficient for energy transfer. This is also the reason that the microwave frequency is employed in high power microwave oven for heating food.

As the inductive coupling method relies on magnetic field for energy transfer, an interesting point is that the permeability of tissue is the same as the permeability of free space. Hence the magnetic field can penetrate deep into human tissues with little attenuation and reflection losses. This is useful in coupling the energy needed to power the embedded device. This method of inductive coupling has been verified experimentally with the RF system operating at 13.56MHz. The RF system has been shown to induce the required voltage to power the LED in the receiver device successfully through the thick slices of bacon tissue. The receiver device showed no power loss when the energy is coupled into the bacon tissue. It is crucial that the circuit of the receiver is tuned to the resonant frequency of the transmitter. A tuned resonant circuit of the receiver generates a higher current to the LED. A higher number of coil turns and optimum diameter of the transmitter coil generate maximum magnetic field and concentrate the magnetic flux density into the receiver coil. When the operating frequency of the RF transmitter is increased, fewer coils are needed for the receiver which effectively reduces the size of the receiver. It is suggested that the 27MHz is another possible International Standard Medical frequency for energy transfer with the advantage of a smaller receiver size. In comparison with the microwave system, the RF system utilising inductive coupling

method is a more efficient way to couple energy through the tissue to power the LED device.

The initial objective for undertaking this work, namely developing an innovative and effective method for improving the current PDT treatment modality, has been achieved.

6.1 Future work

Future possibility of work to continue this programme will concentrate on the following area.

- Developing a small scale integrated chip device incorporating the inductor, the capacitor and the LED.

- Production of a complete RF system capable of allowing investigation into a set of RF parameters allowing optimum energy coupling into tissue.

- Investigating a suitable method to implant the device into tissue easily and safely.

- Investigating a suitable method to accurately quantifying the photodynamic damage occurring in the tumour after treatment for clinical trial test.

- Developing a suitable method for doctors to assess the improvement of treatment in the patients using the embedded light source for PDT.

- Improving theoretical computer models to include more complex tissues geometries and modelling the light and photodynamic process more accurately.

- Investigating other potential applications of an embedded light source in the medical field. Examples are low power bio-stimulation for wound healing and phototherapy for inflammation of subcutaneous tissue using red and blue LED.

175

REFERENCES

1. Cancer Research UK; "Cancer statistic incidence in United Kingdom [online]", 2004. Available from: http://www.cancerresearchuk.org/statistics

2. M.D. Daniell, J.S. Hill; "A history of photodynamic therapy", *Australian New Zealand Surgery*, Vol 61, pp. 340, 1991.

3. R. Bonnett; "Photodynamic therapy in historical perspective", *Review in Contemporary Pharmacotherapy*, Vol 10, pp. 1-19, 1999.

4. R.L. Lipson, E.J. Baldes et al; "The use of a derivative of haematoporphyrin in tumour detection", *Journal of National Cancer Institute*, Vol 26, No. 1, 1961.

5. R.L. Lipson, E.J. Baldes et al; "Hematoporphyrin derivative for detection and management of cancer", *Cancer*, Vol 20, pp.2255, 1967.

6. T.J. Dougherty, G.B. Grindey et al; "Photoradiation therapy II. Cure of animal tumours with hematoporphyrin and light", *Journal of National Cancer Institute*, Vol 55, pp.115, 1975.

7. T.J. Dougherty, J.E. Kaufman et al; "Photoradiation therapy for the treatment of malignant tumours", *Cancer Research*, Vol 38, pp.2628, 1978.

8. Axcan Pharma; "Patients guide – Photofrin® [online]", Axcan Scandipharma, USA 2003. Available from: http://www.photofrin.com

9. C. Hopper; "Photodynamic therapy: a clinical reality in the treatment of cancer", *Lancet Oncology*, Vol 1, No. 4, pp. 212-219, 2000.

10. K. Svanberg, T. Andersson et al; "Photodynamic therapy of nonmelanoma malignant tumours of the skin using topical delta-amino levulinic acid sensitization and laser irradiation", *British Journal of Dermatol*, Vol 130, pp. 743, 1994.

11. B.D. Wilson, T.S. Mang et al; "Photodynamic therapy for the treatment of basal cell carcinoma", *Archives of Dermatology*, Vol 128, pp.1597-1601, 1992.

12. M. Ochsner; "Photophysical and photobiological processes in the photodynamic therapy of tumours", *Journal of Photochemical and Photobiology B: Biology*, Vol 39, pp. 1–18, 1997.

13. C.S Foote, "Singlet oxygen production from photodynamic sensitizers"; *Journal of Photochemistry*, Vol 25, p.p 549,1984.

14. M.S. Westley, M.A. Cynthia et al; "Photodynamic therapeutics: basic principles and clinical applications", *Journal of Drug Discovery Today*, Vol 4, No. 11, 1999.

15. J. M. Fernandez et al, "Singlet oxygen generation by photodynamic agents" *Journal of Photochemical and Photobiology B: Biology*, Vol 46, pp. 147–160, 1987.

16. S. Miskoski, E. Sanchez et al, "Singlet molecular oxygen-mediated photo-oxidation of tetracyclines: kinetics, mechanism and microbiological implications", *Journal of Photochemistry and Photobiology B: Biology*, Vol 43, pp. 164-171, 1998.

17. J.N. Mark, J.S. Andrea et al; "In vitro tests of the validity of singlet oxygen luminescence measurements as a dose metric in photodynamic therapy", *Cancer Research*, Vol 63, pp 7986–7994, 2003.

18. R.R. Anderson, J.A. Parrish; "Selective photothermolysis: precise microsurgery by selective absorption of pulsed radiation", *Science*, Vol 220 pp. 524, 1983.

19. T.M. Sitnik, J.A. Hampton et al; "Reduction of tumour oxygenation during and after photodynamic therapy in vivo: effects of fluence rate", *British Journal of Cancer*, Vol 77, pp. 1386–1394, 1998.

20. D.J. Robinson, H.S. de Bruijn et al; "Fluorescence photobleaching of ALA-induced protoporphyrin IX during photodynamic therapy of normal hairless, mouse skin: the effect of light dose and irradiance and the resulting biological effect", *Journal of Photochemical and Photobiology*, Vol 67, pp. 140–149, 1998.

21. T.H. Foster, R.S. Murant, et al; "Oxygen consumption and diffusion effects in photodynamic therapy", *Radiation Research*, Vol 126, pp. 296–303, 1991.

22. S. Muller, H. Walt, et al "Enhanced photodynamic effects using fractionated laser light", *Journal of Photochemical and Photobiology B: Biology*, Vol 42, pp. 67–70.1998.

23. P. Charlesworth, T.G. Truscott et al; "The use of 5-aminolevulinic acid (ALA) in photodynamic therapy", *Journal of Photochemical and Photobiology*, Vol 18B pp. 99, 1993.

24. I.E. Kochevar, J.A. Parrish et al; "Photophysics, photochemistry, photobiology", in T.B. Fitzopatrick et al, Dermatology in general medicine, Vol 1, New York McGraw-Hill 1993

25. R.S. Wooten, K.C. Smith et al; "Prospective study of cutaneous phototoxicity after systemic hematoporphyrin derivative", *Lasers in Surgery and Medical*, Vol 8, pp 294, 1988.

26. T.J. Dougherty, M.T. Cooper et al; "Cutaneous phototoxic occurrences in patients receiving Photofrin", *Lasers in Surgery and Medical*, Vol 10, pp. 485, 1990.

27. T.J. Dougherty, W.R. Potter et al; "Photodynamic therapy for the treatment of cancer: cancer status and advances", in Photodynamic therapy of neoplastic disease, Boca Raton, Vol 1, Fla, CRC, 1990.

28. R.M. Szeimies, C. Abels et al; "Wavelength dependency of photodynamic effects after sensitization with 5-aminolevulinic acid in vitro and in vivo", *Journal of Investigating Dermatology*, Vol 105, pp. 672, 1995.

29. S.L. Marcus, R.S. Sobel et al; "Photodynamic therapy (PDT) and photodiagnosis using endogenous photosensitisation induced by 5-aminolevulinic acid (ALA): current clinical and development status", *Journal of Clinical Laser in Medical and Surgery*, Vol 14, pp. 59, 1996.

30. M.G. Dilkes, M.L. Dejode et al; "M-THPC photodynamic therapy for head and neck cancer", *Lasers Medical Science*, Vol 11 pp. 23, 1996.

31. T.W. Poate, M.G. Dilkes et al; "Use of photodynamic therapy for the treatment of squamous cell carcinomas of the soft palate", *British Journal of Oral Maxillofacial Surgery*, Vol 34 pp. 66, 1996.

32. J. Lenard, A.Rabson, R. Vanderoef; *Proceeding of National Academy of Science USA*, Vol 90, pp 158–162, 1993.

33. L. Lilge; "Therapeutic application of light – specific techniques", *Proceeding of Medical Physics and Imaging*, Ontario Cancer Institute, Ontario, Canada 2004.

34. A.J. Welch, M.J.C. Van Gemert et al; "Practical models for light distribution in Laser-Irradiated Tissue"; *Laser in Surgery and Medicine*, Vol 6, pp. 488, 1987.

35. A. Dunn, R. Richards; "Light scattering from cells and organelles of arbitrary shape", *Proceeding of International Society for Optical Engineering*, Vol 2979 pp. 548-555, 1997.

36. H.G. Van der Hulst; "Multiple Light Scattering Vol II", Academic Press, New York 1980.

37. E. Hecht; "Optics", Addison-Wesley Publishing Company, New York, pp 219-266 1974.

38. M.J.C. Van Gemert et al; "Skin Optics", *IEE Transactions on Biomedical Engineering*, Vol 36, No. 12, pp. 1146-1154 1989.

39. L.G Henyey, J.L Greenstein; "Diffuse radiation in the galaxy", *Astrophysical Journal*, Vol 93, pp. 70-83, 1940.

40. M. Motamedi et al; "Light and temperature distribution in laser irradiated tissue: the influence of anisotropic scattering and refractive index", *Applied Optics*, Vol 28, No 12, pp. 2230-2237, 1989.

41. A.E. Profio; "Light transport in tissue", *Applied Optics*, Vol 28, No. 12, pp. 2216-2222, 1989.

42. R.R. Anderson, J.A. Parrish; "Optical properties of human skin", *Science of Photomedicine*, pp. 147-194, 1982.

43. C. Diamantopoulos; "Bioenergetics and tissue optics", Therapeutic Lasers Theory and Practice, Churchill Livingstone, New York, pp. 67-88, 1995.

44. D.N. Dederich; "Laser-tissue interactions", *Alpha Omegan*, Vol 4 No 84, 1991.

45. R.R. Anderson, J.A.Parrish; "The optics of human skin", *Journal of Investigative Dermatology*, Vol 77, pp.13-19, 1981.

46. M.A. Everett, E. Yeargers et al; "Penetration of epidermis by ultraviolet rays", *Journal of Photochemical Photobiology*, Vol 5, pp. 533, 1966.

47. C. Diamantopoulos, "Bioenergetics and tissue optics", Therapeutic Lasers Theory and Practice, Churchill Livingstone, New York, pp 67-88, 1995.

48. R.R. Anderson, J.A. Parrish; "Microvasculature can be selectively damaged using dye lasers: a basic theory and experimental evidence in human skin", *Lasers in Surgery and Medicine*, Vol 1, pp. 263-276, 1981.

49. D.J. Smithies, P.H Butler; "Modelling the distribution of laser light in port-wine stains with the Monte-Carlo method", *Physics in Medicine and Biology*, Vol 40, pp. 701-731, 1995.

50. G.W Lucassen et al; "Light distribution in a port wine stain model containing multiple cylindrical and curved blood vessels", *Lasers in Surgery and Medicine*, Vol 18, pp. 345-357, 1996.

51. A.J. Welch, C.M.Gardner; "Monte Carlo model for determination of the role of heat generation in laser-irradiated tissue", *Lasers in Surgery and Medicine*, Vol 11, pp. 616-618, 1991.

52. A.J. Welch; "Laser irradiation of tissue", Heat transfer in Medicine and Biology, Plenum Press, New York, pp. 145-182, 1985.

53. S. Chandrasekhar; "Radiative Transfer", Dover Publications Inc., New York 1960.

54. A. Ishimaru; "Wave propagation and scattering in random media", *Academic Press*, New York, 1978.

55. G.Yoon et al; "Accuracies of the diffusion approximation and its similarity relations for laser irradiated biological media", *Applied Optics*, Vol 28, No 12, pp. 2250-2255, 1989.

56. T. Anderson; "A Monte-Carlo method for the simulation of laser-tissue interaction", M.Sc. Dissertation, pp. 18-28, 1992.

57. S.A. Prahl; "The Diffusion Approximation in Three Dimensions", *Optical-Thermal Response of Laser-Irradiated Tissue*, Plenum Press, New York, pp. 207-230, 1995.

58. S. Prahl; "Optical absorption of water [online]", Oregon Medical Laser Center, 1998. Available from: http://omlc.ogi.edu/spectra/water/index.html

59. G.M. Hale, M.R. Querry, "Optical constants of water in the 200 nm to 200 μm wavelength region," *Applied Optics*,Vol 12, pp. 555-563 1973.

60. S. Jacques; "Optical absorption of melanin [online]", Oregon Medical Laser Center, 1999. Available from: http://omlc.ogi.edu/spectra/melanin/index.html

61. D.H. Sliney, W.A. Palmisano; "The evaluation of laser hazards", *Journal of AIHA*, Vol. 20 pp. 425, 1968.

62. S.L. Jacques, D.J. McAuliffe; "The melanosome: threshold temperature for explosive vaporization and internal absorption coefficient during pulsed laser irradiation". *Journal of Photochemical and Photobiology*, Vol 53, pp. 769-775, 1991.

63. S. Prahl; "Optical absorption of haemoglobin [online]", Oregon Medical Laser Center, 1999. Available from: http://omlc.ogi.edu/spectra/hemoglobin/index.html

64. H.H Pennes; "Analysis of tissue and arterial blood temperatures in the resting human foreman", *Journal of Applied Physiology*, pp. 93–122, 1948.

65. M.G. Skinner, M.C.Kolios et al; "A theoretical comparison of energy sources—microwave, ultrasound and laser—for interstitial thermal therapy", *Physics in Medicine and Biology*, Vol 43, pp. 3535–3547, 1998.

66. A.J. Welsh; "The thermal response of laser irradiated tissue", *IEEE Journal of Quantum Electronics*, Vol QE20, pp 1471, 1984.

67. B.S. Polla, R.R. Anderson; 'Thermal injury by laser pulses: protection by heat shock despite failure to induce heat shock response", *Laser in Surgery and Medical*, Vol 7, pp. 398, 1987.

68. W.Kroy et al; "Laser coagulation: practical advice from a theoretical viewpoint", *Applied Optics*, Vol 19, pp. 6-8, 1980.
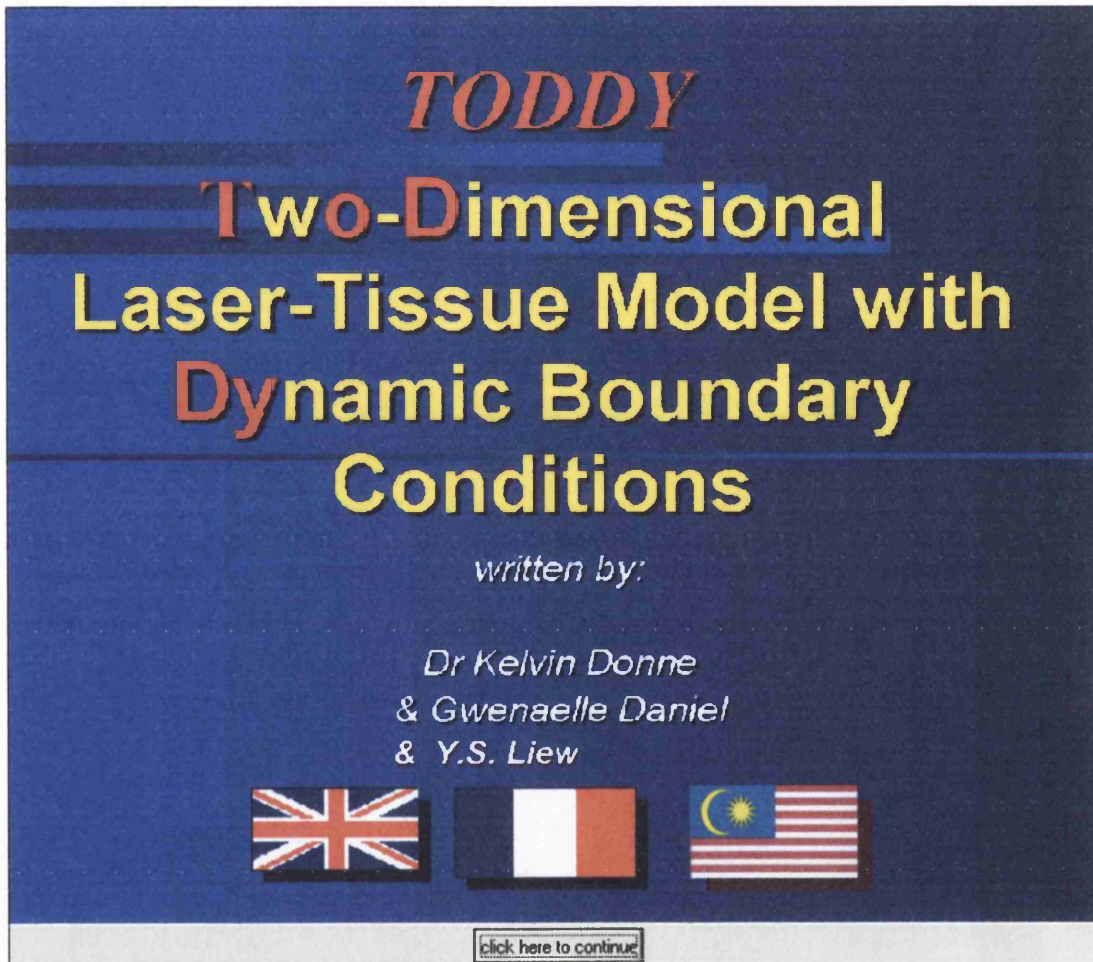
69. J.S. Nelson, T.E. Milner et al; "Laser pulse duration must match the estimated thermal relaxation time for successful photothermolysis of blood vessels", *Lasers in Medical Science*, Vol 10, No 1, 1995.

70. M.N.Kiernan; "An analysis of the optimal laser parameters necessary for the treatment of vascular lesions", PhD Thesis, University of West of England, 1997.

71. R. Bonnett; "Chemical aspects of photodynamic therapy", Advance Chemistry Text, Vol 1, Gordon and Breach Science Publishers, pp. 1-20, 2000.

72. J.E. Van Lier; "Light in biology and medicine", Plenum Press, pp. 133–141 1988.

73. J.V. Moore, C.M.L. West, et al; "The biology of photodynamic therapy", *Physics in Medicine and Biology*, Vol 42, pp. 913-935, 1997.

74. J. Moan, G. Streckyte, et al; "Photobleaching of protoporphyrin IX in cells incubated with 5-aminolevulinic acid", *International Journal of Cancer*, Vol 70, pp. 90-97, 1997.

75. J.D. Spikes; "Quantum yields and kinetics of the photobleaching of haematoporphyrin, Photofrin II, tetraporphyrin and uroporphyrin", *Journal of Photochemical and Photobiology*, Vol 55, pp. 797-808, 1992.

76. S. Iinuma, K.T. Schomacker et al; "In vivo fluence rate and fractionation effects on tumour response and photobleaching: photodynamic therapy with two photosensitiser in an orthotropic rat tumour model", *Cancer Research*, Vol 59, pp. 6164-6170, 1999.

77. H.J.C.M. Sterenborg, M.J.C. Van Gemert; "Photodynamic therapy with pulsed light sources: a theoretical analysis"; *Physics in Medicine and Biology*, Vol 41, pp. 835-849, 1996.

78. K. Langmack, R. Mehta et al; "Topical photodynamic therapy at low fluence rates – theory and practice", *Journal Photochemical and Photobiology B: Biology*, Vol 60, pp 31-43, 2001.

79. H. Rezzoug, L. Bezdetnaya et al; "Parameters affecting photodynamic activity of Foscan® or m-THPC in vitro and in vivo"; *Lasers in Medical Science*, Vol 13, pp. 119-125, 1998.

80. DJ Robinson, HSD Bruijin et al; "Fluorescence photobleaching of ALA-induced protoporphyrin IX during photodynamic therapy of normal hairless mouse: the effect of light dose and irradiance and the resulting biological effect", *Journal of Photochemical and Photobiology*, Vol 67, pp 140-149, 1998.

81. S.A. Blant, A. Woodtli et al; "In vivo fluence rate effect in photodynamic therapy of early cancers with tetra(m-hydroxyphenyl) chlorine", *Journal of Photochemical and Photobiology*, Vol 64, No. 6, pp. 963-968, 1996.

82. T.M. Busch, S.M. Hahn et al; "Depletion of tumour oxygenation during photodynamic therapy", *Cancer Research*, Vol 60, pp. 2636-2642, 2000.

83. H. Messmann, P. Mlkvy et al; "Enhancement of photodynamic therapy with 5-aminolaevulinic acid-induced porphyrin photosensitisation in normal rat colon by threshold and light fractionation studies", *British Journal of Cancer*, Vol 72, pp. 589–594, 1995.

84. H. Messmann, R.M. Szeimies et al; "Enhanced effectiveness of photodynamic therapy with laser light fractionation in patients with oesophageal cancer", *Endoscopy*, Vol 29, pp. 275-280, 1997.

85. S. Muller, H. Walt et al; "Enhanced photodynamic effects using fractionated laser light", *Journal of Photochemical and Photobiology B: Biology*, Vol 42, pp 67-70, 1998.

86. B.W. Pogue, T Hasan; "A theoretical study of light fractionation and dose rate effects in photodynamic therapy", *Radiation Research*, Vol 147, pp. 551-559, 1997.

87. M. Uehara, T. Inokuchi et al; "Expression of vascular endothelial growth factor in mouse tumours subjected to photodynamic therapy", *European Journal of Cancer*, Vol 32, pp. 2111-2115, 2001.

88. D. Kessel, Y. Luo et al; "Rapid initiation of apoptosis by photodynamic therapy", *Journal of Photochemical and Photobiology*, Vol 63, pp. 528-534, 1996.

89. E.D. Cashwell, C.J. Everett, "A practical manual on the Monte Carlo method for random walk problems", Editor N. Metropolis, Pergamon Press, 1959.

90. B.C Wilson, "A Monte Carlo model for the absorption and flux distribution of light in tissue", *Medical Physics*, Vol. 10, No 6, pp 824-830, 1983.

91. A.J. Welch, C.M. Gardner; "Monte Carlo model for determination of the role of heat generation in laser-irradiated tissue", *Lasers in Surgery and Medicine*, Vol 11, pp. 616-618, 1991.

92. C. Gabriel; "Compilation of the dielectric properties of body tissues at RF and microwave frequencies", Brooks Air Force Base 1996.

93. G. Daniel, "An investigation of thermal radiation and thermal transport in laser-tissue interaction", PhD Thesis, Swansea Institute, 2002.

94. A.D. Olver; "Microwave and optical transmission – Microwaves in lossy media", John Wiley & Sons Ltd, England, 1992.

95. R.G. Carter; "Electromagnetic waves: microwave components and devices", Chapman and Hall, London, 1990.

96. M.N. Sadiku; "Elements of electromagnetics", Saunders College Publishing, New York, 1994.

97. W.H. Hayt; "Engineering electromagnetics" McGraw-Hill International Edition, 1989.

98. K. Finkenzeller; "RFID handbook: Fundamentals and applications in contactless smart cards and identification" Second Edition, John Wiley Publishers, New York, 2003.

99. F.R. Connor; "Antennas", Edward Arnold Publishers, London, 1972.

100. J. Conway, A.P. Anderson; "Electromagnetic techniques in hyperthermia", *Clinical Physics and Physiological Measurement*, Vol. 7, No 4, pp 287-318, 1986.

101. Y. Lee; "Antenna circuit design for RFID applications", Microchip Technology Inc., 2003.

102. UPM Rafsec; "Overview of inductively coupled RFID Systems", UPM Rafsec, 2003.

103. F.A. Benson, D. Harrison; "Electric-circuit theory", Edward Arnold Publishers, London, 1975.

104. E N. Marieb; "Human anatomy and physiology", Third edition Benjamin and Cummings, Redwood City, California 1995.

105. D.R. Croft, D.G. Lilley; "Heat transfer calculations using finite difference equations", Applied Science Publishers Ltd., London, pp. 61-65, 1977.

Appendix 1

TODDY SOFTWARE G.U.I.

Toddy startup screen

Tissue optical properties and tissue dimensions data input entry box

Melanin distribution data input entry box

thermal data dialog ✕

thermal properties

	k (W/m/K)	rho (Kg/m3)	C (J/Kg/K)
epidermis	1.06	1050	3350
basal	1.06	1050	3350
dermis	1.06	1050	3350
blood	0.62	1000	3500

pulse characteristics

risetime (us)	50
holdtime (us)	100
falltime (us)	150
toff	1e+006
fluence (J/cm2)	2.5
number of pulses	1
heat transfer coeff (W/m2/K)	0
speed mm/s	0

thermal calculation parameters

	dt (s)	1e-006
NI 400	tmax (s)	0.001
NJ 400	plot every	25 time steps
dx (um) 0		
dy (um) 0	Fourier stability criterion must be < 0.25 and is	0.25

OK   Cancel

Thermal properties data input entry box

Photodynamic properties data input entry box

(12) **UK Patent Application** (19) **GB** (11) **2 376 891** (13) **A**

(43) Date of A Publication 31.12.2002

(21) Application No 0115737.9

(22) Date of Filing 27.06.2001

(71) Applicant(s)
ICN Photonics Limited
(Incorporated in the United Kingdom)
Units 1 & 2 Heol Rhosyn,
Parc Dafen Industrial Estate, LLANELLI,
Carmarthenshire, SA14 8QG,
United Kingdom

(72) Inventor(s)
Michael Noel Kiernan
Robert Marc Clement

(74) Agent and/or Address for Service
Urquhart-Dykes & Lord
Alexandra House, 1 Alexandra Road,
SWANSEA, SA1 5ED, United Kingdom

(51) INT CL⁷
A61N 5/06 // A61B 18/18

(52) UK CL (Edition T)
A5R RAP REHR

(56) Documents Cited
WO 2001/032262 A1   WO 1998/022034 A2
WO 1996/024406 A1   US 5616140 A
US 5445608 A   US 4846743 A

(58) Field of Search
UK CL (Edition T) A5R RAP REHR
INT CL⁷ A61B 18/18 18/20, A61N 5/06
Other: ONLINE WPI/PAJ/EPODOC

(54) Abstract Title
METHOD AND APPARATUS FOR INTERACTING WITH BONE TISSUE USING ILLUMINATING RADIATION

(57) A device comprising an illuminating radiation source 3, and control means 4, to regulate the intensity and/or duration of the radiation emitted from the source which is internally implanted in tissue adjacent to the target bone and illuminating it in a controlled regime comprising at least one period of illumination. The radiation source may be LEDs or laser diodes and the wavelength may be in the range 400 nm-1000 nm and be emitted in pulses. The apparatus may comprise a power source 10, connected to the implanted radiation source. Other embodiments specify that the radiation source and control means are both implanted, or the radiation source, control and a power source be implanted. The implanted device may be powered by converting electromagnetic signals received 9, from outside the body 7, 8, into electricity. Methods of implanting and using the device are described.
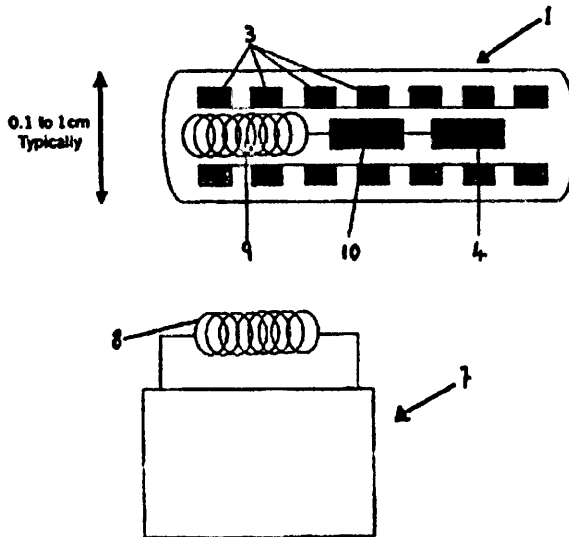
FIGURE 5

GB 2 376 891 A

METHOD AND APPARATUS FOR INTERACTING WITH BONE TISSUE USING ILLUMINATING RADIATION

Description of WO03002201

Method and apparatus for interacting with bone tissue using illuminating radiation
The present invention relates to a method and apparatus for interacting with bone tissue using illuminating radiation.

Many bone disorders, such as osteoporosis, lead to degradation of bone structure and strength. Thus, a treatment which results in new bone being formed at the treatment site may improve bone integrity and relieve disease symptoms.

Bone mainly consists of collagen and calcium deposits with an associated microvasculature blood supply. It is known that low doses of light, specifically visible or near infrared light, may induce an inflammatory response leading to an increase in the production of collagen by fibroblasts (collagen producing cells). Fibroblasts are typically triggered by mediators released by the vasculature which is generally stimulated by low doses of light.

Osteoblasts (bone producing cells) at a target zone of bone tissue when stimulated by illuminating radiation advantageously synthesise new bone tissue ideally improving the structure, strength and general integrity of bone at the target zone of bone tissue.

A trans-dermal delivery system, for example including a fibre optic cable or the like, may be used to deliver illuminating radiation to a target zone of bone tissue.

Surgical incision is usually necessary to insert the fibre optic cable in the vicinity of the bone tissue. The fibre optic cable is generally connected to an external source of illuminating radiation and acts as a means of delivering the illuminating radiation to the bone tissue.

Following completion of a period of illuminating radiation, the fibre optic cable is typically removed from the subjects body. It therefore follows that for each further period of illuminating radiation that may be required, surgical intervention is generally necessary which is time consuming, expensive and may lead to complications prevalent with any type of surgery.

An improved method of interacting with a target zone of bone tissue using illuminating radiation has now been devised.

According to the present invention there is provided a method of interacting with a target zone of bone tissue using illuminating radiation, which method comprises; (i) providing apparatus comprising an illuminating radiation source and control means capable of controlling the intensity and/or duration of illuminating radiation emitted by the radiation source; (ii) implanting the radiation source in tissue of a subject substantially in the vicinity of (preferably in or adjacent to) the target zone of bone tissue, such that the radiation source is implanted substantially below the external surface of the subjects skin; and (iii) controlling the intensity and/or duration of illuminating radiation emitted by the radiation source; wherein the target zone of bone tissue is interacted with *e according to a controlled regime in which at least one period of illuminating radiation is emitted by the implanted radiation source.

The illuminating radiation source may be implanted on the surface of the target zone of bone tissue, or implanted within the bone tissue. Alternatively, the illuminating radiation source may be implanted in the vicinity of the target zone of bone tissue, for example, for anatomical areas whereby the target zone of bone tissue is surrounded by minimal internal biological tissue, the radiation source may be implanted in, adjacent to, or on the surface of the surrounding tissue provided the illuminating radiation emitted by the illuminating radiation source can penetrate through the surrounding tissue and stimulate osteoblasts in the target zone of bone tissue.

As the radiation source is implanted in the vicinity of the target zone of bone tissue, the bone tissue can advantageously receive more than one temporally spaced period of illuminating radiation emitted by the implanted radiation source without the need for further surgical intervention.
It is preferred that the controlled regime of interaction with the target zone of bone tissue comprises temporally spaced periods of illuminating radiation emitted by the implanted radiation source. The control means advantageously allows the radiation source to be activated and deactivated as and when required, according to the controlled regime.

The control means preferably enables a predetermined intensity and/or duration of illuminating radiation to be selected. The intensity and/or duration of illuminating radiation selected is ideally the optimum intensity and/or duration of illuminating radiation for osteoblast stimulation.

It is preferred that the illuminating radiation emitted by the radiation source is substantially in the range 400 nm to 1000 nm, preferably the illuminating radiation comprises a primary wavelength or narrow wavelength band substantially in the range 570 nm to 600 nm or 800 nm to 900 nm.

The illuminating radiation may be pulsed or continuous wave. Pulsed energy may be preferred in order to avoid overheating of the tissue in which the illuminating radiation source is implanted and may produce the optimum conditions for osteoblast stimulation. Pulse duration is preferably substantially in the range 0 to 0.5 seconds. The present invention further provides apparatus for interacting with a target zone of bone tissue using illuminating radiation, which apparatus comprises an illuminating radiation source and control means capable of controlling the intensity and/or duration of illuminating radiation emitted by the radiation source, wherein the radiation source is dimensioned and configured to be implanted in tissue of a subject, such that the radiation source is implanted substantially below the external surface of the subjects skin.

The illuminating radiation source is preferably arranged to emit temporally spaced periods of illuminating radiation. The target zone of bone tissue can thus receive more than one temporally spaced period of illuminating radiation using apparatus of the present invention without the need for further surgical intervention.

The illuminating radiation source is preferably arranged to emit illuminating radiation substantially in or about the range 400nm to 1000 nm, preferably in the range 570 nm to 600 nm or 800 nm to 900 nm.

The illuminating radiation source preferably emits illuminating radiation at an energy density substantially in the range 0.5 J/cm2 to 5 J/cm2. The apparatus is preferably configured to inhibit output energies substantially above this range. Desirably, the apparatus (preferably the control means) is configured to permit variable selection of energy densities within the range.

The illuminating radiation source is preferably arranged to emit pulsed illuminating radiation with a pulse duration substantially in the range 0 to 0.5 seconds.

It is preferred feature of the present invention that the illuminating radiation source comprises a Light Emitting Diode (LED). Alternatively, other light emitters may be used, such as Laser Diodes. Beneficially, a plurality of light emitters are provided, preferably housed in a device housing and operable in concert and/or selectively individually or in sub-groups.

It is preferred that the radiation source is substantially inert so that the radiation source can be implanted into tissue of a subject for a prolonged period of time without inducing an immune response in the subject.

Apparatus of the present invention may include an implant device comprising the illuminating radiation source and at least one further element comprising a power supply system for the illuminating radiation source and/or a control system for the illuminating radiation source. The device is dimensioned and configured to be implanted in tissue of a subject, such that the device is implanted substantially below the external surface of the subjects skin.

The implant device is preferably substantially surrounded by a housing including at least a transparent portion. The housing is advantageously transparent to allow illuminating radiation emitted by the radiation source to pass through the housing of the device and penetrate the target zone of bone tissue once the device has been implanted.

The implant device (at least the device housing) is preferably substantially inert so that the device can be implanted into tissue of a subject for a prolonged period of time without inducing an immune response in the subject.

The implant device may be substantially elongated and flattened. Alternatively the device may be substantially spherical. An elongated and flattened or spherical geometry advantageously allows maximum illumination angles.

Apparatus of the present invention preferably includes a power source. The power source generally powers the illuminating radiation source. The power source may also power the control means and other features which may be included in apparatus of the present invention.

The power source may be an external power source intended to remain outside a subjects body. Additionally or alternatively, an internal power source may be provided, for example, the implant device may include a power source such as a battery.

When an external power source is provided, the external power source may be connected to the implanted radiation source via one or more electrical connectors. It is therefore preferred in one embodiment that apparatus of the present invention includes an electrical connector arranged to connect the radiation source to the power source.

A first electrical connector may be connected at one end to the illuminating radiation source, which radiation source is implanted in tissue of a subject. The opposing end of the first electrical connector may be implanted in the subjects skin. The end of the first connector implanted in the subjects skin can then be connected to the external power source via a second electrical connector.

Upon completion of a period of illuminating radiation emitted by the implanted illuminating radiation source, the second electrical connector can be disconnected from the first electrical connector. The first connector typically remains implanted in the subjects skin so that if further periods of illuminating radiation are required, the second connector can easily be reconnected to the first connector to provide power from the external power source to the implanted radiation source.

A remote control and/or power source or supply system may be used, typically comprising a respective power or control sub-unit respectively mounted on-board the implant device.

An external power/control unit interacts with the device on-board sub-unit to power/control operation of the device.

An electromagnetic signal remote control system (for example, using Radio-frequency signals) may be employed in the present invention. Apparatus of the present invention may therefore include means for receiving electromagnetic control signals (such as an antennae capable of receiving Radio-frequency signals). It is preferred that the signal receiving means is mounted on-board the implant device.

Commands such as activate (operate), deactivate (render inoperable), output power, illuminating radiation wavelength, emission duration and the like can be encoded into such signals and transmitted to the signal receiving means from a remote control unit so as to control the intensityand/or duration of illuminating radiation emitted by the radiation source. The remote control unit may therefore include means for transmitting electromagnetic control signals (such as an antennae capable of transmitting radio-frequency signals).

When apparatus of the present invention includes means for receiving control signals from a remote controller unit as hereinbefore described, the apparatus may further include conversion means (preferably mounted on-board the implant device) capable of converting control signals received by the receiving means into electrical power. The electrical' power generated by the conversion means, may be used to power the radiation source, the control system or any other feature included in the apparatus of the present invention.

There is further provided by the present invention a method of setting up apparatus according to the present invention for interacting with a target zone of bone tissue using illuminating radiation, which method comprises implanting the illuminating radiation source or the implant device in tissue of a subject substantially in the vicinity of (preferably in or adjacent to) the target zone of bone tissue, such that the radiation source or the device is implanted substantially below the external surface of the subjects skin.
The present invention further provides use of apparatus according to the present invention for interacting with a target zone of bone tissue using illuminating radiation.

The illuminating radiation source or the implant device is implanted in tissue of a subject substantially in the vicinity of (preferably in or adjacent to) the target zone of bone tissue, such that the radiation source or the device is implanted substantially below the external surface of the subjects skin.

The present invention further provides use of a source of illuminating radiation in the manufacture of medicament implant apparatus for interacting with a target zone of bone tissue using illuminating radiation.

There is further provided by the present invention bone tissue with an illuminating radiation source implanted therein.

According to a further aspect, the present invention provides apparatus as hereinbefore defined for use in interacting with a target zone of bone tissue, the apparatus including an illuminating radiation source implanted in the vicinity of the target zone of bone tissue to be substantially below the surface of a subjects skin.

Apparatus for interacting with a target zone of bone tissue using illuminating radiation will now be further described in specific embodiments, and by way of example only, with reference to the accompanying drawings in which:
Figure 1 is a schematic plan view of an exemplary apparatus according to the invention;
Figure 2 is a schematic side view of an exemplary apparatus according to the invention;
Figure 3 is a schematic view of an alternative exemplary apparatus according to the invention;
Figure 4 is a schematic view of a further alternative apparatus in accordance with the invention; and
Figure 5 is a schematic view of a further alternative apparatus according to the invention together with a remote external controller and power source.

Referring to the drawings and initially to Figures 1 and 2, there is shown an implant device 1 with an optically transparent housing 2. Device 1 comprises a plurality of individual illuminating radiation emitters 3 (typically Light Emitting Diodes (LEDs) or Laser Diodes) positioned within transparent housing 2 (shown most clearly in Figure 2). The housing 2 of device 1 is transparent to enable illuminating radiation emitted by illuminating radiation emitters 3 to penetrate surrounding tissue which device 1 may be implanted therein. The illuminating radiation emitters 3 may be operated in unison, or individually, or in sub-groups.

Figure 2 shows a control system 4 and a power source 5 encased within the body of device1. Power source 5 typically provides power to illuminating radiation emitters 3. Control system 4 typically controls the intensity and/or duration of illuminating radiation emitted by illuminating radiation emitters 3. For example, illuminating radiation emitters 3 are typically controlled to emit illuminating radiation in a pulsed regime in which the inter-pulse interval is sufficient to prevent overheating of the tissue.

Device 1 is preferably inert so that it can be implanted into tissue of a subject for a prolonged period of time without inducing an immune response in the subject. Device 1 can be flat and elongated as shown in Figures 1 and 2 or spherical as shown in Figure 4. The illuminating radiation emitters 3 shown in Figure 4 are not within the housing 2 of device 1 but are instead position on the surface of device 1.

Figure 3 shows an alternative apparatus according to the present invention where an external power source (not shown) is provided instead of, or in addition to, an internal power source. An external power source can be connected to device 1 via electrical connectors 6 which pass from device 1 to the surface of a subject's skin.

The electrical connectors 6 at the skin surface can be connected to an external power source via further connectors (not shown).

The apparatus shown in Figure 5 has a remote external controller 7 with transmitter 8 capable of transmitting electromagnetic control signals, such as Radio-frequency signals. The control signals transmitted by transmitter 8 can be received by receiver 9 positioned on-board device 1.

Both transmitter 8 and receiver 9 may be antennae capable of transmitting and receiving Radio-frequency signals respectively. Receiver 9 is connected to a power converter * 10 within the body of device 1.. Power converter 10 can convert control signals received by receiver 9 into electrical power to power illuminating radiation emitters 3. Additionally or alternatively, control signals sent by controller 7 via transmitter 8, can be used to control the intensity and/or duration of illuminating radiation emitted by illuminating radiation emitters 3. Control signals are typically received by receiver 9 and transmitted to control system4 to control illuminating radiation emitters 3.

Commands such as activate/deactivate, output power, illuminating radiation wavelength and emission duration can be encoded into the control signals transmitted to receiver 9 and acted upon by control system 4.

METHOD AND APPARATUS FOR INTERACTING WITH BONE TISSUE USING ILLUMINATING RADIATION

Claims of WO03002201

CLAIMS:1. A method of interacting with a targetzonerof bone tissue using illuminating radiation, which method comprises ; (i) providing apparatus comprising an illuminating radiation source and control means capable of controlling the intensity and/or duration of illuminating radiation emitted by the radiation source; (ii) implanting the radiation source in tissue of the subject substantially in the vicinity of the target zone of bone tissue, such that the radiation source is implanted substantially below the external surface of the subjects skin; and (iii) controlling the intensity and/or duration of illuminating radiation emitted by the radiation source; wherein the target zone of bone tissue is interacted with according to a controlled regime in which at least one period of illuminating radiation is emitted by the implanted radiation source.

2. A method according to claim 1, wherein the radiation source is implanted substantially in or adjacent to the target zone of bone tissue.

3. A method according to claim 1 or 2, wherein the controlled regime of interaction with the target zone of bone tissue comprises temporally spaced periods of illuminating radiation emitted by the implanted radiation source.

4. A method according to any preceding claim, wherein the illuminating radiation emitted by the radiation source is of a predetermined wavelength, preferably corresponding to the optimum wavelength for osteoblast stimulation.

5. A method according to any preceding claim, wherein the illuminating radiation emitted by the radiation source is substantially in the range 400 nm to 1000 nm.

6. A method according to claim 5, wherein the illuminating radiation comprises a primary wavelength or narrow wavelength band substantially in the range
570 nm to 600 nm or 800 nm to 900 nm.

7. A method according to any preceding claim, wherein the illumination radiation emitted by the illuminating radiation source is pulsed.

8. A method according to claim 7, wherein the pulse duration is substantially in the range 0 seconds to 0.5 seconds.

9. Apparatus for interacting with a target zone of bone tissue using illuminating radiation, which apparatus comprises an illuminating radiation source and control means capable of controlling the intensity and/or duration of illuminating radiation emitted by the radiation source, wherein the radiation source is dimensioned and configured to be implanted in tissue of a subject, such that the radiation source is implanted substantially below the external surface of the subjects skin.

10. Apparatus according to claim 9, wherein the illuminating radiation source is arranged to emit temporally spaced periods of illuminating radiation.

11. Apparatus according to claims 9 or10, wherein the illuminating radiation source comprises a Light Emitting Diode (LED) and/or Laser Diode.

12. Apparatus according to any of claims 9 to 11, wherein the radiation source is substantially inert.

13. Apparatus according to any of claims 9 to 12, wherein the illuminating radiation source is arranged to emit illuminating radiation substantially in or about the range 400 nm to 1000 nm.

14. Apparatus according to claim 13, wherein the illuminating radiation source is arranged to emit illuminating radiation substantially in or about the range 570 nm to 600 nm or 800 nm to 900 nm.

15. Apparatus according to any of claims 9 to 14, wherein the illuminating radiation source is arranged to emit illuminating radiation at an energy density substantially in the range 0.5J/cm2 to5 J/cm2.

16. Apparatus according to any of claims 9 to 15, wherein the illuminating radiation source is arranged to emit illuminating radiation in a pulsed wave with a pulse duration substantially in the range 0 seconds to 0.5 seconds.

17. Apparatus according to any of claims 9 to 16, including a power source.

18. Apparatus according to claim 17, including an electrical connector arranged to connect the radiation source to the power source.

19. Apparatus according to any of claims 9 to 18, including a device comprising the illuminating radiation source and at least one further element comprising a power supply system for the illuminating radiation source and/or control system for the illuminating radiation source, which device is dimensional and configured to be implanted in tissue of a subject such that the device is implanted substantially below the external surface of the subjects skin.

20. Apparatus according to claim 19, wherein the device is substantially surrounded by a housing including at least a transparent portion.

21. Apparatus according to claim 20, wherein the housing of the device is substantially inert.

22. Apparatus according to any of claims 19 to 21, wherein the device is substantially elongated and flattened. 23. Apparatus according to any of claims 19 to 21, wherein the device is substantially spherical.

24. Apparatus according to any of claims 19 to 23, wherein the device includes means for receiving electromagnetic signals (such as Radio-frequency signals).

25. Apparatus according to claim 24, wherein the device further includes conversion means arranged to convert electromagnetic signals received by the signal receiving means into electrical power.

26. A method of setting up apparatus according to any of claims 9 to 18 for interacting with a target zone of bone tissue using illuminating radiation, which method comprises implanting the illuminating radiation source in tissue of a subject substantially in the vicinity of (preferably in or adjacent to) the target zone of bone tissue, such that the radiation source is implanted substantially below the external surface of the subjects skin.

27. A method of setting up apparatus according to any of claims 19 to 25, for interacting with a target zone of bone tissue using illuminating radiation, which method comprises implanting the device in tissue of a subject substantially in the vicinity of (preferably in or adjacent to) the target zone of bone tissue, such that the device is implanted substantially below the external surface of the subjects skin.

28. Use of apparatus according to any of claims 9 to 18, for interacting with a target zone of bone tissue using illuminating radiation.

29. Use according to claim 28, wherein the illuminating radiation source is implanted in the tissue of a subject substantially in the vicinity of (preferably in or adjacent to) the target zone of bone tissue, such that the radiation source is implanted substantially below the external surface of the subjects skin.

30. Use of apparatus according to any of claims 19 to 25, for interacting with a target zone of bone tissue using illuminating radiation.

31. Use according to claim 30, wherein the device is implanted in tissue of a subject substantially in the vicinity of (preferably in or adjacent to) the target zone of bone tissue, such that the device is implanted substantially below the external surface of the subjects skin.

32. Use of a source of illuminating radiation in the manufacture of medicament implant apparatus for interacting with a target zone of bone tissue using illuminating radiation.

33. Bone tissue with an illuminating radiation source implanted therein. 34. Apparatus for use in interacting with a target zone of bone tissue, which apparatus includes an illuminating radiation source implanted in the vicinity of the target zone of bone tissue, to be substantially below the surface of a subjects skin.